

DISS. ETH NO. 22979

SYNTHESIS AND REACTIVITY OF PHOSPHORUS HETEROCYCLES USING SODIUM
PHOSPHAETHYNOLATE AS THE BUILDING BLOCK

A thesis submitted to attain the degree of
DOCTOR of SCIENCES of ETH ZURICH

Presented by
XIAODAN CHEN

Dipl.-Chem., Southeast University China

born on 01.09.1986

citizen of P. R. China

Accepted on the recommendation of
Prof. Dr. Hansjörg Grützmacher, Examiner
Prof. Dr. Antonio Togni, Co-Examiner

2015

ACKNOWLEDGEMENTS

This work would not have been possible without the support and the contribution of various people, to whom I would like to express my deep gratitude.

I would like to thank my supervisor Prof. Dr. Hansjörg Grützmacher who gave me the opportunity to work on a highly interesting research topic. He provided me with the freedom that I needed to pursue the quest into unknown chemical lands and pointed me into the right direction with his insight and creativity when I most needed it. I would like to thank Prof. Dr. Antonio Togni for kindly agreeing to be the co-referee for my thesis.

I would like to thank Dr. Hartmut Schönberg and Ms. Christine Rüegg for their general assistance and support. I would like to thank Dr. René Verel for his support in NMR related problems and Dr. Michael Würle for his help whenever I was facing problems to measure or to solve X-ray structures.

In general, I would like to thank the entire Grützmacher research group for the nice collaborative working atmosphere and for discussing various chemical and non-chemical topics and problems during my theses. Their insight often led to elegant solutions for difficult problems or shone light on my research related problems from a different angle. Surely many parts of this work would be missing without their creative ideas and insights. Especially, I would like to thank Dr. Dominikus Heift, Vittorio Sacchetti, Andreas Beil, Matthew Baker and everybody else who shared the laboratory with me and always supported me in chemical and non-chemical matters.

In particular I would like to thank my husband Dr. Zhongshu Li who is very helpful not only in my life but also in scientific problems. Last but not least, I would like to thank my parents and my friends, who enriched my life and always encouraged and supported me.

PUBLICATIONS

- Z. Li, X. Chen, M. Bergeler, M. Reiher, C.-Y. Su, H. Grützmacher, "A Stable Phosphanil Phosphaketene and Its Reactivity" *Dalton Trans.*, **2015**, *44*, 6431-6438.
- X. Chen, S. Alidori, F. F. Puschmann, G. Santiso-Quinones, Z. Benko, Z. S. Li, G. Becker, H. F. Grutzmacher, "Sodium Phosphaethynolate as a Building Block for Heterocycles" *Angew. Chem.Int. Ed.*, **2014**, *53*(6): 1641-1645.
- X. Chen, Z. Li, H. Grützmacher, "Synthesis and Photoluminescence properties Cu(I) Complexes with Chelating Phosphinito Phosphinine Ligands" *Eur. J.Inorg. Chem.*, invitation topic, accepted.
- X. Chen, R. Rong, B. Sun, "Three Novel Copper-Radical Complexes: Syntheses, Crystal Structures, and Magnetic Properties." *Eur. J. Inorg. Chem.*, **2010**, (22): 3506-3512.
- B. Sun, X. Chen, "A novel large Ni-azido circle with tridentate (NNO) Schiff base co-ligands: hexagonal structure and ferromagnetic properties." *New J. Chem.*, **2010**, *34*(2): 190-192.
- B. Sun, X. Chen, "Hydrothermal Synthesis of a 3D Polymeric Cobalt(II) Carboxylate Derivative from 1,2,4,5-Benzenetetracarbonitrile." *Z. Anorg. Allg. Chem.*, **2009**, *635*(15): 2375-2377.

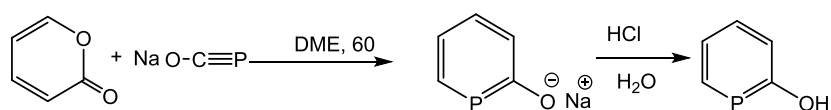
PRESENTATIONS

- Poster presentation: Heterophosphorous phenol
Swiss Chemical Society Fall Meeting, ETH Zurich, Switzerland, September 9, **2011**
- Poster presentation: Cycloaddition of NaOCP
10th European Workshop on phosphorus Chemistry, March 18–20, **2013**
- Oral presentation: Unexpected results: from Cycloaddition of NaOCP and tetracyclone
Swiss Chemical Society Fall Meeting, EPFL, Lausanne, Switzerland, September 9, **2012**
- Poster presentation: Simple dimeric Cu(I) complexes bridged by μ^2 -P of phosphinine
12th European Workshop on phosphorus Chemistry, March 18–20, **2015**

ABSTRACT

Phosphorus-containing heterocycles have evolved from laboratory curiosities to functional components, such as ligands in catalytically active metal complexes or molecular constituents in electronic devices. However, the straightforward synthesis of functionalized heterocycles on a larger scale remains a challenge. The phosphoethynolate anion $(\text{OCP})^-$ is indeed a valuable building block, which can be obtained in a simple one-pot procedure from sodium, elemental phosphorus, and ethylene carbonate. In this work, the use of the phosphoethynolate anion $(\text{OCP})^-$ as a building block for various sterically unprotected and functionalized hydroxy substituted phosphorus heterocycles will be described. As the resulting heterocycles are themselves anions, they constitute building blocks for further facile functionalization.

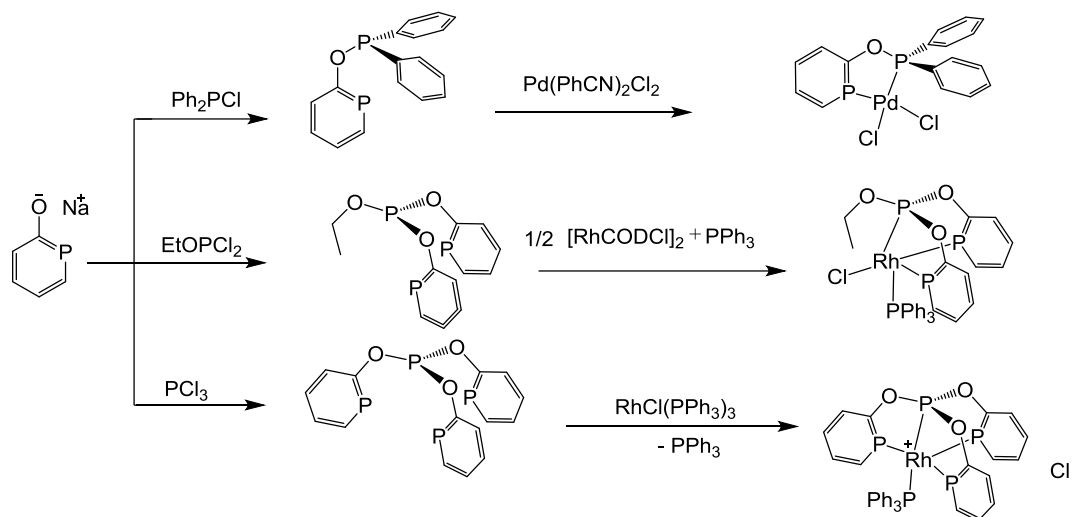
A phosphinine was simply synthesized through the Diels Alder reaction between $\text{Na}(\text{OCP})$ and α -pyrone under mild reaction condition, in which the phosphinine ring only carries an oxy-substituent in 2-position. Sodium 2-phosphaphenolate is an air stable compound from which, after the protonation with hydrochloric acid in water, 2-hydroxyphosphinine was synthesized. 2-hydroxyphosphinine was experimentally and theoretically proven to show no tautomerization unlike its nitrogen analogue of 2-Hydroxypyridine. Additionally, 2-hydroxyphosphinine with the pKa value of 8.16 is more acid than phenol.



Scheme A1

Sodium 2-phosphaphenolate reacts with electrophiles easily and generates fascinating derivatives, which can be applied as ligands to transition metal complexes and to stabilize electron rich metal centers. In chapter 3, the synthesis of three compounds is presented which contain one-, two- or three- phosphinine rings respectively (Scheme A2). Additionally, the coordination modes of these compounds were studied. Compared with the ipso-C-P-C-angle in the parent phosphinine, the ipso-C-P-C-angle turns to be more open for 2-diphenylphosphinite phosphinine

(POP') in Pd(II) complex. This decreases the aromaticity and stability of the phosphinine ring. Additionally, the diphosphinyl-ethyl phosphite ligand and its Rh(I) complex have been synthesized. Preliminary experiments have shown that the ligand in the Rh(I) complex can undergo a Arbuzov-like reaction under certain conditions. The obtained complex containing phosphonate is stabilized by one equivalent of lithium iodide. Additionally, the coordination of triphosphinyl phosphite to Rh(I) indicates its abilities to stabilize electron rich metal centers.



Scheme A2

So far, the coordination chemistry of phosphinines as ligands were developed considerably, but other potential applications of the phosphinine moiety have been much less regarded and reported. In chapter 4, the luminescent, dimeric $[\text{Cu}_2(\text{X})_2(\mu_2\text{-POP}')_2]$ ($\text{X}=\text{Cl}, \text{Br}, \text{I}$) complexes are described which were obtained in good yields in reactions between CuX and 2-phosphininonate-diphenylphosphine (POP'). In these dimeric complexes, the phosphinine units take bridging positions and induce Cu-Cu interactions while the halogen ligands are in terminal positions. These complexes show red phosphorescence at room temperature with relatively long decay time (Figure A1). The wavelengths of the emission bands are modulated by the halogen ligands whereby the strong field ligand chloride leads to the lowest emission energy (longest wavelength) and the weakest ligand iodide to the highest emission energy (shortest wavelength). Additionally, the cluster $[\text{Cu}_4(\mu_2\text{-POP}')_2(\mu^2\text{-Cl})_2(\mu^2\text{-Cl})_2(\text{THF})_2]$ was synthesized by the reaction of POP' and 2 equivalents of CuCl in THF. In CH_3CN , POP' changes its coordination from μ^2 -mode to η_1 -mode

and a new cluster $[\text{Cu}_4(\eta^1\text{-POP}')_2(\mu^3\text{-Cl})_2(\mu^2\text{-Cl})_2(\text{CH}_3\text{CN})_2]$ is formed. Both of these complexes are phosphorescent as well.

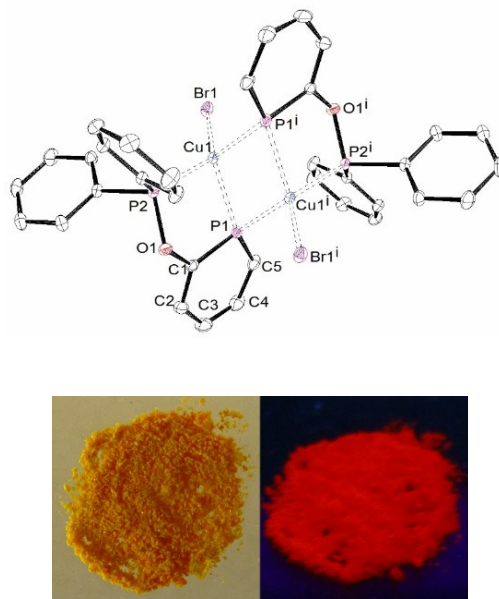
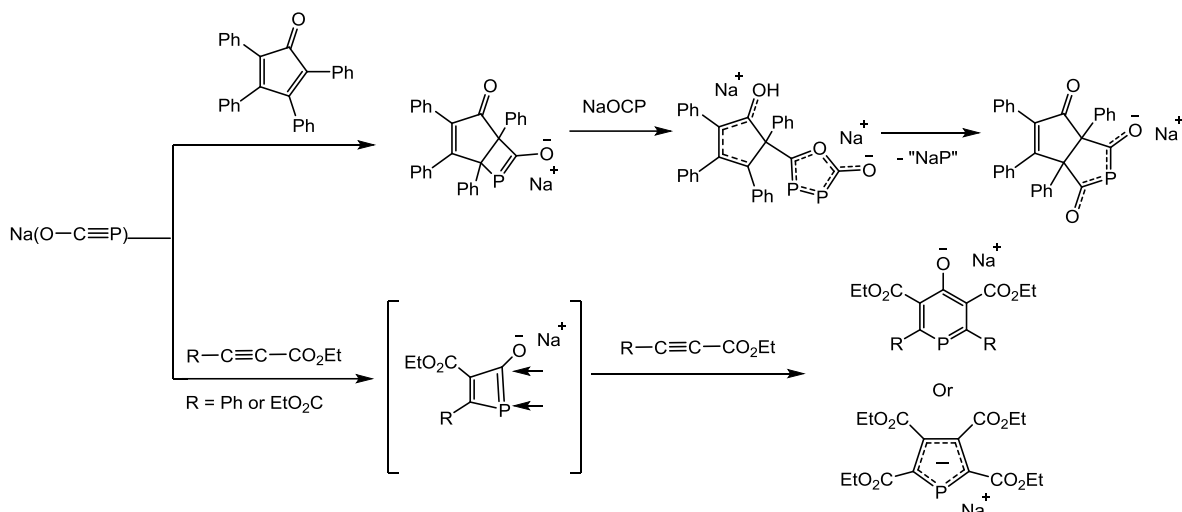


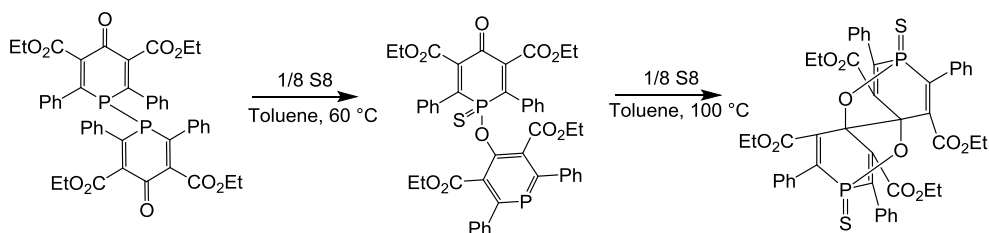
Figure A1

The reactivity of $\text{Na}(\text{OCP})$ towards tetracyclone and acetylenes was investigated in chapter 5. NMR studies at low temperature show that $[2+2]$ cycloaddition intermediates are formed at the beginning of the reaction (Scheme A3). On the basis of these experimental results, it is revealed that the cycloadditions of $(\text{OCP})^-$ with different unsaturated compounds proceed with high regioselectivity. When $\text{Na}(\text{OCP})$ is treated with the asymmetrical alkyne $(\text{EtO}_2\text{CC}\equiv\text{CPh})$, a phosphinine ring is formed. Nevertheless, the reaction between $\text{Na}(\text{OCP})$ and the more electron deficient alkyne $(\text{EtO}_2\text{CC}\equiv\text{CCO}_2\text{Et})$ does not only produce phosphinine, but also phospholide under loss of CO .



Scheme A3

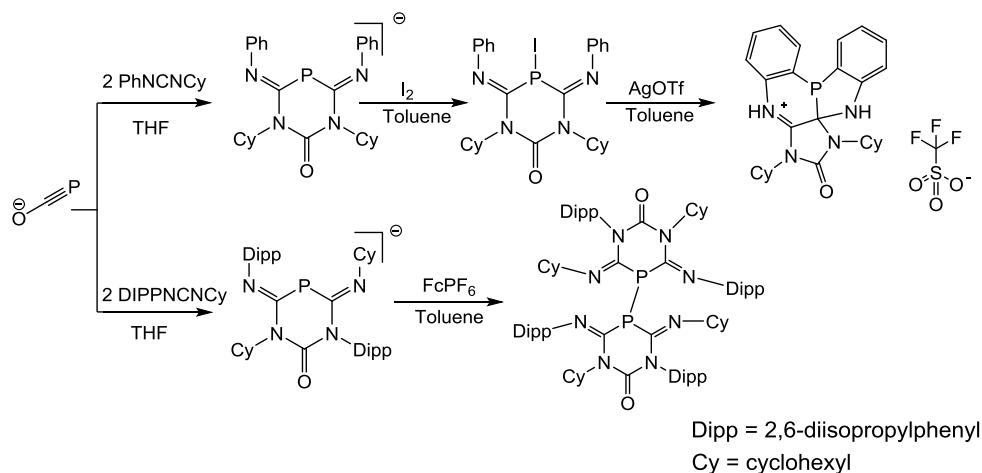
The 4-oxy-phosphinine (sodium salt of diethyl 4-hydroxy-2,6-diphenylphosphinine -3,5-dicarboxylate, Scheme A3) was synthesized by the reaction between Na(OCP) and ethyl phenylpropiolate. The reactivity of this 4-oxy-phosphinine was also investigated and it is revealed that it is not as stable as 2-oxy-phosphinine. It is unreactive to water but is oxidized by oxygen or sulfur. Additionally, the corresponding bisphosphinone was obtained by one-electron oxidation of the sodium salt of 4-oxy-phosphinine, a formation that has never been studied before. By oxidizing the bisphosphinone with sulfur, a series of intermolecular rearrangements are induced in this compound (Scheme A4).



Scheme A4

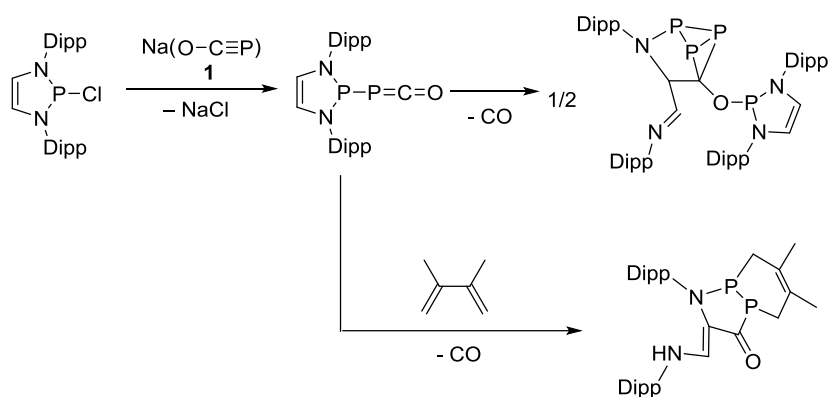
Similarly to the reaction of Na(OCP) with unsaturated C-C bonds, the cycloaddition between Na(OCP) and 2 equivalents of carbodiimide forms anionic 1,3,5-diazaphosphinane heterocycles. The experimental results show that the substituents of carbodiimide will affect the activation barriers of the reaction as well as the conformations (Scheme A5) and the reactivity of the obtained heterocycles. One electron oxidation of both symmetric and asymmetric heterocycles

will form the corresponding diphosphanes. For the symmetric heterocycle with two phenyl substituents, after two-electron oxidation, the P^+ activates the aromatic C-H bonds of phenyl groups. DFT calculations were performed to gain deeper insight into the mechanism of the insertion of P^+ to the C-H of phenyl groups. In contrast, the two-electron oxidation of the asymmetric heterocycles is very complicated due to various components in the products, which makes purification impossible.



Scheme A5

Na(OCP) reacts with the bulky P-chloro-diazaphosphole yielding a phosphanyl phosphaketene, which is stable for weeks under an inert atmosphere in the solid state. This compound is best described as a tight ion pair with a remarkably long P–P bond distance (2.44 Å). In solution, this phosphaketene dimerizes under loss of CO to give 1,2,3-triphosphabicyclobutane identified by an X-ray diffraction study. As an intermediate, a five-membered heterocyclic diphosphene was trapped in a Diels–Alder reaction with 2,3-dimethylbutadiene. The formation of this intermediate in a hetero-Cope-rearrangement as well as dimerization/CO loss were computed with various DFT methods which allowed us to propose a reaction mechanisms.



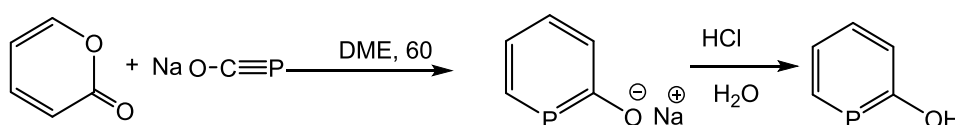
Scheme A6

In summary, using the $(\text{OCP})^-$ anion as building block, a variety of phosphorus-containing five- and six-membered heterocycles can be prepared in practically quantitative yields. The studies of ligands containing phosphinine rings reveal that they can be applied not only in coordination chemistry but also in photoluminescence materials. The experimental results of the reactions between $\text{Na}(\text{OCP})$ and unsaturated compounds indicate that they do not proceed in a concerted fashion, but are stepwise initiated by a nucleophilic attack of the phosphorus atom in $(\text{OCP})^-$. Meanwhile, by the reaction between $\text{Na}(\text{OCP})$ and P-chloro-diazaphosphole, a stable phosphanyl phosphaketene with unusually long P–P bond is obtained. Compared with the reactivity of $\text{Na}(\text{OCP})$, the phosphanyl phosphaketene is more likely to lose CO in reactions.

ZUSAMMENFASSUNG

Phosphor-Heterozyklen haben sich von einer Laborkuriosität zu funktionalen Materialien, wie etwa Liganden katalytisch aktiver Metallkomplexe oder molekularer Bestandteile elektronischer Bauteile, entwickelt. Dabei ist die direkte Synthese grösserer Mengen funktionalisierter Heterozyklen immer noch eine Herausforderung. Das Phosphaethinolat-Anion (OCP^-) ist dabei ein wertvoller Synthesebaustein, der in einer einfachen Eintopfsynthese aus Natrium, elementarem Phosphor und Ethylencarbonat erhalten werden kann. In dieser Arbeit wird die Verwendung des Phosphaethinolat-Anions (OCP^-) als Synthesebaustein zur Herstellung einer Vielzahl sterisch ungeschützter und funktionalisierter hydroxy-substituierter Phosphor-Heterozyklen beschrieben. Da die erhaltenen Heterozyklen selbst anionisch sind, stellen sie ebenfalls Synthesebausteine dar und können einfach weiter funktionalisiert werden.

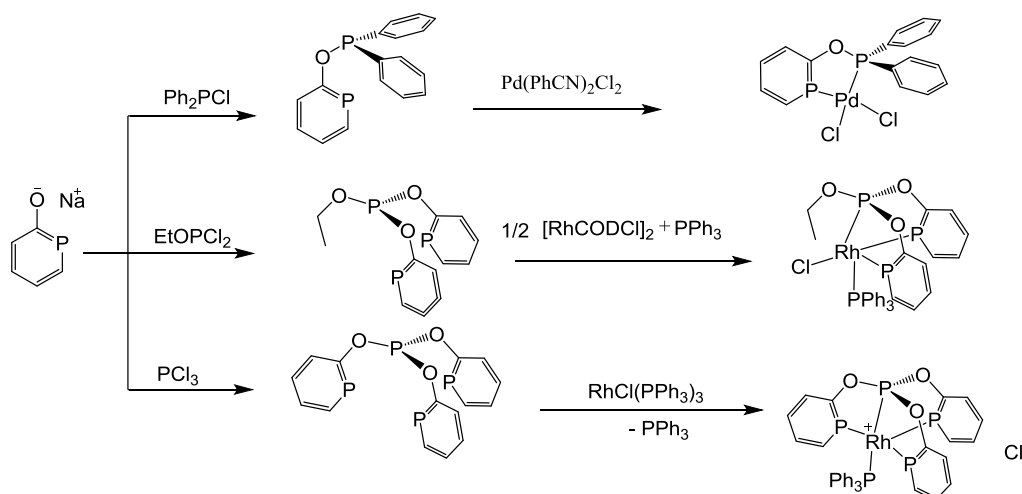
Ein Phosphinin wurde leicht in einer Diels-Alder-Reaktion zwischen Na(OCP) und α -Pyrone unter milden Bedingungen erhalten, wobei der Phosphinin-Ring als einzigen Substituenten eine Oxy-Funktion in 2-Position trägt. Natrium-2-phosphaphenolat ist eine luftstabile Verbindung, aus der durch Protonierung mit HCl in Wasser 2-Hydroxyphosphinin erhalten wird. Dieses zeigt im Gegensatz zu seinem Stickstoffanalogon 2-Hydroxypyridin keine Tautomerie, wie experimentell und theoretisch gezeigt wurde. Zudem ist 2-Hydroxyphosphinin acider als Phenol mit einem pK_a -Wert von 8.16.



Gleichung A1

Natrium-2-phosphaphenolat reagiert gut mit Elektrophilen zu faszinierenden Derivaten, welche als Liganden für Übergangsmetalle eingesetzt werden können. Zudem können diese Derivate elektronenreiche Zentren stabilisieren. In Kapitel 3 wird die Synthese von drei Verbindungen mit einem, zwei beziehungsweise drei Phosphinin-Ringen dargestellt (Gleichung A2). Im Weiteren

wurden die Koordinationsmoden dieser Verbindungen studiert. Der Komplex von 2-Phosphininonadiphenylphosphin (POP') mit Pd(II) zeigt eine Vergrößerung des ipso-Winkels C-P-C im Phosphinin, was zu einer Verminderung der Aromatizität und der Stabilität des Phosphinin-Heterozyklus' führt. Auch wurden der Diphosphininylethylphosphit-Ligand und sein Rh(I)-Komplex synthetisiert. Vorläufige Experimente haben gezeigt, dass der Ligand in diesem Rh(I)-Komplex unter bestimmten Bedingungen Arbusov-ähnliche Reaktionen eingehen kann. Der erhaltene Komplex, welcher Phosphonat enthält, kann mit einem Äquivalent Lithiumiodid stabilisiert werden. Zudem zeigt die Koordination von Triphosphininylphosphit an Rh(I), dass es in der Lage ist, elektronreiche Metallzentren zu stabilisieren.



Gleichung A2

Die Verwendung von Phosphininen als Liganden in der Komplexchemie ist im Wesentlichen bekannt, andere potentielle Anwendungen der Phosphinin-Einheit hingegen wurden weit weniger beachtet und publiziert. In Kapitel 4 werden die lumineszenten, dimeren Komplexe $[\text{Cu}_2(\text{X})_2(\mu_2\text{-POP}')_2]$ ($\text{X}=\text{Cl}, \text{Br}, \text{I}$) beschrieben, welche in guten Ausbeuten in Reaktionen zwischen CuX und 2-Phosphininonadiphenylphosphin (POP') erhalten wurden. In diesen dimeren Komplexen nimmt die Phosphinin-Einheit verbrückende Positionen ein und vermittelt Cu-Cu-Wechselwirkungen, während die Halogenliganden terminale Positionen einnehmen. Diese Komplexe zeigen bei Raumtemperatur eine rote Phosphoreszenz mit relativ langen Relaxationszeiten (Abbildung A1). Die Wellenlänge der Emissionsbanden ist dabei von den Halogenliganden beeinflusst, wobei der Starkfeldligand Chlorid zu den niedrigsten

Emissionsenergien (den längsten Wellenlängen) und der schwächste Ligand Iodid zu den höchsten Emissionsenergien (den kürzesten Wellenlängen) führt. Inzwischen wurde der Cluster $[\text{Cu}_4(\mu_2\text{-POP}')_2(\mu^2\text{-Cl})_2(\mu^2\text{-Cl})_2(\text{THF})_2]$ in der Reaktion von zwei Äquivalenten CuCl mit POP' in THF synthetisiert, was zur Annahme verleitet, dass POP' seinen Koordinationsmodus ändert und einen neuen Cluster $[\text{Cu}_4(\eta_1\text{-POP}')_2(\mu^3\text{-Cl})_2(\mu^2\text{-Cl})_2(\text{CH}_3\text{CN})_2]$ formt, wenn man es in CH_3CN löst. Diese Komplexe sind ebenfalls beide phosphoreszent.

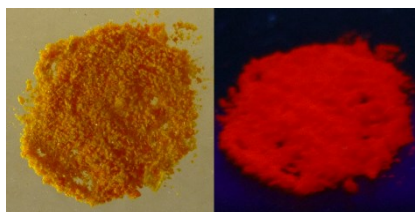
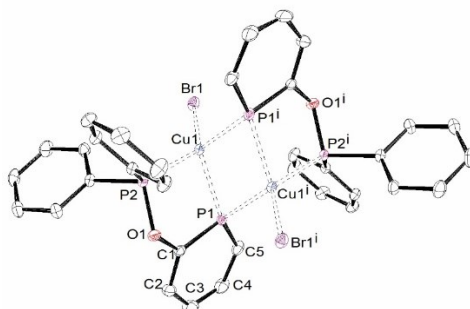
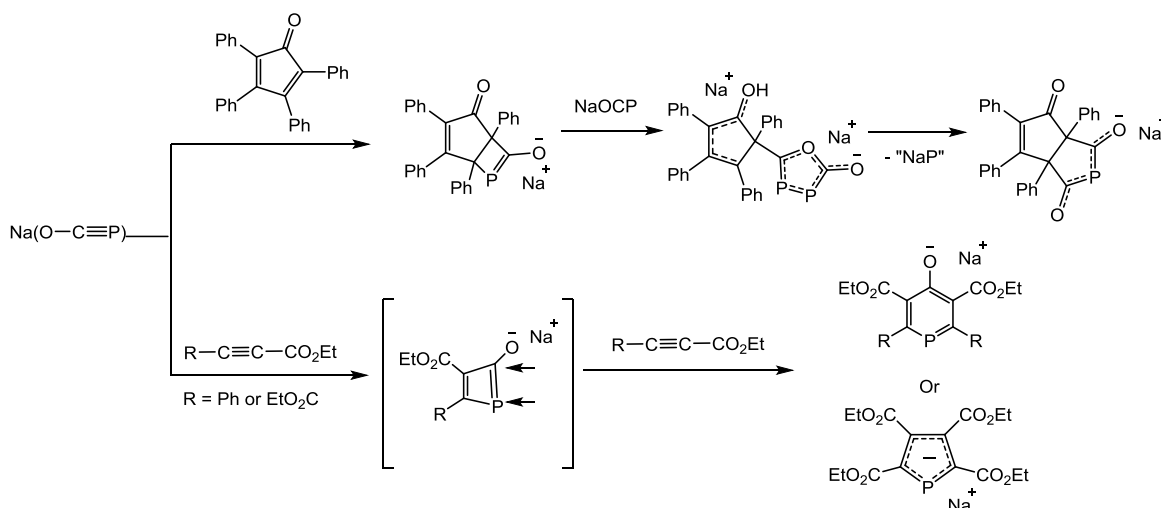


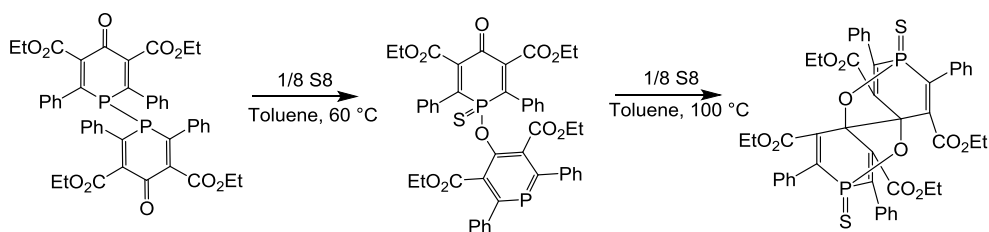
Abbildung A1

Die Reaktivität von $\text{Na}(\text{OCP})$ gegenüber Tetracyclon und Acetylenen wird in Kapitel 5 untersucht. Tieftemperatur-NMR-Studien zeigen, dass Intermediate in $[2+2]$ -Cycloadditionen zu Beginn der Reaktionen gebildet werden (Gleichung A3). Basierend auf diesen experimentellen Befunden wurde gezeigt, dass die Cycloadditionen von $(\text{OCP})^-$ mit verschiedenen ungesättigten Verbindungen mit hoher Regioselektivität verlaufen. Wenn $\text{Na}(\text{OCP})$ mit dem asymmetrischen Alkin $(\text{EtO}_2\text{CC}\equiv\text{CPh})$ behandelt wird, wird ein Phosphinin-Ring gebildet. Dagegen führt die Reaktion von $\text{Na}(\text{OCP})$ mit dem elektronenärmeren Alkin $(\text{EtO}_2\text{CC}\equiv\text{CCO}_2\text{Et})$ nicht nur zu dem Phosphinin-Ring, sondern unter Abspaltung von CO auch zu einem Phospholid.



Gleichung A3

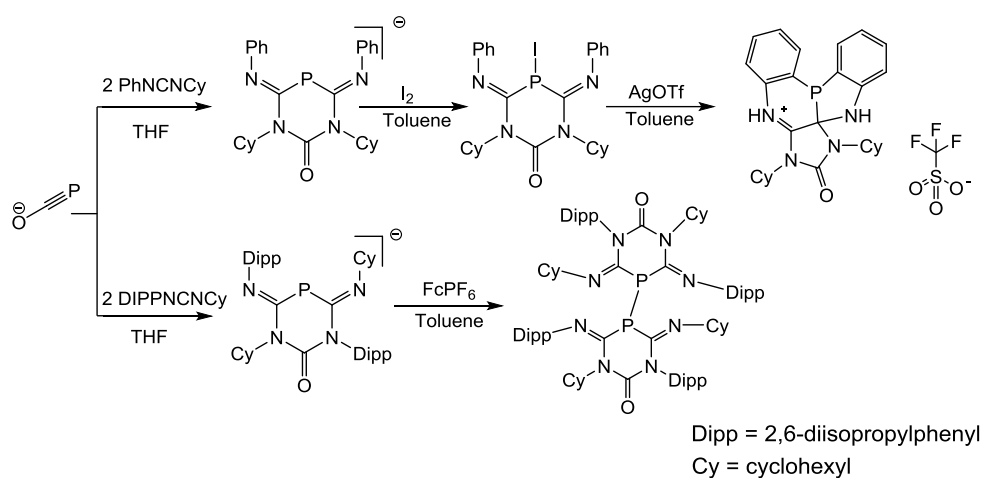
Das 4-Oxyphosphinin (Natrium-Salz von Diethyl-4-hydroxy-2,6-diphenylphosphinin-3,5-dicarboxylat, Gleichung A3) wurde in der Reaktion zwischen $\text{Na}(\text{OCP})$ und Ethylphenylpropiolat synthetisiert. Die Reaktivität dieses 4-Oxyphosphinin wurde ebenfalls untersucht und es wurde gezeigt, dass es nicht so stabil ist wie 2-Oxyphosphinin. Es reagiert nicht mit Wasser, wird aber von Sauerstoff und Schwefel oxidiert. Zwischenzeitlich wurde durch Einelektronenoxidation des Natriumsalzes das entsprechende Bisphosphinin erhalten, dessen Bildung zuvor noch nicht untersucht worden ist. Durch die Oxidation des Bisphosphinons mit Schwefel wird eine Reihe neuer Bindungsumlagerungen zwischen den beiden Heterozyklen in dieser Verbindung induziert (Gleichung A4).



Gleichung A4

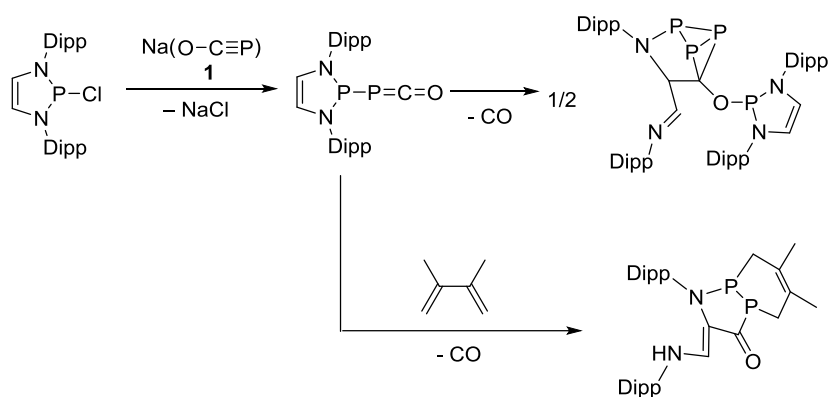
Ähnlich wie in der Reaktion von $\text{Na}(\text{OCP})$ mit ungesättigten C-C-Bindungen, werden in der Cycloaddition zwischen $\text{Na}(\text{OCP})$ und zwei Äquivalenten Carbodiimid anionische 1,3,5-Diazaphosphinan-Heterozyklen gebildet. Die experimentellen Befunde zeigen, dass die Substituenten des Carbodiimids sowohl die Orientierung der Addition (Gleichung 5) als auch die

Reaktivität der erhaltenen Heterozyklen beeinflussen. Die Einelektronenoxidation sowohl des symmetrischen als auch des asymmetrischen Heterozyklus führt zur Bildung der entsprechenden Diphosphane. Im Fall des symmetrischen Heterozyklus aktiviert das P^+ nach einer Zweielektronenoxidation die Kohlenstoff-Wasserstoff-Bindungen der Phenylsubstituenten. Um einen tieferen Einblick in den theoretischen Mechanismus der P^+ -Insertion in die C-H-Bindungen der Phenylgruppen zu erhalten, wurden DFT-Rechnungen angestellt. Im Gegensatz dazu führt die Zweielektronenoxidation der asymmetrischen Heterozyklen zu einer Mischung vieler Verbindungen, welche nicht aufgetrennt werden konnten.



Gleichung A5

Na(OCP) reagiert mit dem sperrigen P-Chlordiazaphosphol unter Ausbildung eines Phosphanylphosphaketens, welches als Feststoff in einer inerten Argon-Atmosphäre über Wochen stabil ist. Diese Verbindung kann man am besten als ein starkes Ionenpaar mit einer bemerkenswert langen P-P-Bindungslänge (2.44 Å) beschreiben. In Lösung dimerisiert dieses Phosphaketen unter CO-Abspaltung zu einem 1,2,4-Triphosphabicyclobutan, welches in einer röntgenkristallographischen Studie identifiziert worden ist. Als Intermediat wurde ein fünfgliedriges heterozyklisches Diphosphen in einer Diels-Alder-Reaktion mit 2,3-Dimethylbutadien abgefangen. Die Bildung dieses Intermediates in einer Hetero-Cope-Umlagerung wurde ebenso wie die Dimerisierung und die CO-Abspaltung mit verschiedenen DFT-Methoden berechnet, was uns erlaubte, die Reaktionsmechanismen zu verstehen.



Gleichung A6

Zusammenfassend wurden durch die Verwendung des $(\text{OCP})^-$ -Anions als Synthesebaustein eine Vielzahl fünf- und sechsgliedriger Heterozyklen in praktisch quantitativer Ausbeute erhalten. Die Untersuchungen von Liganden, welche Phosphinin-Ringe enthalten, zeigten, dass diese nicht nur in der Koordinationschemie benutzt werden können, sondern auch in photolumineszenten Materialien. Die experimentellen Befunde über die Reaktionen zwischen $\text{Na}(\text{OCP})^-$ und ungesättigten Verbindungen zeigen, dass diese Reaktionen nicht konzertiert sondern stufenweise verlaufen, wobei die Reaktionen von einem nukleophilen Angriff des Phosphoratoms in $(\text{OCP})^-$ initiiert werden. Zwischenzeitlich wurde in der Reaktion zwischen $\text{Na}(\text{OCP})^-$ und P-Chlordiazaphosphol ein stabiles Phosphanylphosphaketen mit einer ungewöhnlich langen P-P-Bindung erhalten. Im Vergleich mit $\text{Na}(\text{OCP})^-$ ist es für das Phosphanylphosphaketen wahrscheinlicher, in Reaktionen CO abzuspalten.

1	Introduction	1
1.1	Phosphorus-carbon triple bonds	1
1.2	Phosphinine	3
1.3	Coordination modes of phosphinine with transition metals	5
1.4	Other phosphorus-containing heterocycles	6
1.5	Thesis objective and outline	7
2	Synthesis and property studies of 2-Hydroxyphosphinine	8
2.1	Introduction	8
2.2	Reaction of sodium phosphacyanate with α -pyrone	10
2.2.1	Synthesis of sodium phosphinin-olate [Na(2)] and 2-hydroxyphosphinine (2H) 10	
2.2.2	NMR Diffusion experiment of (2H)	13
2.2.3	The pK_a value of 2H	15
2.3	Computational Investigations	17
2.3.1	DFT Calculation for 2H and 3	17
2.3.1	Aromaticity studies of 2, 2H and 3	18
2.4	The reactivity of Sodium phosphinin-2-olate	19
2.5	Conclusion	21
3	The coordination studies of phosphinine derivatives	23
3.1	Introduction	23
3.2	Synthesis of derivatives for phosphinine	24
3.3	Pd(II) complex of 2-diphenylphosphinite phosphinine: Synthesis, Structure, and Reactivity	25
3.3.1	The coordination of ligand 4 to Pd(II)	25
3.3.2	Reactivity with water	27
3.4	A new Ethyl diphosphinylphosphinite chelated Rhodium complex and its Arbuzov-like dealkylation reactions	28
3.4.1	Coordination of 8 to Rh(I)	29

3.4.2	Arbuzov reaction of 12.....	30
3.5	Synthesis of Rh complex 16.....	33
3.6	Conclusion	35
4	Synthesis and Photoluminescence properties of Phosphinine–Cu(I) Complexes	36
4.1	Introduction.....	36
4.2	The synthesis and characterization of Copper(I) complexes	38
4.3	The luminescence properties	42
4.4	DFT calculations.....	45
4.5	Conclusions.....	46
5	Na(OCP) as precursor to phosphaketenes and various phosphorus heterocycles.....	47
5.1	Introduction.....	47
5.2	The reaction of Na(OCP) with tetracyclone	48
5.2.1	Formation of phosphorus heterocycles.....	48
5.2.2	The crystal structures of 24 and 25.....	50
5.3	Synthesis of phosphinin-4-olate and phospholide.....	52
5.3.1	Reactions between Na(OCP) and acetylene	52
5.3.2	The crystal structure of 26 and 28	53
5.3.3	Comparison of selected structure parameters in [PC ₄ R ₄] – phospholide rings	55
5.4	Reactivity of phosphinin-4-olate	56
5.4.1	Oxidation of 26 with oxygen and sulfur	57
5.4.2	Synthesis of biphosphininone (31).....	58
5.4.3	The oxidation of biphosphininone	60
5.5	Conclusion	62
6	Synthesis and reactivity of the 1,3,5-diazaphosphinane anions	64
6.1	Introduction.....	64
6.2	The synthesis and characterization of two diazaphosphanes.....	65
6.3	Discussion on the reaction mechanism.....	68

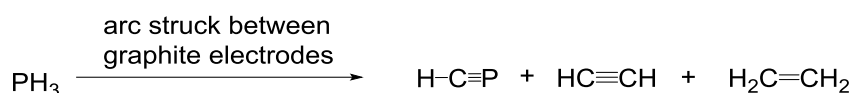
Contents

6.4	Oxidation of the anionic diazaphosphinane 37.....	69
6.5	Mechanistic studies on the formation of the 1, 3, 5- diazaphosphinane anion ..	71
6.6	Reactivity of the anionic diazaphosphinane 38.....	71
6.7	Conclusion	76
7	A Stable Organic Phosphaketene and Its Reactivity	77
7.1	Introduction.....	77
7.2	Preparation of the stable organic phosphaketene.....	78
7.3	Trapping the intermediate for the dimerization	80
7.4	Computational investigation on the rearrangement of 48	82
7.5	The reactivity of 48.....	84
7.6	Compound 48 as P–P triple bond source	85
7.7	Conclusion	87
8	Summary and Outlook	88
9	Experimental section	90
9.1	General Information.....	90
9.2	Sodium phosphoethynolate reacted with α -pyrone	93
9.3	Coordination studies with phosphinine derivatives.....	98
9.4	The synthesis of copper (I) complexes	104
9.5	Na(OCP) as precursor to phosphaketenes and phosphorus heterocycles.....	108
9.6	Synthesis and reactivity of 1,3,5-diazaphosphinane anion.....	114
9.7	A Stable Organic Phosphaketene and Its Reactivity.....	118
10	Appendix	124
10.1	Crystallographic information.....	124
10.1.1	Experimental Details.....	124
10.1.2	Crystallographic data and tables.....	124
10.2	Crystallographic tables	125
11	References.....	140

1 INTRODUCTION

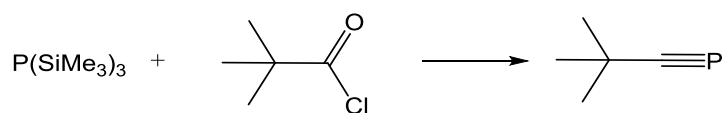
1.1 PHOSPHORUS-CARBON TRIPLE BONDS

Organophosphorus chemistry has attracted wide interests for several decades.¹⁻⁷ For a long time, the so called “double-bond rule” suggested that sp^2 -hybridization could not be extended for heavier elements because of a weak overlap between 3s and 3p atomic orbitals.⁸ Chemists are accustomed to use phosphorous derivatives in their usual oxidation state trivalent, tricoordinate ($\lambda^3\sigma^3$) and pentavalent, tetracoordinate ($\lambda^5\sigma^4$).⁹ However, with the development of the synthetic technologies, more and more unsaturated phosphorous compounds were obtained. This firmly demolished the “double-bond rule”. In the 1960s, Gier¹⁰ reported the generation of the extremely reactive phosphacetylene, $H-C\equiv P$, from phosphine in a rotating arc struck between graphite electrodes.



Scheme 1 Generation of phosphacetylene from phosphane

The synthesis of the molecules containing P-C triple bonds encouraged researchers to obtain relatively stable derivatives. Around ten years later, relative bulky substituents to stabilize the P-C triple bond in $tBu-C\equiv P$ were reported by Becker et al.¹¹ It was synthesized from trisilylphosphane $P(TMS)_3$ and pivaloyl chloride, $BuCOCl$ (Scheme 2). This synthetic method allowed to build up a large number of new phosphalkynes with various bulky substitutions.

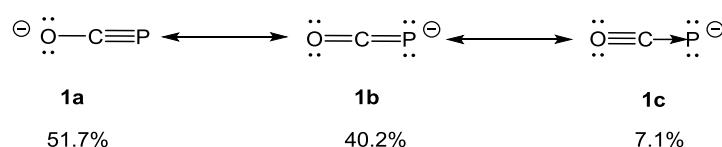


Scheme 2 synthesis of tert-butyl-phosphaacetylene

After the initial synthesis of lithium phosphaethynolate $Li(OCP)$ from $Li[P(SiMe_3)_2]$ and dimethylcarbonate, $(MeO)_2CO$, by Becker et al.,¹² the sodium salt, $Na(OCP)$, was also prepared from $NaPH_2$ and carbon monoxide¹³ or by a bond metathesis reaction from a niobium phosphido

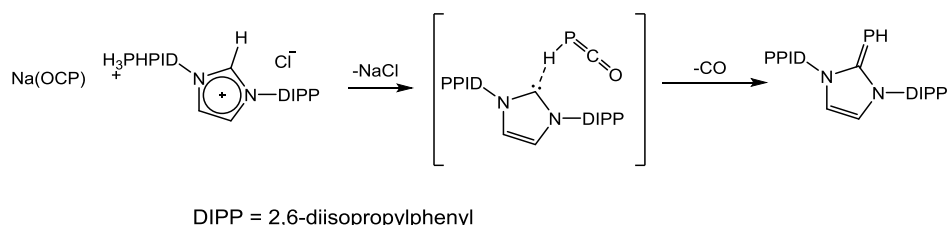
complex, $\text{Nb(L)n}\equiv\text{P}$ and CO_2 .¹⁴ Very recently, the reaction between K_3P_7 and CO in presence 18-crown-6 was reported to yield $[\text{K}(18\text{-crown-6})(\text{OCP})]$ in DMF at $150\text{ }^\circ\text{C}$.¹⁵ To the best of our knowledge, the simplest procedure is the reaction of NaPH_2 with ethylenecarbonate which gives $[\text{Na}(\text{OCP})(\text{dioxane})_x]$ with $x \approx 2.5$ in reproducible yields (up to 65% based on P).¹³

The $(\text{OCP})^-$ anion in the alkaline phosphoethynolate salts, $\text{M}(\text{OCP})$ ^{12,16} ($n = 1$: $\text{M} = \text{Li}, \text{Na}, \text{K}, \text{Cs}$), is the simplest stable compound isolated, containing an unsaturated phosphorus-carbon bond. This anion is best described as a superposition of the resonance structures **1a** (phosphaethynolate), **1b** (phosphaketenide) (Scheme 3). According to Natural Resonance Theory (NRT) calculations **1a** and **1b** are the two predominant structures with **1a** of a slightly higher weight than **1b** in the electronic ground state of this anion.¹⁷⁻¹⁸



Scheme 3 Resonance structures of the phosphaethynolate anion

Beside these two resonance structures, though with a much smaller contribution, structure **1c** was found. **1c** is a donor-acceptor complex of a P^- ion and carbon monoxide. As a proof of this concept, it was demonstrated that the reaction of an imidazolium salt with $\text{Na}(\text{OCP})$ formed the adduct of the parent phosphinidene (P-H) with the corresponding N-heterocyclic carbene ($^{\text{DIPP}}\text{NHC}=\text{PH}$).¹⁹ The proposed mechanism for this reaction is that the parent phosphaketenide H-PCO is formed as intermediate, which delivers the PH fragment in a concerted reaction step under the elimination of CO (Scheme 4).



Scheme 4 Synthesis of $^{\text{DIPP}}\text{NHC}=\text{PH}$

1.2 PHOSPHININE

Almost at the same period of the discovery of phosphalkyne, another type of unsaturated phosphorous compounds, phosphinines, was also obtained as stable compound. 2,4,6-triphenylphosphinine was the first example of phosphinines obtained by Märkl²⁰ in 1966. The parent phosphinine (Scheme 3) was reported by Ashe III in 1971.²⁰⁻²¹ In phosphinine, the reactive P=C double bond were stabilized by incorporating the aromatic systems. This opened up an access to phosphorous systems with significantly different electronic and steric properties compared with classical ligands based on trivalent phosphorus.²²⁻²⁵



Scheme 3 2,4,6-triphenylphosphinine and the parent phosphinine

As planar and aromatic heterocycles, one of the methylene groups (CH) of benzene in phosphinines is replaced by an isoelectronic, low-coordinate, trivalent and formally sp^2 -hybridized phosphorus atom.²⁰⁻²¹ Additionally, phosphinines have an aromatic stability as high as 88% of benzene²⁶⁻²⁷ according to theoretical calculations of bond separation enthalpies. Although phosphinines are the analogue of pyridines, their electronic properties differ significantly. This was verified by photoelectron and electron transmission spectroscopy as well as by theoretical calculations.^{18,28-30} The molecular orbital (MO) diagram of the frontier orbitals of phosphinine and pyridine are shown in Figure 1. In phosphinine the HOMO⁻² (in red) has a high electron localization at the phosphorus atom and represents essentially the lone pair at the heteroatom; while in pyridine the HOMO (in red) represents the lone pair located at the nitrogen atom. In addition, the lone pair at the phosphorus occupies a more diffuse and less directional orbital than that at the nitrogen in pyridine. Furthermore, phosphinines have a LUMO (π^* -orbital) with a high electron localization at phosphorus. This enables the heterocycle to act as a π -acceptor ligand, once coordinating to the metal centre. Compared to phosphinine, the LUMO of pyridine occupies a higher energy level. Consequently, phosphinines are much better π -acceptor ligands, but less good σ -donors compared to pyridines. With these particular electronic properties, phosphinines

are attractive ligands for electron rich metal centers, and suitable precursors for the synthesis of stable radical anions and dianions.³¹⁻³³

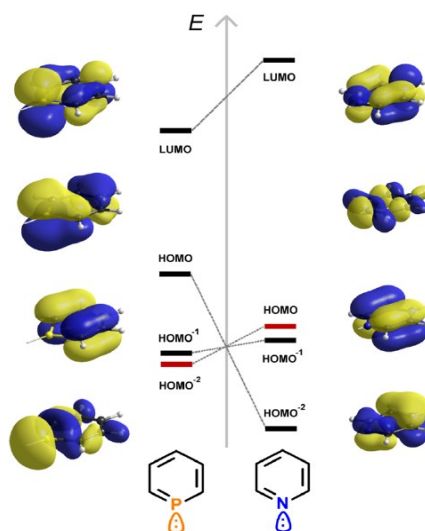


Figure 1. Qualitative MO diagram of the frontier orbitals of phosphinine and pyridine. The MOs representing the lone-pair are given in red.

Furthermore, the lone pair energy on phosphorus atom corresponding to the third highest occupied level of phosphinine is about -10.0 eV, which is higher than that of -10.6 eV for PH_3 . As a result, phosphinine is also of significant σ -donor capacity.^{25,34-35} With these two valuable electronic properties, phosphinine is believed to be an ideal alternative to carbon monoxide, which is by far probably the most important and versatile ligand in transition metal chemistry.³⁶⁻³⁷

To determine the aromaticity of a compound, nuclear magnetic resonance spectroscopy is one of the most popular methods. All peripheral protons in ^1H NMR spectrum of the phosphinine heterocycle are shifted to lower field similar to that of benzene. This can be attributed to the presence of a diamagnetic ring current.³⁸ In the ^{31}P NMR spectrum³⁹ a typical downfield shift of about $\delta = 180\text{--}200$ ppm is observed for phosphinines. Nucleus-independent chemical shift (NICS) values of phosphinines have led to the same conclusion.⁴⁰

1.3 COORDINATION MODES OF PHOSPHININE WITH TRANSITION METALS

There are two different ways for phosphinines to coordinate to a metal centre: via the lone pair of the phosphorus atom or via the aromatic π -system. Since the orbitals for σ -donation (HOMO⁻²) and π -donation (HOMO⁻¹, HOMO) are close in energy, a range of coordination modes are possible (Figure 2).

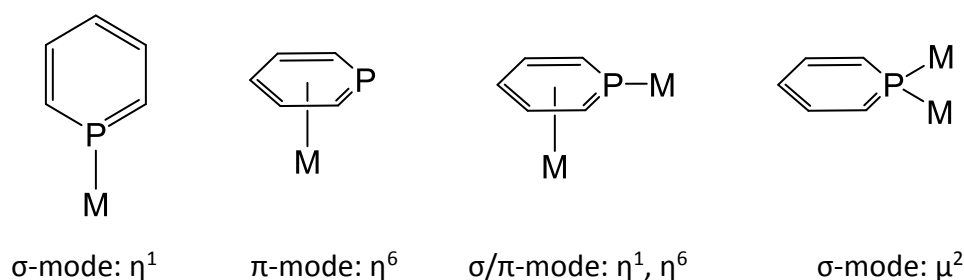


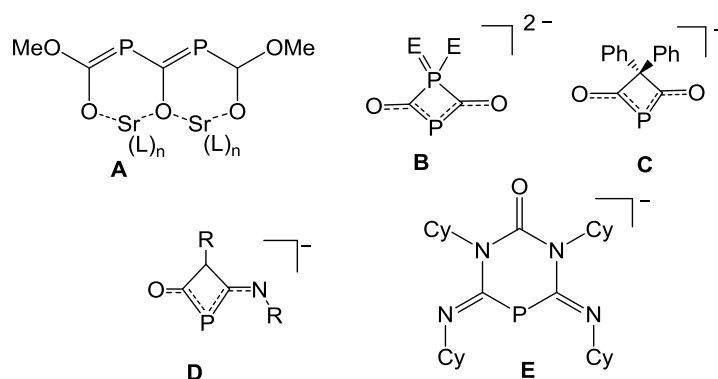
Figure 2. The most common coordination modes of phosphinines

The η^6 -binding mode (via the π -electrons) is typically observed with early transition metals in higher oxidation states in order to compensate for the electron deficiency of the metal centre (Figure 2). Vanadium (0) and titanium (0) complexes have been reported as the type $[\eta^6\text{-LM}(\text{CO})_3]$ (M: Cr, Mo, W; L: phosphinines) with additional π -acceptor ligands.⁴¹⁻⁴³ The coordination mode also depends on the substitutions, especially on the 2- and 6- positions of the phosphorus heterocycle. When substituents become increasingly bulky, such as *t*Bu- or Me₃Si- groups, steric effects may cause the coordination mode to change from η^1 to η^6 or might completely prevent coordination to the metal centre.⁴⁴⁻⁴⁵ Transition metals in-between early and late tend to exhibit mixed η^1 - η^6 binding, such as manganese, where the phosphinine behaves as an $8e^-$ donor.⁴⁶ The η^1 - coordination (via the lone pair) of phosphinines is the most common mode and generally observed for the late transition metals in low oxidation states due to the strong π -acceptor properties of the phosphinine ligand. Breit et al. reported on the Rh(I) complex $[\text{Rh}(\text{L})(\text{CO})\text{Cl}]$ (L: phosphinines), and Elschenbroich et al. described the homoleptic phosphinine complexes of the type $[\text{Ni}(\eta^1\text{-C}_5\text{H}_5\text{P})_4]$ and $[\text{Fe}(\eta^1\text{-C}_5\text{H}_5\text{P})_5]$.⁴⁷⁻⁴⁹ Compared with other late metals, it is surprising that the coordination chemistry of phosphinine with Cu(I) has been limited so far to only a few examples.⁵⁰⁻⁵²

1.4 OTHER PHOSPHORUS-CONTAINING HETEROCYCLES

Compared to nitrogen, oxygen or sulfur heterocycles, phosphorus heterocyclic chemistry cannot yet compete at such a level of complexity but, nevertheless, is undergoing very rapid development. A lot of the classic heterocycles (N, O, S) have already been applied in catalyst, drugs, dyes and numerous other materials.⁵³⁻⁵⁴ The phosphorus heterocycles are expected to be versatile, their potential applications are thus exciting. Few specialized fields of molecular chemistry present such a potential for growth and applications.

(OCP)⁻ anion with a carbon phosphorus triple bond is an ideal precursor for building new phosphorus heterocycles, however, the use of the (OCP)⁻ anion as building block for organophosphorus compounds has been scarcely exploited. Remarkably, while the alkali metal salts are rather stable and can be even briefly treated with water, the alkaline earth salts are unstable and must be kept at low temperature^{12,16}. For the strontium salt, the product of a dimerization reaction in presence of an excess of (MeO)₂CO to the [P₂C₃O₂(OMe)₂]²⁻ dianion **A** was observed (Scheme 4). In the reaction of Li(OCP) with sulphur or selenium the formation of the four-membered cycle **B** is suggested and recently Jupp and Goicoechea reported the heterocycles **C** and **D** as products from the reaction of K(OCP) with a ketene or a carbodiimide¹⁵. The reaction of Na(OCP) with carbodiimide formed a six-membered heterocycle (**E**), which was reported by Dr. Dominikus Heift from our group⁵⁵.



Scheme 7 Organophosphorus compounds **A – D** obtained with M(OCP).

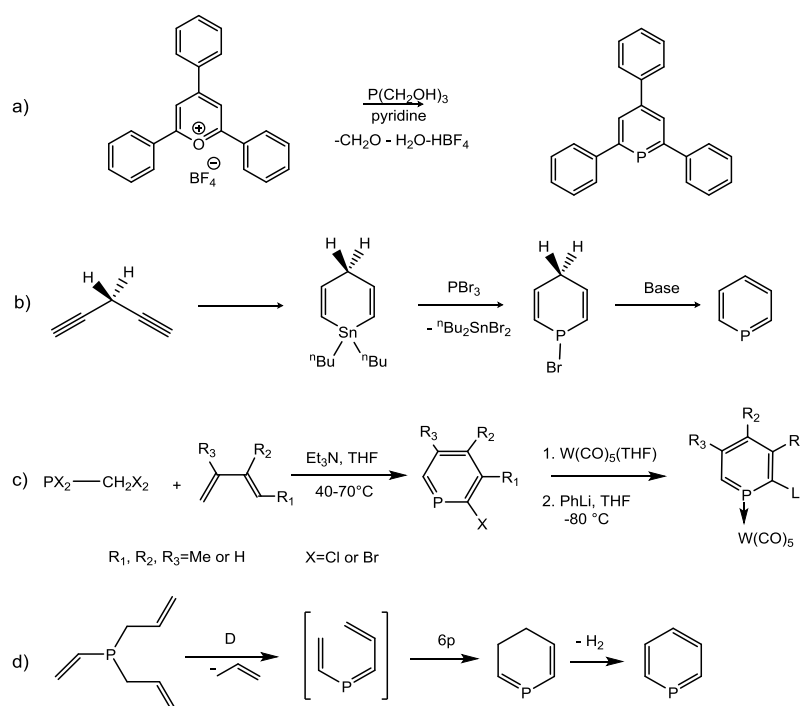
1.5 THESIS OBJECTIVE AND OUTLINE

To date, using sodium phosphoethynolate Na(OCP) as the building block, more and more phosphorus heterocycles have been synthesized and characterized in our group. Inspired by the broad studies of cycloaddition chemistry involving C-P triple bond in phosphoalkynes species, the reactivity of the (OCP)⁻ anion to similar substances was studied. Firstly, in the reaction of Na(OCP) and α -pyrone, the aimed compound sodium phosphinin-2-olate was obtained. As an anion, the phosphinin-2-olate can be facilely functionalized to produce new ligands with phosphinine rings. These ligands are worthily applicable in coordination chemistry, as phosphinines are widely considered as ideal electron stabilizing ligands. Secondly, the formation of heterocycles, based on Na(OCP) as the building block, were unpredictable. It is interesting to study all of these reactions and the properties of the heterocycle products. Last but not least, by replacing sodium cations for an organic substituent, a rather stable phosphaketene (R-PCO) was formed. The reactivity of the organic phosphaketene is comparable with Na(OCP) and also very attractive.

2 SYNTHESIS AND PROPERTY STUDIES OF 2-HYDROXYPHOSPHININE

2.1 INTRODUCTION

Phosphinines, the phosphorus analogue of pyridine, have been found to display good stability because of a significant aromatic character.⁵⁶⁻⁵⁸ Extensive studies have focused on the synthesis of phosphinines, but there is still a lack of convenient methods to obtain phosphinines. The first phosphinine, 2,4,6-triphenylphosphorine, was synthesized by Gottfried Märkl²⁰ in 1969 from the corresponding pyrylium salt and phosphorus sources, such as phosphine, $P(\text{SiMe}_3)_3$, $P(\text{CH}_2\text{OH})_3$ (Scheme 1a). This is still a typical procedure for synthesizing phosphinines widely used by the groups of Breit⁴⁷ and BASF.⁵⁹

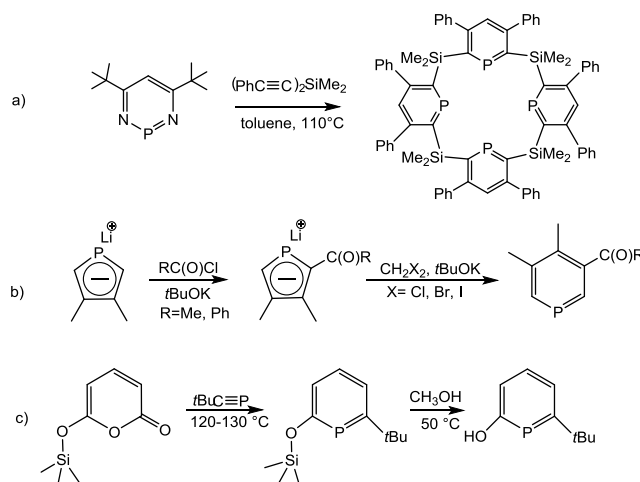


Scheme 1 a) Synthesis of the first phosphinine; b) Synthesis of the unsubstituted phosphorine; c) 2-halogen substituted phosphorines; d) Unsubstituted phosphorine synthesized from vinyl diallyl phosphine at high temperature.

About two years later, the unsubstituted phosphorine was reported by Arthur J. Ashe III as a distillable liquid that is somewhat air-sensitive but stable against hydrolysis (Scheme 1b).²¹

In 1990s, François Mathey developed a series of methods to synthesize phosphinines, such as 2-halogen⁶⁰⁻⁶¹ substituted phosphinines, from the reaction of dihalogenmethyl-dihalogenphosphine with conjugated dienes in the presence of triethylamine (Scheme 1c). Later, they also reported another method to generate unsubstituted phosphinine from thermolysis of vinylallylphosphine at 700°C and 10⁻³ Torr (Scheme 1d), as well as some other functionalized phosphinines using transition metal mediated reactions including palladium- or nickel-catalyzed coupling reactions.⁶²

Furthermore, in late 1990s Pascal Le Floch et. al. (Scheme 2a) reported⁶³⁻⁶⁴ the synthesis of polyphosphinine macrocycles, which consist of a 16 membered rings with four phosphorus atoms and a 12 membered ring with three phosphorus atoms, formed by cycloaddition of 1,3,2-diazaphosphinines with alkynes. Such polyphosphinine macrocycles have strong π -acceptor properties and are useful for stabilizing negative oxidation states and also useful for reductive catalysis. More recently, Mathey and Grundy⁶⁵ developed a new ring-expansion approach to synthesize a six-membered phosphinine ring in a one-pot method from a five-membered phosphole ring (Scheme 2b).



Scheme 2 a) Synthesis of the polyphosphinine macrocycles; b) Ring-expansion approach for synthesize phosphinine; c) Diels-Alder reaction between carbon phosphorus triple bond and pyrone.

In addition, there was one report on the Diels-Alder reaction of phosphoalkyne with cyclic 1,3-dienes to generate phosphinines by Märkl,⁶⁶ et.al. They reacted 2-tert-butylphosphoalkyne with α -pyrone (Scheme 2c). The reaction was performed at 120-130 °C and elevated pressures of 2-3

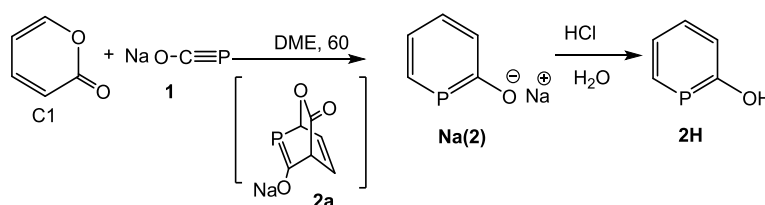
bar. The disadvantage of this method is that reacted phosphoethynes always require a bulky substituent in order to be stable.

All the efforts to obtain various compounds with phosphinine rings inspired us to use sodium (I) phosphocyanate (Na(OCP), **1**) in the form of the adduct [Na(OCP)(dioxane)_{2.5}] as the building block for constructing phosphinines. Na(OCP) is synthesized in a simple one-pot procedure from sodium, elemental phosphorus and ethylene carbonate; it is quite a stable compound and even survives for hours in air. So Na(OCP) is an economical chemical and can be easily handled as a starting material.

2.2 REACTION OF SODIUM PHOSPHACYANATE WITH α -PYRONE

2.2.1 Synthesis of sodium phosphinin-olate [Na(**2**)] and 2-hydroxyphosphinine (**2H**)

In the reaction of Na(OCP) with α -pyrone,⁶⁷ the proposed mechanism for the procedure goes via the unstable bicyclic intermediate formed through a [4+2] cycloaddition. However it could neither be observed nor isolated under the given reaction conditions. The final product, sodium phosphinin-2-olate [Na(**2**)], is then formed through a [4+2] cycloelimination of CO₂ (Scheme 3). Although the obtained structure of [Na(**2**)] cannot reveal the orientation of the nucleophilic attack of (OCP)⁻ to α -pyrone, the isomer resonance analysis of **1** suggested that the negative charge of (OCP)⁻ mainly located on the O–C side. That means the carbon atom in (OCP)⁻ prefers to attack the more electrophilic position (C1) in pyrone. As a result, **2a** is the proposed conformation of the intermediate in the reaction (Scheme 3).



Scheme 3 Synthesis of the sodium phosphinin-olate [Na(**2**)] and 2- hydroxyphosphinine (**2H**)

In solution, **2** shows a singlet in the ³¹P NMR spectrum at 151.6 ppm, which is a characteristic

value for phosphinines.⁶⁸ Additionally, the chemical shifts of the protons in the ^1H NMR are observed between 6.47 and 8.12 ppm within the typical range of 6.5 to 9.0 ppm for aromatic protons. Pale crystals of **2** were obtained in dimethoxyethane (DME) layered with n-hexane. The crystal structure was determined by single crystal X-ray diffraction. The unique unit in the crystal structure contains a distorted cubane core $[\text{Na}_4(\text{DME})_4(\mathbf{2})_4]$, which is formed by four sodium cations and four oxygen atoms from phosphinin-2-olate. The four phosphinine rings, located around the cubane core, can rotate freely. Each sodium cation is chelated by one DME solvent molecule at the same time. The bond lengths within the phosphinine rings and the ispo-C1-P1-C5 angle are comparable with the data available for the parent phosphinine PC_5H_5 (P-C1 1.76 Å, C1-C2 1.45 Å, C2-C3 1.38 Å, C3-C4 1.35 Å, C4-C5 1.40 Å, C1-O1 1.31 Å, C1-P1-C5 102°)⁶⁸, and indicate that **2** is aromatic.

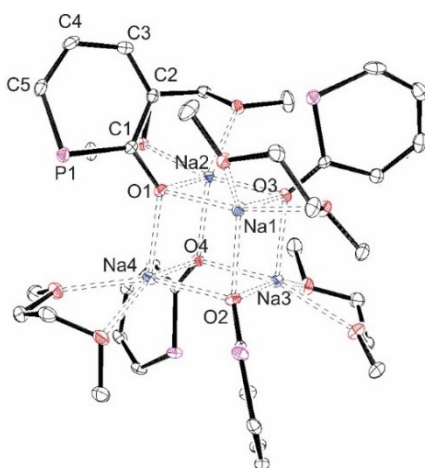


Figure 1. Crystal structure of $[\text{Na}(\text{DME})(\mathbf{2})]$. Ellipsoids are drawn at a 30 % probability level. Hydrogen atoms are omitted for clarity. Selected bond distances [Å] and angles [$^\circ$]: Na-O 2.3110~2.3560, P1-C1 1.761(2), P1-C5 1.713(3), C1-C2 1.451(5), C2-C3 1.387(5), C3-C4 1.355(4), C4-C5 1.402(1), C1-O1 1.315(2); C1-P1-C5 102.22(12), C2-C1-P1 119.7(2), C1-C2-C3 124.1(3), C4-C3-C2 124.0(1), C3-C4-C5 122.6(2), C4-C5-P1 126.9(2), O1-C1-C4 120.9(2), O1-C1-P1 119.39(16).

The crystals of **2** were observed to have a cubane structure when they were growing from DME/n-hexane solution. However, pale yellow crystals of the composition $[\{2-(\text{NaO})-(\text{PC}_5\text{H}_4)\} \times \{2-(\text{HO})-(\text{PC}_5\text{H}_4)\} \times (\text{dioxane})]$ $[2\text{Na} \times 2\text{H} \times (\text{dioxane})]$ were obtained when **2** was recrystallized from dioxane containing small amounts of water. In the crystal structure of $2\text{Na} \times 2\text{H} \times (\text{dioxane})$, the bond lengths in the ring and the C1-P1-C5 angle were also in the range of the data available for

the parent phosphinine PC_5H_5 . Furthermore, the value for the C2-O1 bond in $[\text{Na}_4(\text{DME})_4(\mathbf{2})_4]$ of 1.315(2) and the C5-O2 bond in $[\mathbf{2Na} \times \mathbf{2H} \times (\text{dioxane})]$ of 1.338(1) Å were both close to the typical C-O single bond length range in sodium phenolate of 1.32-1.34 Å ($\text{R}_2\text{C}=\text{O}$ 1.20-1.23 Å).⁶⁹⁻⁷⁰

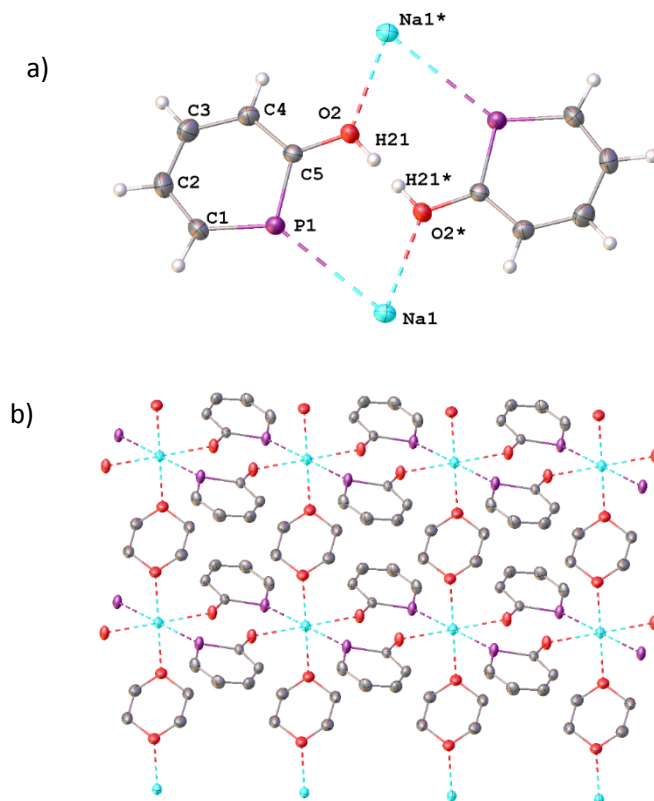
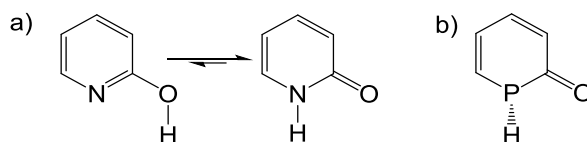


Figure 2 a) Structure of $[\{2-(\text{NaO})-(\text{PC}_5\text{H}_4)\} \times \{2-(\text{HO})-(\text{PC}_5\text{H}_4)\} \times (\text{dioxane})]$ $[\mathbf{2Na} \times \mathbf{2H} \times (\text{dioxane})]$. Ellipsoids are drawn at a 30% probability level. Dioxane molecules coordinated to Na are omitted for clarity. The bridging hydrogen atom H21 resides on two disordered positions on the $\text{O2} \cdots \text{O2}^*$ axis). Selected bond distances [Å] and angles [°]: P1-C1 1.732(1), P1-C5 1.758(1), C1-C2 1.374(2), C2-C3 1.394(2), C3-C4 1.382(1), C4-C5 1.402(1), C5-O2 1.338(1), P1-Na1 3.116(1), Na1-O2 2.384(1); C1-P1-C5 101.7(1), C2-C1-P1 126.0(1), C1-C2-C3 121.9(1), C4-C3-C2 124.0(1), C3-C4-C5 124.6(1), C4-C5-P1 121.9(1), O2-C5-C4 118.4(1), O2-C5-P1 119.7(1). b) Packing diagram of **2** in solid state. Hydrogen atoms are omitted for clarity.

After the reaction with HCl, **2** was converted to 2-hydroxyphosphinine (**2H**) and isolated as yellowish oil (Scheme 3). **2H** is an analogue of 2-hydroxypyridine. It is well known that 2-hydroxypyridine will tautomerize to 2-pyridone easily in solution or in the solid state (Scheme 4a).⁷¹ Furthermore, 2-pyridone is demonstrated to be the predominant form in solid state and in polar solvents.⁷¹

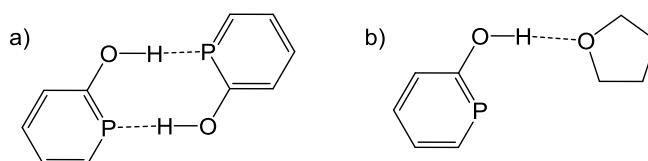


Scheme 4 a) Tautomerization between 2-hydroxypyridine and 2-pyridone; b) The calculated stable confirmation of 2-phosphapyridon

In 2007, Feng and co-workers⁷² reported theoretical calculations of 2-phosphapyridon (Scheme 4b) and pointed out that unlike 2-pyridone, the hydrogen on phosphorus in 2-phosphapyridon is not co-planar with the heterocycle. This means the heterocycle is anti-aromatic. Based on their reports, it will not be difficult to analyze whether tautomerization occurs in **2H** in solution by NMR analysis of **2H**. The ¹H NMR chemical shift for hydroxyl group is a singlet at 5.76 ppm in (deuterated chloroform) CDCl₃ and 9.50 ppm in (deuterated tetrahydrofuran) D₈-THF. The remaining peaks in ¹H NMR of **2H** are in the typical range of 6.5 to 9.0 ppm for aromatic protons.⁷³ Second, the ³¹P NMR chemical shift of **2H** appears at around 149 ppm in both apolar and polar solvents. This is close to the chemical shift for phosphinines.⁷⁴ Last but not least, the J_{PH} coupling constant of 42 Hz implies that there is no proton directly bonded to phosphorus, as the $^1J_{\text{PH}}$ coupling constant should be around 200 Hz.⁷⁵ The obtained coupling is the $^2J_{\text{PH}}$ to the proton on the adjacent carbon in accordance with the previous reports by Le Floch.⁷⁶ From our observations, we conclude that the protonation of **2** only leads to the formation of 2-hydroxyphosphinine, which does not undergo tautomerization in solution.

2.2.2 NMR Diffusion experiment of (2H)

In solution the dimeric form of 2-hydroxypyridine is present with two hydrogen bonds,⁷⁷ the ratio of dimerization is strongly dependent on the polarity of the solvent. The ratio is lower in polar solvent than in apolar solvents, because of the hydrophobic effects⁷⁸. It is worth to investigate whether the 4 ppm difference between the ¹H NMR chemical shifts of OH group for **2H** in CDCl₃ and in D₈-THF is due to the dimerization for **2H** in solutions (Scheme 5a).



Scheme 5 a) Dimeric form of **2H** and b) Hydrogen bonding between **2H** and THF

We carried out a ^1H diffusion NMR experiment,⁷⁹ which is an efficient method for studying the molecular dimensions in solution. Here, we aimed to determine the dimensions of compound **2H** in CDCl_3 and $\text{D}_8\text{-THF}$. From the modified Stokes-Einstein equation (1) shown below, the hydrodynamic size (r_H) can be calculated from the self-diffusion coefficient (D). Repetitions of the experiment with increasing gradient strengths (G) afford a set of signals from which the D can be calculated the linearized equation (Eq. 2).

$$D = k_B T / c \pi \eta r_H \quad \text{Eq. 1}$$

$$\ln(I/I_0) = -\gamma_X^2 \delta^2 \left(\Delta - \frac{\delta}{3} \right) D G^2 \quad \text{Eq. 2}$$

In Eq.1, k_B is the Boltzmann constant, T is the absolute temperature, c is the friction constant and η the solution viscosity. If the solute is considered to be a spherical particle the friction constant equals to 6.⁸⁰

γ_X in Eq.2 is the gyromagnetic ratio of the nucleus X, δ is the length of the gradient pulse, G is the gradient strength, Δ is the inter-gradient delay. The observed intensity changes, $\ln(I/I_0)$, would be a linear directly proportional to G^2 .⁸⁰

To determine the diffusion coefficients, the diffusion coefficient of HDO in D_2O was used as a reference ($D_{\text{HDO}} = 1.9 \times 10^{-9} \text{ m}^2 \cdot \text{s}^{-1}$),⁸¹ which means that the diffusion of HDO was detected at the same temperature, gradient pulse and inter-gradient delay as those for **2H**. The linear slopes of $\ln(I/I_0)$ to G^2 (see Figure 3) are labeled as m_x for diffusion molecular and m_{HDO} for HDO, so Eq. 3 was obtained.⁸⁰

$$\frac{m_x}{m_{\text{HDO}}} = \left(\frac{\gamma_x}{\gamma_{\text{HDO}}} \right)^2 \left(\frac{\delta_x}{\delta_{\text{HDO}}} \right)^2 \left(\frac{(\Delta - \pi/3)_x}{(\Delta - \pi/3)_{\text{HDO}}} \right) \left(\frac{D_x}{D_{\text{HDO}}} \right)$$

$$D_x = \frac{m_x * D_{\text{HDO}}}{m_{\text{HDO}}} \quad \text{Eq. 3}$$

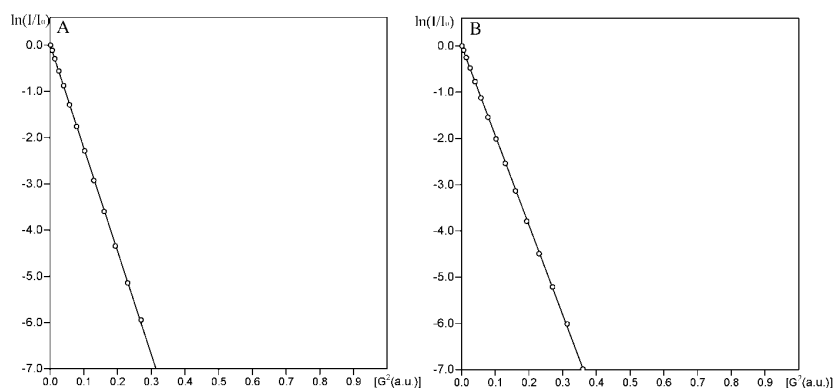


Figure 3. The Plot of the observed intensity changes, $\ln(I/I_0)$, to the gradient strengths G^2 for **2H** in CDCl_3 (A) and D^8 -THF(B)

From Eq.3, the self-diffusion coefficient was calculated (Table 1), the solvent viscosities ($10^{-3} \text{ kg s}^{-1} \text{ m}^{-1}$) used for the calculation of the hydrodynamic radii were $\eta(\text{CHCl}_3) = 0.53$, $\eta(\text{THF}) = 0.46$.⁸¹ The temperature for the experiment was $T = 298 \text{ K}$, according to Eq.1 the hydrodynamic radii r for **2H** is $2.145 \times 10^{-11} \text{ m}$ in CDCl_3 and $2.824 \times 10^{-11} \text{ m}$ in D^8 -THF, namely $r_2(\text{D}^8\text{-THF}) = 1.32 r_2(\text{CDCl}_3)$. The radii difference for **2H** in D^8 -THF and CDCl_3 is close to the dimension of one THF molecule. As a result, the proton chemical shift difference for the hydroxyl group in **2H** in CDCl_3 and THF is attributed to a hydrogen bond between **2H** and the oxygen center in THF.

Table 1 The diffusion coefficients of **2** in D^8 -THF and CDCl_3

	$D_x / \text{m}^2 \cdot \text{s}^{-1}$		Slope(exp.)
HDO	1.90×10^{-9}	ref	-0.002195587390
2 in D^8 -THF	1.68×10^{-9}		-0.001939131884
2 in CDCl_3	1.92×10^{-9}		-0.002216248562

2.2.3 The pK_a value of **2H**

The comparison of the UV-Vis spectra of **2** and the protonated form of **2H** showed that both absorption maxima of **2** and **2H** were well separated at 348 and 312nm respectively (Figure 4). When the spectra of **2** and **2H** were recorded in aqueous buffer solutions at different pH values, an isosbestic point was observed at 323 nm. This result indicated that only compounds **2** and **2H** were involved in the protonation equilibrium. The slope of the titration curve indicated that **2H** was a weak acid. These results enabled the evaluation of the pK_a value for **2** using the following

form of the Henderson-Hasselbalch equation.⁸²

$$\text{pK}_a = \text{pH} - \log[(A - A^0_{\text{H}})/(A^0_{\text{ion}} - A)]$$

A: Absorption of **2** at 346 nm at different pH values

A^0_{H} : Absorption of **2** at 346 nm at a pH value of 4.7.

A^0 : Absorption of **2** at 346 nm at a pH value of 10.38.

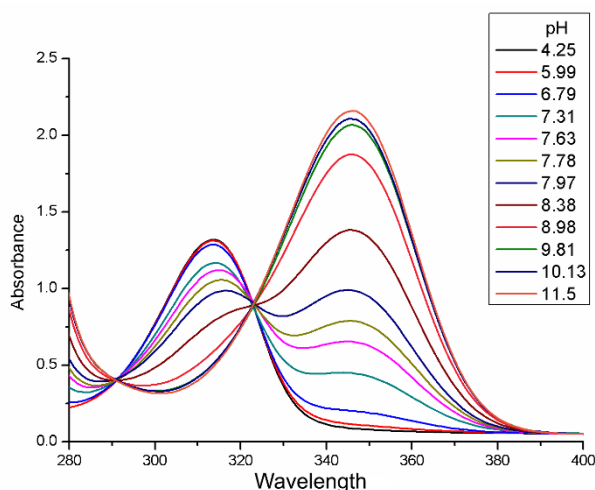


Figure 4 UV-vis spectra photometric titration of **2H** by measurement of **2H** in 0.18 mg pH adjusted ammonia / ammonium chloride (0.02 M) or acetic acid / sodium(I) acetate (0.02 M) buffer solutions.

Consequently, the pK_a was obtained through a linear regression where $\log[(A - A^0_{\text{H}})/(A^0_{\text{ion}} - A)]$ was plotted against the corresponding pH values.⁸³ Where the term $\log[(A - A^0_{\text{H}})/(A^0_{\text{ion}} - A)]$ in the linear regression became equal to zero, the pK_a value is equal to the pH value^[28]. The obtained pK_a value for **2H** was $\text{pK}_a = 8.16$. In comparison with the pK_a value in water for 2-hydroxy pyridine ($\text{pK}_a = 11.6^{84}$), **2H** is 2500 times more acidic.⁸⁵ Phosphinines are generally weak bases compared to their nitrogen hetero analogues, which is mostly due to the higher *s*-character of the phosphorus compared to the nitrogen lone pair.⁸³ In fact, calculations revealed an *s*-character of 65% for the phosphorus lone pair in phosphinine (PC_5H_5), whereas the *s*-character at the nitrogen lone pair in pyridine was only 29%.²⁵ In addition, phosphorus and carbon lie on a diagonal line in the periodic table, therefore, the pK_a value for **2H** ($\text{pK}_a = 8.16$) should be closer to the one for phenol ($\text{pK}_a = 9.99$) than to the one for 2-pyridone ($\text{pK}_a = 11.6^{84}$), which was indeed observed.

2.3 COMPUTATIONAL INVESTIGATIONS

2.3.1 DFT Calculation for 2H and 3

According to the NMR spectra, 2- hydroxyphosphinine **2H** behaves as a hetero-phenol without tautomerization. Computational studies of **2H** and its proposed tautomer, 2-phosphapyridon (**3**), also indicated **2H** is more stable than **3** by 17.07 kcal mol⁻¹ (Figure 5). The geometry optimization of the two compounds has been calculated using B3LYP level of theory with 6-311++G(2d,2p) basis set.

Table 2: The calculation results of NMR spectrum for **2** and its supposed tautomer **3** and the experimental data of **2** in CDCl₃.

		C1	C2	C3	C4	C5	P1	H1	H2	H3	H4	H(O)
2	Isotropi	19.04	58.98	46.26	52.54	20.8	127.1	24.1	24.1	24.1	22.9	26.3
	NMR	202.8	124.8	137.5	131.2	162.	171.4	7.7	7.7	7.7	8.9	5.6
3	Isotropi	33.18	48.70	36.39	48.88	32.4	317.4	25.4	24.4	24.8	24.5	25.9
	NMR	216.9	135.0	147.4	134.9	151.	-18.9	6.4	7.3	6.9	7.3	5.9
Experimental		188.7	121.6	132.5	127.9	153.	148.9	7.3	7.49	7.49	8.56	5.7

Compound **2H** has a stable planar aromatic conformation and is 17.07 kcal mol⁻¹ more stable than **3**. The energy gap is too large for facile conversion of **2H** to its supposed tautomer, while the tautomers of its nitrogen analogue are of similar energy with only 0.6 kcal mol⁻¹ difference in the gas phase. Additionally, the activation energy for tautomerization is 62.48 kcal mol⁻¹ at room temperature. With such a high energy barrier, even two compounds of similar enthalpy cannot convert to each other freely. Therefore, from the calculation results, the tautomerization between these two compounds is forbidden. Furthermore, as previously mentioned, the minimum energy conformation of 2-phosphapyridon (**3**) is not planar, the sum of bond angles for this tri-coordinated phosphorus is 303.9°. The hydrogen on phosphorus vibrates from one side of the ring to the other, the planar transition state is 11.21 kcal mol⁻¹ higher in energy than the energy minimum.

For comparing the results of NMR studies, the nucleus independent chemical shifts of 2-

hydroxyphosphinine and 2-phosphapyridon were calculated at the B3LYP/GIAO/6-311++G(2d,2p) level of theory. All the chemical shifts from calculation for 2- hydroxyphosphinine matched well with experimental results (Table 2). For instance, the ^{31}P NMR of **2H** and **3** were 171.4 and -18.9 ppm from calculation, while the experimental one was 151.5 ppm which was more close to 171.4 ppm. Therefore, the protonation of **2** formed **2H** unambiguously and the tautomerization between 2- hydroxyphosphinine and 2-phosphapyridon is forbidden according to our experimental and calculational results.

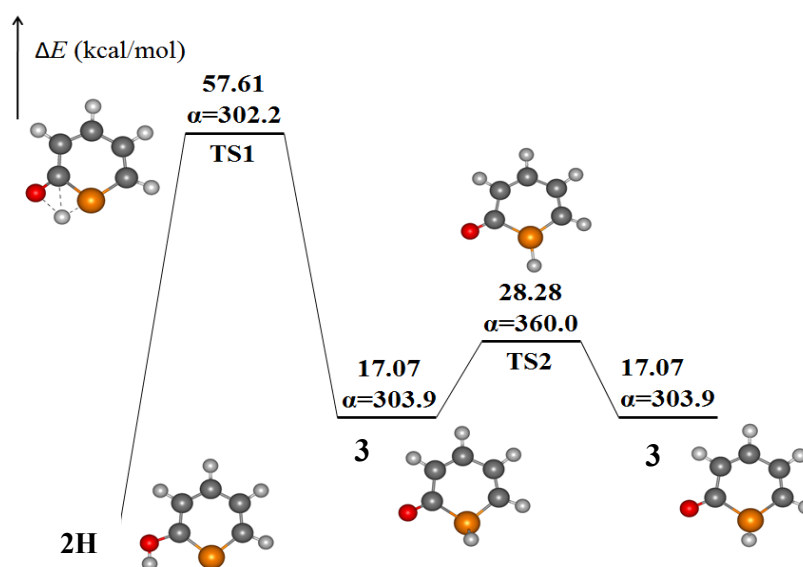


Figure.5 The calculated tautomerization process from **2H** to **3** (the analogue structure of 2- Pyridone); α : bond angles summed for tri-coordinate phosphorus atoms.

2.3.1 Aromaticity studies of **2**, **2H** and **3**

The nucleus-independent chemical shift (NICS)⁸⁶ is a computational method that calculates the chemical shift of a hypothetical lithium ion positioned directly inside or above the ring. This is a simple and efficient aromaticity criterion for a wide range of molecules. Aromaticity is defined by a negative NICS value (given in ppm), whereas anti-aromaticity by a positive value and nonaromaticity by a NICS value close to zero.⁸⁷⁻⁸⁸

In order to further confirm the aromaticities of the 2-phospha-phenolate ion and 2-hydroxyphosphinine, we calculated the NICS values of their geometric centers and 1 Å from the center normal to the plane using the GIAO-B3LP method with corresponding basis sets, which is

listed in Table 3. The NICS values of the two species are both negative, confirming their aromaticity. Relative to the NICS values of benzene at the same level of theory, the aromaticity percentages relative to benzene for **2** and **2H** are 25.1, 44.0% and 86.2, 94.0% for center and 1.0 Å above respectively. For further comparison, we also calculated the NICS value of phenolate ions and phenol at the same level of theory. Their NICS values are 49.1, 56.7 % and 114.2, 95.1% relative to benzene for center and 1.0 Å of phenolate ions and phenol respectively. Therefore, the phenolate ion is also less aromatic than phenol according to their calculated NICS values. Clearly, the NICS values of 2-phospha-phenolate ions and 2- hydroxyphosphinine are close to those of corresponding carbon analogues (typical aromatic compounds) especially at 1.0 Å above the rings. Compared to the NICS value -1.37 of 2-pyridone center reported before,⁷² 2-phospha-phenolate and 2-hydroxyphosphinine are more aromatic than the corresponding nitrogen analogues as expected.

Table 3 Calculated NICS values (in ppm) at the GIAO-B3LYP method

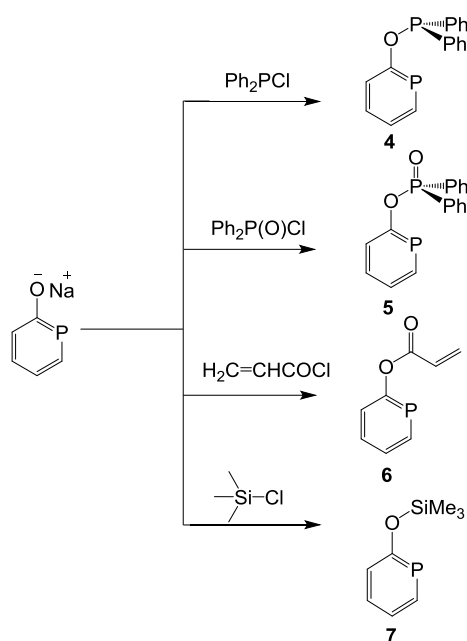
Species	B3LYP	
	NICS(0.0)	NICS(1.0)
2-phospha-phenolate	-1.903	-4.368
2- hydroxyphosphinine	-7.463	-8.878
Benzene	-7.575	-9.922
phenolate ions	-3.717	-5.634
phenol	-8.653	-9.440

2.4 THE REACTIVITY OF SODIUM PHOSPHININ-2-OLATE

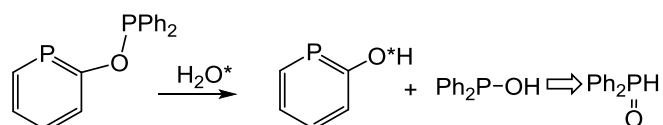
In general, phosphinin-2-olates can serve as nucleophiles in various reactions. To date, no synthesis of a phosphinine derivative using phosphinin-2-olate salts has been reported. It would be interesting to figure out which site (phosphorus or oxygen) on the phosphinin-2-olate anions the electrophiles will attack. Viewing the electronic analysis of sodium phosphinin-2-olate above, it can be expected that the phosphinin-2-olate salt will react similarly to the phenolate salt. Herein, a series of reactions of electrophilic compounds with phosphinin-2-olate forming new derivatives

(Scheme 6) are described.

All these electrophilic reactions were performed under mild conditions, in THF solution stirring at room temperature for 10 minutes. The ^{31}P NMR spectrum of **4** has two doublets located at 164 ppm and 114 ppm with P-P coupling constant of 97.5 Hz. Compound **5** also showed two doublets in ^{31}P NMR with chemical shifts of 177 ppm and 30 ppm with P-P Coupling of 10.9 Hz. Compound **4** decomposes when a trace of water is present (Scheme 7). The decomposition products are assigned to be the mixture of 2-hydroxyphosphinine and diphenylphosphine oxide according to the ^{31}P NMR spectrum. Compound **5** is stable in both water and air. In fact, the properties of both compounds were very similar to their respective phenol analogues ⁸⁹. The ^{31}P NMR spectra of **6** and **7** showed peaks at 183.4 and 168.9 ppm, which indicated the modification of **2** always occurring on the 2-oxy-position. Among these derivatives of sodium phosphinin-2-olate, only **5** is a white solid, while others are all isolated as colorless oil.



Scheme 6: Synthesis of the phosphinine derivatives, all reactions were carried out in THF solution and the sodium chloride (NaCl) precipitated from the solution.



Scheme 7 The decomposition of **4** in water

The single crystal X-ray analysis revealed that compound **5** crystallized in the monoclinic group $P2_1/n$ containing three aromatic rings, two phenyl substituents connected to phosphinoyl-P and one phosphinine ring. In the phosphinine ring, the bond distances are 1.740 and 1.746 Å for the bonds C5-P2 and C1-P2, respectively, which are typical distances for carbon phosphorus bonds phosphinines. The C-C distances in the phosphinine ring ranged from 1.374 to 1.383 Å, a little shorter than the C-C bonds of 1.39 Å in phenyl groups. Compared with the geometry parameters of sodium phosphinonate (**2**), the *ispo*-C1-P2-C5 angle of 98.56(16)° is smaller than the one in **2** (102.22(12)°), the C-C and C-P bond lengths of the heterocycle have a smaller range of values in **5**. Additionally, the C1-O2 distance is close to the single bond length with a value of 1.429(3) Å,⁷⁰ which is longer than the one in **2** (1.315(2) Å).

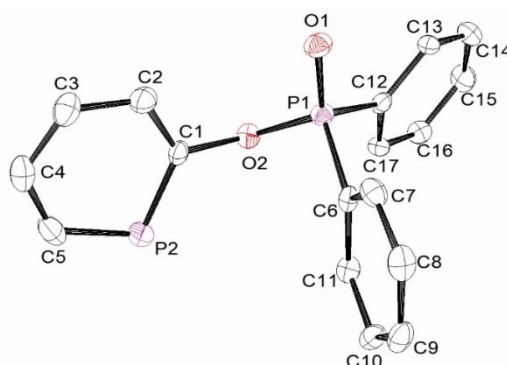


Figure 4 X-ray structure of compound **5**, ellipsoids are drawn at a 30 % probability level. The hydrogen atoms have omitted for clarity. Selected bond distances [Å] and angles [°]: P2-C1 1.746(3), P2-C5 1.740(4), C1-C2 1.383(4), C2-C3 1.396(5), C3-C4 1.385(5), C4-C5 1.389(5), P1-O1 1.484(2), P1-O2 1.621(5), C1-O2 1.429(3); C1-P2-C5 98.56(16), P2-C1-C2 126.6(2), C1-C2-C3 122.5(3), C2-C3-C4 122.9(3), C3-C4-C5 122.8(3), C4-C5-P2 126.5(3).

2.5 CONCLUSION

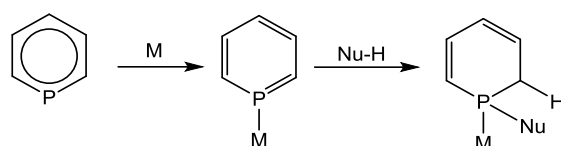
In summary, Na(OCP) is indeed a valuable building block, which can be obtained via a simple synthesis route. Sodium phosphinin-2-olate [Na(**2**)] was synthesized through Diels Alder reaction of Na(OCP) with α -pyrone under mild reaction condition. Na(**2**) is an air stable compound. The protonation of Na(**2**) with hydrochloric acid in water forms 2-hydroxyphosphinine (**2H**). It is experimentally and theoretically proven that **2H** does not tautomerize in solution. The UV-vis

spectra of Na(**2**) in various pH conditions revealed that **2H** is more acid than phenol with pKa value of 8.16. In addition, sodium phosphinin-2-olate is easily modified by reaction with electrophiles generating different functionalized derivatives. These are remarkable ligands for transition metals and to stabilize electron rich centers, as will be discussed in the following chapters.

3 THE COORDINATION STUDIES OF PHOSPHININE DERIVATIVES

3.1 INTRODUCTION

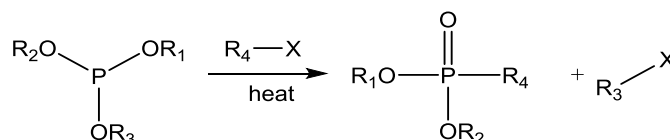
Soon after the discovery of phosphinines by Märkl,²⁰ research on the coordinating behavior of these heterocycles started and some classical complexes of metal carbonyls were reported. However, the lack of efficient synthetic approaches to functionalized derivatives hampered their use in coordination chemistry and catalysis. For a long time, the 2,4,6-triphenyl substituted phosphinine remained the most easily accessible derivative. As previously mentioned, there have been various advances in synthesis of phosphinine derivatives, which helped the development of phosphinine as a ligand in coordination chemistry.^{21,33,35,90}



Scheme 1 The aromaticity of the phosphinine ring decreases when coordinating to metal center (M) in a higher oxidation state

Heterocycles with sp^2 -hybridized phosphorus (III) in aromatic systems are significantly different to classical ligands based on trivalent phosphorus with respect to electronic, steric, coordination and reactivity properties.³² As discussed in the previous chapter, and in contrast to pyridines, phosphinine-based ligands are suitable for the stabilization of electron-rich metal centers due to the pronounced π -acceptor properties of the aromatic phosphorus heterocycle.^{31,91-93} On the other hand, the aromaticity of the phosphinine heterocycle is significantly disrupted upon coordination to metal centers especially those in higher oxidation states and with reduced π -back-donation capabilities (Scheme 1). Accordingly, the phosphinine core behaves like a cyclophosphahexatriene containing a highly reactive P=C double bond.⁹³ Recently, there have been several reports on nucleophilic attack at the phosphorus atom of phosphinine-based ligands in complexes.⁹⁴⁻⁹⁶

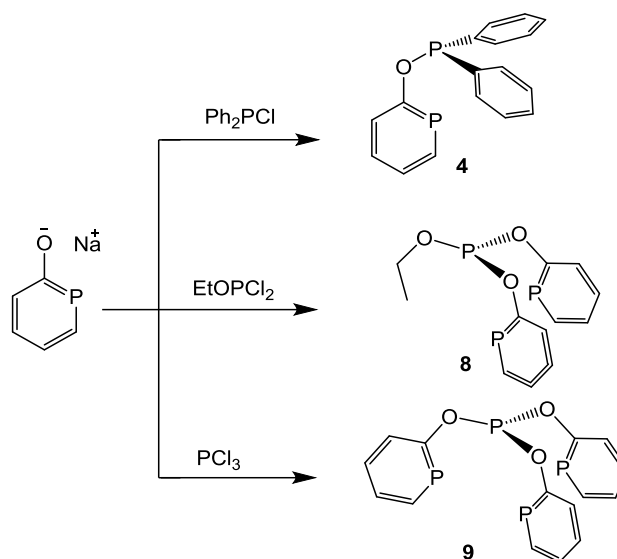
The Arbuzov reaction is well known for the alkyl phosphite among the organophosphorus chemists (Scheme 2).⁹⁷⁻⁹⁹ In the classical Arbuzov reaction, a nucleophilic X^- of the alkyl halide attacks the α -carbon of the phosphorus (III) ester, forming an organophosphorus (V) compound with alkyl transfer. As a prevalent ligand in transition metal chemistry, alkyl phosphites were considered relatively unreactive once coordinated to a metal center. However, some reports revealed that the dealkylation reaction can proceed with transition-metal-bonded phosphite ligands, leading ultimately to metal phosphonate complexes. Reactions involving transition-metal complexes are less predictable, occurring rapidly at room temperature for some compounds while not at all for others.¹⁰⁰ As a result, most complexes containing phosphonate ligands are not prepared by the Arbuzov-like dealkylation reaction.¹⁰¹⁻¹⁰⁴



Scheme 2 Arbuzov reactions (R1, R2, R3 and R4 are frequently alkyl or aryl groups, X is halide)

3.2 SYNTHESIS OF DERIVATIVES FOR PHOSPHININE

Since we can synthesize sodium phosphinin-2-olate¹⁰⁵ [Na(**2**)] through a convenient route, we were encouraged to do further research on such a stable phosphinine. As an alkali salt, it is easy to replace the sodium cations in Na(**2**) with electrophiles. The reaction between **2** and diphenylchlorophosphine has been described in chapter 2, forming bidentate ligand **4** (2-phosphininonate- diphenylphosphine, POP'). Similarly, 2 equivalents of **2** and ethyl dichlorophosphite¹⁰⁶ (Scheme 3) form ethyl diphosphininylphosphinite (**8**), and 3 equivalents of **2** and trichlorophosphite yield the tetra-dentate ligand **9** (triphosphininyl phosphite). All three of these ligands are colorless oils, compound **4** is very sensitive to water as described in chapter 2, while **8** and **9** are quite stable like normal phosphite compounds. In this chapter, the coordination properties of these ligands and reactivity of the obtained complexes are described.

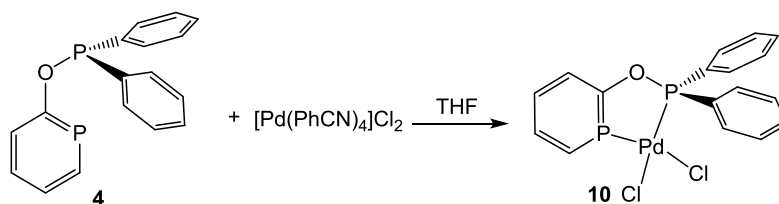


Scheme 3 Synthesis of the three ligands containing one, two or three phosphinines

3.3 Pd(II) COMPLEX OF 2-DIPHENYLPHOSPHINITE PHOSPHININE: SYNTHESIS, STRUCTURE, AND REACTIVITY

3.3.1 The coordination of ligand **4** to Pd(II)

The reaction between **4** and 1 equivalent of $[\text{PdCl}_2(\text{PhCN})_4]$ led to a yellow solution, with the corresponding Pd(II) complex, $[\text{PdCl}_2(\mathbf{4})]$, formed within several minutes and isolated as a bright-orange solid over 90% yield (Scheme 4).



Scheme 4 Reaction of **4** and $[\text{Pd}(\text{PhCN})_4\text{Cl}_2]$

Complex **10** was characterized in solution by NMR spectroscopy. The ^{31}P NMR spectrum of **10** shows two doublets at $\delta = 164.8$ and 156.8 ppm with $^3J_{\text{PP}}$ of 19.6 Hz. According to the $^{31}\text{P}\{^1\text{H}\}$ NMR, the signal at 164.8 ppm belongs to the P atom of the phosphinine ring with $^2J_{\text{PH}}$ of 20.2 Hz, which is in the expected region for phosphinine-metal complexes with a η^1 -coordination mode of

the phosphorus atom.⁹⁶ Orange crystals of **10** suitable for x-ray diffraction were obtained by slow diffusion of (diethyl ether) Et₂O into a diluted mixture of [PdCl₂(CH₃CN)₄] and **4** in dichloromethane (CH₂Cl₂).

Complex **10** crystallizes in the monoclinic space group P2₁/c and the asymmetric unit consists of one molecule of the metal complex. The structure of **10** is given in Figure 1 and selected bond lengths and angles are presented below the figure.

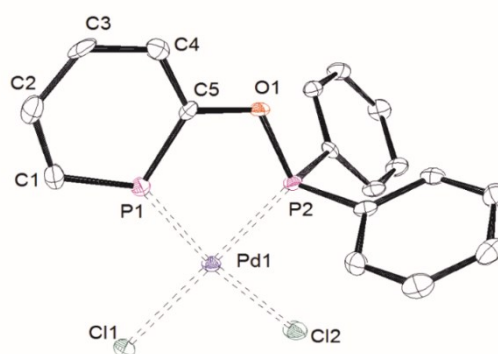


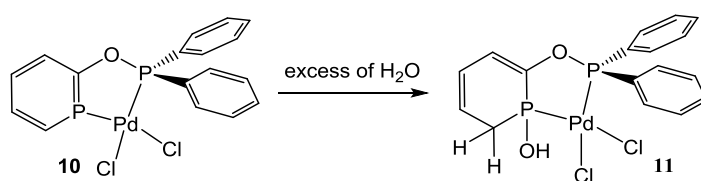
Figure 1 ORTEP drawing of the molecular structure of **10**. Thermal ellipsoids are drawn at 50% probability level. Non relevant hydrogen atoms have been removed for clarity. The values reported for selected bond distances and angles correspond to the average. Selected bond distances [Å] and angles [°]: Pd1-P1 2.1889(9), Pd1-P2 2.3919(9), Pd1-Cl1 2.3377(9), Pd1-Cl2 2.3227(8), P1-C1 1.701(3), P1-C5 1.715(3), C1-C2 1.391(5), C2-C3 1.395(5), C3-C4 1.382(5), C4-C5 1.381(4); P1-Pd1-P2 83.77(3), P1-Pd1-Cl1 93.55(3), P2-Pd1-Cl2 87.50(3), Cl1-Pd1-Cl2 94.97(3), C1-P1-C5 105.87(16), C2-C1-P1 120.3(3), C1-C2-C3 124.0(3), C4-C3-C2 125.4(3), C5-C4-C3 121.3(3).

The crystal structure confirms the spectroscopic data and reveals the mononuclear nature of the compounds with slightly distorted square-planar coordination geometries around the metal center. To form a strong bond with a Lewis acidic metal center the lone-pair at the phosphorus atom, having a high *s* character in the free ligand, must gain considerable *p* character upon coordination. This leads to an opening of the ispo-C-P-C angle, which is around 101.345°¹⁰⁷⁻¹⁰⁹ in free phosphinine. The higher the oxidation states of the metal centers, the more open the ispo-C-P-C angle is. This means the phosphinine heterocycle will be less aromatic. In fact, it was stated that for phosphinine, the preparation of complexes with transition-metal centers in higher oxidation states is difficult, with few examples reported in the literature of phosphinine-Pd(II) complexes.¹¹⁰ It is interesting to compare the <C-P-C angle in complex **10** with selected literature

data, since the \angle C-P-C angle is correlated with the electron accepting character of a metal fragment. In the Cr(0)¹¹¹ complex the opening of the \angle C-P-C angle is 104.4 and the Ru(II)⁹⁶ complex with \angle C-P-C angle of 103.7°. These compounds are very stable towards nucleophilic attack. In contrast, the Pd(II), Pt (II) complexes with angles of 107.3 and 107.6 ° are sensitive towards nucleophilic attack,¹¹⁰ which indicates the disruption of aromaticity upon coordination to a more electrophilic metal center. Here, we also expected our PdCl₂ fragments to have high Lewis acidities, which should be reflected in a large ispo-C-P-C angle. Indeed, we found a value of 105.87° in **10**, which is in between the angles reported for stable and unstable phosphinine complexes. As a result, it is worth studying the reactivity of complex **10** towards nucleophilic reagents.

3.3.2 Reactivity with water

Compound **10** reacted immediately when drops of water were added to the THF solution of complex **10** (Scheme 4). Upon concentrating the red solution, the product precipitated and was isolated as bright orange powder with 95% yield. The ³¹P NMR spectrum of [PdCl₂(**4H**•OH)] **11** shows two doublets at δ = 151.0, 82.1 ppm with a ³J_{PP} coupling constant of 50.65 Hz, which is bigger than the one in complex **10**. Coordination stabilizes the arylphosphine-PO bond in the ligand, while activating the CP double bond of the phosphinine.



Scheme 4. Reaction of [PdCl₂(**4**)] **10** and water

The crystal structure of **11** unambiguously shows that the H₂O molecule has been added to the P1=C1 double bond. The phosphorus atom shows a distorted tetrahedral geometry with a P1-C1 bond length of 1.785(7) Å and a P1-C5 distance of 1.797(5) Å, which reflects the sp² hybridization of C1 and the sp³ hybridization of C5. Moreover, the C-C bond distances in the phosphorus heterocycle are in agreement with a diene structure, with bond lengths for C1-C2 of 1.331, C2-C3

of 1.467, C3-C4 of 1.331, and C4-C5 of 1.499 Å. The P1-O1 distance of 1.585(5) Å is in the typical range of phosphinite–Pd complexes. The palladium center shows a slightly distorted square planar coordination geometry with a Cl1-Pd1-Cl2 angle of 96.77° and a bite angle P1-Pd1-P2 of 85.33°.

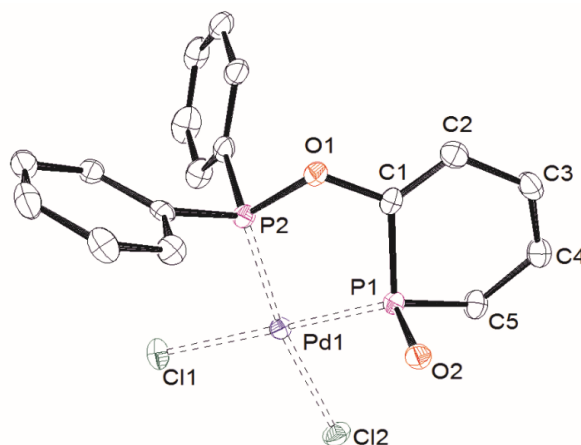


Figure 2 ORTEP drawing of the molecular structure of **11**. Thermal ellipsoids are drawn at 50% probability level. Non relevant hydrogen atoms have been removed for clarity. The values reported for selected bond distances and angles correspond to the average. Selected bond distances [Å] and angles [°]: Pd1-P1 2.1959(7), Pd1-P2 2.2120(8), Pd1-Cl1 2.3568(7), Pd1-Cl2 2.3826(7), P1-C1 1.797(3), P1-C5 1.785(3), P1-O1 1.5847(18), C1-C2 1.499(4), C2-C3 1.331(4), C3-C4 1.467(4), C4-C5 1.331(4); C5-P1-C1 101.43(15), C5-P1-O2 104.58(12), P1-C1-C2 123.5(2), C1-C2-C3 120.9(3), C2-C3-C4 124.5(3), C3-C4-C5 124.5(3), C4-C5-P1 113.1(2), P1-Pd1-P2 85.33(3), Cl1-Pd1-Cl2 96.77(3).

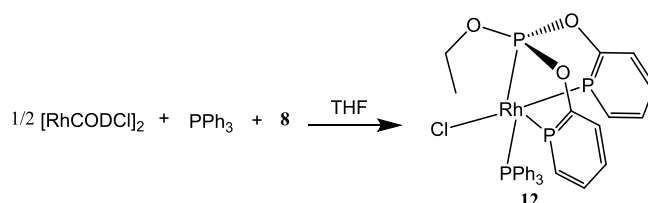
3.4 A NEW ETHYL DIPHOSPHININYLPHOSPHINITE CHELATED RHODIUM COMPLEX AND ITS

ARBUZOV-LIKE DEALKYLATION REACTIONS

A previous report referring to the Arbuzov-like reaction focused on a mono-coordinated phosphite ligand.¹¹²⁻¹¹⁴ Here the synthesis of a rhodium complex with ethyl diphosphininyolphosphinite as the chelating ligand will be discussed as well as its Arbuzov-like dealkylation reactions under different conditions.

3.4.1 Coordination of **8** to Rh(I)

The synthesis of complex $[\text{Rh}(\mathbf{8})(\text{PPh}_3)\text{Cl}]$ (**12**) is straightforward and proceeds with excellent yields. To a solution of $[\text{Rh}(\text{COD})\text{Cl}]_2$ in THF, 2 equivalents of triphenylphosphine and 2 equivalents of Diphosphinyl-ethyl phosphite (**8**) in THF were added sequentially. After 30 minutes stirring, the obtained orange precipitate was filtered, washed with THF and dried under vacuum. Crystals of $[\text{Rh}(\mathbf{8})(\text{PPh}_3)\text{Cl}]$ (**12**) were obtained by layering a CHCl_3 solution of the precipitate with n-hexane. (Scheme 5)



Scheme 5 Synthesis of complex **12**

The crystal structure of complex **12** is shown in Figure 3. The geometry about rhodium(I) is a distorted trigonal bipyramid. The phosphite-P and triphenylphosphine-P are coordinated in axial positions while the two phosphinine-P and one chloride are in equatorial position. The P3-Rh1-P4 angle is 175.438° and the P1-Rh1-P2 angle is 126.639° . The ^{31}P NMR spectrum of **12** indicated that in the solution, the triphenylphosphine remains trans to the phosphite-P with a $^2J_{\text{PP}}$ coupling constant of 516.38 Hz,¹¹⁵ which is a typical value for the $^2J_{\text{PP}}$ coupling through Rh(I) in a trans conformation. Complex **12** is quite stable in both the solid state and in solution, even with heating to 60°C , no Arbuzov-like reaction was observed. That means the bond between chloride and rhodium(I) is relatively strong, and will not dissociate in the solution under heating.¹⁰⁰

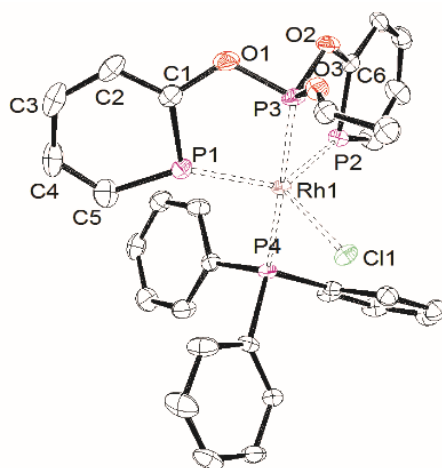
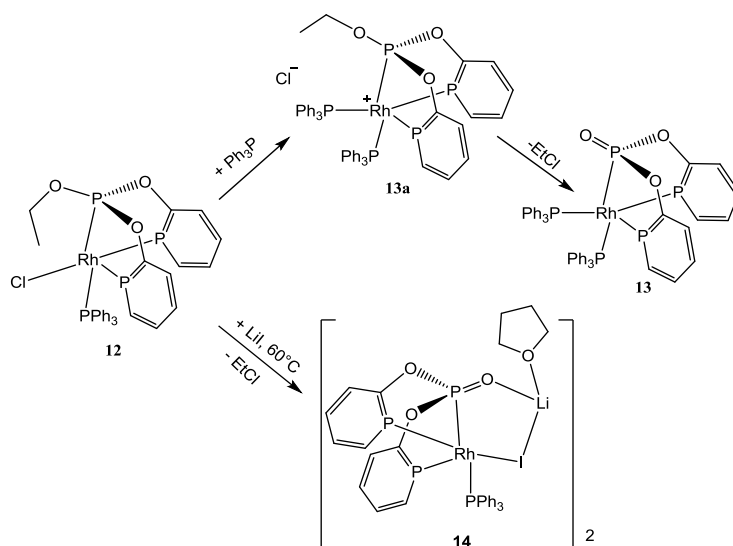


Figure 3 ORTEP drawing of the molecular structure of **12**. Thermal ellipsoids are drawn at 50% probability level. Non relevant hydrogen atoms and the solvent atoms have been removed for clarity. The values reported for selected bond distances and angles correspond to the average. Selected bond distances [Å] and angles [°]: Rh1-P1 2.2169(8), Rh1-P2 2.2360(8), Rh1-P3 2.2250(8), Rh1-P4 2.3423(7), Rh1-Cl1 2.5244(7), P1-C1 1.734(3), P1-C5 1.717(3), P3-O1 1.626(2), P3-O2 1.617(2), P3-O3 1.563(4). P3-Rh-P4 175.44, P3-Rh-Cl1 94.67, P3-Rh-P1 81.67, P3-Rh-P2 81.38, C5-P1-C1 101.13.

3.4.2 Arbuzov reaction of **12**

When adding another equivalent of triphenylphosphine to complex **12**, the phosphine will replace the chloride forming the intermediate **13a**. Once the chloride ion is released, it will attack the ethyl group on the phosphite and compound **13** will form at the end (Scheme 6).



Scheme 6 Synthesis of complexes **13** and **14**

The intermediate **13a** was observed via ^{31}P NMR spectroscopy immediately after addition of PPh_3 to **12** in CDCl_3 , while the dealkylation required above 5 hours. Kinetic studies of this reaction suggest the rate law for the dealkylation obeys first order reaction kinetics, $[\mathbf{13}] = Ae^{-kt}$ with $k = 0.00017 \text{ L mol}^{-1} \text{ s}^{-1}$, which is much slower than the one previously reported ($k_{\text{obs}} = 0.011$).¹¹⁶ In the crystal structure of **13**, the rhodium(I) resides in a distorted trigonal bipyramidal coordination sphere (Figure 4) created by five phosphorus atoms with Rh-P distances in range of 2.307 to 2.399 Å. Since the phosphite-P(III) converted to phosphonate-P(V) in complex **13**, the bond length for Rh-P should shorten, however because of steric effects, it lengthened from 2.225 to 2.307 Å. The structure is remained in solution. There are five separate multiplets in ^{31}P NMR spectrum for the five phosphorus atoms in **13**. The $^2J_{\text{PP}}$ for two phosphorus atoms in axial position (P3 and P4) decreases by 100 Hz compared with the value for **12**.

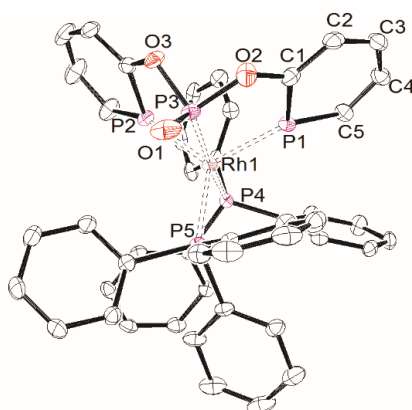


Figure 4 ORTEP drawing of the molecular structure of **13**. Thermal ellipsoids are drawn at 50% probability level. Non relevant hydrogen atoms and the solvent atoms have been removed for clarity. The values reported for selected bond distances and angles correspond to the average. Selected bond distances [Å] and angles [°]: Rh1-P1 2.2382(8), Rh1-P2 2.2275(8), Rh1-P3 2.3075(8), Rh1-P4 2.3301(7), Rh1-P5 2.3986(7), P1-C1 1.732(3), P1-C5 1.715(3), P3-O1 1.465(2), P3-O2 1.660(2), P3-O3 1.670(2). P3-Rh-P4 170.78(3), P3-Rh1-P5 89.80(3), P3-Rh1-P1 82.14(3), P3-Rh1-P2 81.39(3), C5-P1-C1 101.72(16).

Another way to promote the Arbuzov reaction for complex **12** is the addition of lithium iodide (LiI) to a suspension of **12** in THF. After heating the mixture to 60°C for 2 hours the suspension changes to a clear red solution. ^{31}P NMR spectroscopy reveals that a new complex **14** was formed. In the crystal structure, the iodide atom replaces the chloride coordinated to Rh1, the ethyl group on phosphite is eliminated as ethyl chloride and replaced by the lithium cation which coordinates to

iodide and the oxygen atom of the P=O unit. The coordination environment of Rh(I) is similar to that in complex **12**. That is, both the bond length and angles are close to those in **12**. In solution, the ^{31}P NMR chemical shift of the phosphonate-P, 170.7 ppm, differs to that of the phosphite-P, 205.49 ppm. However the splitting for all the chemical shifts were similar to those of **12** with the $^2J_{\text{PP}} = 476.4$ Hz of the two phosphorus atoms in axial position (P3, P4). We hope that compound **14** would release LiI in solution such that a lewis-basic P=O and lewis-acidic rhodium center is generated.¹¹⁷

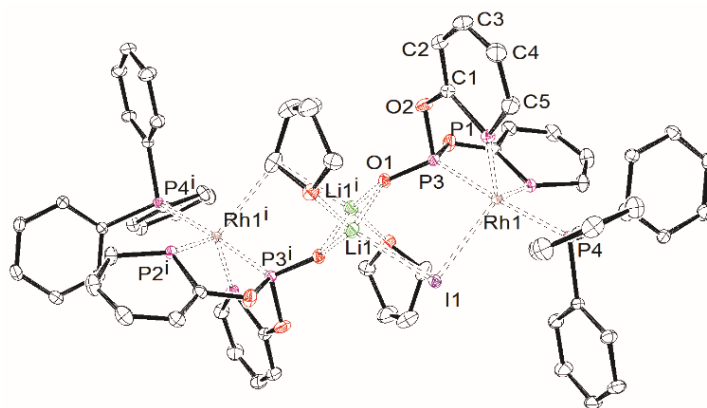
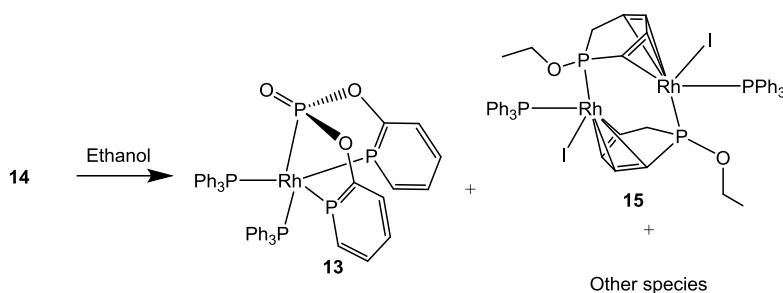


Figure 5 ORTEP drawing of the molecular structure of **14**. Thermal ellipsoids are drawn at 50% probability level. Non relevant hydrogen atoms have been removed for clarity. The values reported for selected bond distances and angles correspond to the average. Selected bond distances [Å] and angles [°]: Rh1-P1 2.2328(5), Rh1-P2 2.2057(4), Rh1-P3 2.2708(4), Rh1-P4 2.3426(4), Rh1-I1 2.83139(15), Li1-I1 2.742(3), Li1-O1 1.946(3), Li1'-O1 1.903(3), P1-C1 1.7415(18), P1-C5 1.713(2), P3-O1 1.5012(13). P3-Rh-P4 170.78, P3-Rh1-I1 92.421(11), P3-Rh1-P1 82.195(17), P3-Rh1-P2 81.434(16), C5-P1-C1 102.23(9).

Unfortunately, compound **14** is unreactive towards H_2 and decomposes in ethanol. When dissolving complex **14** in ethanol, a clear reddish solution forms initially, then, after a few seconds a yellow precipitate forms which was collected by filtration. The ^{31}P NMR of the filtrate revealed that complex **14** had decomposed, and several new species were formed in solution. The yellow precipitate was complex **13** according to ^{31}P NMR. Crystals of complex **15** were obtained from the reddish filtrate. The structure of **15** indicates that ligand **8** has been decomposed by ethanol.



Scheme 7 Decomposition of **14** in ethanol

The X-ray structure of complex **15** revealed that a dimeric Rhodium (I) complex. The phosphorus containing heterocycles serve as bridging ligands. As ^{31}P NMR spectroscopy contained very little information to indicate the identity of the other species, the process of forming this dimeric Rhodium(I) complex remains obscure.

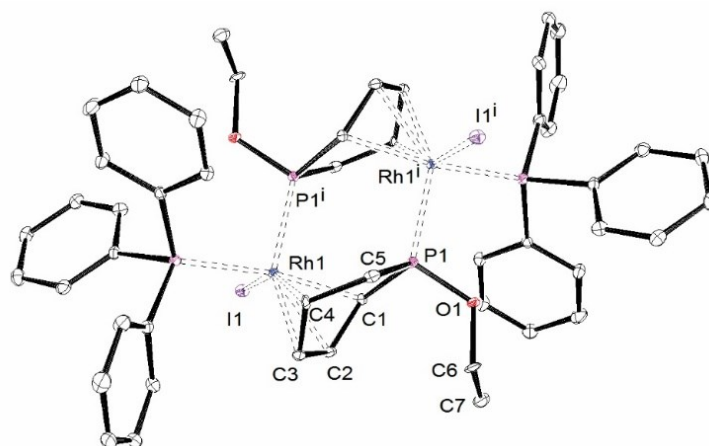
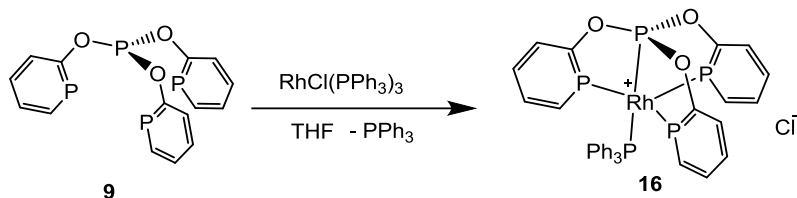


Figure 6 ORTEP drawing of the molecular structure of **15**. Thermal ellipsoids are drawn at 50% probability level. Non relevant hydrogen atoms have been removed for clarity. The values reported for selected bond distances and angles correspond to the average. Selected bond distances [\AA] and angles [$^\circ$]: Rh1-I1 2.7566(4), Rh1-P2 2.3179(10), Rh1-C 2.177(4), 2.157(4), 2.187(4), 2.131(4), Rh1-P1' 2.2769(4), P1-C1 1.797(4), P1-C5 1.834(4), P1-O1 1.615(3). P1-Rh-P2 97.41(4), P1'-Rh1-I1 92.91(3), C5-P1-C1 99.53(19).

3.5 SYNTHESIS OF RH COMPLEX 16

It has been demonstrated in one particular case that the phosphinine ligand is able to stabilize a 19-electron radical anion, which confirms the high π -acceptor capacity. Here we will introduce ligand **9**, containing three phosphinine heterocycles, which should have good properties for stabilizing metal centers in low oxidation state.[lit] To a solution of $\text{Rh}(\text{PPh}_3)_3\text{Cl}$ in THF, 1 equivalent of triphosphinyl phosphite (**9**) was added. After 30 minutes stirring, the obtained

orange-red precipitate was filtered, washed with THF and dried under vacuum. Crystals of $[\text{Rh}(\mathbf{9})(\text{PPh}_3)\text{Cl}]$ (**16**) were obtained by layering a (acetonitrile) CH_3CN solution of precipitate with n-hexane.



Scheme 8 Synthesis of complex **16**

There have been many examples of 4-coordinate, 16 electron Rh(I) complexes with trialkyl or triaryl phosphine ligands reported¹¹⁸, since the discovery of Wilkinson's catalyst, $\text{Rh}(\text{PPh}_3)_3\text{Cl}$. However, examples of 5 coordinate 18 electron complexes of Rh(I) with phosphorus ligands were rarely reported. Coordination of 5 phosphorus atoms leads to a crowded 18 electron Rh(I) complex, and usually Rh(I) complexes are sufficiently as 16 electron complexes.. The crystal structure of product **16** was determined and shows a trigonal bipyramidal conformation (Figure 7).

The rhodium (I) is located in the center of a distorted trigonal bipyramidal structure with phosphite-P and triphenylphosphine-P on the vertical axis combined with three phosphinine-P in the equatorial plane. The chloride anion is not coordinated to the Rh(I) center. The P3-Rh1-P5 angle is 179.561° and the average for the P-Rh-P angle on equatorial plane is 117.2° . The metal atom lies 0.356 \AA above the plane containing the three donor atoms from phosphinine rings. The distance for Rh-P5, 2.341 \AA , is in the normal range for rhodium(I) coordinated by trialkyl or triaryl phosphine ligands. The distances for Rh-P(Phosphinine) of $2.276\text{-}2.282 \text{ \AA}$ are shorter than classical rhodium(I) phosphine distances, which might be caused by the back donation effects between metal center to the phosphinine rings. The angles for $\langle\text{C-P-C}\rangle$ are between $101.9 - 102.1^\circ$. Therefore, the phosphinines in complex **16** are quite stable with respect to nucleophilic attack. Indeed, no reaction occurs when a few drops of water are added to the THF solution of **16**.

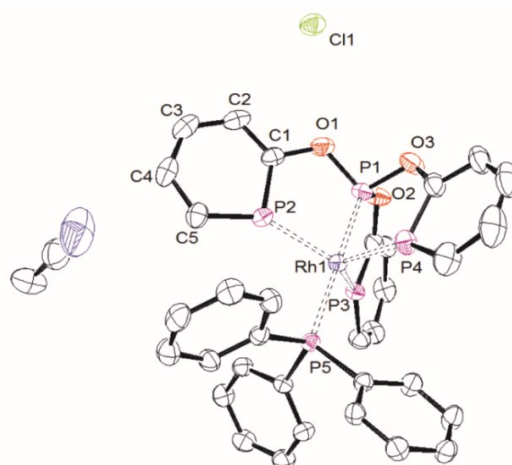


Figure 7 ORTEP drawing of the molecular structure of **16**. Thermal ellipsoids are drawn at 50% probability level. Non relevant hydrogen atoms have been removed for clarity. The values reported for selected bond distances and angles correspond to the average. Selected bond distances [Å] and angles [°]: Rh1-P1 2.1978(6), Rh1-P2 2.2736(6), Rh1-P3 2.2850(7), Rh1-P4 2.2829(7), Rh1-P5 2.3407(6). P1-Rh-P5 179.56(2), P2-Rh1-P3 116.00(2), P3-Rh1-P4 119.15(2), P2-Rh1-P4 117.66(3), C5-P2-C1 101.93(12).

3.6 CONCLUSION

This chapter described the synthesis of three ligands which contain one, two or three phosphinine rings for **4**, **9** and **10** respectively. The coordination of 2-phosphininonate-diphenylphosphine **4** to Pd(II) led to a more open ispo \angle C-P-C angle in phosphinine, which caused a decrease in both the aromaticity and stability of the phosphinine heterocycle. At the same time, the diphosphininylyl phosphite ligand and its rhodium (I) complex have been synthesized. To give the complexes **13** and **14**, complex **12** can undergoes Arbuzov-like reactions under certain conditions. Complex **14** is stabilized by coordination with one lithium iodide. An interesting challenge will consist of removing the lithium iodide to release the basic and acidic sites in the complex. As sad, complex **14** is unreactive with hydrogen gas and unstable in alcohol solvent. The coordination of ligand **9** (triphosphininylyl phosphite) to Rh(I) indicated the ability of **9** to chelate electron rich metal centers.

4 SYNTHESIS AND PHOTOLUMINESCENCE PROPERTIES OF PHOSPHININE–Cu(I) COMPLEXES

4.1 INTRODUCTION

MLCT (metal to ligand charge transfer) electronic transitions in coordination compounds are normally more intense than MC (metal-centered) ones since they do not have the same restrictions imposed by orbital symmetry; accordingly MLCT absorption bands exhibit relatively high molar extinction coefficients. As far as emission is concerned, when MLCT excited states are the lowest-lying, they are generally characterized by long lifetimes, and potentially intense luminescence. Complexes exhibiting long-lived MLCT excited states have been extensively investigated in the last decades, both for a better comprehension of fundamental phenomena¹¹⁹⁻¹²⁰ and for potential applications in solar light harvesting and conversion. The most attention has been devoted to Ru (II)¹²¹⁻¹²², Os (II)¹²³ and, more recently, Ir (III)¹²⁴ complexes, however, economic and environmental considerations make Cu (I)¹²⁵⁻¹²⁶ compounds interesting alternatives.

As discussed extensively in the literature, long-lived luminescent MLCT excited states of d⁶ metal complexes, in particular those of Ru (II)¹²¹, can be strongly affected by the proximity of energetically higher lying MC levels. The latter can be partially populated through thermal activation from the MLCT states and prompt non-radiative deactivation pathways and photochemical degradation. Closed shell d¹⁰ copper(I) complexes¹²⁷ will not suffer these kinds of problems. An orbital diagram illustrating the electronic transitions of Cu (I) complexes is reported in Figure 1.

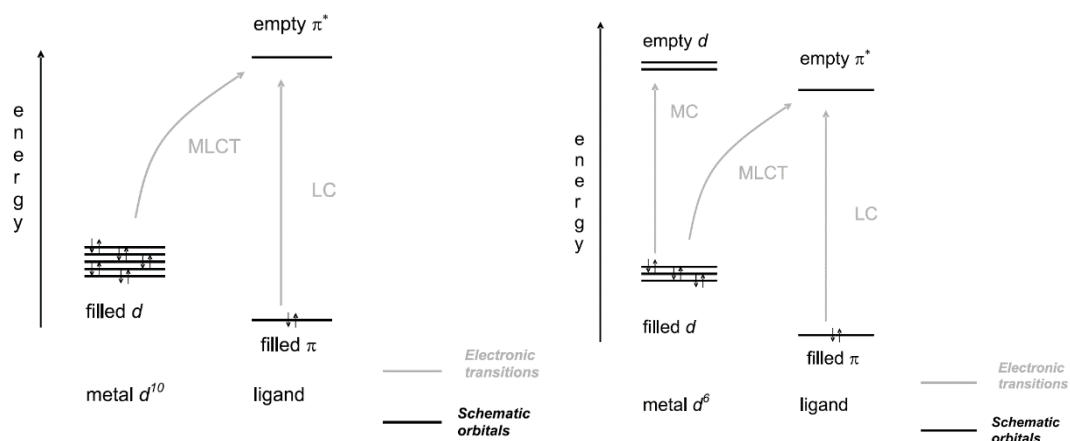
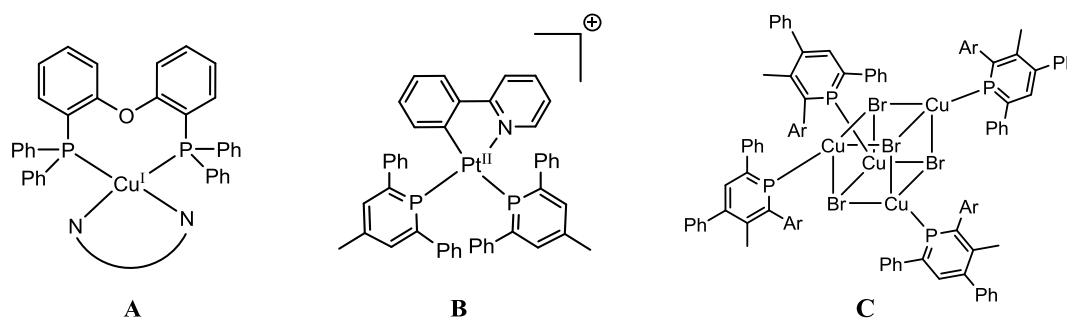


Figure 1 Qualitative comparison of orbitals and related electronic transitions in metal complexes having d^6 (e.g. Ru(II)) (right) and d^{10} (e.g. Cu(I)) (left) configurations

Because of these advantages of Cu (I), more and more phosphorescent and delayed-fluorescent tetrahedral Cu (I) complexes have been reported.¹²⁸⁻¹³¹ Most of these complexes were formed by a Cu (I) center and two bidentate ligands (Scheme 1 **A**) (bisimine and/or bisphosphine ligands).¹³²⁻¹³⁴

As we discussed in Chapter 1, due to both an inversion of the π and n -orbital sequence between phosphinine and pyridine and the presence of an energetically low-lying LUMO,^{29-30,40,96,135-136} phosphinines usually act as weak σ -donor but rather strong π -acceptor ligands, which can stabilize efficiently metal centers in low oxidation states.^{91,137} The fundamental organometallic chemistry of monodentate phosphinines as ligands for transition metals has been developed considerably,⁴⁷⁻⁴⁹ but other potential applications of the phosphinine moiety have been far less regarded and reported. Due to the increasing interest in phosphorus-containing π -conjugated molecular materials, the photophysical properties of some aryl-substituted phosphinines⁹¹ have been explored. These classes of compounds display readily observable phosphorescence in solution as well as the solid state. Inspired by these discoveries, the studies on phosphorescent properties of transition metals with coordinated phosphinines have attracted attention as well. Last year, there were two examples of a phosphinine-based complex reported which exhibit phosphorescence. The first example is a platinum (II) (Scheme 1 **B**) complex¹³⁸ with phosphinine as co-ligand reported by Hani Amouri, et. al. However, this complex only has detectable emission at low temperature (77 K). The other example is a $[\text{Cu}_4\text{Br}_4]$ cluster (Scheme 1 **C**)¹³⁹ containing

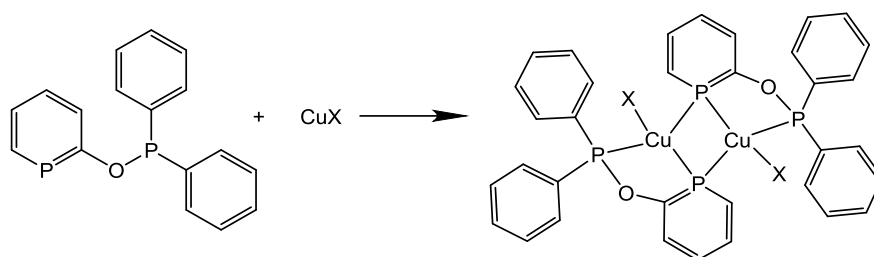
phosphinine moieties reported by the group of Christian Müller, which exhibited orange phosphorescence at low (77 K) and room temperature. In both of these complexes, the phosphinine ligands are aryl-substituted derivatives.¹³⁵ Such π -conjugated substitutions lead to significant fluorescent properties to the ligands. In order to reduce such effects caused by π -conjugated substituents, we developed a new phosphinine containing molecule sodium phosphinin-2-olate [Na(**2**)]¹⁰⁵ where no aryl substituents are present. In addition, due to the low cost and stable supply of copper metal, and the advantages of closed shell d^{10} copper (I) for OLED applications, phosphorescent and delayed/fluorescent tetrahedral copper (I) complexes have received increasing attention as dopants,¹³²⁻¹³⁴ over the past two decades.^{131,140-143} In this chapter, we describe the synthesis and photophysical properties of a series of Cu(I) halide complexes with the bidentate ligand 2-diphenylphosphinite phosphinine (**3**, POP') which contains one "classical" phosphine group, PR_2 , and one low-coordinate phosphorus donor center in the phosphinine moiety.



Scheme 1 The popular bisphosphine ligand (POP) in Cu(I) complexes (the anions are omitted here, **A**); the Pt(II) complex with phosphinine (the anions are omitted here, **B**) and phosphinine-Cu₄Br₄ cluster (**C**).

4.2 THE SYNTHESIS AND CHARACTERIZATION OF COPPER(I) COMPLEXES

When the bidentate ligand **4** was mixed with one equivalent of CuX (X=Cl (**17**), Br (**18**), I (**19**)) in THF (Scheme 2), a series of simple dimeric copper (I) complexes [Cu₂X₂(POP')₂] were formed. Single crystals of **17** – **19** suitable for X-ray analysis were grown from the THF solution via slow evaporation of the solvent.



Scheme 2 Synthesis of the dimeric copper complexes (X=Cl for **17**, Br=**18**, I for **19**)

Single crystal X-ray diffraction with crystals of **17** – **19** gave detailed insight into the structures of these compounds. All compounds have similar structures and only the structure of **18** is shown, as a representative, in Figure 2 (see the chapter 9 for the structures of **17** and **19**). Remarkably, the phosphorus center of the phosphinine ring bridges the two copper centers and the halide centers occupy terminal positions. Usually the halides are found in bridging positions in classical Cu(I) halide phosphine complexes such as **C**.^{139,144} The Cu...Cu bond distances are in the range of 2.655 – 2.694 Å, which are significantly shorter than the sum of the Van der Waals radii of Cu (2.8 Å)¹⁴⁵ and indicate copper–copper interactions.¹⁴⁶⁻¹⁴⁸ Each copper (I) center resides in a slightly distorted tetrahedral coordination sphere. Complexes with a phosphinine acting as a bridging μ^2 -P ligand are rare.¹⁴⁹⁻¹⁵⁴ In these reported examples, the inter-plane angles φ between the phosphinine ring and the M_2P plane is close to 90°. In complexes **17** – **19**, the inter-plane angle is reduced to $\varphi = 71.6^\circ - 75.8^\circ$ which possibly enhances the interaction between the Cu_2X_2 core with the π -system of the phosphinine ring.

The *ipso*-C-P-C angles in the phosphinine rings vary within a narrow range from 101.9 to 102.5°, which is very close to the corresponding angle in the uncoordinated phosphinine (101.345°).¹⁰⁷⁻¹⁰⁹ In agreement with previous studies, **17** – **19** are relatively stable in the presence of nucleophiles such as water and alcohols¹⁵⁵⁻¹⁵⁷ and can be handled in air, at least for short periods in the solid state.

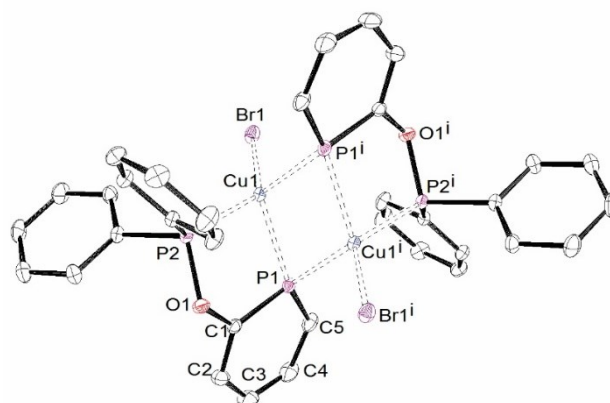
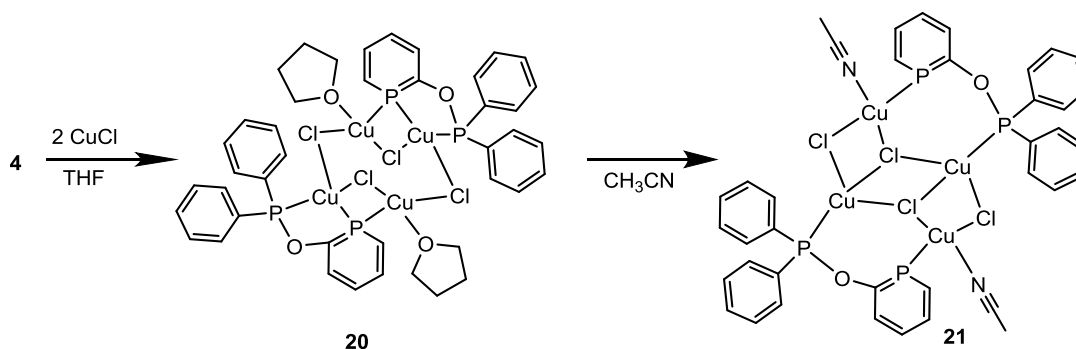


Figure 2. ORTEP drawing of the molecular structure of **18**. Thermal ellipsoids are drawn at 50% probability level. Non relevant hydrogen atoms have been removed for clarity. The values reported for selected bond distances and angles correspond to the average. Selected bond distances [Å] and angles [°]: Cu1-P1 2.3511(5), Cu1-P2 2.2440(5), Cu1-Br1 2.3346(3), P1-C1 1.7364(19), P1-C5 1.7153(19), C1-C2 1.378(3), C2-C3 1.393(3), C3-C4 1.393(3), C4-C5 1.387(3).

Additionally, the reaction between 2 equivalents of CuCl and **4** in THF afforded another complex **20** (Scheme 3), a $[\text{Cu}_4(\mu^2\text{-Cl})_2(\mu^2\text{-Cl})_2]$ cluster, comparable reactions did not take place with CuBr or CuI. Complex **20** rearranges when crystals are dissolved in acetonitrile, forming complex **21**, a $[\text{Cu}_4(\mu^3\text{-Cl})_2(\mu^2\text{-Cl})_2]$ cluster.



Scheme 3 Synthesis of the tetra copper complexes **20** and **21**

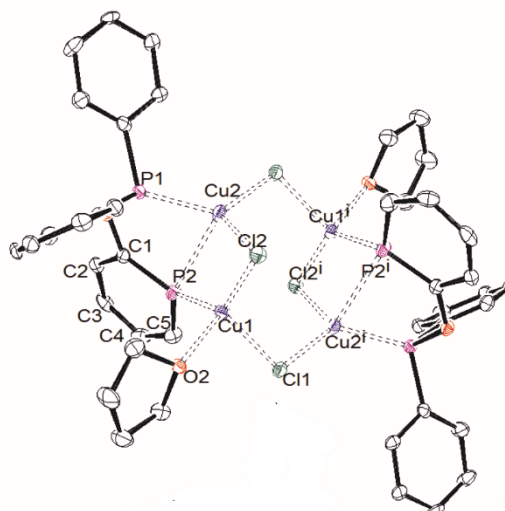


Figure 3. ORTEP drawing of the molecular structure of **20**. Thermal ellipsoids are drawn at 50% probability level. Non relevant hydrogen atoms have been removed for clarity. The values reported for selected bond distances and angles correspond to the average. Selected bond distances [Å] and angles [°]: Cu1-P1 2.3511(5), Cu1-P2 2.2440(5), Cu1-Cl1 2.3346(3), P1-C1 1.7364(19), P1-C5 1.7153(19), C1-C2 1.378(3), C2-C3 1.393(3), C3-C4 1.393(3), C4-C5 1.387(3).

The crystal structure of complex **20** (Figure 3) consists of a $[\text{Cu}_4(\mu^2\text{-Cl})_2(\mu^2\text{-Cl})_2]$ cluster formed by a centrosymmetric ring of alternating copper (I) and chloride ions. The four copper (I) and two chloride atoms (Cl2, Cl2') are almost coplanar. Outside the cluster, two molecules of ligand **4** act as bridges with $\eta^1\text{-P}$ of diphenylphosphine and $\mu^2\text{-P}$ of phosphinine. There are two different coordination geometries of copper(I), one (Cu1) displays a normal tetrahedral geometry with two bridging chloride atoms, one $\mu^2\text{-P}$ and one oxygen atom from THF as the vertex; the other (Cu2) is in a distorted tetrahedron bonded by $\eta^1\text{-P}$, $\mu^2\text{-P}$ and two bridging chloride atoms. The $\mu^2\text{-P}$ and $\mu^2\text{-Cl}$ bridged copper–copper distance of 2.594 Å is shorter than those in **17** – **19** which indicate that a stronger metal–metal interaction. The inter-plane angles φ between the phosphinine ring and the M_2P plane is small in complexes **17** – **19** ($\varphi = 71\text{-}76$). In **20**, the inter-plane angle is even smaller $\varphi = 52.6^\circ$ which favours interaction between the copper centers and the π -system of the phosphinine ring.

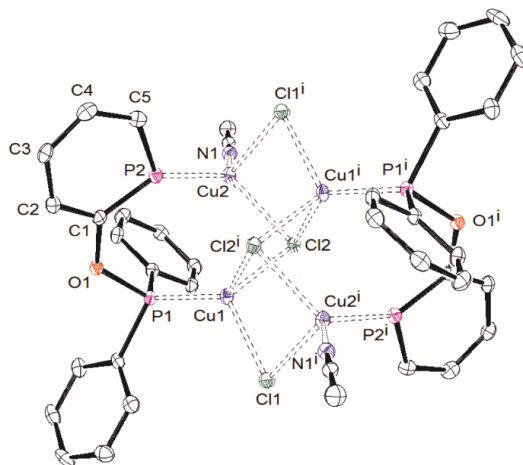


Figure 4. ORTEP drawing of the molecular structure of **21**. Thermal ellipsoids are drawn at 50% probability level. Non relevant hydrogen atoms have been removed for clarity. The values reported for selected bond distances and angles correspond to the average. Selected bond distances [Å] and angles [°]: Cu1-P1 2.3511(5), Cu1-P2 2.2440(5), Cu1-Br1 2.3346(3), P1-C1 1.7364(19), P1-C5 1.7153(19), C1-C2 1.378(3), C2-C3 1.393(3), C3-C4 1.393(3), C4-C5 1.387(3).

The μ^2 -P coordination mode for phosphinane in complex **20** rearranges to the η^1 -P mode forming complex **21** (Figure 4) upon exchange of the coordinated THF with acetonitrile.¹⁵⁸ The molecular structure of **21** consists of a $[\text{Cu}_4(\mu^2\text{-Cl})_2(\mu^3\text{-Cl})_2]$ core containing two ligands **4** and has crystallographically imposed centro-symmetry. The $[\text{Cu}_4(\mu^2\text{-Cl})_2(\mu^3\text{-Cl})_2]$ core shows a “stair-step” geometry with each of the 10 edges defined by a Cu-Cl bond. The Cu1 and Cu2 atoms both adopt distorted tetrahedral geometry coordination. The Cu-P distances are similar 2.195 and 2.189 Å, while the Cu-Cl bond lengths vary appreciably, ranging from 2.399 to 2.438. As expected, the Cu-Cl distances involving the triply bridging chlorine atoms (Cl1 and Cl1ⁱ) are longer than those to the doubly bridging chlorine atoms (Cl2 and Cl2ⁱ). The four copper atoms are exactly coplanar, with Cu...Cu distances Cu1...Cu2 = Cu1ⁱ...Cu2 = 3.276, and Cu1...Cu2ⁱ = 3.100. The Cl-Cu-Cl angles (Cl1-Cu1-Cl2 = 108.697 and Cl1-Cu2-Cl1ⁱ = 95.678) are larger than the Cu-Cl-Cu angles, which range from 75.94 (2) to 81.71 (3).¹⁵⁹⁻¹⁶⁰

4.3 THE LUMINESCENCE PROPERTIES

The absorption spectra of POP' (**4**) and the copper (I) complexes **17** – **21**, recorded as 10^{-5} M solution of dichloromethane (DCM), are shown in Figure 5a. The spectrum of uncoordinated **4** is

characterized by a broad absorption centered at $\lambda = 307$ nm ($\epsilon = 2860$ M⁻¹ cm⁻¹) which is close to the intense absorption at $\lambda = 300$ nm of simple aryl phosphines containing Ph₂P groups as in POP.¹⁶¹ The highest occupied molecular orbital (HOMO) in phosphinines is a π -type orbital delocalized over the heterocycle which is also valid for **4**. The second occupied orbital (HOMO-1) is constituted mainly from the non-bonding electron pairs on the two phosphorus atoms. Therefore, the absorption bands around 307 nm are assigned to overlapping $\pi \rightarrow \pi^*$ and $n(\text{P}) \rightarrow \pi^*$ transitions. The $\pi \rightarrow \pi^*$ excitations stem from the phosphinine ring or the phenyl groups of the PPh₂ group. The $n \rightarrow \pi^*$ transitions correspond to an excitation of an electron from the lone pair of electrons at the phosphinine phosphorus center into the π^* -orbitals of the phosphinine ring or from the free electron pair at the phosphorus atom of the PPh₂ group into the π^* orbitals of the phenyl rings.¹⁶²

The UV/Vis absorption spectra of complexes **17** – **19** show two broad bands in solution; a broad band with maxima at $\lambda = 325$ nm (**17**), $\lambda = 325$ nm (**18**), and $\lambda = 335$ nm (**19**) and in addition a shoulder at longer wavelengths, $\lambda_{\text{max}} = 382$ nm for **17** and $\lambda_{\text{max}} = 378$ nm for **18** and **19**. The broad absorption band observed in the range 320 – 340 nm is again assigned to overlapping $\pi \rightarrow \pi^*$ and $n(\text{P}) \rightarrow \pi^*$ transitions into which $n(\text{X}) \rightarrow \pi^*$ transitions involving the non-bonding pairs at the halogen centers are merged (X = Cl, Br, I). Because the π^* orbitals in phosphinines are lower in energy than those in the phenyl substituents, the absorptions we observed are red shifted compared to a previous report about the complexes of copper(I) with other POP type ligands containing only aryl phosphine moieties, R₂P.^[8a] The absorption spectra of complex **20** and **21** are broader than those of complexes **17** – **19**. The most intense absorptions are at $\lambda = 341$, 382 nm for **20** and **21**, respectively. The shoulders at $\lambda_{\text{max}} = 372$; 375 nm aside the maximum peaks are significantly more intense than those of **17** – **19**. In the solid state, complexes **17** – **19** show broad absorptions with a maximum at $\lambda = 412$ nm (**19**), $\lambda = 421$ nm (**18**), and $\lambda = 450$ nm (**17**) (see chapter 9).

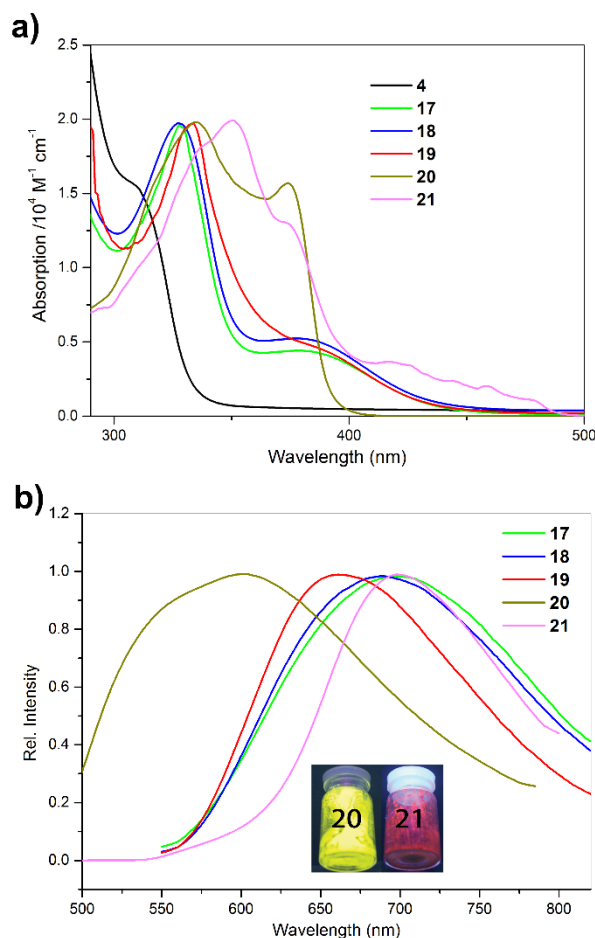


Figure 5. Absorption (a) in CH_2Cl_2 and corrected emission spectra (b) in solid state of POP' (black), **17** (purple), **18** (red), and **19** (green), **20** (yellow), **21** (blue). The inset shows the luminescence of **20** (yellow) and **21** (red) Under UV-irradiation.

The photoluminescent properties, at room temperature, of complexes **17** – **21** are presented in Figure 5b. Compound **4** as a pure liquid does not have an observable emission under UV light. However, all complexes show phosphorescence and emit red light. The phosphorescence lifetimes of the three complexes **17-19** were measured after laser excitation at 420 nm. The phosphorescence decay profiles are given in the SI, from which life times of 19.94 μs (**17**), 22.56 μs (**18**), and 25.07 μs (**19**) were calculated in the solid state. The longest wave emission maxima for **17** – **19** are at $\lambda_{\text{max}} = 700$, $\lambda_{\text{max}} = 688$, and $\lambda_{\text{max}} = 660$ nm, respectively, which translates into an increasing order of emission energies 1.771 eV (**17**) < 1.802 eV (**18**) < 1.878 eV (**19**). The ligand-field strength of the halogen ligands in **17** to **19** decreases in the order $\text{Cl}^- > \text{Br}^- > \text{I}^-$. Consequently, the metal centered HOMOs will be highest in energy for the Cu-Cl complex **17**, while the HOMOs of the Cu-I complex **19** will have the lowest energy. If we assume that emission occurs from a

triplet state, with the highest singly occupied orbital located in a phosphinine π^* -orbital, into a metal centered orbital, the ordering of the emission energies can be explained (little drawing). A comparable analysis has been made for series of copper halide complexes with a simple chelating diphosphenobenzene ligand, in which the halide anions occupy bridging positions between the copper centers.¹⁴⁴ Complex **20** emits yellow phosphorescence (λ_{max} 595 nm) under irradiation with UV light in the solid state. After the rearrangement of **20** in acetonitrile, the obtained complex **21** exhibits an intense red-shift luminescence (λ_{max} 704 nm). The difference between **20** and **21** can be explained by the cuprophilic interaction which occurs when $d_{\text{Cu-Cu}} < 2.8 \text{ \AA}$, which is absent in **21** (Figure 4; $d_{\text{Cu-Cu}} = 3.200 - 3.276 \text{ \AA}$). The average emission lifetime of **20** and **21** are 55.36 and 72.82 μs respectively, which is relatively long for copper(I) complexes.

4.4 DFT CALCULATIONS

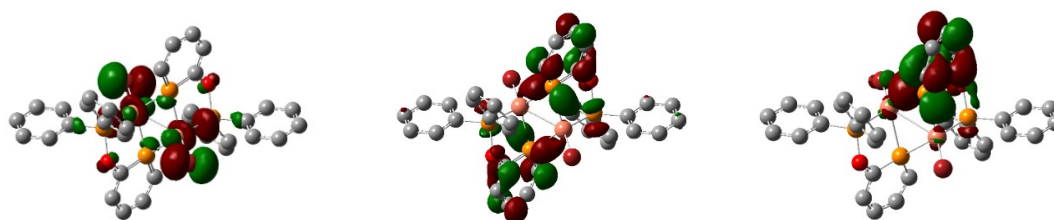


Figure 4. HOMO (left) and LUMO (middle) of the optimized ground state S_0 and the highest singly occupied orbital of the triplet state (right) of **18** (isovalue 0.035)

In order to gain further insight into the mechanism of the fluorescence of these dinuclear copper complexes, DFT calculations of complex **18** were carried out as a representative example. The DFT calculations at the level of PBE0/LANL2DZ show that the HOMO of **18** is indeed largely located on the copper and halogen centers with a small contribution of the Cu-P σ^* -orbitals (see left hand side of Figure 4). An analysis of the molecular orbital diagram of the ground state of **18** reveals that the HOMO to HOMO-7 orbitals are mainly Cu-Br located orbitals with large contributions of Br(p) orbitals. The LUMO to LUMO+5 orbitals are phosphinine centered (see middle of Figure 4). This result is consistent with previous studies that show phosphinines to be strong π -acceptor ligands with energetically low-lying LUMOs. Consequently, TD-DFT studies confirm the lowest energy absorption $S_0 \rightarrow S_1$ at λ 412 nm ($f = 0.0134$), the value of which is in agreement with the

experimental value of $\lambda = 421$ nm. The lowest excitation and subsequent 8 excitations between λ 412 and 305 nm are assigned to charge-transfer bands of XMLCT character, i.e., charge transfer from Cu and Br to the phosphinine ligand ($X = \text{Br}$, $M = \text{Cu}$). Similar observations and analyses were reported for other Cu(I) halide clusters for which the transitions of lowest energies were also assigned to XMLCT charge transfer bands.^{131,140-142,144} The computed highest singly occupied orbital of the triplet state is shown on the right side of Figure 4. The spin density of the unpaired electron is delocalized over one of the phosphinine ligands with a minor contribution of a copper and a bromine atom. Consequently, we assume that the phosphorescence $S_0 \leftarrow T_1$ in complexes **17** – **19** is best described by an electron relaxation from a π^* -orbital of the phosphinine into Cu-X located orbitals.

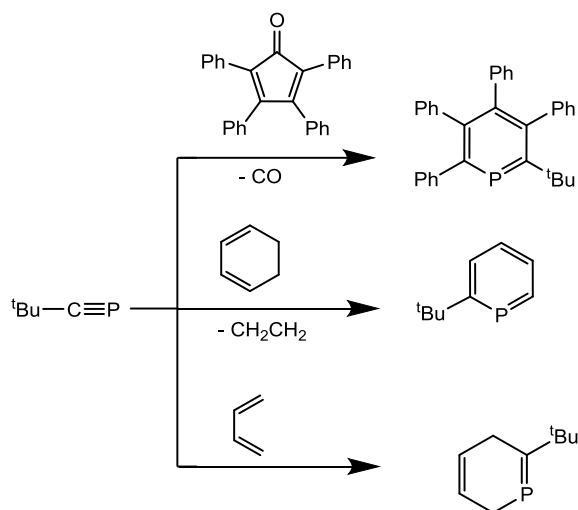
4.5 CONCLUSIONS

In conclusion, three examples of luminescent, dimeric $[\text{Cu}_2(\text{X})_2(\mu_2\text{-POP}')_2]$ complexes, **17**, **18**, and **19**, were obtained in good yields with $X = \text{Cl}$, Br , I and POP' a new chelating ligand with one “classical” diarylphosphino and one unsaturated π -conjugated phosphinine donor group. In these dimeric complexes, the phosphinine units occupy bridging positions and induce Cu-Cu interactions while the halogen centers are in terminal positions. Compounds **17** - **19** show red phosphorescence at room temperature with relatively long decay times. The wavelengths of the emissive bands is modulated by the halogen ligands whereby the strongest ligand (Cl) leads to the lowest emission energy (longest wavelength) and the weakest ligand (I) to the highest emission energy (shortest wave length). Although the complexes are structurally and electronically rather different, the same observation has been made with another series of Cu(I) halide complexes $[\text{Cu}_2(\mu_2\text{-X})_2(\text{dppb})_2]$ ($\text{dppb} = \text{diphenyl-phosphinobenzene}$).¹⁶³ Two examples of tetranuclear copper complexes **20** and **21** were synthesized in different solvents. This finding demonstrates that there are several possible structures for complexes formed between **4** and copper halides. Additionally, it remains to be investigated to what extent varying the substitution pattern of the phosphinine unit and exchange of the terminal halide centers in **17** – **19** allows tuning of the optical properties.

5 Na(OCP) AS PRECURSOR TO PHOSPHAKETENES AND VARIOUS PHOSPHORUS HETEROCYCLES

5.1 INTRODUCTION

In the [4+2] cycloaddition between Na(OCP) and α -pyrone, the (OCP)⁻ anions act as the typical carbon-phosphorus triple bond as in *t*BuCP (phosphaacetylene).¹⁶⁴⁻¹⁶⁵ *t*BuCP,¹⁶⁶⁻¹⁶⁸ it reacts with various dienes to form phosphorus containing heterocycles (Scheme 1). However, Na(OCP) is not as reactive as *t*BuCP and only with tetracyclone a reaction was observed. Through careful investigation of the reaction it was observed that, unlike the [4+2] cycloaddition of tetracyclone with *t*BuCP, there is no elimination of carbon monoxide during the reaction of tetracyclone with Na(OCP) even at the temperature of 80 °C. In this chapter, the investigation of the reactivity of Na(OCP) towards tetracyclone is presented. The heterocycles formed in this reaction are not the expected heterocycle.¹⁰⁵



Scheme 1 Reactivity of *t*BuCP with diene

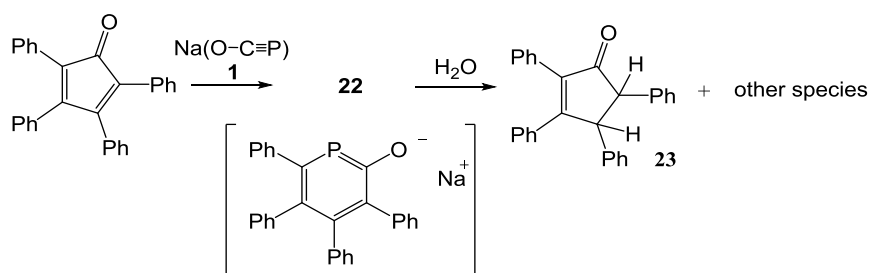
Not only does the reaction between Na(OCP) and tetracyclone form unprecedented products, but reactions with other reagents also yield unexpected results. Tetracyclone contains two functional groups. One is the unsaturated diene unit, and the other is the electrophilic carbonyl group. The

reaction of Na(OCP) towards acetylene reagents was also investigated. A new phosphinine heterocycle was formed by the reaction of Na(OCP) and the asymmetrical alkyne (ethyl phenylpropiolate, EtOCC≡CPh) as the only product of this reaction. The more electron-deficient alkyne (diethyl acetylenedicarboxylate, EtOCC≡CCOOEt) did not generate only the six-membered phosphinine ring but also the five-membered phospholide ring with the loss of CO.

5.2 THE REACTION OF Na(OCP) WITH TETRACYCLONE

5.2.1 Formation of phosphorus heterocycles

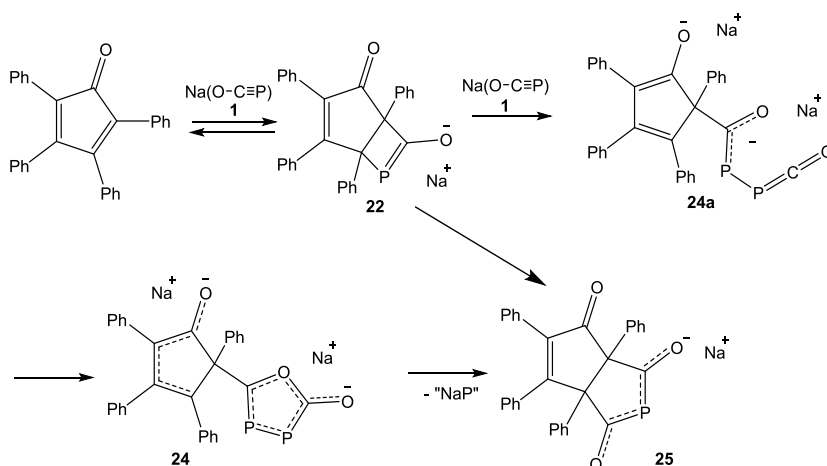
After the reaction of tetracyclone with Na(OCP), a signal in the ^{31}P NMR at 154.9 ppm is observed, which is close to the chemical shift for phosphinines. Initially, it was assumed that the reaction proceeds as [4+2] Diels Alder reaction with loss of one equivalent of carbon monoxide, forming product **22** as 2-hydroxy-3,4,5,6-tetraphenyl-phosphinine. However, product **22** was very sensitive to water and decomposes to 2,3-dihydratetracyclone (**23**),¹⁶⁹ as a white precipitate from aqueous solution. Other undefined species remains in solution with multiple signals in the ^{31}P NMR spectrum around 0 ppm. The formation of **23** revealed that only one double bond in the diene was attacked by (OCP)⁻ in the reaction between (OCP)⁻ and tetracyclone.



Scheme 2 The reaction between compound **22** and water.

The reaction between Na(OCP) and tetracyclone was studied carefully by varying the ratio between the two reagents. At room temperature, when adding more than 1 equivalent of Na(OCP) was added to tetracyclone, one singlet at 154.9 ppm and two doublets at 159.2 and -35.5 ppm were observed in the ^{31}P NMR spectrum. The two doublets belong to one compound

with a J_{PP} coupling constant of 361 Hz. The color of the reaction mixture in THF turned from deep red to orange after adding a second equivalent of Na(OCP). Only the two doublets remained in the ^{31}P NMR spectrum. After filtration, yellow crystals were obtained by leaving the filtrate undisturbed for 1 hour. The structure of the crystals was unequivocally identified as a disodium salt of the 1,3,4-oxadiphospholonide derivative **24** which is a new phosphorus heterocycle (see below for X-ray diffraction study). Compound **24** was not stable in solution; it slowly converted to compound **25** in 24 hours (Scheme 3). The new phosphorus containing compound **25** had a chemical shift at 66.5 ppm in the ^{31}P NMR spectrum. After work up, the sodium salt of the 2-phosphapentalene-1,3-dione derivative **25** was obtained in good yield as a pale yellow crystalline substance under extrusion of "NaP" from **24**. The crystal structure of **25** was determined by X-ray diffraction and NMR spectroscopy. These results confirm that only one double bond in tetracyclone reacts with $(\text{OCP})^-$.



Scheme 3. Synthesis of oxadiphospholonide **24** and 2-phosphapentalene-1,3-dione **25**.

As mentioned above, when Na(OCP) reacted with tetracyclone in a 1:1 ratio in THF, a clean reaction was observed within 10 minutes. In the ^{31}P NMR spectrum of compound **22** a singlet resonance at 154.9 ppm was observed.¹⁷⁰ This was assumed to be phosphinine. But **22** was not stable in solution and converted to **25** upon heating to 60 °C for 3 hours or stirring at room temperature for 12 hours. The structure of intermediate **22** is assumed to be a [2+2]-cyclo adduct as shown in Scheme 3. This proposition is bolstered by the low temperature, -40 °C, ^{13}C NMR spectrum. Three carbon atoms and one phosphorus atom form the [2+2] adduct, the chemical

shift at 225.5 ppm with $^1J_{CP} = 47.3$ Hz is assigned to the carbon from $(OCP)^-$ anion; while singlet at 78.9 ppm and doublet at 54.4 ppm with $^1J_{CP} = 16.1$ Hz are belonging to the carbons from cyclone. All the values for chemical shifts in ^{13}C NMR spectrum are reasonable for the structure of the intermediate **22**.

5.2.2 The crystal structures of **24** and **25**

In the crystal structure of **24**, two $(OCP)^-$ anions from $Na(OCP)$ form a five-membered heterocycle with two phosphorus atoms, two carbon atoms and one oxygen atom in the cycle. Such a heterocycle has never been observed before. The bond lengths of P1-P2, P1-C1 and P2-C2 are 2.15, 1.69, and 1.75 Å respectively. The P-P distance is between a typical single bond (2.23 Å) and double bond (2.03 Å). The C-P distances are in the range of C-P double bonds. The C1-O1 and C2-O1 bond lengths of 1.385 and 1.400 Å are in the range of C-O single bond distances, while the C2-O2 distance of 1.27 Å is close to a C-O double bond length. These structural parameters can be interpreted as the delocalization of electron density in the fragment C1-P1-P2-C2-O2. In the asymmetric unit, there are two sodium cations which are bridged by oxygen atoms (O2, O3') in a μ_2 mode. Generation of the complete unit cell shows that the complete molecule has the tetranuclear structure shown in Figure 1. There are two different coordination environments around the sodium atoms. The two sodium cations in the middle are located in tetrahedral environments coordinated by two oxygen atoms from the heterocycle, one oxygen atom from the tetracyclone and one oxygen atom from a THF molecule. The other two sodium cations are in square pyramidal geometry. The sodium cation is nearly coplanar with the equatorial plane in the tetragonal pyramid formed from one oxygen atom of the tetracyclone and three oxygen atoms from THF molecules. The axial position is occupied by one oxygen atom of the heterocycle. The P_2C_2O heterocycle is connected with the C_5 -ring of the cyclone ring through the C1-C4 bond. The C3-O3 in the carbonyl moiety of 1.29 Å is in between the typical C-O single bond (1.43) distance and carbonyl (C=O) bond length of 1.20 Å, indicating delocalization of the negative charge.

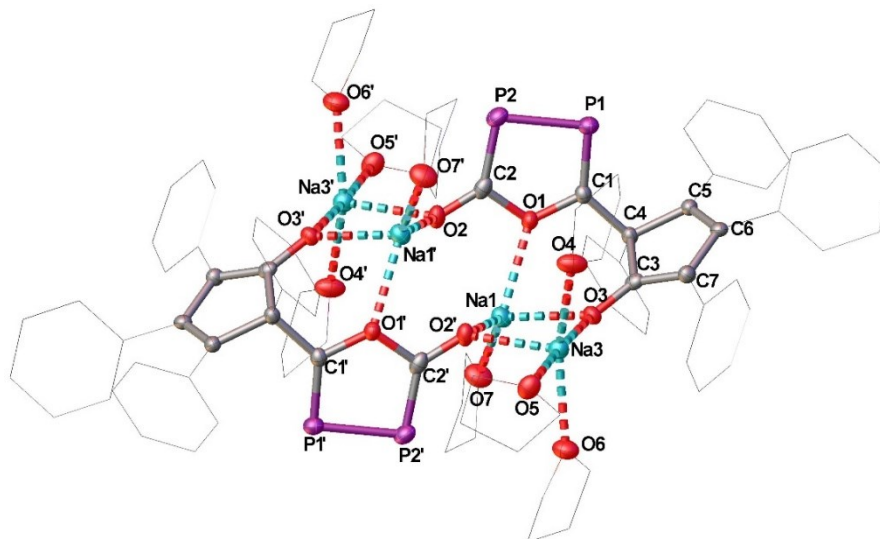


Figure 1 ORTEP plot (30% ellipsoid probability-except the THF solvent molecules) showing the X-ray structure of compound **24**. The hydrogen atoms and the phenyl groups have been omitted for clarity. P1–P2 2.1516(1), P1–C1 1.694(3), P2–C2 1.750(3), C1–O1 1.382(3), C2–O1 1.401(3), C2–O2 1.267(3), Na1–O 2.285(2)–2.791(2), Na1–Na3 3.347(2); P2–P1–C1 93.9(1), P1–C1–O1 119.2(2), C1–O1–C2 116.9(2), O1–C2–P2 116.6(2), C2–P2–P1 93.2(1).

Maroon crystals of compound **25** were crystallized from THF and n-hexane solution, which decomposes in the presence of water to dihydro- tetraphenylcyclopentadienone and phosphate salt. In Figure 2, the crystal structure of compound **25** is shown, which can be expanded to a chain structure. In the phosphorus heterocycle, which shares one edge with tetracyclone, two carbonyl moieties bind to the phosphorus atom. The C-P-C bond angle is approximately 90° . Usually $2\lambda^3$ phospho-1,3-dionates have two coordination modes¹⁷¹: either the metal is coordinated by the oxygen atoms or by the phosphorus atom. In the crystal structure of **25**, the carbonyl oxygen atoms coordinate to sodium. The P-C bond lengths of 1.78 Å and the C-O bond lengths of 1.22 Å are slightly different from those of the normal bond length for a P-C single bond (1.83 Å)¹⁷² and C-O double bond (1.20 Å). So the negative charge is not localized on an oxygen or phosphorus atom but is delocalized over the whole $2\lambda^3$ phospho-1,3-dionate part. The sodium cations are located in a pyramidal geometry and coordinated by five oxygen atoms. Two oxygen atoms from THF molecules and three from two separate phosphorus heterocycles. Furthermore, they are bridged by the heterocycles forming a polymer chain structure.¹⁶³

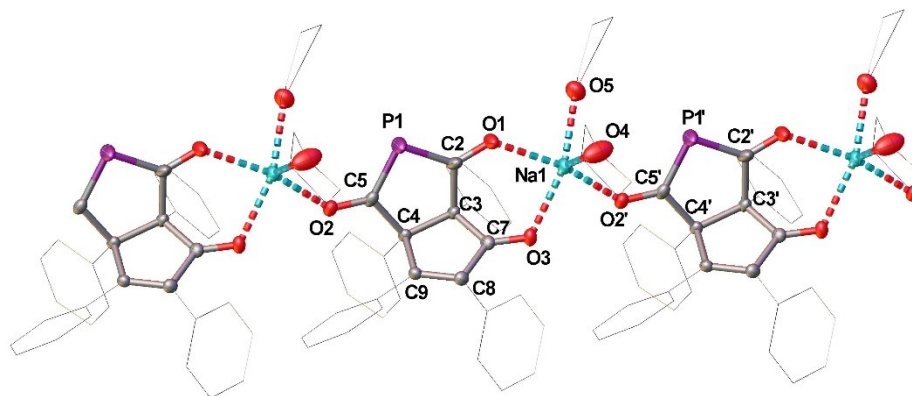


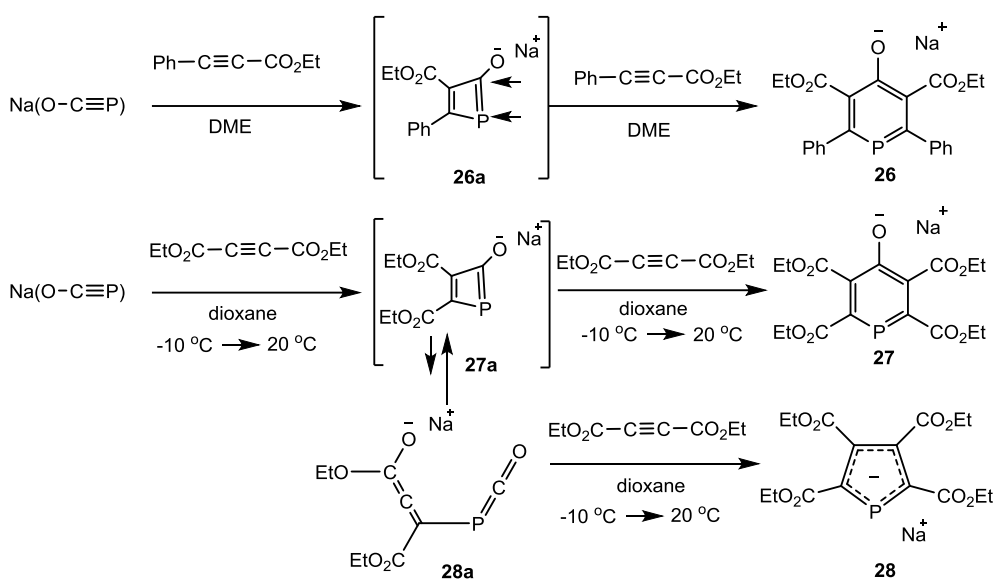
Figure 2 ORTEP plot (30% ellipsoid probability, except the THF solvent molecules) showing the X-ray structure of compound **24**. The hydrogen atoms have been omitted for clarity. c) P1–C2 1.783(4), P1–C5 1.783(4), C4–C5 1.554(5), C3–C4 1.553(5), C2–C3 1.576(5), O1–C2 1.224(4), C5–O2 1.220(4), Na1–O 2.295(3)–2.391(2); C5–P1–C2 92.4(2), C3–C2–P1 114.6(3), C4–C5–P1 114.6(2), O6–C2–P1 126.7(3), C3–C4–C5 109.6(3), C4–C3–C2 107.9(3).

5.3 SYNTHESIS OF PHOSPHININ-4-OLATE AND PHOSPHOLIDE

5.3.1 Reactions between Na(OCP) and acetylene

The reaction between Na(OCP) and tetracyclone inspired us to test other reagents with unsaturated CC bonds. It was found that acetylenes with one or two electrophilic substitutions (R-CC-CO₂Et, R = phenyl or CO₂Et) react with Na(OCP). In this case, six-membered heterocycles (phosphinine) are formed when the R is a phenyl group. However, when R is carboxyl group, the reaction will form five-member heterocycles (phospholide) as well as phosphinine (Scheme 4).

The reaction of Na(OCP) (**1**) in form of its dioxane adduct, [Na(OCP) (dioxane)_{2.5}], and two equivalents of phenylethylnylcarboxylic ethylester in refluxing DME yields the sodium salt of diethyl 4-hydroxy-2,6-diphenylphosphinine- 3,5-dicarboxylate [Na(**26**)] in a clean reaction (Scheme 4). An intermediate compound, with a ³¹P chemical shift of 153.2 ppm, was observed in the yellow reaction solution which we assign to the [2+2] cycloadduct **26a**.¹⁷⁰ Likely, **26a** reacts further with a second alkyne in a subsequent [2+2] cycloaddition to give an undetected Dewar-benzene analogue, which rearranges to the final product Na(**26**) in excellent yield as pale yellow crystals. The ³¹P NMR shifts of this sodium phosphinin-4-olate are strongly solvent dependent with ³¹P = 91.9 ppm in [D₈]THF and 66.2 ppm in [D₆]DMSO.



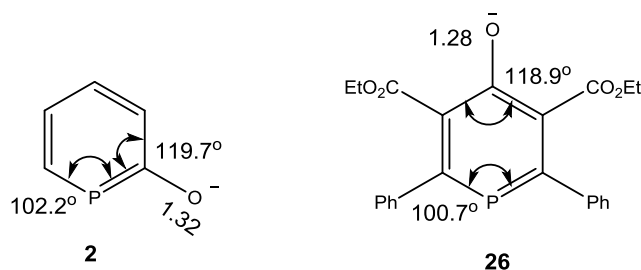
Scheme 4. Synthesis of the phosphinin-4-olate **26**, **27** and of the phospholide **28**. The centers in the intermediates **26a**, **27a**, and **28a** which are involved in either a [2+2] or [3+2] cycloaddition are indicated by small arrows.

In contrast to **26**, the more-electron-deficient diethyl but-2-ynedioate does not only form the 2,3,5,6-tetracarboxyphosphinin-4-olate (**27**), but also the phospholide anion **28** in a ratio of approximately 1:1. A detailed reaction mechanism cannot be provided, but we propose that the cyclic intermediate **27a** is in equilibrium with the acyclic phosphaketene **28a**, which is likely the primary product formed by nucleophilic attack of the $(\text{OCP})^-$ anion on the activated alkyne. This intermediate may then further react with a second equivalent of alkyne **28a** to give the phospholide **28** under loss of CO.

5.3.2 The crystal structure of **26** and **28**

Single crystals of **26** (yellow-orange) and **28** (yellow) were investigated by X-ray diffraction, and the structures of these compounds were determined. The sodium salt **26** (Figure 3) forms dimeric aggregates in the solid state with Na_2O_2 rings as a common structural motif. Na^+ ions in $\text{Na}(\mathbf{26})$ are five-coordinate and adopt a square pyramidal configuration (Figure 3) with four oxygen atoms from two heterocycles in the equatorial plane and one oxygen atom from THF in the axial position. A comparison of relevant bond lengths and angles in the phosphinin-4-olate (**26**) anion and phosphinin-2-olate (**2**) is given in Scheme 5. In **26**, the six-membered ring is stretched along the

O...P axis with a short C-O bond [1.284(3) Å] and a long-short sequence of C-C bonds in the ring. Both ipso angles in the para-position at C3 [118.8(2)°] and P1 [100.7(1)°] are compressed, indicating a quinonoid-type distortion of the π -system.¹⁷³⁻¹⁷⁴



Scheme 5 Comparison of selected structure parameters of the phosphinin-4-olate anion in **26** and the phosphinin-2-olate anion in **2**.

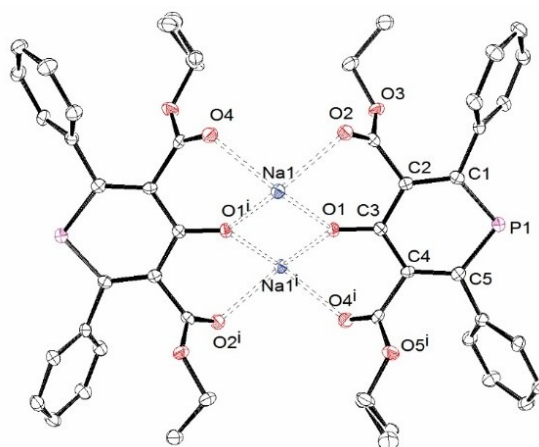


Figure 3 Structure of **26**. Ellipsoids are drawn at a 30% probability level. Hydrogen atoms and the coordinated THF molecules have been omitted for clarity. Selected bond distances [Å] and angles [°]: P1-C1 1.749(3), P1-C5 1.750(3), C1-C2 1.378(4), C2-C3 1.428(4), C3-C4 1.434(4), C4-C5 1.391(4), C3-O1 1.284(3), Na-O 2.275(2)~2.366(2); C5-P1-C1 100.7(1), P1-C1-C2 124.8(2), C1-C2-C3 125.5(3), C2-C3-C4 118.8(2), C3-C4-C5 125.2(3), C4-C5-P1 124.9(2).

In the sodium salt of 2,3,4,5-tetra(ethylcarboxy)phospholide Na(**28**), a two-dimensional coordination polymer is formed containing octahedrally coordinated sodium cations. In one dimension (*a* axis), the carbonyl oxygen centers O1/O3 and O5/O7 of the four COOEt groups are coordinated to sodium cations to form $\{\text{Na}[\text{PC}_4(\text{COOEt})_4]\}_1$ ¹⁷⁵ ribbons, which are then linked along the *b* axis by two dioxane molecules bound in a cis-fashion to Na1 to form a layered structure. The phosphorus-containing heterocycles in all compounds are flat, and the distances indicate delocalized π -systems in all cases. The phospholide ring in **28** is the only known example in which the PC₄ ring is “free” and not coordinated to a metal center; however, this has no systematic influence on the bond parameters.

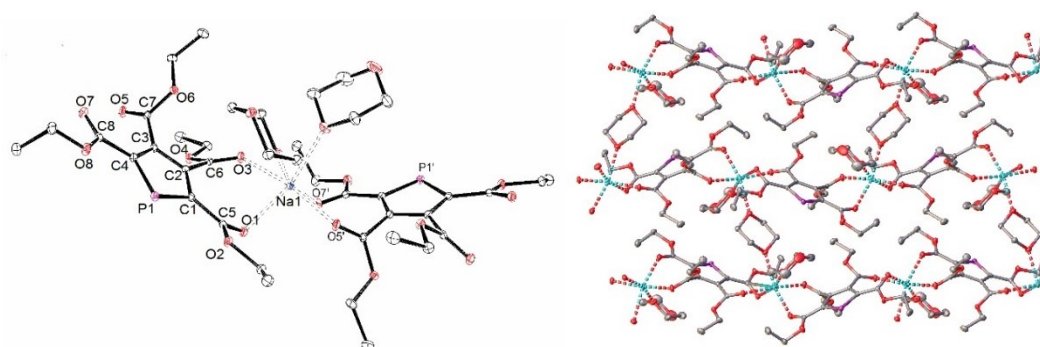
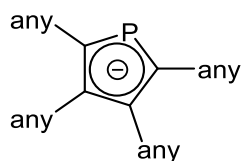


Figure 4 Structure of **28** (left) and packing diagram of **28** (right) in solid state. Hydrogen atoms have been removed for clarity. Ellipsoids are drawn at a 30% probability level. Hydrogen atoms have been removed for clarity. Selected bond distances [Å] and angles [°]: P1–C1 1.747(1), P1–C4 1.754(1), C1–C2 1.417(2), C2–C3 1.401(2), C3–C4 1.414(2), Na1–O 2.249(1)–2.467(1); C1–P1–C4 90.4(1), P1–C1–C2 112.4(1), C1–C2–C3 112.4(1), C2–C3–C4 112.6(1), C3–C4–P1 112.2(1).

5.3.3 Comparison of selected structure parameters in [PC4R4] – phospholide rings

For the general structure motif shown below about 340 structures are listed in the CCDC data bank.



Scheme 6 General structure of phospholide anions

In all cases the counter cation is a metal, M, which include metals such as M = Fe, Zr, Ru, Mn, Tl, Sm, Rh, Pt, Ca, W, Mo, Ni, Co, Cr, Ti, Ba, Sr and others. In most of the structures the metal is η^5 -coordinated (see coordination modes below). In many of these complexes a second metal center is coordinated to the phosphorus atom too. Few examples (Cu, Ga, W, Mo, Mn, Ag, Au, Sn, Li) show only a η^1 - η^3 or an “out of plane” P–metal coordination.

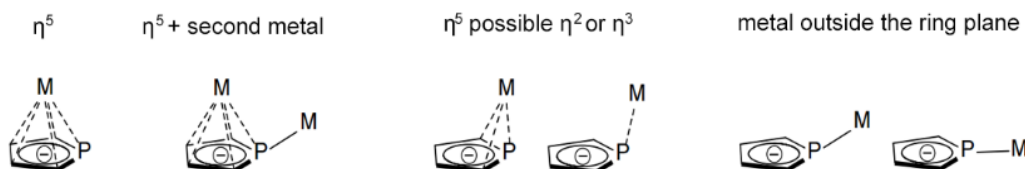
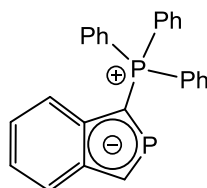


Figure 5 The coordination mode for phospholide

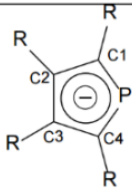
The only structures that do not show a metal-coordination at the PC₄R₄ – ring were reported by Gudat et al.¹⁷⁶(Scheme 7, CCDC: 161501-161504).



Scheme 7 Uncoordinated phospholide

With one exception (a lithium salt reported in CCDC 57728 by E. Niecke, et al.¹⁷⁷ showing an η^1 coordination), all structures with alkali metals (Na^+ , K^+) as counter ions always display an η^5 coordination (See for example CCDC 215122).¹⁷⁸ For comparison, Table 1 lists pertinent bond lengths (\AA) within the PC₄ rings.

Table 1. Comparison for different M-PC₄ X-ray structures

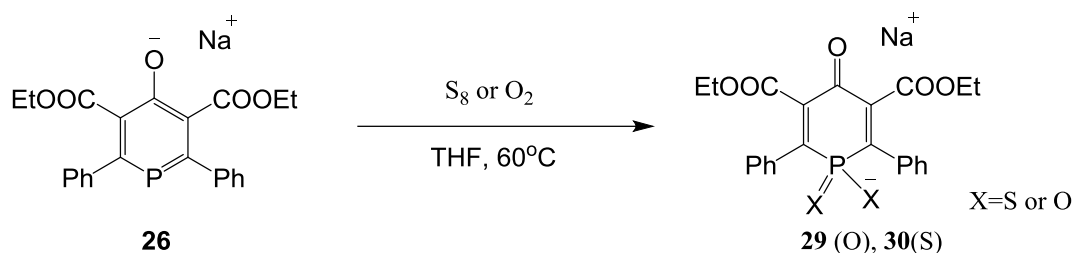
	Li^+ (η^1) ^[s9]	Li^+ (η^5) ^[s11]	Na^+ (η^5) ^[s10]	K^+ (η^5) ^[s10]	Cu^+ (η^2) ^[s12]	Ag^+ "out of plane" ^[s13]	Au^+ "out of plane" ^[s14]	28
P-C ₁	1.77	1.75	1.75	1.76	1.75	1.72	1.71	1.747
P-C ₄	1.79	1.75	1.79	1.76	1.77	1.72	1.72	1.754
C ₁ -C ₂	1.394	1.396	1.408	1.401	1.421	1.444	1.453	1.417
C ₂ -C ₃	1.443	1.423	1.432	1.427	1.447	1.421	1.420	1.401
C ₃ -C ₄	1.431	1.396	1.377	1.401	1.426	1.444	1.443	1.414
C-C _{avg}	1.42	1.41	1.41	1.41	1.43	1.436	1.438	1.411

5.4 REACTIVITY OF PHOSPHININ-4-OLATE

In chapter 2, the reactivity of sodium(I) phosphinin-2-olate [$\text{Na}(\mathbf{2})$] has been discussed, it is quite stable to oxygen and water. The comparison of the structure parameters in **26** and **2** indicate that **26** has a quinonoid-type distortion of the π -system. As a result, **26** should be more reactive than **2**.

5.4.1 Oxidation of **26** with oxygen and sulfur

The phosphinin-4-olate anion is also stable towards water, when drops of water are added to the THF solution of Na(**26**). No reaction or decomposition was observed in the ^{31}P NMR spectrum. However, **26** can be oxidized by oxygen at room temperature or sulfur at 60 °C (Scheme 8). The NMR spectrum and X-ray diffraction study revealed that the oxidation occurs at the phosphorus atom.



Scheme 8 Oxidation of the phosphinin-4-olate anion **26** by oxygen or sulfur

The crystals of compounds **29** and **30** contain both contact ion pairs (Figure 6). A two-dimensional aggregation is observed for **29** and a one-dimensional linear chain for **30**. The six-membered ring in the anionic part of **29** is almost planar, with two oxygen atoms bonding to phosphorus below and above the plane. The sodium cation resides in a distorted tetrahedral environment formed by three oxygen atoms from three heterocycles and one oxygen atom from THF. Unlike the coordination mode in **29**, the sodium cations in **30** are five-coordinate and are in the center of a trigonal bipyramidal structure (Figure 6c). Two oxygen atoms of two heterocycles are on the vertical axis and three oxygen atoms from THF lie in the equatorial plane.

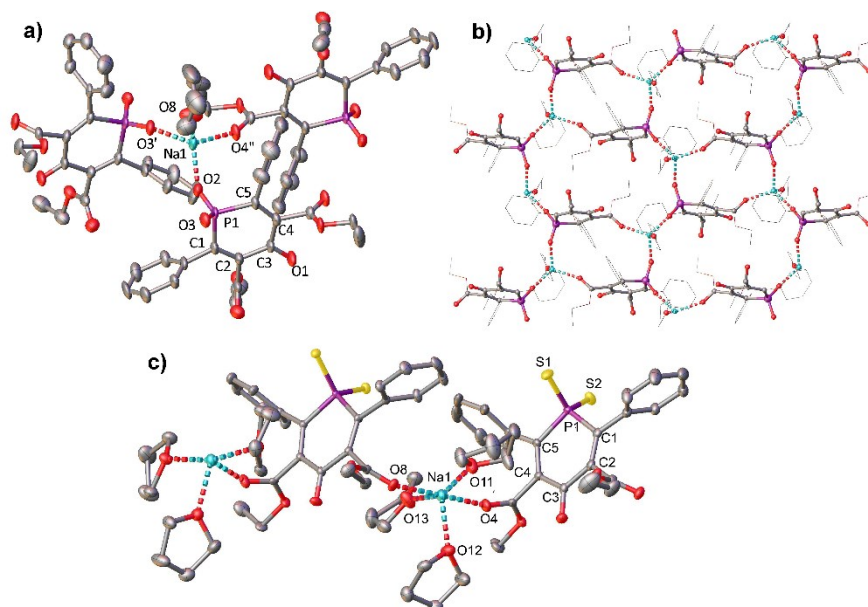
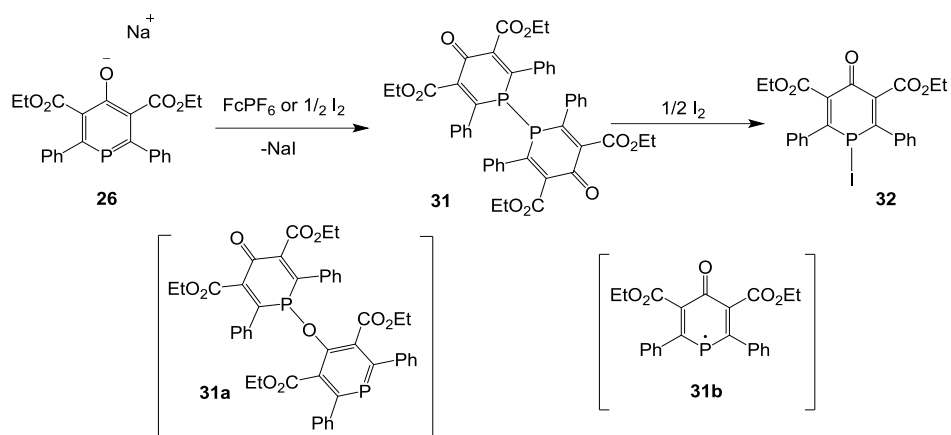


Figure 6 a) Structure of **29**. Ellipsoids are drawn at a 30% probability level. Hydrogen atoms have been removed for clarity. Selected bond distances [Å] and angles [°]: P1-C1 1.749(3), P1-C5 1.750(3), C1-C2 1.378(4), C2-C3 1.428(4), C3-C4 1.434(4), C4-C5 1.391(4), C3-O1 1.284(3), O1-Na1 2.293(2), O1-Na1' 2.275(2), O2-Na1 2.366(2), O4'-Na1' 2.358(2); C5-P1-C1 100.7(1), P1-C1-C2 124.8(2), C1-C2-C3 125.5(3), C2-C3-C4 118.8(2), C3-C4-C5 125.2(3), C4-C5-P1 124.9(2). b) 2D layer for extended construction of **29**. c) Structure of **30**. Ellipsoids are drawn at a 30 % probability level. Hydrogen atoms have been removed for clarity. Selected bond distances [Å] and angles [°]: P1-C1 1.749(3), P1-C5 1.750(3), C1-C2 1.378(4), C2-C3 1.428(4), C3-C4 1.434(4), C4-C5 1.391(4), C3-O1 1.284(3), O1-Na1 2.293(2), O1-Na1' 2.275(2), O2-Na1 2.366(2), O4'-Na1' 2.358(2); C5-P1-C1 100.7(1), P1-C1-C2 124.8(2), C1-C2-C3 125.5(3), C2-C3-C4 118.8(2), C3-C4-C5 125.2(3), C4-C5-P1 124.9(2).

5.4.2 Synthesis of biphosphininone (**31**)

Oxidation of Na(**25**) with stoichiometric amounts of ferrocenium hexafluorophosphate (FcPF₆) or elemental Iodine (I₂), leads to three potential configurations for dimers of the heterocycle: a compound with persistent a P-O-P unit as in compound **31a**, a phosphorus centered radical species **31b**, and the biphosphininone **31** (Scheme 3). The ³¹P NMR spectrum of the product displayed only one singlet at -38.2 ppm, revealing that the product is biphosphininone **31**.



Scheme 9 Oxidation of the phosphinin-4-olate anion **26** with iodine

It is known that the PP bond of diphosphanes bearing bulky substituents can undergo reversible dissociation. In the temperature range 133 K to 323 K no signals could be detected in the EPR spectrum of **31** in toluene. This indicates that **31** cannot generate measurable amounts of the corresponding P centered radical. In addition, DFT calculations revealed an energy difference of -29 kcal/mol between **31** and **31b**, which is relatively high for the dissociation of PP bond in **31**. By adding one more equivalent of iodine, the dimer can be oxidized further, to give iodophosphane **32**.

Yellow single crystals of **31** and orange single crystals of **32** were obtained from saturated toluene and THF solutions, respectively. The results of the X-ray diffraction studies are shown in Figure 7. The solid state structure of **31** exhibits crystallographic orthorhombic symmetry; the asymmetric unit contains one six-membered ring (Figure 7a). The six atoms of the heterocycle are nearly coplanar. The P atom deviates by a 0.154 Å from this plane. The dihedral angle between the two six-membered rings is 42.38° to minimize steric repulsion between the phenyl substitutions. The P-P bond length is 2.207 Å, which is a typical value for P-P single bonds in the literature.¹⁴ Similar to the phosphorus center in biheterocycles formed from phospholes, the phosphorus atom is the apex of a trigonal pyramid and thus not conjugated with the “dieneacetone” unit. The crystal structure of **31** shows one iodophosphane molecule, upon coordination of iodine, the phosphorus atom deviates from the plane of the heterocycle by 0.383 Å (Figure 1b), which is more twisted than in **30**.

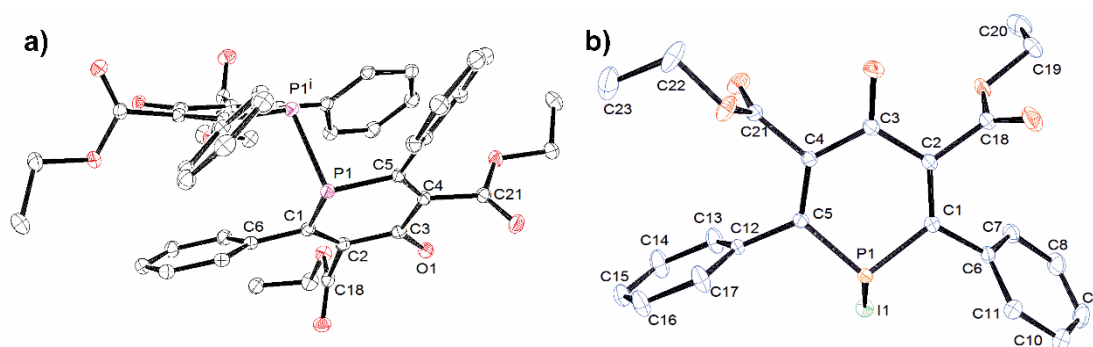
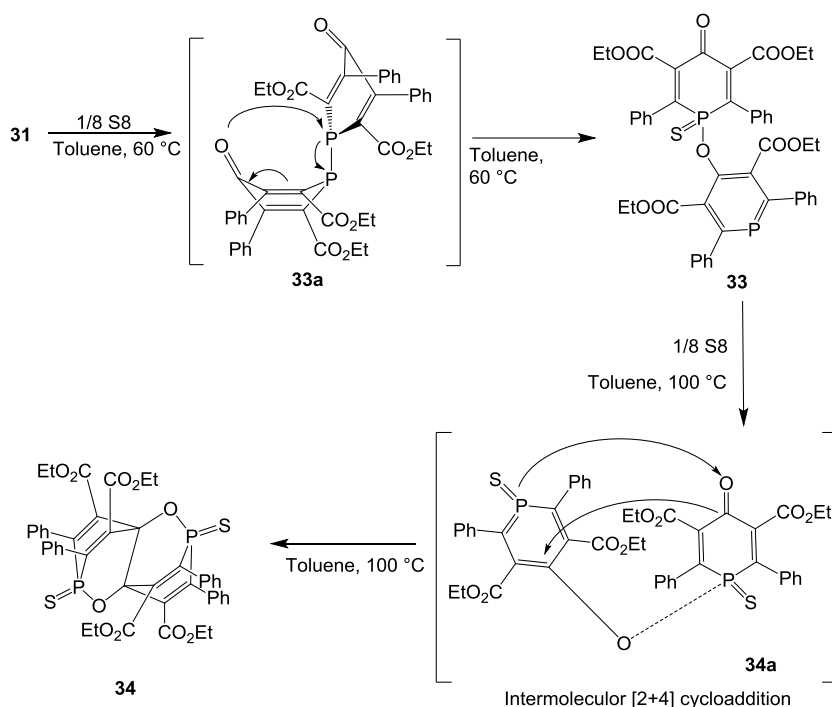


Figure 1 a) Structure of **31**. Ellipsoids are drawn at a 30% probability level. Hydrogen atoms have been removed for clarity. Selected bond distances [Å] and angles [°]: P1-P1' 2.2071(16), P1-C1 1.798(3), P1-C5 1.793(3), C1-C2 1.343(5), C2-C3 1.468(5), C3-C4 1.43470(5), C4-C5 1.340(5), C3-O1 1.236 (4); C5-P1-P1' 99.71(12), C5-P1-C1 103.72(15), P1-C1-C2 122.1(3), C1-C2-C3 125.2(3), C2-C3-C4 120.8(3), C3-C4-C5 125.4(3), C4-C5-P1 122.0(3). b) Structure of **32**. Ellipsoids are drawn at a 30 % probability level. Hydrogen atoms have been removed for clarity. Selected bond distances [Å] and angles [°]: P1-I1 2.4590(4), P1-C1 1.8163(15), P1-C5 1.8154(15), C1-C2 1.3466(19), C2-C3 1.481(2), C3-C4 1.473(2), C4-C5 1.348(2), C3-O1 1.2265(18); C5-P1-I1 102.71(4), C5-P1-C1 102.11(7), P1-C1-C2 116.77(10), C1-C2-C3 125.96(13), C2-C3-C4 119.84(12), C3-C4-C5 124.93(13), C4-C5-P1 122.98(11).

5.4.3 The oxidation of biphosphinone

Since it is very convenient to obtain the unprecedented Biphosphinone (**31**), it would be interesting to study its oxidation properties. The cyclic voltammetry of **31** in THF at room temperature with tetrabutylammonium hexafluorophosphate ($n\text{Bu}_4\text{NPF}_6$) as a supporting electrolyte showed irreversible redox waves, which revealed the oxidation states (one electron or two electrons) were highly reactive and unstable in solution.



Scheme 10 The oxidation of biphosphininone **31** by sulfur

However, the oxidation of dimer **31** by 1 equivalent sulfur gave a stable product **33** with two doublets at 171.8 and 40.1 ppm of $J_{PP} = 7.8$ Hz observed in ^{31}P NMR spectrum. The low field chemical shift indicated that one phosphinine ring was released. Crystal structure and NMR spectra analysis revealed a structure formed where one of the heterocycles was oxidized at the phosphorus atom by sulfur and the other heterocycle reformed with the phosphinine ring bonding the oxidized phosphorus atom with the phosphininolic oxygen atom (Scheme 10).

By adding another equivalent of sulfur and raising the reaction temperature, **33** could be further oxidized. A singlet at 45.1 ppm for **34** was observed instead of the two doublets in the ^{31}P NMR spectrum. The analysis of the crystal structure for compound **34** revealed it underwent an intramolecular [2+4] cycloaddition reaction (Scheme 10). A symmetric tetracyclic structure was formed. Colorless crystals of compound **34**, of good enough quality for X-Ray diffraction, were obtained directly from the reaction mixture in toluene.

The single crystal X-ray analysis revealed that compound **33** crystallized in the P_{-1} space group. The asymmetric unit contains two molecules of **33**, one of them is shown in Figure 2a. After oxidization, by sulfur, of one phosphorus atom (P1) in biphosphininone (**31**), the P1-P2 bond dissociates and the heterocycle (containing P2) rotates and bonds with the oxidized P1 through

O2. The heterocycle (containing P2) reforms as a phosphinine ring. The bond lengths and angles in oxidized heterocycles are similar to those in biphosphininone (**30**), while the geometric parameters of the six-membered ring (containing P2) are in the typical range of those for phosphinine rings.

The crystal structure of **34** is built up from two symmetric heterocycles, which are bonded to each other with C3-O1 adding to C3'-P1'. Phosphorus atoms (P1 or P1') are located in tetrahedral environment bonded to sulfur with a distance of 1.9028(4) Å, which is in the range of a typical P-S double bond. At the same time, C3(') are also in tetrahedral environments with the bond length C3-C3' of 1.6239(19) which is much longer than normal carbon carbon single bond distances ¹⁷⁹⁻

181.

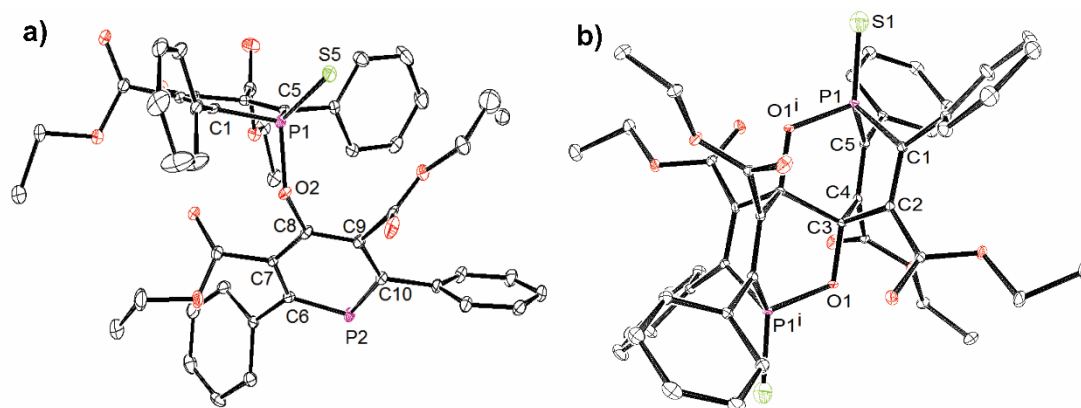


Figure 2 a) Structure of **33**. Ellipsoids are drawn at a 30% probability level. Hydrogen atoms have been removed for clarity. Selected bond distances [Å] and angles [°]: P1-C1 1.802(3), P1-C5 1.809(3), P2-C6 1.740(3), P2-C10 1.748(3), C-C in phosphinine 1.393(4)- 1.400(4), C-C in P1-heterocycle: 1.340(3)-1.490(3), C8-O2 1.404(4), P1-O2 1.634(4), P1-S1 1.917(5); C5-P1-C1 106.02(12), C6-P2-C10 101.78(14), P2-C6-C7 124.0(2), C6-C7-C8 122.9(2), C7-C8-C9 124.7(3), C8-C9-C10 121.6(3), C9-C10-P2 124.8(2), P1-O2-C8 126.63(16). b) Structure of **34**. Ellipsoids are drawn at a 30 % probability level. Hydrogen atoms have been removed for clarity. Selected bond distances [Å] and angles [°]: P1-C1 1.8254(11), P1-C5 1.8058(10), C1-C2 1.3455(14), C2-C3 1.5246(14), C3-C4 1.5200(14), C4-C5 1.3367(14), C3-O1 1.4200(12), P1-S1 1.9028(4), P1-O1' 1.6352(8), C3-C3' 1.6239(19); C5-P1-C1 100.65(5), P1-C1-C2 111.36(8), C1-P1-O1' 98.45(4), C5-P1-O1' 101.85(4), C1-C2-C3 116.89(9), C2-C3-C4 110.14(8), C3-C4-C5 118.43(9), C4-C5-P1 110.69(7).

5.5 CONCLUSION

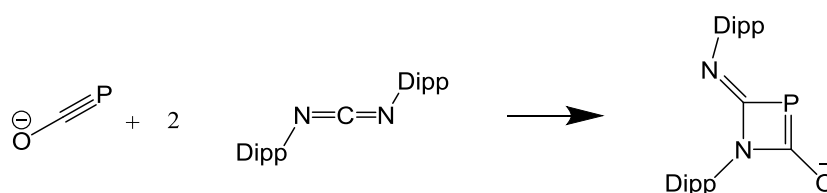
In this chapter, all reactions of Na(OCP) with unsaturated compounds proceed under disruption lead to the dissociation of the carbon-phosphorus bond in the (OCP)⁻ anion. Low temperature

NMR studies revealed that the reactions were initiated by the [2+2] cycloadditions. Additionally, the formation of phosphaketenes, **24a** and **28a**, is proposed as highly reactive intermediates. Following the subsequent loss of P^- or CO, for **24** and **28** respectively, the final products were obtained. Thus phenomena reflect formally the resonance structure $[P\leftarrow CO]^-$, which indicates that $(OCP)^-$ can act as a P^- transfer reagent. Additionally, the one pot synthesis of sodium phosphinin-4-olate (**26**) is remarkably selective and atom economical with respect to phosphorus. It is unreactive to water but oxidized by oxygen or sulfur. From the one electron oxidation of **26**, the corresponding biphosphinone (**31**) was obtained. The novel biphosphinone **31** can be oxidized by sulfur step by step wherevly subsequently a significant rearrangement followed by an intermolecular cycloaddition is initiated.

6 SYNTHESIS AND REACTIVITY OF THE 1,3,5-DIAZAPHOSPHINANE ANIONS

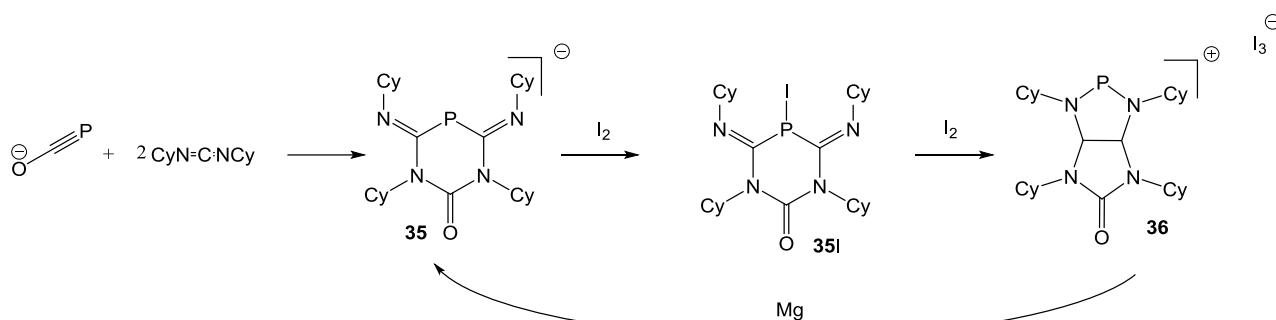
6.1 INTRODUCTION

As shown in chapter 5, the $(\text{OCP})^-$ anion reacts with tetracyclone or alkynes to form four-membered heterocycles as an intermediate in these reactions.¹⁰⁵ Goicoechea^{182,183} and his group obtained a four-membered PC_2N ring in the reaction of **1a** with bis(2,6-diisopropylphenyl) carbodiimide (DippNCNDipp) (Scheme 1) at room temperature. The four-membered ring has a chemical shift of $\delta = 18.6$ ppm in ^{31}P NMR. They also mentioned in their report that this [2+2] cycloaddition adduct is strongly dependent upon the nature of the substituents on the carbodiimide, the mixture of **1a** and dicyclohexylcarbodiimide (CyNCNCy) showed no evidence for a reaction to form the cycloaddition product even upon prolonged heating.¹⁸³



Scheme 1 Formation of [PC₂N] four-membered ring

Independently, Heift from our group found that the reaction of $[\text{Na}(\text{dioxane})_{2.5}(\text{OCP})]$ (**1**) with CyNCNCy afforded a six-membered heterocycle, namely the diazaphosphinane (**35**), after refluxing in THF overnight¹⁸⁴. Additionally, a redox reversible interconversion (Scheme 2) occurs between the six-membered heterocycle (**35**) and diazaphospholenium **36**. In this reaction, the elemental iodine cleaved the phosphorous halogen bond in **35I** to form a phosphonium cation, which rearranged to form the diazaphospholenium in an exothermic reaction. When silver triflate was used in the reaction with **35I**, but the chemical shifts in the ^{31}P NMR spectrum is obtained for the reaction mixture and none of the chemical shifts is correspond to **36**. Note that $[\text{Na}(\text{dioxane})_{2.5}(\text{OCP})]$ (**1**) reacts with DippNCNDipp to give exclusively the [2+2] cycloadduct likely because the carbodiimide is sterically too bulky.

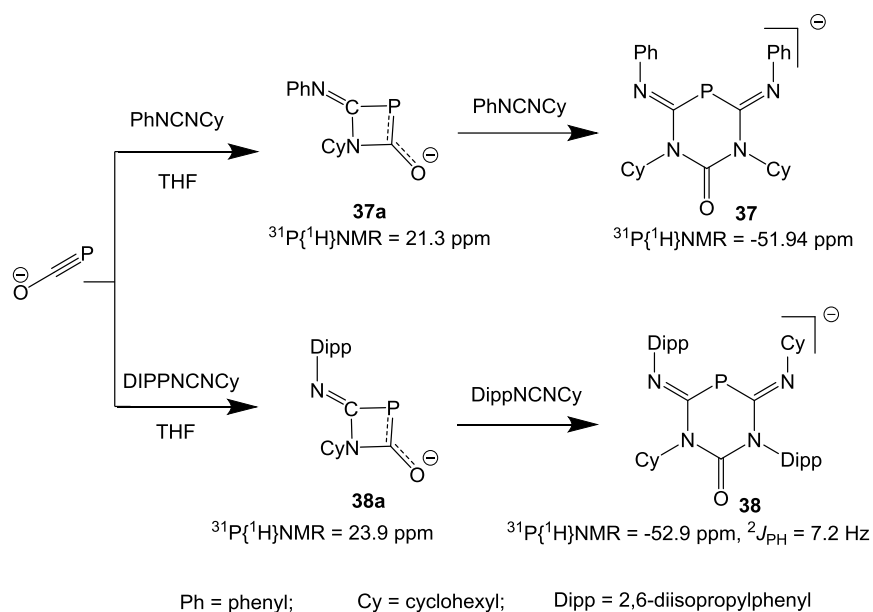


Scheme 2 Redox reversible interconversion between **35** and **36**

To gain further insight into substituent effects in the reactions between **1** and carbodiimides, we describe the reactivity of **1** with non-symmetric carbodiimides in this chapter. The products obtained from these reactions were fully characterized, and the reactivity of the products was studied.

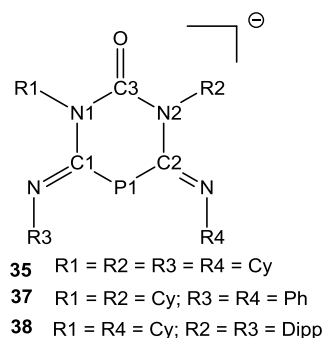
6.2 THE SYNTHESIS AND CHARACTERIZATION OF TWO DIAZAPHOSPHINANES

The reaction of **1** and 2 equivalents of cyclohexylphenylcarbodiimide (PhNCNCy) yielded cleanly one product with a singlet at -51.4 ppm in ^{31}P NMR after stirring for 2 hours at room temperature. According to the previous reports,¹⁸⁴ a chemical shift of $\delta = -51.4$ ppm is typical for a six-membered heterocycle. A singlet at $\delta = 21.3$ ppm in ^{31}P NMR spectrum was observed during the reaction. This chemical shift belongs to the [2+2] cycloaddition¹⁸³ intermediate and its relative intensity decreased with prolonged stirring. It is notable that the chemical shift for the [2+2] cycloaddition intermediate was not observed in the reaction of Na(OCP) with CyNCNCy. The final product **37** was then unequivocally identified by X-ray diffraction analysis, which revealed that both phenyl groups are located adjacent to the phosphorus atom (Figure 1a).



Scheme 3 Formation of the six membered ring anion **37** and **38**

When **1** is reacted with another asymmetric carbodiimide, *N*-(2,6-diisopropylphenyl)-*N*-cyclohexyl-carbodiimide (DIPPNCNCy), the formation of [2+2] adduct can also be observed $\delta = 23.9$ ppm in ^{31}P NMR spectrum of the reaction mixture. After stirring for two hours in THF at room temperature, one doublet of -52.9 ppm with a proton coupling of $J_{\text{PH}} = 2.1$ Hz is observed in the $^{31}\text{P}\{\text{H}\}$ NMR spectrum. The proton coupling is assigned to the hydrogen on the cyclohexyl group, this means that one of cyclohexyl groups (Cy) is close to the phosphorus atom in **38** (Scheme 3). The X-ray structures of **37** and **38** are shown in Figure 1. The sodium cation is coordinated by three solvent molecules of 1,2-dimethoxyethane (DME) which are omitted for clarity in the figure. The six-membered heterocycle of phosphide **37** is non-planar. Compared with **35**, the maximum deviation from planarity in **37** is smaller (Table 1). The P-C distances in **37** are shorter while the N-C(O), C(O)-N are longer than those in compound **35**. The X-ray diffraction study of **38** confirmed the NMR results that it is one Dipp and one cyclohexyl group are located beside the phosphorus atom (Figure 1b). As there are two bulky Dipp groups attached to the six-membered heterocycle of phosphide **38**, the structure of the cycle is more twisted compared with that of **37**. The deviation from planarity is higher and the central C1-N2 and C2-N2 bond lengths are larger than those in **37** and **35** (Table 1).



Scheme 4

Table 1 Comparison of the bond length in the six-member ring for **37**, **38** and **35**

Bond length(Å)	P1-C1	P1-C2	C1-N2	C2-N1	N1-C3	N2-C3	Planarity
37	1.791	1.789	1.412	1.409	1.379	1.385	0.244
38	1.809	1.769	1.424	1.424	1.392	1.365	0.390
35	1.802	1.789	1.445	1.441	1.365	1.374	0.254

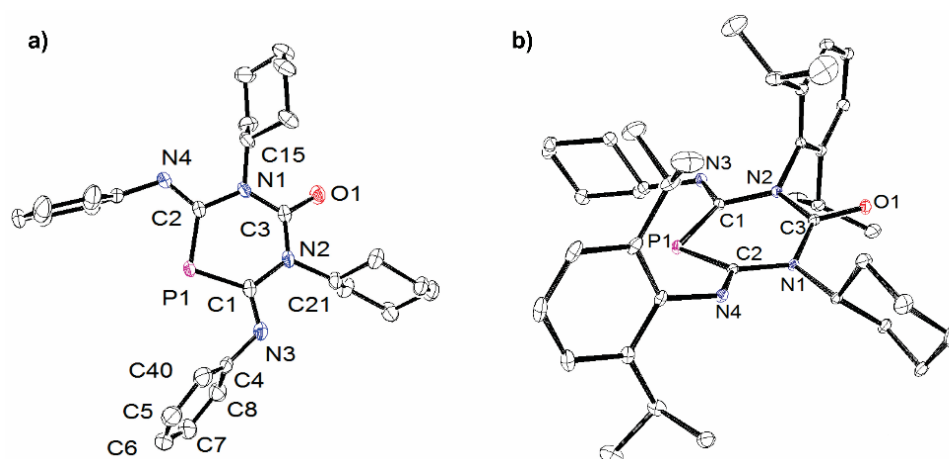


Figure 1 ORTEP plot of anions **37** (a) and **38** (b) (thermal ellipsoids drawn at 50% probability). Hydrogen atoms, sodium cation and solvents have been omitted for clarity. Selected bond lengths (Å) and angles (°) for **37**: P1-C1 1.7913(14); P1-C2 1.7894(14); C2-N1 1.4096(17); C1-N2 1.4120(18); C3-O1 1.2257(17); N1-C3 1.3794(18); N2-C3 1.3794(19); C2-N4 1.3026(18); C1-N3 1.301(2). C1-P1-C2 100.28(6); P1-C1-N2 122.87(11); P1-C2-N1 122.76(10); C2-N1-C3 124.68(12); C1-N1-C3 124.51(12); N1-C3-N2 121.01(12). **38**: P1-C1 1.8095(11); P1-C2 1.7689(12); C2-N1 1.4243(16); C1-N2 1.4237(15); C3-O1 1.2298(14); N1-C3 1.3921(15); N2-C3 1.3646(15); C2-N4 1.3006(14); C1-N3 1.2855(15). C1-P1-C2 99.36(5); P1-C1-N2 120.54(8); P1-C2-N1 122.02(8); C2-N1-C3 123.20(9); C2-N1-C3 123.20(9); N1-C3-N2 119.26(10).

6.3 DISCUSSION ON THE REACTION MECHANISM

The mechanism of the reaction between **1** and CyNCNCy has been studied via DFT calculations and was reported by our group recently.¹⁸⁴ It revealed that the first step is the [2+2] cycloaddition, which is also the rate-determining step in the reaction with a rather high activation barrier for the model compound dimethylcarbodiimide. The following steps to form the six-membered heterocycle are nearly barrierless. The computational results are in accordance with the experimental observation that the reaction needs to be performed at elevated temperature and need longer reaction times for the alkyl substituted carbodiimide.

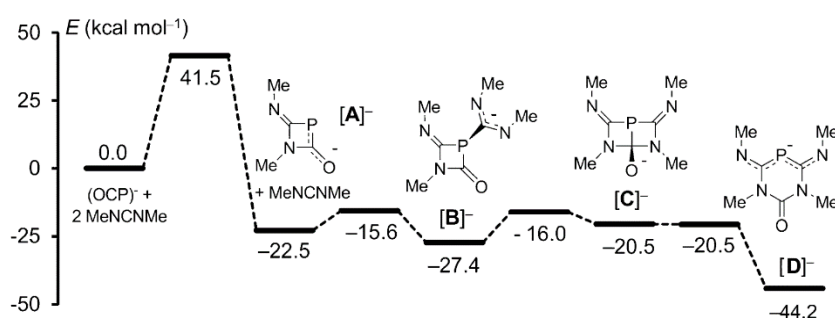


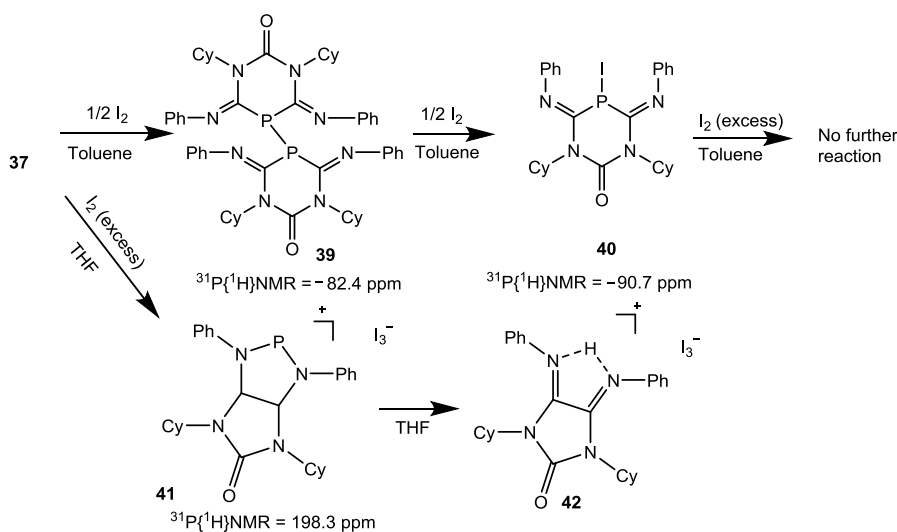
Figure 2 The minimum energy reaction pathway of the reaction between Na(OCP) and two dimethyl carbodiimide molecules at the CBS-QB3 level. Na⁺ ions were included in the computations but not shown.

When carbodiimides have one aryl substituent, like phenyl or DIPP, the activation barrier for the first step decreases and the reaction with Na(OCP) can proceed at room temperature. As described in the experimental section for **37**, at the beginning of the reaction, two singlets at $\delta = 21.3$ and -51.4 ppm are observed in the ³¹P NMR spectrum. This indicated the formation of [2+2] adducts (**37a**) and the six-membered ring **37**. The (OCP)⁻ anion is so small that dimensions of the substituents on carbodiimide do not affect the first step. The electrophilic carbon of (OCP)⁻ interacts with the more nucleophilic imide-N, which is bonded with the cyclohexyl group to give ring like **37a** as sole product. In the next step, the phosphorus center of the [2+2] adduct attacks the central carbon atom of another carbodiimide molecule. As the phenyl group on carbodiimide is smaller than cyclohexane, the steric effects lead to the formation of the symmetric product **37**. The results of this reaction support the previously proposed mechanism. The reaction between DippNCNCy and Na(OCP) gives a non-symmetric product. In the first step, the four-membered

ring [Na(**38a**)] formed with the aryl substituent beside the phosphorus atom similar to that in the reaction with PhNCNCy. Because the bulky Dipp substituent requires more space, the second molecule of DippNCNCy added to [Na(**38a**)] in a way that the non-symmetric structure of [Na(**38**)] is generated.

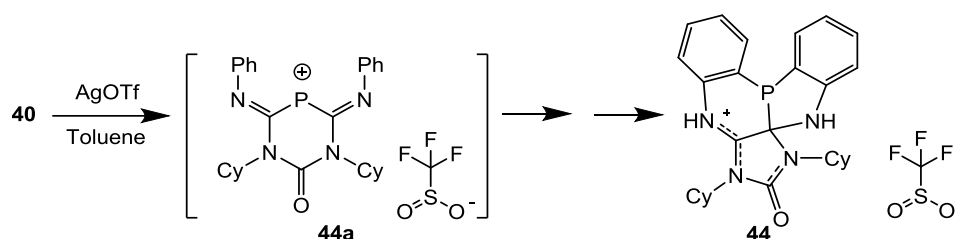
6.4 OXIDATION OF THE ANIONIC DIAZAPHOSPHINANE **37**

In the attempt to prepare compounds comparable to **36** with two fused five-membered heterocycles,¹⁸⁴ iodine was reacted with **37** (scheme 4). The diphosphane **39** was obtained and shows a singlet at $\delta = -82.4$ ppm in the ^{31}P NMR spectrum when half an equivalent of iodine (I_2) was added to diazaphosphinane **37** in toluene. After adding an excess of I_2 to the reaction mixture, the iodophosphane **40** was formed with a singlet at $\delta = -90.7$ ppm in ^{31}P NMR spectrum. But no further reaction was observed (Scheme 2) in toluene. The reaction is solvent-dependent. In THF or diethyl ether several chemical shifts are observed in the ^{31}P NMR spectrum after 30 minutes. The major signal appears at $\delta = 198.2$ ppm in the ^{31}P NMR spectrum which is the typical value for a diazaphospholenium cations like **41**. This decomposed in a few hours (the peak at 198.2 ppm disappeared in 5 hours stirring), and the solvent was removed completely under vacuum. The remaining solid was extracted by dichloromethane, after filtration, the filtrate was layered by hexane. After one day diffusion, yellow crystals were obtained, the structure was proved as drawn for **42**.



Scheme 4 Oxidation of the six-membered ring anion **37** with iodine

When the iodophosphane **40** was treated with silver trifluoromethanesulfonate (AgOTf) in toluene, a clean reaction was observed and one product is obtained which shows a singlet at -7.9 ppm in the ^{31}P NMR spectrum. After workup, a white solid was collected, which is stable under inert atmosphere was collected. The product was studied by X-ray diffraction and as a result structure **44** is obtained. This reaction is also solvent dependent and **44** is not formed in THF or diethyl ether.

**Scheme 5** Formation of compound **44** from the reaction between iodophosphane and silver triflate

Crystals of compound **41** could not be grown; instead, crystals of **42** were obtained by slow evaporation of the solvent for **41** in DME/n-hexane solution. The structure of **42** is similar to the diazaphospholenium cation with a proton replacing P^+ in the ring. From the phosphorus chemical shift at 198.2 ppm for the reaction mixture and the structure of **42**, it is inferred that the diazaphospholenium **41** was probably formed during the reaction. The crystal structure of **42** (Figure 3) consists of two fused five-membered rings. Compared with **36**, the $\angle\text{C1-N1-C4}$ in **42** is smaller by 4° and the distance between N1 and N2 is longer by 0.3 \AA , these differences are attributed to loss of P^+ . The proton H1 is located in between N1 and N2, with bond distances of 1.414 and 1.619 \AA respectively.

The structure of **44** is shown in Figure 3b. The bond length for N2-C2 of $1.308(4) \text{ \AA}$ is close to normal nitrogen carbon double bond, while C1-N1 distance is close to a single bond with a value of $1.449(3) \text{ \AA}$. As a result, the positive charge is probably mainly localized on the imine proton N2-H $^+$. The ^1H NMR spectrum in CD_3Cl shows two singlets at low field of 10.5 and 6.2 ppm, which indicates the different chemical environment for these two N-H units. In the fragment of C1-N3-C3-N4-C2, the N4-C2 and C3-N3 bond lengths are $1.328(3)$ and $1.351(3)$, respectively, indicating

the delocalization of electrons in the fragment. The other bond lengths (N2-C6, N1-C7, C1-N3) are closer to single bond lengths.

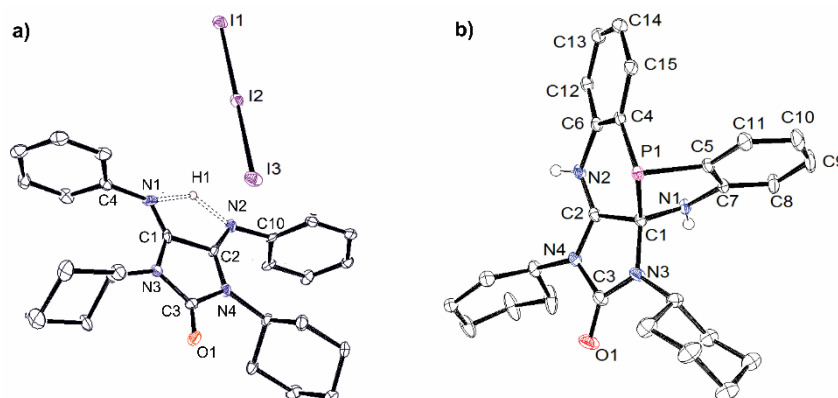


Figure 3 Ortep plot of compound **42** (a) and **44** (b) (thermal ellipsoids are drawn at 50% probability). Hydrogen atoms (except the Nitrogen-H) have been omitted for clarity. Selected bond lengths (Å) and angles (°) for **42**: C1-C2 1.526(10); N1-C1 1.289(10); N2-C2 1.223(11); N1-C4 1.448(9); C1-N3 1.327(11); C2-N4 1.404(11); C3-N4 1.373(11); C3-N3 1.431(9); O1-C3 1.204(11); N1-H1 1.414; N2-H1 1.689. N2-H1-N1 122.595; N1-C1-N3 134.0(7); C4-N1-C1 122.6(8). **44**: P1-C1 1.892(3); P1-C4 1.840(3); P1-C5 1.820(3); C1-N1 1.449(3); N1-C7 1.405(2), N2-C6 1.431(3), N2-C2 1.308(4); C2-N4 1.328(3); C1-N3 1.453(3); N3-C3 1.351(3); N4-C3 1.457(4); C3-O1 1.202(4). C5-P1-C1 88.34(12); C5-P1-C4 96.81(12); C4-P1-C1 93.85(12); C6-N2-C2 123.3(2); C7-N1-C1 112.6(2); N2-C2-N4 127.3(2); N1-C1-N3 114.2(2); C2-C1-P1 110.83(18); C2-C1-N1 111.4(2); C2-C1-N3 100.6(2); N1-C1-P1 105.55(17); C2-N4-C3 109.5(2); C1-N3-C3 112.9(2); N3-C3-N4 106.4(2).

6.5 MECHANISTIC STUDIES ON THE FORMATION OF THE 1, 3, 5- DIAZAPHOSPHINANE ANION

Interestingly, the iodophosphane **40** reacted with silver triflate affording one clean product **44** as white powder. Monitoring of the reaction progress via ^{31}P NMR spectroscopy did not reveal any observable intermediate leading to compound **44**.

To further investigate the mechanism for the unexpected formation of **44** instead of the phospholenium cation, the minimum-energy reaction pathway (MERP) for the formation of a model cationic compound **A**, in which the cyclohexyl groups in **44** were replaced by methyl groups and the OTf^- anion is omitted, was calculated at the B3LYP/6-31+G(d,p) level of theory with density functional theory (DFT) (Figure 4). The first intermediate is calculated to be **A_Int1** resulting from the nucleophilic attack of the neighboring carbon to the electron poor phosphorus atom. The P-C bond distance is contracted to 1.93 Å as compared to the relative bond length of

3.25 Å in parent phospholenium cation **A**. The intermolecular cycloaddition rearrangement triggers the positive charge transferring from the phosphorus atom to one of the nitrogen atom. Subsequently, **A_Int1** undergoes a proton transfer cascade rearrangement from its initial position on the carbon atom bonded with the phosphorus atom to neighboring carbon (**A_Int2**), then to the nitrogen atom (**A_Int3**) in sequence. This process is highly exothermic by 37.2 kcal mol⁻¹ as compared to the model compound **A**. Note that, as far as we know, such intramolecular C_{sp}²-H activation process with a cationic phosphorus atom has never been reported before. In a similar manner, this phosphorus atom activated the second aromatic C-H bond to form a zwitterionic heterocycle **A_Int4**. This asymmetric molecule contains two positive charge and one negative charge separated from each other, which makes it the most unstable intermediate through this rearrangement process. Through a proton transfer rearrangement, a C₂-symmetric intermediate **A_Int5** is formed with two positive charge located separately on two nitrogen atom, while the negative charge is centered on phosphorus atom. Finally, after the rearrangement of one P-C bond breaking and one C-C bond forming, the product **B** is formed through a highly exothermic process, which is 55.8 kcal mol⁻¹ more stable than the starting compound **A**. The bulky cyclohexyl groups are believed to favor this rearrangement more than methyl groups, since the bulky cyclohexyl groups should push the phenyl groups closer to the phosphorus atom. Therefore, the highly exothermic process calculated with the model compound is in agreement with our experimental results that no intermediates were observed.

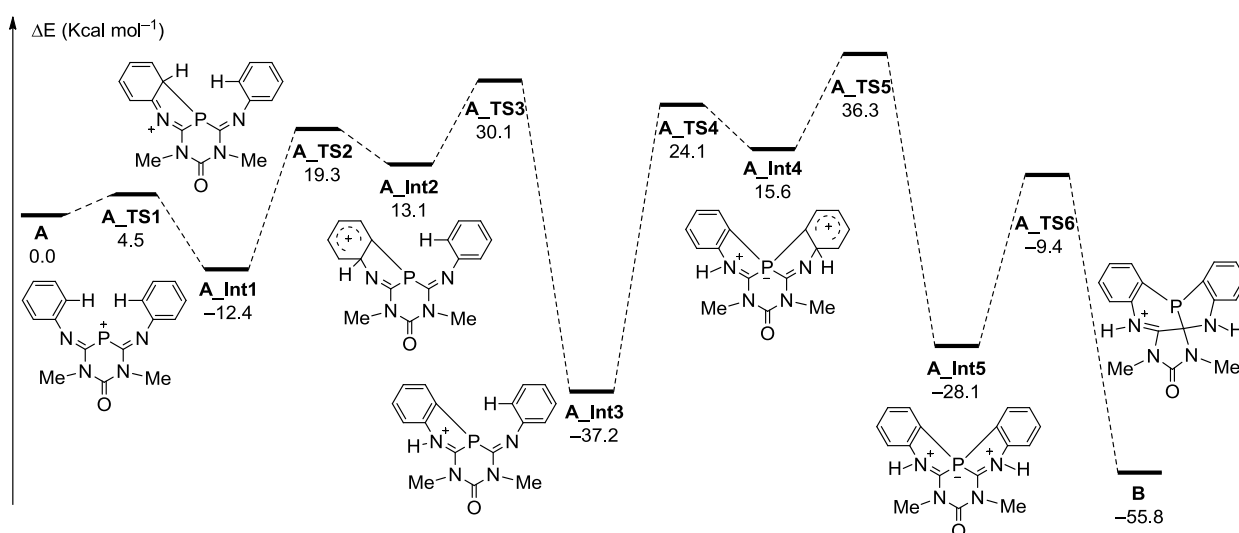
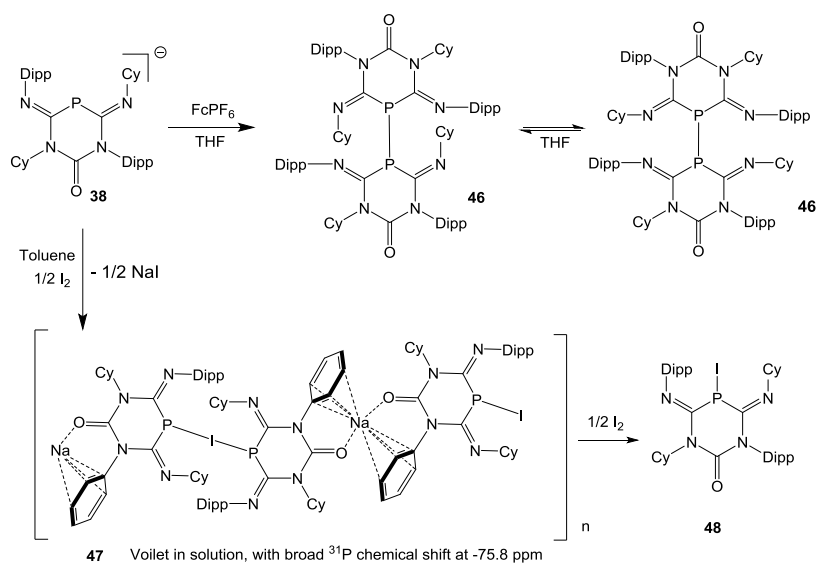


Figure 4 MERP of the formation for the model compound B from phospholenium cations A at the B3LYP/6-31+G(d,p) level, all the structures of minimum–energy intermediates are attached in the figure.

6.6 REACTIVITY OF THE ANIONIC DIAZAPHOSPHINANE **38**

In order to test whether the substituents on **38** are bulky enough to stabilize a phosphorous centered radical, ferrocenium hexafluorophosphate (FcPF_6) was used as one electron oxidizing reagent. Yellow crystals were obtained from saturated n-hexane solution via slow evaporation of the solvent, and were determined to be the diphosphane **46** by X-ray diffraction. The toluene solution of **46** was yellowish and EPR silent. The ^{31}P NMR spectrum of this crystalline compound showed two peaks at -12.5 and -13.9 ppm at room temperature. The temperature dependent ^{31}P NMR spectra of **46** in THF revealed that there are two isomers for **46** (Figure 5). At 257 K, the chemical shift is a doublet at -12.5 ppm with J_{PH} of 3.1 Hz. While the intensity of the singlet at -13.9 ppm increases with rising temperature. As the chemical shifts for the isomers of **46** are close to each other, the difference is attributed to the position of the cyclohexyl substituents. The proton on cyclohexyl substituent is closer to phosphorus in cis isomer (**46**) than that in trans isomer (**46'**). As a result, the doublet in ^{31}P NMR is assigned to chemical shift for **46**, which is the preferred configuration at low temperature. Consequently, the singlet belongs to **46'**, which is the less stable isomer and will dominate at higher temperatures.



Scheme 6 Oxidation of the six-membered ring anion [Na][**38**] with iodine and FcPF₆, the isopropyl groups at the arena rings coordinated to the sodium cations have been omitted for clarity.

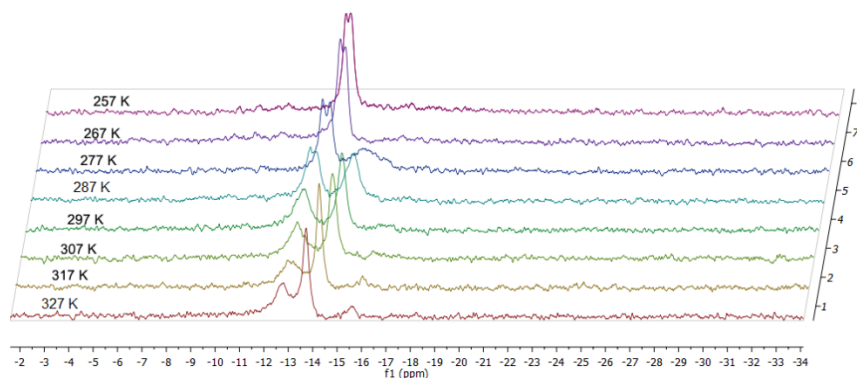


Figure 5 Temperature depended ³¹P NMR spectra for compound **46** for 257 K to 327 K.

After adding half an equivalent of iodine to **38** in toluene, rather than forming diphosphane **46**, the color of the solution turned violet and a broad ³¹P NMR chemical shift at -76.2 ppm was observed. At first it was thought that the phosphorous centered radical species might be obtained in the reaction. However, the solution is still EPR silent. After filtration, the filtrate was left undisturbed and violet crystals formed in half an hour, which were characterized as compound **47** by X-ray diffraction.

When adding one equivalent of I₂ to Na(**38**) in toluene, the iodophosphane **48** was formed with chemical shift at $\delta = -102.3$ ppm in ³¹P NMR. The reactions of both silver triflate and excess iodine with **48** form a mixture which contain a complex mixture of compounds which could not be purified.

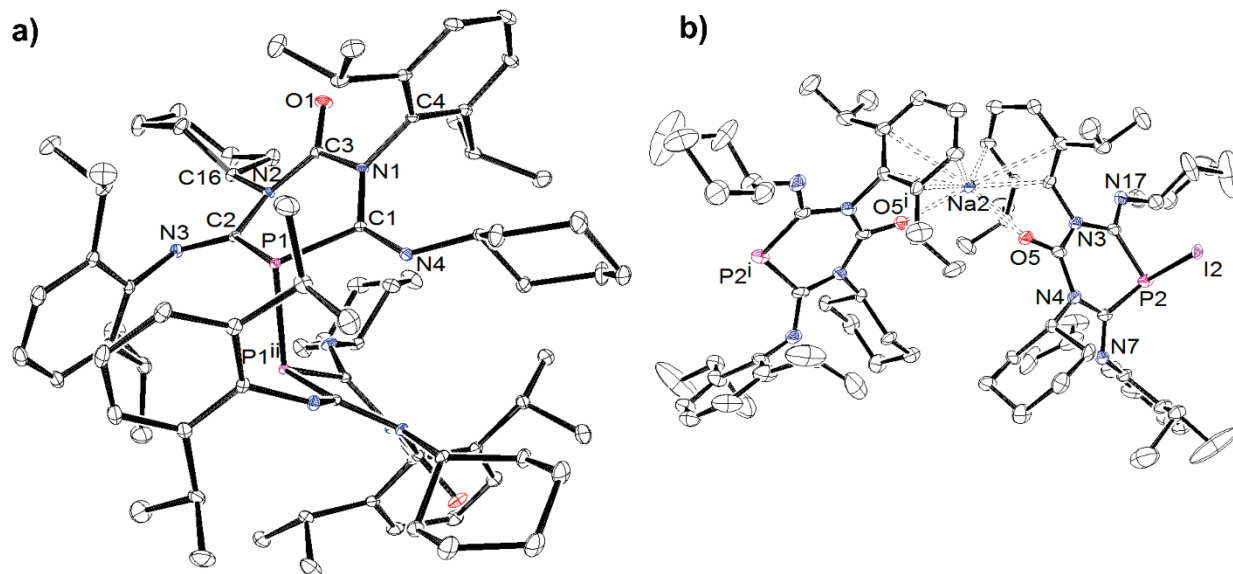
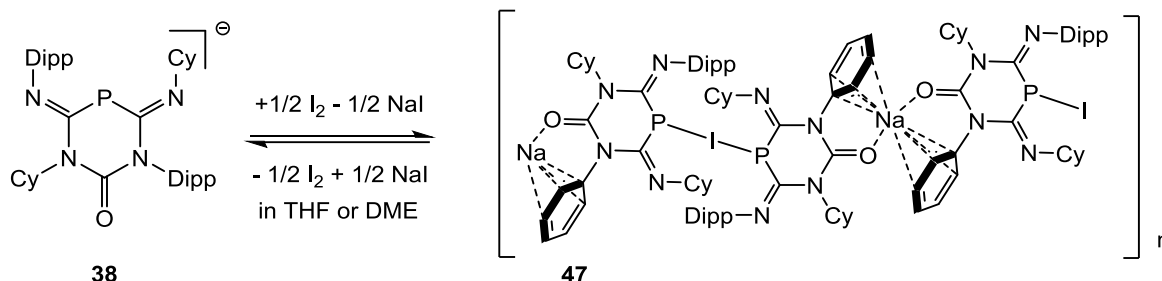


Figure 6 Ortep plot of compound **46** (a) and **47** (b) (thermal ellipsoids are drawn at 50% probability). Hydrogen atoms have been omitted for clarity. Selected bond lengths (Å) and angles (°) **46**: P1-P1ⁱ 2.2278(5), P1-C1 1.8374(10); P1-C2 1.8531(9); C1-N1 1.4183(12); C1-N4 1.2688(12); C3-O1 1.2161(12); N1-C3 1.4104 (12); N2-C3 1.[Na][38]99(12); C2-N2 1.4168(12); C2-N3 1.2704(12). C1-P1-C2 100.98(4); P1-C1-N1 116.44(7); P1-C2-N2 118.58(7); C1-N1-C3 128.21(8); C2-N2-C3 124.28(8); N1-C3-N2 120.285(8).

The solid state of **46** exhibits crystallographic monoclinic symmetry; the asymmetric unit contains one six-membered heterocycle (Figure 6a). To minimize steric repulsion between the Dipp substituents, the atoms of P1 and C2 deviate from the plane formed by the other four atoms of the heterocycle by 0.880 and 0.586 Å, respectively. Application of the symmetric operation, generates the dimeric structure. The P-P bond length is 2.2278(5) Å, which is a typical value for P-P single bonds reported in the literature.¹⁴

The crystals of **47** grew too fast and, as such, disorder in the orientation of the molecules was observed. As a result, the quality of the data is not good enough to allow a structural refinement. However, the gross structure of **47** is seen (Figure 6b). It contains a fascinating chain with diazaphosphinane anions bridged by sodium and iodine alternatively. The sodium cation is coordinated by two oxygen atoms and two aryl rings from two diazaphosphinane anions. The iodine atom is bonded to two phosphorus atoms from two diazaphosphinane units. To the best of knowledge, this is the first example for such a combination between iodine and phosphorus. The observation of **47** indicates that phosphorus radicals are eventually not involved in the formation of diphosphenene **46**. The phenomena is similar for the reaction between iodine and

38 in THF or DME, but the crystals obtained from these solvents were yellowish and proved to be the sodium salts $[\text{Na}(\mathbf{38})]$. This is probably because of that sodium iodide is soluble in THF or DME, there is an equilibrium between **38** and **47** in these solvents (Scheme 7).



Scheme 7 The equilibrium between **38** and **47** in THF or DME

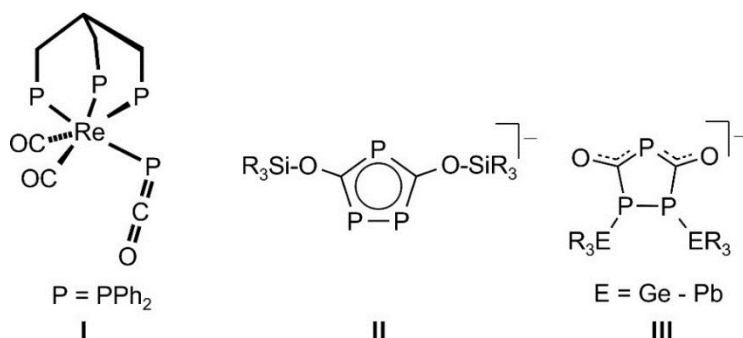
6.7 CONCLUSION

The heterocycles of anionic 1,3,5-diazaphosphinane (**37** and **38**) were obtained by the cycloaddition of $\text{Na}(\text{OCP})$ with carbodiimides. The experimental results revealed that the substituents on carbodiimides will affect the activation barrier of the reaction as well as the conformation and the reactivity of the obtained products. Compound **37** with symmetric conformation was obtained by the reaction of $\text{Na}(\text{OCP})$ and PhNCNCy , in which the phenyl groups were besides the phosphorus atoms. When the carbodiimide (DippNCNCy) with bulky aryl substituents was reacted with $\text{Na}(\text{OCP})$, **38** was formed as a non-symmetric structure. One-electron oxidation of both **37** and **38** will result in the formation of diphosphane. After two-electron oxidation of **37**, the P^+ will activate the carbon-hydrogen bonds on phenyl substituents. DFT calculations were performed to gain deeper insight into the rearrangement mechanism of the insertion of P^+ into the C-H bond on phenyl groups. Additionally, the diphosphane **46** from **38** can be obtained by reacting with FcPF_6 and had two isomers in solution, while a fascinating chain of **47** forms when **38** is treated with half an equivalent of iodine.

7 A STABLE ORGANIC PHOSPHAKETENE AND ITS REACTIVITY

7.1 INTRODUCTION

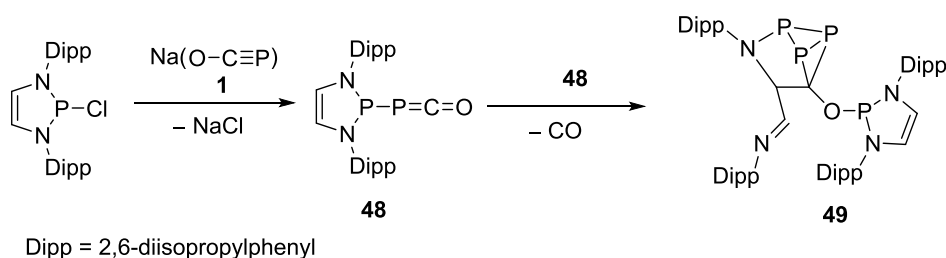
The search and synthesis of new reactive intermediates is an eternally active research field. Often these species allow elegant syntheses of new molecules and materials or help in understanding reaction mechanisms.¹⁸⁵ Prominent examples are carbenes, CR_2 ,¹⁸⁶ and isolobal phosphinidenes, RP ,¹⁸⁷⁻¹⁹⁰ which have not yet been isolated as stable entities. The development of synthetic strategies for precursor molecules which allow the generation or the transfer of such reactive intermediates is therefore an active area of research. Phosphinidene metal complexes, $\text{L}_n\text{M}=\text{PR}$, as spectroscopically observable intermediates¹⁹¹ or even isolated stable compounds are established “RP” transfer reagents for the synthesis of a multitude of organophosphorus compounds.¹⁶⁴ Cummins and co-workers have recently reported a very elegant method which allows the transfer of RP and P_2 units from simple organophosphorus precursor molecules.¹⁹²⁻¹⁹³ We developed a simple large scale synthesis of sodium(phosphaethynolate), $\text{Na}(\text{OCP})$,^{12,194-197} and showed that this serves as a P-transfer reagent with loss of carbon monoxide.¹⁹ Experimental and computational results indicate that phosphaketenes, $\text{R-P}=\text{C}=\text{O}$, are present in these reactions. These are easily obtained in salt metathesis reactions between main group or transition metal halides and $\text{Na}(\text{OCP})$, however, they are remarkably reactive.¹⁹⁸⁻²⁰⁰ So far, only the rhenium(I) phosphaethynolate¹⁹⁸ complex **I** could be fully characterized including a structural analysis using X-ray diffraction methods. Trisorganyl tetrel substituted phosphaketenes, $\text{R}_3\text{E-P}=\text{C}=\text{O}$ ($\text{E} = \text{Si} - \text{Pb}$),¹⁹⁹ show a surprising reactivity and may rearrange into new heterocycles **II**, **III** which contain three phosphorus centers. These reactions proceed under loss of CO and formal transfer of “P⁻” units.²⁰⁰ Since R_3E groups can be regarded as π -acceptor substituents through negative hyperconjugation we became interested in the synthesis of phosphaketenes with π -donor substituents. Note, in this context, computations predict that phosphinidenes with π -donor substituents such as amino or phosphanyl groups lead to stabilized RP species with a singlet ground state.²⁰¹



Scheme 1. A stable Re(I) phosphaketene complex **I** and triphosphaheterocycles **II** and **III** obtained by complex rearrangement reactions of trisorganyl tetrel phosphaketenes, $R_3E-P=C=O$ ($E = Si - Pb$).

7.2 PREPARATION OF THE STABLE ORGANIC PHOSPHAKETENE

The reaction between $Na(OCP)$ (**1**), in form of its dioxane adduct, and simple chlorophosphanes, R_2PCl , yielded inseparable mixtures of products. Reactions with haloamines, R_2N-X , led to oxidation of $Na(OCP)$ to $[Na_2(C_4P_4O_2)]^{202}$ which is not surprising given the rather negative irreversible oxidation potential of the OCP^- anion¹⁹⁸ making this a strong reductant. However, the reaction between **1** and P-chloro-diazaphosphole, with the very bulky bis(2,6-diisopropyl)phenyl substituent (Dipp, Scheme 2) on the nitrogen atoms, leads cleanly to the desired phosphanyl phosphaketene **48** (Scheme 2). This was isolated as a crystalline yellow solid and characterized by structural determination of single crystals by X-ray diffraction. The result is displayed in Figure 1.



Scheme 2. Synthesis of phosphaketenes **48**, and **48** in solution afford phosphorus heterocycles **49**.

The most notable feature of the structure of **48** is the very long P-P distance of 2.4414(5) Å which is much longer than typical P-P distances in diphosphanes (about 2.2 Å),²⁰³⁻²⁰⁶ and even significantly exceeds the distance in the highly sterically crowded diphosphane $[(TMS)_2CH]_2P-P[CH(TMS)_2]_2$ (2.3 Å).²⁰⁷ To the best of our knowledge, the only diazaphospholyl-phospholes with

similar or longer PP bonds than **48** were reported by Burck et al., in systems where it exists as "diazaphospholenium" and "phospholide anion".²⁰⁸⁻²⁰⁹ The P2 center deviates only by 0.236 Å from the plane passing through N1-C8-C9-N2 which supports the assumption that **48** retains a large (diazaphospholenium)⁺ OCP⁻-anion character. The ³¹P NMR data show that **3** preserves its structure in solution indicated by the ¹J_{PP} coupling constant of 253 Hz and the chemical shifts, δ P1 = -233 ppm and δ P2 = 165 ppm. Computations show that the phosphaketene-type isomer, "P-P=C=O", is about 18 kcal mol⁻¹ more stable than the oxy-phosphaalkyne isomer, "P-O-C≡P". This result is in accordance with our previous findings which show that all R₃E-P=C=O compounds (with E = C – Pb) are more stable than R₃E-O-C≡P.¹⁹⁹

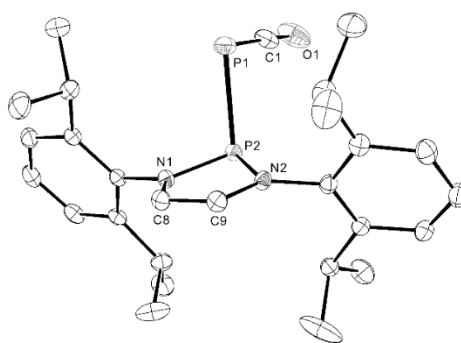


Figure 1. Molecular structure of **48** in the solid state (H atoms omitted for clarity; 50% probability thermal ellipsoids). Selected distances [Å] and angles [°]: P1-P2 2.4414(5), P1-C1 1.6418(14), C1-O1 1.1695(17), P2-N1 1.6965(9), P2-N2 1.6942(9), N1-C8 1.4082(13), C8-C9 1.3361(16), C9-N2 1.4009 (13), O1-C1-P1 179.13(11), C1-P1-P2 86.60(4), P1-P2-N1 102.60(3), P1-P2-N2 101.93(3), P2-N1-C8 112.80(7), P2-N2-C9 113.09(7), N1-C8-C9 111.62(9), C8-C9-N2 111.88(9).

Under an inert atmosphere, solid **48** can be stored for at least a couple of weeks. However, in solution **48** rearranges cleanly, at room temperature over 60 h, to give **49** as the only product. (Scheme 2). This rearrangement is complete in 2 h in toluene at 60 °C.

Species **49** was unequivocally identified as a compound with 1,2,3- triphosphabicyclobutane substructure by X-ray diffraction with a single-crystal which was obtained from a 4:1 acetonitrile / diethylether solution. The structure is shown in Figure 2. The P–P distances within the P₃ unit in this new tricyclic compound are about 2.2 Å, which are close to values previously found for P₃

units.²¹⁰⁻²¹⁴ Clearly **49** is very different from 1,3-diphosphetane-2,4-diones which have been reported as “classical” dimers of other organic phosphaketenes.²¹⁵⁻²¹⁶

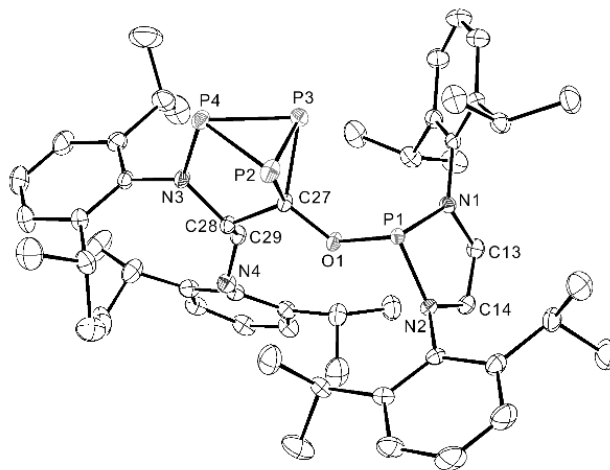
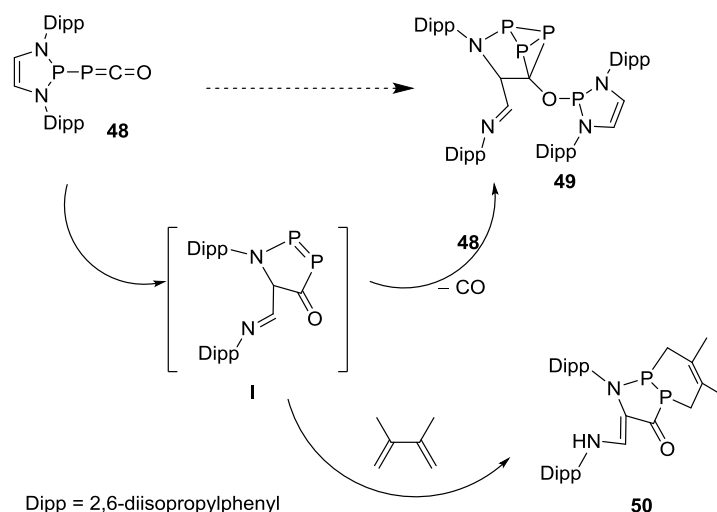


Figure 2. Molecular structure of **49** in the solid state (H atoms omitted for clarity; 50% probability thermal ellipsoids). Selected distances [Å] and angles [°]: P1-N1 1.7061(9), N1-C13 1.4030(15), C13-C14 1.3371(16), C14-N2 1.4157(14), P1-N2 1.6976(10), P1-O1 1.6864(8), O1-C27 1.4019(13), P3-C27 1.8900(12), P2-C27 1.8974(11), C27-C28 1.5250(15), P2-P3 2.2124(5), P3-P4 2.2104(4), P4-P2 2.1922(4), P4-N3 1.7053(10), N3-C28 1.4546(14), C28-C29 1.5041(16), C29-N4 1.2564(15), P1-N1-C13 111.97(8), P1-N2-C14 111.70(8), P1-O1-C27 116.83(7), O1-P1-N1 101.74(4), O1-P1-N2 99.66(4), O1-C27-P3 118.39(7), O1-C27-P2 120.50(7), O1-C27-C28 110.85(9), C27-P3-P4 78.66(3), C27-P3-P2 54.41(3), C27-P2-P4 78.98(3), C27-C28-N3 105.59(9), C27-C28-C29 113.32 (9), C28-C29-N4 119.93(11), P2-P3-P4 59.427(14), P3-P4-P2 60.331(15), P4-P2-P3 60.242(15), P3-P4-N3 96.68(4), P2-P4-N3 97.66(4), P4-N3-C28 115.72(7).

7.3 TRAPPING THE INTERMEDIATE FOR THE DIMERIZATION

As a possible intermediate in the remarkable rearrangement reaction of **48** the cyclic diphosphene **I** is proposed.³³ This may form from **48** via cleavage of one intra-cyclic P–N bond and displacement of the imino unit, RN=CH, with simultaneous insertion of the CO group. The resulting five-membered P₂NC₂ heterocycle is retained in the final product **49** which may result from the reaction of **I** and a second equivalent of “P–PCO” **48** under loss of one CO molecule.



Scheme 3. Rearrangement of phosphaketene **48** and formation of **49** and **50** with **I** as assumed intermediate.

In order to strengthen this hypothesis, a solution of compound **48** was stirred at room temperature in neat 2,3-dimethylbutadiene (2,3-DMB) as trapping agent for **I**. Frequently, 2,3-DMB has been successfully used to capture reactive P–P triple and P–P double bonds.^{217–219} Indeed, after 72 hours at room temperature, 11% of the bicyclic compound **50** with an aza-1,2–diphosphane moiety was isolated together with compound **49** as main product. Compound **50** is the product of the [2+4] Diels-Alder-cycloaddition between the P–P double bond in **I** and the diene unit 2,3–DMB and was isolated in pure form and fully characterized by NMR spectroscopy and single-crystal X-ray diffraction. The structure of **50** is shown in Figure 3.²²⁰

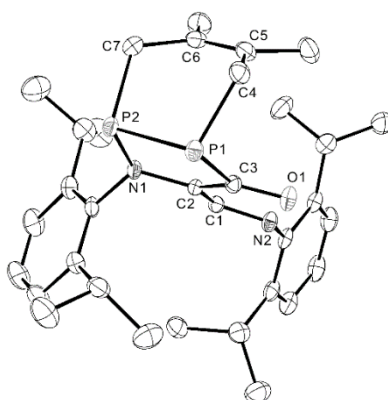
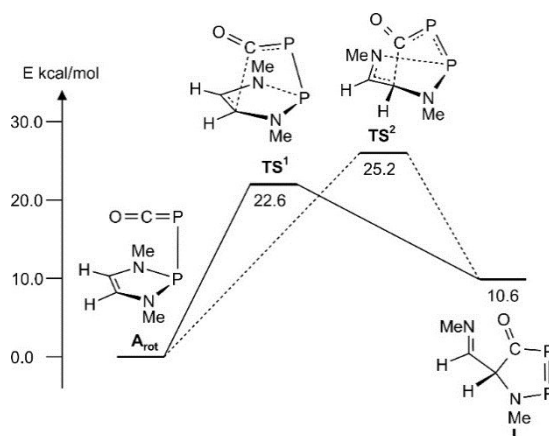


Figure 3. Molecular structure of **50** in the solid state (H atoms omitted for clarity; 50% probability thermal ellipsoids). Selected distances [Å] and angles [°]: P1–P2 2.2064(6), P1–C3 1.8765(16), C3–O1 1.2383(19), C3–C2 1.436(2), C2–C1 1.364(2), C1–N2 1.343(2), C2–N1 1.433(2), N1–P2 1.7239(14), P2–C7 1.873(2), C7–C6

1.501(2), C6-C5 1.337(3), C5-C4 1.505(3), C4-P1 1.874(2), P2-P1-C3 92.23(5), P1-C3-O1 120.52(12), P1-C3-C2 114.89(11), C3-C2-C1 122.16(14), C2-C1-N2 125.43(15), C3-C2-N1 116.39(13), C2-N1-P2 119.37(10), N1-P2-P1 94.04(5), N1-P2-C7 105.64(8), P2-C7-C6 115.72(14), C7-C6-C5 119.53(17), C6-C5-C4 120.08(15), C5-C4-P1 112.33(12), C4-P1-P2 95.80(8), P1-P2-C7 97.61(6).

7.4 COMPUTATIONAL INVESTIGATION ON THE REARRANGEMENT OF **48**

These experiments give strong evidence that the heterocycle **I** with a P=P double is indeed the key intermediate in the reactions shown in Scheme 3. Possible Minimum Energy Reaction Pathways (MERP's) were calculated for the formation of **I** from the phosphanyl phosphaketene (Scheme 4).

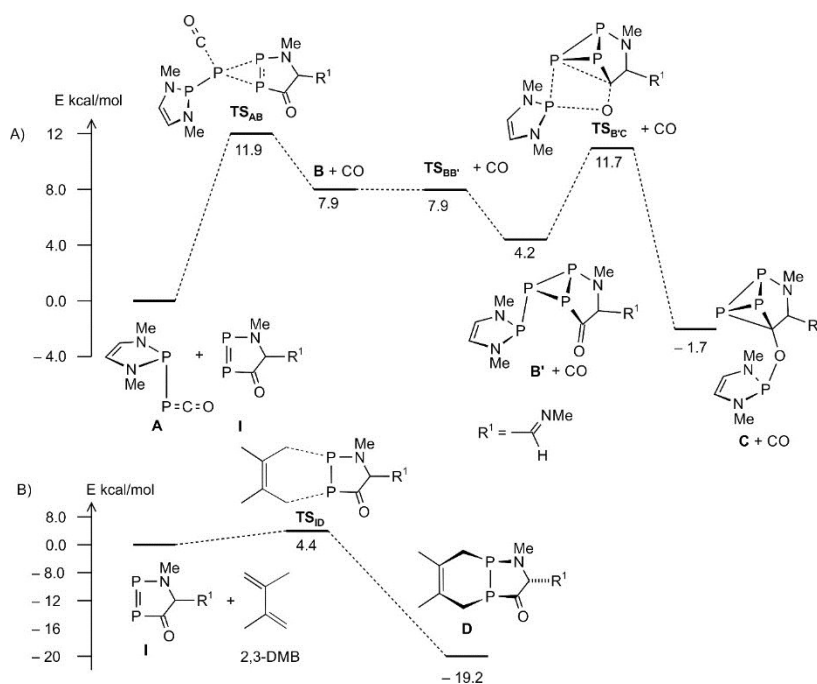


Scheme 4. BP86/RI/def2-TZVP transition path from structure **A_{rot}** to **I**.

In addition, the further rearrangement of **I** to the tricyclic triphosphane **50** (Scheme 5A), as well as the trapping reaction with 2,3-DMB (Scheme 5B) were computed. Model compounds in which the Dipp substituents were replaced by methyl groups were used in calculations at the BP86/RI/def2-TZVP level.

The ground state rotamer **A** with an OCP group turned outwards with respect to the PN₂C₂ heterocycle will not lead to the product **I**. Hence, we investigated its rotamer **A_{rot}** which is only 1 – 2 kcal mol⁻¹ higher in energy. The rearrangement of **A_{rot}** to **I** may proceed via two slightly different reaction pathways as shown in Scheme 4. Educt and product are connected via only one active complex, either **TS¹** or **TS²**. **TS¹** is at slightly lower energy (22.6 kcal mol⁻¹), and the carbon center in the PN₂C₂ heterocycle can be viewed as part of an electron rich *cis*-diamino olefin which

attacks the electrophilic carbon center of the phosphaketene under concomitant opening of the P–N bond on the opposite side. The newly formed C···C interaction (1.9 Å) is rather long while the breaking P–N bond remains rather short (1.9 Å). The opposite is seen in the (25.2 kcal mol⁻¹) **TS**², slightly higher in energy, which better resembles the final product (late TS) with a shorter new C–C (1.6 Å) and longer P···N (2.6 Å) interaction. On both pathways, **I** is formed as product of an endothermic heteroatom Cope-rearrangement ($\Delta H_r = 10.6$ kcal mol⁻¹). The heterocycle **I** reacts further with non-reacted starting material **A** to give a cyclo-triphosphane **B** which, in a practically barrier-less reaction, rearranges to **B'**. Both, **B** and **B'** have very similar structures and are merely rotamers with respect to the orientation of the diazaphosphole unit, (CH)₂(NMe)₂P. The reaction **A** → **B** proceeds via the activated complex **TS**_{AB} in a transition state at 11.9 kcal mol⁻¹ which is the highest barrier along the MERP from **A** to **C**. Note that the activated complex **TS**_{AB} can be viewed as a complex of a phosphanyl phosphinidene, (HC)₂(NMe)₂P–P, coordinated by a CO molecule and the P=P bond in **I**. A similar observation was made for the activated complex computed for the reaction of PH₂⁻ and CO which is best described as a P⁻ anion coordinated by an H₂ and CO molecule.¹⁹⁵ In the final step the diazaphosphol moiety migrates from the *exo*-cyclic phosphorus atom to the C=O group with simultaneous formation of a C–P bond which closes the P₃C cage in **C**. This reaction is associated with a barrier of 7.5 kcal mol⁻¹ at **TS**_{B'c}.

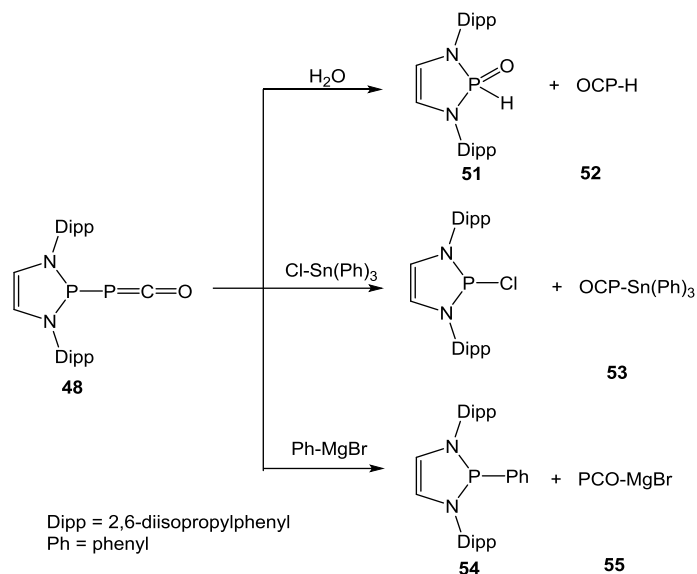


Scheme 5. A) BP86/RI/def2-TZVP transition path from **A** and **I** to **C**. B) BP86/RI/def2-SVP transition path for the Diels-Alder reaction between **I** and 2,3-DMB to **D**.

The MERP of the trapping reaction of the heterocyclic intermediate **I** with 2,3-DMB was also computed. An activated complex **TS_{ID}** with a remarkably low energy (4.4 kcal mol⁻¹) was found for this Diels-Alder type [2+4] reaction, which proceeds with normal electronic demands (the HOMO of the P=P interacts favorably with the LUMO of 2,3-DMB). The product **D** is found to be 19.2 kcal mol⁻¹ more stable than the educt. At first glance the computations are not in accordance with the experimental results, which show that the triphosphabicyclobutane **49** is obtained as major product even when the reaction is performed with 2,3-DMB in large excess as solvent. However, the [2+4] cycloreversion of **D** which leads back to **I** and 2,3-DMB has an activation barrier of 23.6 kcal mol⁻¹ which is in the same range as the Cope-rearrangement **A** → **I** and is accessible under the experimental conditions. Indeed, a kinetic modelling of the reaction starting from the phosphaketene **A**, with the energies shown in Scheme 4 and 5, shows that the reaction evolves slowly to the product **E** which is formed irreversibly because of the loss of the CO. It is possible that the bulky Dipp substituents, instead of methyl substituents, and the inclusion of solvent effects would further favor the formation of the triphosphabicyclobutane **49**.

7.5 THE REACTIVITY OF **48**

The reactivity of the polar P–P bond in **48** with other reagents was studied. The compound **48** reacts with H₂O within a few minutes at room temperature via cleavage of the polar P–P bond to yield 2-oxodiazaphospholene **51** quantitatively (Scheme 3). The PCO moiety can't be detected in the reaction solution, there is only one phosphorus peak with a big H-P coupling constant $^1J_{\text{HP}} = 639$ Hz at a chemical shift $\delta = 2.9$ ppm in the ³¹P NMR spectrum. Actually, we observe gas evolution from the reaction solution. We propose that besides product **51**, the PCO moiety is likely to form the HPCO **52**,²²¹⁻²²² and after rearrangement is released from solution as some gaseous species (Scheme 7). Unfortunately, we failed to trap this species with 2,3-dimethylenebutane. The reactivity of **48** with H₂O is similar to the previous report for such polar P–P bonds.²²³



Scheme 6. The reactivity of **3** with its polar P–P bond.



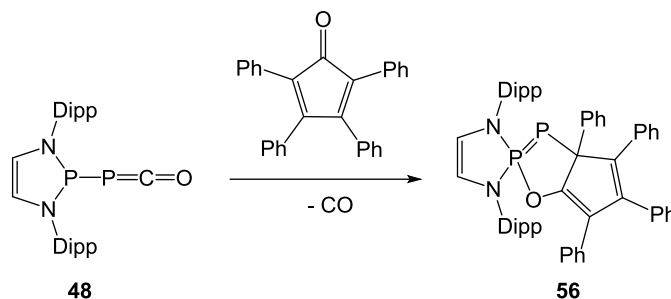
Scheme 7. The proposed decomposition of HPCO.

Diphosphane **48** reacts quantitatively with Ph_3SnCl to yield the chlorodiazaphospholene and OCP-Sn(Ph)_3 **53** at room temperature.²²⁴ In addition to the metathesis reaction with polar single bond, the diphosphane **48** exhibits an interesting reactivity towards the Grignard reagent Ph-MgBr as nucleophile, which yields phenyldiazaphospholene **54** and the alkaline earth metal phosphoethynolate salt PCO-MgBr **55**. In contrast to alkaline earth metal bisphosphoethynolate salts, which are quite unstable,²²⁵ **55** was isolated as grey solid, and it is stable at room temperature under inert atmosphere. From NMR spectroscopic study, the PCO unit coordinates to Mg^{2+} via the oxygen atom and not via the center phosphorus. The carbon phosphorus coupling constant of 60 Hz in **55** is close to the reported value for Na(OCP) of 62 Hz and differs significantly from the value for phosphaketene **48** or the phosphaketene Rhenium complex of 90 Hz.

7.6 COMPOUND **48** AS P–P TRIPLE BOND SOURCE

To a certain extent the reaction between the phosphanyl phosphaketene **48** and the cyclic diphosphene intermediate **I** can be regarded as a Michael-addition of the stabilized OCP^- anion in

48 to the activated P=P-C=O unit of **I**. Therefore the reaction between **48** and the tetracyclone was investigated (Scheme 8).



Scheme 8. Synthesis of the diphosphinylidene **56**.

Through the [2 + 3] cycloaddition reaction between **48** and tetracyclone, it produces phosphanylidene phosphorane **56** by eliminating CO gas (Scheme 4). Phospha-Wittig reagents, such as **56**, are normally very reactive and are especially unstable in solution. Thus there is only limited synthetic viability for the isolation of free phosphanylidene phosphoranes.²²⁶⁻²²⁸ **56** is not only stable in the solid state, but also in solution for several days. Additionally, there are no observable changes in the ^{31}P spectrum after heating to 60 °C for two hours. Formally this corresponds to a cleavage of a P=C double bond. Although there are few similar examples reported of metal assisted reactions.²²⁹⁻²³⁰ The mechanism for this reaction is still not completely clear. **56** was isolated as a yellow solid and has been characterized by single-crystal X-ray crystallography (Figure 4); the short P–P bond distances (2.0688(8) Å) suggest a strong interaction between these two atoms. The NMR spectra (^{31}P , ^{13}C , and ^1H) in benzene- d_6 solution are consistent with the observed solid-state structure, and the ^{31}P data (two doublets with P-P coupling constant $J_{\text{PP}} = 651$ Hz at a chemical shift, $\delta = 115$ and -143 ppm) confirms the existence of the P–P bond.²¹⁷

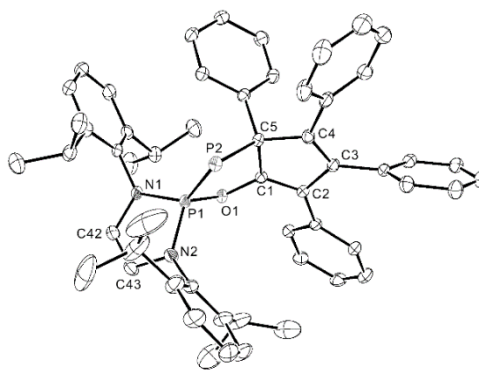


Figure 6. Molecular structure of **56** in the solid state (H atoms omitted for clarity; 50% probability thermal ellipsoids). Selected distances [Å] and angles [°]: P1-P2 2.0688(8), P1-O1 1.6569(16), O1-C1 1.389(3), C1-C2 1.351(3), C1-C5 1.494(3), C2-C3 1.490(3), C3-C4 1.359(3), C4-C5 1.521(3), C5-P2 1.916(2) P1-N1 1.6785(19), P1-N2 1.664(2), N1-C42 1.411(3), C42-C43 1.328(3), C43-N2 1.415(3), O1-P1-P2 102.92(6), O1-P1-N1 101.64(9), O1-P1-N2 113.11(10), N1-P1-P2 130.48(7), N2-P1-P2 116.70(8), N2-P1-N1 91.33(10), C5-P2-P1 89.40(7), C1-O1-P1 109.40(13), C42-N1-P1 111.62(15), C43-N2-P1 112.19(16), C3-C4-C5 109.41(19), C1-C2-C3 105.24(19), C4-C5-P2 114.85(15), C1-C5-P2 103.48(15), C1-C5-C4 100.57(17), O1-C1-C5 117.57(18), O1-C1-C2 127.8(2), C2-C1-C5 114.01(19), C2-C3-C4 110.44(19), C42-C43-N2 111.9(2), C43-C42-N1 112.3(2).

7.7 CONCLUSION

The reaction between Na(OCP) (**1**) and the unsaturated P-chlorophosphanes yields **48** as stable compound in high yield. This compound was isolated and characterized as a phosphanyl phosphaketene with an unusually long P-P bond. This ketene undergoes a variety of unexpected reactions such as a hetero-Cope-rearrangement to a five-membered heterocycle **I** with a P=P double bond. This heterocycle contains a highly reactive P=P bond and could be successfully trapped with a diene in [2+4] Diels-Alder reaction. A phosphanyl phosphinidene, $R_2P\equiv P$, as an intermediate in these reactions reported here is highly unlikely.²³¹

8 SUMMARY AND OUTLOOK

The phosphoethynolate anion $(\text{OCP})^-$ is indeed a valuable building block in phospho-organic chemistry. In present work, a series of phosphorus heterocycles were synthesized and studied. Sodium phosphinin-2-olate was simply synthesized through Diels-Alder reaction of $\text{Na}(\text{OCP})$ with α -pyrone in good yield. The protonation of sodium 2-phosphinin-2-olate formed 2-hydrophosphinine. Rather than 2-hydroxyridine, 2-hydrophosphinine behaved more similar to phenol. The facile functionalization of the sodium 2-phosphinin-2-olate produced a series of compounds containing one-, two- or three- phosphinine rings. These compounds were applied in coordination with $\text{Pd}(\text{II})$ and $\text{Rh}(\text{I})$ forming complexes. $\text{Cu}(\text{I})$ complexes with phosphinito phosphinine ligands showed phosphorescence at room temperature with relatively long decay time.

It will be worthwhile to obtain substituted 2-phosphinin-2-olates, especially on the 5-position. Afterwards, introducing these substituted ones in coordination with metal centers will form complexes with new reactivity and properties. For example, in $\text{Rh}(\text{I})$ complexes, the substituent on 5-position of phosphinine might avoid the coordination of one triphenylphosphine on the vertical axis. At the same time, the substituents on phosphinines will affect the LUMO energy. Consequently the emission wavelength will shift for the corresponding $\text{Cu}(\text{I})$ complexes.

Compared to the common phosphoacetylene (such as *t*BuCP), the chemical behavior of $(\text{OCP})^-$ anion shows fairly unique character and delivers unpredictable reactions. In the reaction of $\text{Na}(\text{OCP})$ with unsaturated compounds (such as alkynes and carbodiimides) they were initiated by the [2+2] cycloadditions. These reactions may proceed under cleavage of C-P triple bond in the $(\text{OCP})^-$ anion. Formally a P^- source is delivered and some unprecedented heterocycles are formed. The CO group either remained in the heterocycles or is released as carbon monoxide. The reactivity of these heterocycles discussed in the present work is dependent on the substituents on the heterocycles. Several unusual compounds were formed by oxidizing these new rings. The application of these cycles as ligands in transition metal complexes is expected to open new perspectives for catalytic or photo-physical research.

The phosphanyl phosphaketene obtained by the reaction of Na(OCP) with P-chlorodiazaphosphole showed different chemical behavior from (OCP)⁻ anion. It also displayed a variety of unexpected reactions. Generally, the reactivity of phosphaketene revealed that the CO group was likely to be released as carbon monoxide during the reaction. The further reactivity of phosphanyl phosphaketene is still under investigation. It has a potential of forming phosphanyl phosphinidene with P-P triple bond, which has not been reported so far.

9 EXPERIMENTAL SECTION

9.1 GENERAL INFORMATION

Unless otherwise noted, all reactions and manipulations were routinely performed under dry nitrogen or argon atmosphere using standard Schlenk techniques. The argon was provided by PANGAS and further purified with an MBraun 100 HP gas purification system. Solvents were distilled under argon from sodium/benzophenone (THF, diethyl ether, n-hexane), sodium (toluene), potassium (DME) or calcium hydride (methylene chloride). Air sensitive compounds were stored and weighed in a glovebox (*M Braun: 150-GI or lab master 130*). Reactions in small quantities were performed within a glovebox. Substances are classified as: *air sensitive*: decompose rapidly on air (seconds to minutes); *slightly air sensitive*: decompose on air in solution in hours and as solid in hours to days, *air stable*: stable on air in solution and as solid (in the period observed, usually days).

Basic chemicals were ordered at ABCR, Acros, Aldrich, Fluka, Lancaster or STREM. Chemicals used for catalysis were purified as described in the corresponding section.

Analytical methods and instruments

NMR

NMR spectra were recorded on *Bruker Avance 500, 400, 300, 250 and 200* spectrometers. The chemical shifts (δ) are measured according to IUPAC^[1] and expressed in parts per million (ppm) relative to TMS, CCl₃, and H₃PO₄ for ¹H, ²H, ¹³C, ¹⁹F and ³¹P respectively. Coupling constants *J* are given in Hertz (Hz) as absolute values, unless otherwise stated. The multiplicity of the signals is indicated as *s, d, t, q, or m* for singlets, doublets, triplets, quartets, or multiplets, respectively. The abbreviation *br.* is given for broadened signals.

IR

IR spectra were recorded on a *Perkin-Elmer-Spectrum 2000* FT-IR-Raman spectrometer with KBr beam splitter (range 500-4000 cm^{-1}). For solid compounds the ATR technique was applied. The absorption bands are described as follows: strong (*s*), very strong (*vs*), middle (*m*), weak (*w*), or broad (*br*).

Elemental Analysis

Elemental analyses were performed by the microanalytical laboratory of the ETH Zürich.

High resolution MS (HiRes MS)

High resolution ESI-MS, EI-MS and MALDI-MS were performed using a Bruker Daltonics maxis ESI-QTOF and a Varian HiResMALDI by ETH Zürich DCHAB/LOC MS-Service. Values are given as *m/z*.

Melting Point

Melting points were determined with a Büchi melting point apparatus and are not corrected.

Computational Methods

The calculation were performed by Dr. Zhongshu Li and Maïke Bergeler.

Method for chapter 2

The molecular orbital calculations have been performed by using the GAUSSIAN 03, vs. 6.1 program package²³² using the BH&HLYP/6-311+G (3df,2p)//BH&HLYP/6-31+G(d) functionals. M. W. Wong and L. Radom have recommended a similar procedure as a good compromise between theoretical accuracy and computational time for molecular orbital calculations of larger systems. The hybrid density functional Becke-half-and-halfLYP (BH&HLYP) is supposed to give more realistic results for the calculation of transition states. All structures were optimized with the basis set 6-31+G(d) and the harmonic vibrational analysis was performed at the same level of theory. All calculations of stable species did not show any imaginary vibration frequencies, while those of the transition state structures were characterized by one imaginary vibration frequency as expected for a saddle point on the potential energy hypersurface of the system. In the case of a transition state, an ICR calculation was performed. The thermal correction of the enthalpy

resulting from the vibrational analysis with BH&HLYP/6-31+G(d) was used to correct the total electronic energy (E_{total}) of the corresponding structure obtained by the single point calculation at the level BH&HLYP/6-311+G(3df,2p). These corrected data (H^{298}) were used to calculate the reaction enthalpies (ΔH^{298} , relative to the combined enthalpies of the educts OCP anion and pyranone molecule) shown in the Table and discussed in the text.

Method for chapter 4

Geometry optimizations were carried out using density functional theory (DFT) using the PBE0 functional within the LANL2DZ ECP basis set. The structural data obtained from the X-ray diffraction studies served as the starting point for the optimization. The unrestricted PBE0 method was used to obtain the energetically lowest triplet state. TD-DFT calculation were performed at the optimized ground state geometry for the singlet and triplet excited states using the same functional and basis sets.

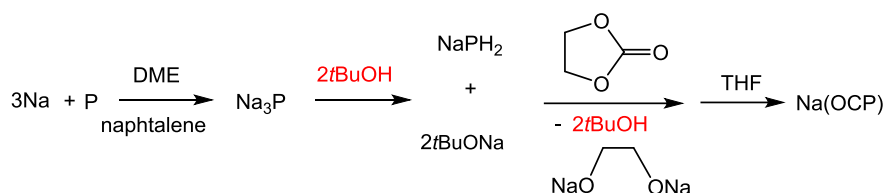
For chapter 6 and 7

We performed density functional calculations with the Turbomole²³³ (versions 6.3.1 and 6.5) and Gaussian²³² (version 09, Revision C.1) program packages. In the Turbomole calculations we employed Ahlrichs' def2-SVP and def2-TZVP basis set²³⁴⁻²³⁵. The BP86²³⁶⁻²³⁷ density functional was chosen in combination with the resolution of the identity (RI) technique and B3LYP²³⁸⁻²⁴⁰. The convergence criterium for the self-consistent-field single-point calculations was set to an energy difference of 10^{-7} hartree between the two last energy iterations and structure optimizations were considered converged when the length of the geometry gradient was below 10^{-4} hartree/bohr. In the Gaussian calculations we employed BP86 with the TZVP basis set.^{234,241} We used the default convergence criteria (scfconv=tight, which means that the energy difference between two iteration steps was less than 10^{-8} hartree, and optimizations were considered converged when the root mean square force was below 3×10^{-4} a.u.). We located the transition state structures by performing a constrained optimization scan with Gaussian, selecting the highest energy structure, calculating the vibrational frequencies and following the lowest eigenvalue mode with the trust-radius image based eigenvector-following procedure

implemented in Turbomole. A preoptimization was carried out with def2-SVP basis set and on the converged structure we performed a TS calculation with def2-TZVP basis set. We performed a vibrational analysis on every structure with vanishing gradient, in order to verify that the structure is a minimum or transition state. The intrinsic reaction coordinates have been calculated with Gaussian to verify that the transition state structure between the correct local minima has been found. Molecular structures were visualized with PyMOL²⁴².

9.2 SODIUM PHOSPHAETHYNOLATE REACTED WITH A-PYRONE

Preparation of Sodium phosphacyanate $[\text{Na}(\text{O}-\text{C}\equiv\text{P})(\text{Dioxane})_{2.5}]_{\infty}$. ($\text{Na}(\text{OCP})$, **1**)

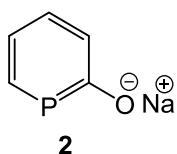


Scheme 1 The synthesis of $\text{Na}(\text{OCP})$

In a 1L schlenk flask equipped with a KPG stirrer, 500ml THF (AR) was added. The whole apparatus was flushed with argon bubble for 20 minutes to get rid of oxygen. In an argon atmosphere, red phosphorus (7 g, 0.226 mol, 1 equiv.), naphthalene (1.5 g, ca. 11.7 mmol) and finely divided sodium (15.6 g, 0.677 mol, 3 equiv.) were added to the flask. The mixture gave a red-brown suspension, which was heated in an oil bath at 60 °C for 24 h, so that the sodium particles stay finely divided and do not form large lumps. During this time, a dark green suspension formed, which was cooled to room temperature. Afterwards, the degassed 10 ml THF solution of $t\text{BuOH}$ (23.77 mL, 0.248 mol, 1.1 equiv.) was added by a dropping funnel to the reaction mixture. After stirring for 3 hours, the reaction flask was immersed in an ice bath, a degassed THF (100ml) solution of ethylene carbonate (19.89 g, 0.226 mol, 1 equiv.) was added dropwise to the flask over a period of 1 hour. The suspension was stirred for another 2 hours at room temperature. Normally the solution becomes too sticky to be filtered. Therefore the mixture was heated at 60 °C overnight and then 2 ml degassed water were added to the mixture to convert $t\text{BuONa}$ into insoluble NaOH . After these operation, the reaction mixture can be easily filtered through a G4

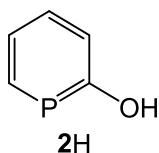
glass frit to remove the insoluble sodium salts. The filtrate was concentrated under reduced pressure to a volume of 100 – 150 mL and layered with 100 mL of dioxane whereby the immediate formation of micro crystals was observed. The yellowish solution was filtered off and the white solid washed with 20 mL of dioxane and dried under high *vacuum*. Finally, 48 g Na(O-C≡P)(dioxane)_{2.5} (yield of 68%) were obtained. The number of dioxane per molecule was determined by ¹H NMR, with naphthalene as the standard.

Sodium phosphinin-2-olate (**2**)



The synthesis of 2H-pyran-2-one can be performed as previously reported. In the glove box, 5mL DME solution of 1.5g 2H-pyran-2-one (15 mmol) was added to a stirring dispersion of 4.5 g Na(O-C≡P)(dioxane)_{2.5} (15 mmol) in 3 mL DME in a 25 mL vial. During that, the solution turned orange with product as red precipitation appearing. To complete the reaction, the reaction mixture was brought out of the box and heated to 60°C in an oil bath under an argon stream. Gas bubbles were observed. After 4 hours heating, the DME solution was removed under reduced pressure. The red sticky precipitate was washed with 20 mL ether to remove all the organic compounds. After that the solid was dried under vacuum. Finally, the pure 1.93g Sodium 2-phosphinin-2-olate was obtained, yield 97%. ¹H NMR (D₆-DMSO, 23°C) δ[ppm]: 8.12 (dd, 1H, ²J_{HP} = 36.5Hz, α-C-H), 7.03 (m, 1H), 6.72 (m, 1H); 6.47 (dd, 1H); ¹³C NMR (D₆-DMSO, 23°C) δ[ppm]: 204.6 (d, ¹J_{CP} = 46.7Hz, α-C-O), 155.2 (d, ¹J_{CP} = 54.3Hz, α-C-H), 131.7 (d, ³J_{CP} = 8.5Hz, γ-C), 123.1 (d, ²J_{CP} = 10.3Hz, β-C), 118.5 (d, ²J_{CP} = 13.9Hz, β-C). ³¹P NMR (D₆-DMSO, 23°C) δ[ppm]: 151.6 (s). IR [golden gate in cm⁻¹]: 3272 (b, CH stretch), 3039, 2975 (wk, CH stretch), 1554 (m, C=CAr), 1520 (wk, C=CAr), 1390(s,P=C), 1332 (s), 1297 (s, C-O), 1186 (s, C-O), 1157 (s), 1115 (s), 1017 (m), 934 (m), 948 (m), 856 (s), 764 (m), 732 (s), 668(wk).

2-Hydroxyphosphinine (**3**):

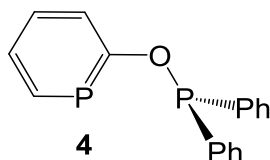


Under the stirring 1 mL 37% HCl(aq) was added drop wise to the 2 mL water solution of 1 g sodium 2-phosphaenolate with the color changing from red to yellow. The mixture was left stirring for 10 minutes, then transferred to a 50 mL separatory funnel and extracted with two 20 mL portions of diethyl ether. After being washed with one 10 mL portion of saturated aqueous sodium chloride, the combined organic extracts are dried over anhydrous sodium sulfate and filtered. Diethyl ether is removed with a rotary evaporator. And the resulting yellow oil can be further purified by silica gel column chromatography (100:10 n-hexanes:diethyl ether) to afford 2-hydroxyphosphinine (506mg, 0.045mol, 60% yield) as a slight yellowish liquid. ^1H NMR (300 MHz, $\text{D}_8\text{-THF}$, 23°C) δ [ppm]: 9.56 (s, 1H, OH), 8.51 (dd, 1H, $^2J_{\text{HP}} = 42$ Hz, $\alpha\text{-C-H}$), 7.34 (2H), 7.15 (1H). ^{13}C NMR (75.5 MHz, $\text{D}_8\text{-THF}$, 23°C) δ [ppm]: 192.7 (d, $^1J_{\text{CP}} = 49.9$ Hz, $\alpha\text{-C-O}$), 154.2 (d, $^1J_{\text{CP}} = 49.3$ Hz, $\alpha\text{-C-H}$), 132.7 (d, $^2J_{\text{CP}} = 14.3$ Hz, $\beta\text{-C}$), 126.9 (d, $^2J_{\text{CP}} = 15.9$ Hz, $\beta\text{-C}$), 121.9 (d, $^3J_{\text{CP}} = 6.7$ Hz, $\gamma\text{-C}$); $^{31}\text{P}\{^1\text{H}\}$ NMR (121.3 MHz, $\text{D}_8\text{-THF}$, 23°C) δ [ppm] 149.0 (d, $J_{\text{PH}}=42$ Hz)

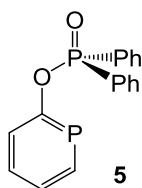
^1H NMR (300 MHz, CDCl_3 , 23°C) δ [ppm]: 5.73 (s, 1H, OH), 8.56 (dd, 1H, $J_{\text{HP}} = 42$ Hz, $\alpha\text{-C-H}$), 7.47 (2H), 7.30 (1H); ^{13}C NMR (75.5 MHz, CDCl_3 , 23°C) δ [ppm]: 188.8 (d, $J_{\text{CP}} = 48.7$ Hz, $\alpha\text{-C-O}$), 153.4 (d, $J_{\text{CP}} = 49.04$ Hz, $\alpha\text{-C-H}$), 132.6 (d, $J_{\text{CP}} = 14.95$ Hz, $\beta\text{-C}$), 127.9 (d, $J_{\text{CP}} = 16.45$ Hz, $\beta\text{-C}$), 121.6 (d, $J_{\text{CP}} = 8.03$ Hz, $\gamma\text{-C}$); $^{31}\text{P}\{^1\text{H}\}$ NMR (121.3 MHz, CDCl_3 , 23°C) δ [ppm]: 148.9 (d, $J_{\text{PH}}=42$ Hz).

IR [golden gate in cm^{-1}]: 3044 (wk, CH stretch), 3025 (wk, CH stretch), 1694 (wk, $\text{C}=\text{C}_{\text{Ar}}$), 1548 (m, $\text{C}=\text{C}_{\text{Ar}}$), 1393(s), 1365 (s), 1297 (s, C-O), 1282 (s, C-O), 1210 (m), 1166 (m), 1117 (m), 1008 (m), 948 (m), 928 (m), 856 (m), 781 (wk), 757 (m), 740 (s), 728 (s), 616 (m).

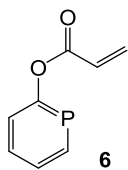
Diphenylphosphinite phosphinine (POP', 4)



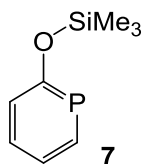
To a solution of 200 mg Ph_2PCI (0.906 mmol) in 10 ml dry THF 121.5 mg sodium phosphin-2-olate (0.906 mmol) were added under an argon atmosphere. After stirring for 10 minutes, the solution was filtered over celite, the filtrate was concentrated by evaporating the solvent leaving a yellow oil as the crude product. The resulting oil can be further purified by alumina column chromatography (n-hexane/diethyl ether 1:1). The filtrate was concentrated under reduced pressure to give **4** (230 mg) as a colorless oil, yield 85.2%. NMR data of **4**: ^1H NMR (300 MHz, $\text{D}_8\text{-THF}$, 300 K) δ [ppm]: 8.51 (dd, 1H, $^2J_{\text{HP}} = 43.2$ Hz, $\alpha\text{-C(H)}$ of phosphinine), 7.59-7.35 (m 13H). ^{13}C NMR (75.5 MHz, $\text{D}_8\text{-THF}$, 300 K) δ [ppm]: 189.3 (dd, $^1J_{\text{CP}} = 45.8$ Hz, $^2J_{\text{CP}} = 14.2$ Hz, $\alpha\text{-C-O}$ of phosphinine), 152.7 (dd, $^1J_{\text{CP}} = 47.3$, $^4J_{\text{CP}} = 9.6$ Hz, $\alpha\text{-C}$ of phosphinine), 138.4 (d, $^2J_{\text{CP}} = 17.1$ Hz, $\beta\text{-C}$ of phosphinine), 133.3 (t, $^2J_{\text{CP}} = 14.2$ Hz, $\beta\text{-C}$ of phosphinine), 132.1 (d, $^1J_{\text{CP}} = 25.4$ Hz, phenyl-C), 130.5 (s, phenyl-C), 129.0 (s, phenyl-C), 128.8 (d, $^3J_{\text{CP}} = 6.2$ Hz, phenyl-C), 126.1 (t, $^3J_{\text{CP}} = 7.8$ Hz, $\gamma\text{-C}$ of phosphinine). ^{31}P NMR (121.3 MHz, $\text{D}_8\text{-THF}$, 300 K) δ [ppm]: 163.6 (d, $^3J_{\text{PP}}=97.5$ Hz, phosphinine-P), 114.5 (d, $^3J_{\text{PP}}=97.5$ Hz, diphenylphosphine-P).



To a solution of 45 mg $\text{Ph}_2\text{P(O)Cl}$ (0.190 mmol) in 5ml dry THF 30 mg sodium phosphin-2-olate (0.172 mmol) were added under argon atmosphere. After stirring for 10 minutes, the solvent was evaporated under reduced pressure and benzene was used to dissolve the resulting solid. The solution was filtered by celite, the filtration was concentrated until it become sticky. Adding n-hexane drop by drop, leads to the formation of colorless crystals of compound **5**. ^1H NMR (300 MHz, $\text{D}_8\text{-THF}$, 23°C) δ [ppm]: 8.51 (dd, 1H, $J_{\text{HP}} = 43.2$ Hz, $\alpha\text{-C-H}$), 7.59-7.35 (mm 13H). ^{13}C NMR (100.5 MHz, $\text{D}_8\text{-THF}$, 23°C) δ [ppm]: 192.4 (dd, $^1J_{\text{CP}} = 47.4\text{Hz}$, $^2J_{\text{CP}} = 12.5\text{Hz}$, Phosphinine $\alpha\text{-C-O}$), 154.0 (dd, $^1J_{\text{CP}} = 52.5$ Hz, Phosphinine $\alpha\text{-C-H}$), 141.2 (d, $J_{\text{CP}} = 18.2$ Hz, phenyl C-P), 134.8 (t, $J_{\text{CP}} = 13.1$ Hz, Phosphinine $\beta\text{-C}$), 132.2 (d, $J_{\text{CP}} = 14.8$ Hz, Phosphinine $\beta\text{-C}$), 131.3 (d, $J_{\text{CP}} = 22.4$ Hz, phenyl C), 130.2 (s, phenyl C), 129.1(s, phenyl C), 128.8 (d, $J_{\text{CP}} = 7.1$ Hz, phenyl C), 125.9 (t, $J_{\text{CP}} = 8.2$ Hz, Phosphinine $\gamma\text{-C}$). ^{31}P NMR (121.5 MHz, THF, 23°C) δ [ppm]: 177.6 (d, $J_{\text{PP}}=10.9$ Hz), 30.2 (d, $J_{\text{PP}}=10.9$ Hz).



Under stirring, a 2 mL THF solution of 20 mg acryloyl chloride (0.22 mmol) was added drop wise to a 2 mL THF solution of 38 mg (0.22 mmol) sodium 2-phosphaenolate. The mixture was left stirring for 20 minutes and then filtered. The filtrate was concentrated by evaporating the solvent leaving a yellow oil as product. The resulting oil can be further purified by silica gel column chromatography (100:10 diethyl ether:ethyl acetate) to afford compound **6** (25mg) as a slight yellowish oil. ^1H NMR (250 MHz, CD_3CN , 23°C) δ [ppm]: 8.51 (dd, 1H, $J_{\text{HP}} = 42.5$ Hz, α -C-H), 7.64 (m, 3H), 6.65 (1H), 6.44 (m, 1H), 6.14 (dd, 1H). ^{13}C NMR (100.5 MHz, CD_3CN , 23°C) δ [ppm]: 184.2 (d, $J_{\text{CP}} = 47.7$ Hz, phosphinine α -C-O), 166.2 (d, $J_{\text{CP}} = 2.5$ Hz, CO), 156.5 (d, $J_{\text{CP}} = 51.1$ Hz, phosphinine α -C-H), 134.3 (s, ethylene C), 133.4 (d, $J_{\text{CP}} = 15.5$ Hz, phosphinine β -C), 133.3 (d, $J_{\text{CP}} = 14.7$ Hz, phosphinine β -C), 130.4 (d, $J_{\text{CP}} = 10.84$ Hz, phosphinine γ -C), 129.2 (d, $J_{\text{CP}} = 1.9$ Hz, ethylene C-CO); ^{31}P NMR (CH_3CN , 23°C , 121.5 MHz) δ [ppm]: 177.0



Compound **7** was prepared using the similar procedure as for compound **6**, trimethylsilyl chloride was used instead of acryloyl chloride. A colorless liquid was obtained for **7**. ^1H NMR (250 MHz, D_8 -THF, 23°C) δ [ppm]: 8.46 (dd, 1H, $J_{\text{HP}} = 45$ Hz), 7.591-7.358 (mm 3 H), 0.32 (mm 9H), ^{31}P NMR (D_8 -THF, 23°C , 121.5 MHz) δ [ppm]: 168.9.

pK_a Value for 2-hydroxyphosphinine (3):

A slight by orange solution of 2-hydroxyphosphinine (14 mg in 6.0 mL of water) was prepared. Subsequently a series of diluted solutions was prepared. With an Eppendorf pipette, 200 μL of the stock solution was placed in 12 different volumetric flasks (25 mL). For the dilution, twelve

0.02 M buffer solutions adjusted at the following pH values were used: 4.5, 6.0, 6.9, 7.8, 8.2, 8.5, 8.8, 9.2, 9.5, 10.0, 10.2, 11.9. The buffer solutions were prepared using NaOAc / HOAc or NH₄Cl / NaOH. The UV-Vis spectrum for each of the twelve solutions was recorded employing the corresponding buffer solution as blank. Subsequently the pH value was measured with a pH-meter. The pH values registered at 20°C were: 4.39, 5.99, 6.79, 7.31, 7.63, 7.78, 7.97, 8.38, 8.98, 9.81, 10.13 and 11.86. Data were recorded based on the absorbance at the maximum of $\lambda_{\max} = 346$ nm versus pH values.

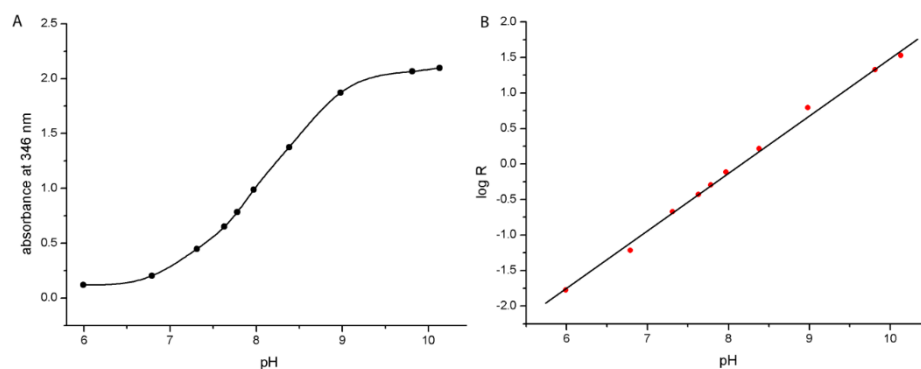


Figure. 1: A) Absorbance at 346 nm of **2** at different pH values in 0.2 M solutions. B) At 346 nm log R vs pH plot.

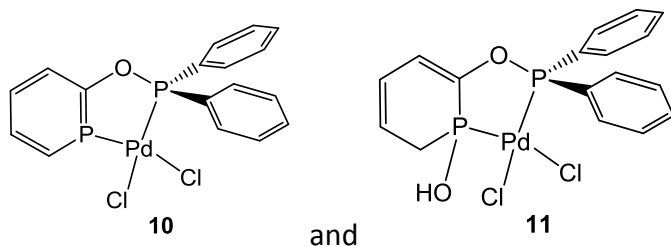
When $\text{pH} \gg \text{pK}_a$, **2** will be ionized completely in solution, the absorbance will belong to phosphinin-2-olate ions; in contrast, $\text{pH} \ll \text{pK}_a$, the absorbance is due to the contribution of unionized compound. Consequently, A_{H^0} 's absorbance equals to **2**'s in solution of $\text{pH} = 4.39$, while A_{ion^0} 's equals to **2**'s in solution of $\text{pH} = 11.5$.

$$\log R = \log \left[\frac{A - A_{\text{H}^0}}{A_{\text{ion}^0} - A} \right]$$

When $\log R = 0$, $\text{pH} = \text{pK}_a$. The line plot of equation $\log R = 0.8185 \text{ pH} - 6.6733$ in Figure 1 was fitting the experimental data well with agreement factor of $R^2 = 0.997$. As a result, when $\log R = 0$, $\text{pH} = 8.158$.

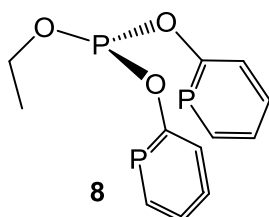
9.3 COORDINATION STUDIES WITH PHOSPHININE DERIVATIVES

Diphenylphosphinite phosphinine reacted with Pd(II)

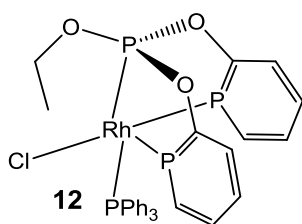


As diphenylphosphinite phosphinine is very sensitive to water, it was better to use the fresh ones for the further reactions. To the stirred 2 ml THF solution of complex $[\text{Pd}(\text{NCPH})_2\text{Cl}_2]$ (40 mg), compound **4** (36 mg oil of compound **4** diluted by 1 ml THF) was added drop wise. During 10 minutes stirring, the mixture turned from yellow to red and was filtered by celite. After one day, the crystals of complex **10** were obtained (yield: 50 mg, 94.2%). Complex **11** was obtained by adding two drops of water to the solution of complex **10** (48 mg, 92.1%). NMR for **10**: ^1H NMR (300 MHz, CD_2Cl_2 , 300 K) δ [ppm]: 8.37 (dd, 1H, $^2J_{\text{HP}} = 45.2$ Hz, $\alpha\text{-C(H)}$ of phosphinine), 7.55-7.21 (m, 13H). ^{13}C NMR (75.5 MHz, CD_2Cl_2 , 300 K) δ [ppm]: 181.4 (dd, $^1J_{\text{CP}} = 34.5$ Hz, $^2J_{\text{CP}} = 7.6$ Hz, $\alpha\text{-C-O}$ of phosphinine), 161.5 (dd, $^1J_{\text{CP}} = 44.1$, $\alpha\text{-C}$ of phosphinine), 141.5 (d, $^2J_{\text{CP}} = 16.2$ Hz, $\beta\text{-C}$ of phosphinine), 132.6 (t, $^2J_{\text{CP}} = 9.15$ Hz, $\beta\text{-C}$ of phosphinine), 131.8 (d, $^1J_{\text{CP}} = 21.3$ Hz, phenyl-C), 130.1 (s, phenyl-C), 129.4 (s, phenyl-C), 128.5 (d, $^3J_{\text{CP}} = 5.0$ Hz, phenyl-C), 126.1 (t, $^3J_{\text{CP}} = 6.1$ Hz, $\gamma\text{-C}$ of phosphinine). ^{31}P NMR (101.3 MHz, CD_2Cl_2 , 23°C) δ [ppm]: 164.96 (d, $^3J_{\text{PP}} = 20.3$ Hz), 156.88 (d, $^3J_{\text{PP}} = 20.3$ Hz); NMR for **11**: ^1H NMR (300 MHz, CD_2Cl_2 , 300 K) δ [ppm]: 7.59-7.35 (m, 13H), 4.39 (dd, 1H, $^2J_{\text{HP}} = 20.3$ Hz, 2H, $\alpha\text{-C(H)}$). ^{13}C NMR (75.5 MHz, CD_2Cl_2 , 300 K) δ [ppm]: 166.2 (dd, $^1J_{\text{CP}} = 36.2$ Hz, $^2J_{\text{CP}} = 4.5$ Hz), 140.7 (d, $^2J_{\text{CP}} = 20.2$ Hz), 133.9 (t, $^2J_{\text{CP}} = 11.3$ Hz), 132.1 (d, $^1J_{\text{CP}} = 22.5$ Hz, phenyl-C), 131.1 (s, phenyl-C), 129.1 (s, phenyl-C), 128.9 (d, $^3J_{\text{CP}} = 7.08$ Hz, phenyl-C), 125.9 (t, $^3J_{\text{CP}} = 8.7$ Hz), 42.3 (d, $^1J_{\text{CP}} = 45.7$ Hz). ^{31}P NMR (101.3 MHz, CD_2Cl_2 , 23°C) δ [ppm]: 151.86 (d, $J_{\text{PP}} = 41.3$ Hz), 100.88 (d, $J_{\text{PP}} = 41.3$ Hz).

Ethyl diphosphininylphosphinite (**8**)

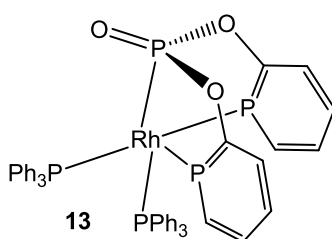


To a solution of 200 mg Ethyl dichlorophosphite (1.370 mmol) in 10 ml dry THF 367.5 mg sodium phosphoethynolate (2.741 mmol) were added under argon atmosphere. After stirring for 10 minutes, the solution was filtered by celite, the filtration was concentrated by evaporating all the solvent leaving yellow oil as a crude product. As the resulting oil can be further purified by silica-gel column chromatography (n-hexane/diethyl ether 1:1), the filtration was concentrated under reduced pressure to give **8** (350 mg) as a colorless oil, yielding 85.7%. NMR data of **8**: ^1H NMR (300 MHz, CDCl_3 , 23°C) δ [ppm]: 8.52 (dd, 2H, $^2J_{\text{HP}} = 41.8$ Hz, $^4J_{\text{HP}} = 9.9$ Hz, $\alpha\text{-C(H)}$ of phosphinine), 7.40-7.65 (m, 6H), 4.24 (m, 2H), 1.31 (t, 3H). ^{13}C NMR (75.5 MHz, $\text{D}_8\text{-THF}$, 23°C) δ [ppm]: 185.3 (dd, $^1J_{\text{CP}} = 48.2$ Hz, $^2J_{\text{CP}} = 8.82$ Hz, $\alpha\text{-C-O}$ of phosphinine), 153.4 (dd, $^1J_{\text{CP}} = 51.9$ Hz, $^4J_{\text{CP}} = 4.78$ Hz, $\alpha\text{-C}$ of phosphinine), 131.7 (m, $\gamma\text{-C}$ of phosphinine), 129.6 (d, $^2J_{\text{CP}} = 16.7$ Hz, $\beta\text{-C}$ of phosphinine), 127.1 (m, $\beta\text{-C}$ of phosphinine), 59.6 (s, $-\text{OCH}_2\text{CH}_3$), 16.7 (t, $^3J_{\text{CP}} = 4.04$ Hz, $-\text{OCH}_2\text{CH}_3$). ^{31}P NMR (121.3 MHz, $\text{D}_8\text{-THF}$, 23°C) δ [ppm]: 169.568 (d, $^3J_{\text{PP}} = 73.8$ Hz, phosphinine-P), 128.984 (t, $^3J_{\text{PP}} = 73.8$ Hz, diphenylphosphine-P).

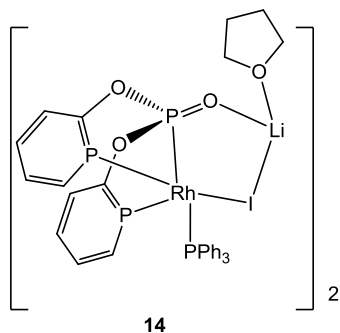


To a stirred solution of $[\text{RhCODCl}]_2$ (56.47 mg, 0.168 mmol) in THF (10 ml) triphenylphosphine (87.97 mg, 0.335 mmol) was added at room temperature. After 5 minutes of vigorous stirring, Ethyl diphosphinylphosphinite **8** (100 mg, 0.335 mmol) were added to the reaction mixture drop wise. During that, the solution turned red with orange precipitates. The reaction mixture was stirred for another 10 min, the orange precipitates were collected by filtration and washed with 1 ml dry THF two times. After that the solid was dried under vacuum. Finally, the pure 150 mg complex **12** was obtained, yielding 64%. NMR data of **12**: ^1H NMR (300 MHz, CD_2Cl_2 , 23°C) δ [ppm]: 7.61-7.10 (br, 21H, H_{ar}), 7.13-7.04 (br, m, 4H, phosphine-H), 6.60 (m, 2H, phosphine-H), 4.57 (m, 2H), 1.44 (t, 3H); ^{13}C NMR (75.5 MHz, CD_2Cl_2 , 23°C) δ [ppm]: 169.8 (dd, $^1J_{\text{CP}} = 22.7$ Hz, $^2J_{\text{RhC}} = 8.13$ Hz $\alpha\text{-C-O}$ of phosphinine), 134.2 (d, $^1J_{\text{CP}} = 12.3$ Hz, Aromatic-C), 133.5 (t, $^1J_{\text{CP}}/^2J_{\text{RhC}} = 12.1$ Hz,

α -C of phosphinine), 133.2 (m, γ -C of phosphinine), 130.7 (s, Aromatic-C), 130.5 (d, $^2J_{CP} = 10.5\text{Hz}$, β -C of phosphinine), 130.1 (s, Aromatic-C), 128.5 (d, $^1J_{CP} = 10.5\text{Hz}$, Aromatic-C), 128.2 (d, $^1J_{CP} = 9.9\text{Hz}$, β -C of phosphinine), 122.9 (d, $^1J_{CP} = 11.5\text{ Hz}$, $^2J_{RhC} = 11.09$, Aromatic-C), 119.9 (d, $^1J_{CP} = 19.7\text{Hz}$, Aromatic-C), 65.7 (s, $-\text{OCH}_2\text{CH}_3$), 15.9 (t, $^3J_{CP} = 7.9\text{ Hz}$, $-\text{OCH}_2\text{CH}_3$). $^{31}\text{PNMR}$ (121.3 MHz, CD_2Cl_2 , 23°C): δ [ppm]: 210.4-203.2 (ddt, $^2J_{PP} = 516.3\text{Hz}$, $^1J_{RhP} = 148.3\text{Hz}$, $^2J_{PP} = 32.6\text{Hz}$, phosphite-*P*), 172.7-170.8 (dm, $^1J_{RhP} = 191.5\text{Hz}$, $^2J_{PP} = 50.0\text{Hz}$, $^2J_{PP} = 32.7\text{Hz}$, phosphinine-*P*), 37.2-30.7 (dm, $^2J_{PP} = 516.3\text{Hz}$, $^1J_{RhP} = 93.1\text{Hz}$, $^2J_{PP} = 49.8\text{Hz}$, triphenylphosphine-*P*). Anal. Calcd for $\text{C}_{31}\text{H}_{29}\text{O}_3\text{P}_4\text{Cl}_4\text{Rh}$: C, 45.51; H, 3.57. Found: C, 45.71; H, 3.63.



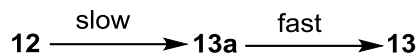
To a stirred suspension of complex **13** (69.8 mg, 0.1 mmol) in THF (5 ml) triphenylphosphine (35.8 mg, 0.12 mmol) were added, after 10 minutes of vigorous stirring, the solution turned yellow together with yellow precipitates. The yellow precipitates were collected by filtration and washed with 1 ml dry THF for 2 times. After that the solid was dried under vacuum. Finally, the pure 88 mg complex **13** was obtained, yielding 64%. NMR data of **13**: $^1\text{HNMR}$ (300 MHz, CD_2Cl_2 , 23°C) δ [ppm]: 7.49-7.05 (br, 36H, H_{ar}), 6.82 (mm 2H, H_{ar}). $^{13}\text{CNMR}$ (75.5 MHz, CD_2Cl_2 , 23°C) δ [ppm]: 185.3 (dd, $^1J_{CP} = 48.2\text{Hz}$, $^2J_{CP} = 8.8\text{Hz}$, α -C-O of phosphinine), 153.4 (dd, $^1J_{CP} = 51.9\text{Hz}$, $^4J_{CP} = 4.7\text{Hz}$, α -C of phosphinine), 131.7 (m, γ -C of phosphinine), 129.6 (d, $^2J_{CP} = 16.7\text{Hz}$, β -C of phosphinine), 127.19 (m, β -C of phosphinine), 59.6 (s, $-\text{OCH}_2\text{CH}_3$), 16.7 (t, $^3J_{CP} = 4.0\text{Hz}$, $-\text{OCH}_2\text{CH}_3$). $^{31}\text{PNMR}$ (161.9 MHz, CD_2Cl_2 , 23°C) δ [ppm]: 177.5-175.6 (m, phosphinine-*P*), 158.3-154.4 (dm, $^2J_{PP} = 418.6\text{ Hz}$, $^1J_{RhP} = 142.1\text{Hz}$, $^2J_{PP} = 49.1\text{ Hz}$, $^2J_{PP} = 24.6\text{Hz}$, phosphite-*P*), 42.4-39.3 (dm, $^2J_{PP} = 418.6\text{Hz}$, triphenylphosphine-*P* trans to phosphite-*P*), 28.7-26.5 (mm, $^2J_{PP}=418.6\text{Hz}$, triphenylphosphine-*P* cis to phosphite-*P*). Anal. Calcd for $\text{C}_{46}\text{H}_{42}\text{O}_3\text{P}_5\text{Rh}$: C, 61.35; H, 4.70. Found: C, 61.41; H, 4.68.



To a stirred suspension of complex **12** (69.8 mg, 0.1 mmol) in THF (5 ml) LiI (16 mg, 0.12 mmol) were added, the solution turned clear red immediately. However, ^{31}P NMR shifts showed that the ethyl group is still on the phosphite. After heating at 60 °C overnight, ^{31}P NMR shifts showed the reaction completed, the mixture was filtered and the filtrate was concentrated. The resulting solid was washed with n-hexane to give the complex **6**. Single crystals were obtained by diffusion of n-hexane in THF (82 mg, yields 92.6%). NMR data of **14**: ^1H NMR (300 MHz, CD_2Cl_2 , 23°C) δ [ppm]: 7.56-7.01 (br, 21H, H_{ar}), 6.91 (m, 2H, H_{ar}), 3.58 (m, 4H), 1.74 (t, 4H). ^{13}C NMR (75.5 MHz, CD_2Cl_2 , 23°C) δ [ppm]: 170.7 (dbr, $^1J_{\text{CP}} = 29.1\text{Hz}$, $\alpha\text{-C-O}$ of phosphinine), 136.0 (dd, $^1J_{\text{CP}} = 46.1\text{Hz}$, $^2J_{\text{RHC}} = 8.0\text{Hz}$, $\alpha\text{-C}$ of phosphinine), 134.5 (br, Aromatic-C), 134.3 (br, Aromatic-C), 133.5 (m, $\gamma\text{-C}$ of phosphinine), 130.1 (s, Aromatic-C), 128.8 (d, $^2J_{\text{CP}} = 8.6\text{ Hz}$, $\beta\text{-C}$ of phosphinine), 128.4 (d, $^1J_{\text{CP}} = 10.1\text{Hz}$, Aromatic-C), 122.3 (t, $^1J_{\text{CP}} / ^2J_{\text{RHC}} = 10.9\text{Hz}$, Aromatic-C), 119.2 (d, $^1J_{\text{CP}} = 9.5$, $\beta\text{-C}$ of phosphinine), ^{31}P NMR (121.3 MHz, $\text{D}_8\text{-THF}$, 23°C) δ [ppm]: 174.5-170.3 (dm, $^1J_{\text{RhP}} = 201.0\text{Hz}$, $^2J_{\text{PP}} = 48.2\text{Hz}$, $^2J_{\text{PP}} = 32.2\text{Hz}$, phosphinine-P), 172.7-170.8 (dm, $^2J_{\text{PP}} = 476.4\text{Hz}$, $^1J_{\text{RhP}} = 131.1\text{Hz}$, $^2J_{\text{PP}} = 32.2\text{Hz}$, phosphite-P), 39.2-34.2 (dm, $^2J_{\text{PP}} = 476.4\text{Hz}$, $^1J_{\text{RhP}} = 97.4\text{Hz}$, $^2J_{\text{PP}} = 46.9\text{Hz}$, triphenylphosphine-P). Anal. Calcd for $\text{C}_{64}\text{H}_{62}\text{Li}_2\text{O}_8\text{P}_8\text{Rh}_2\text{I}_2$: C, 45.74; H, 3.72. Found: C, 45.99; H, 3.67.

Kinetic measurement and analysis for the dealkylation of **12**

From the studies of the reaction for the dealkylation of **12**, the reaction is relatively slow. According to ^{31}P NMR spectrum, once adding one equivalent triphenylphosphine to the solution of **12** in DCM, the intermediate **13a** was formed. So we assumed the speed of the reaction for **12** converting to **13a** is very high, the barrier step is the dealkylation from **13a** to **13**.



The ^{31}P NMR data for kinetic analysis were acquired on Bruker-200 spectrometers. All integrals were normalized versus the started concentration of **13a** and plotted versus the time. The values of the integrals were fit by a non-linear least squares method to the first order equations $[13a] = Ae^{-kt}$ and $[13] = B - Ce^{-kt}$ (where A, B, C and k were allowed to vary freely) using the automated routine of Gnuplot.

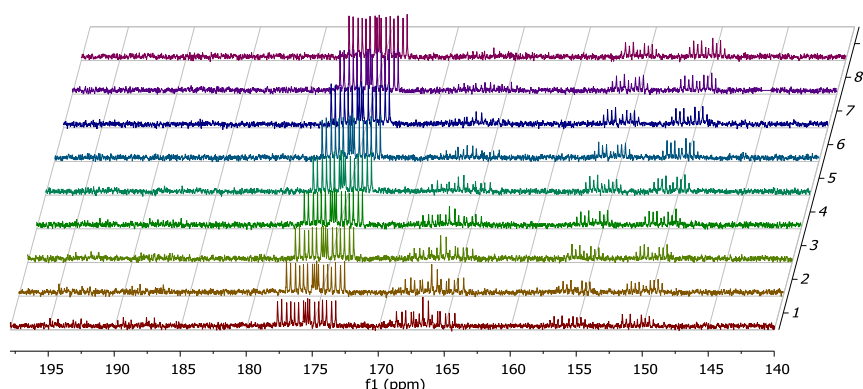


Figure 2. Dealkylation of **13a** (shifts at 164-168 ppm) to **13** (shifts at 174-178 ppm) in toluene (^{31}P NMR) at 0 hour to 4.5 hours (front to back). The left are the multiplets from **13a**, the right is the three multiplets for **13**. The other region of chemical shifts has been omitted.

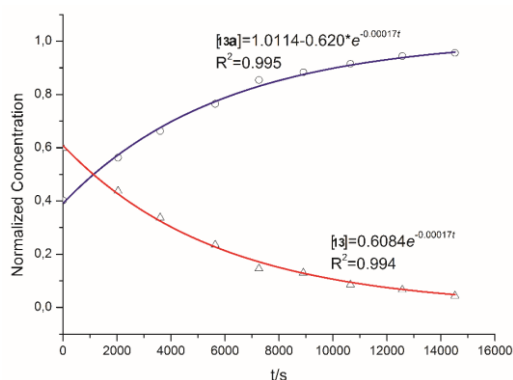
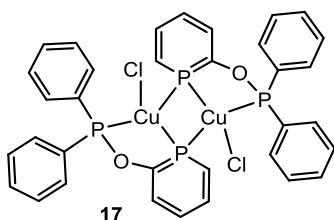
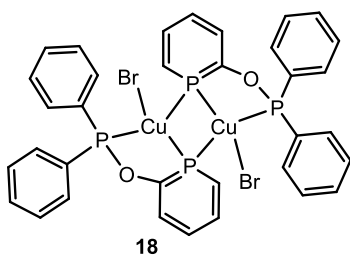


Figure 3. Representative kinetic data on the dealkylation of **13a** to **13** in DCM at 25 °C. The concentration versus time profile of **13a** and **13** fit first order equation: $[13] = Ae^{-kt}$ and $[13a] = B - Ce^{-kt}$, with a rate constant $k_{\text{obs}} = 0.00017 \text{ h}^{-1}$ at 25 °C.

9.4 THE SYNTHESIS OF COPPER (I) COMPLEXES

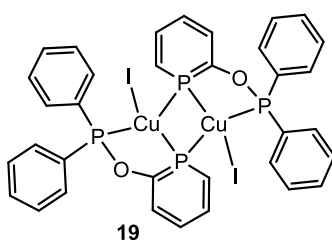


To a solution of POP (100 mg, 0.337 mmol) in THF, Copper (I) Chloride (33.33 mg, 0.337 mmol) was added. The mixture was stirred for around 0.5 h until most of Copper (I) Chloride solid disappeared in solution. The reaction mixture was filtrated, and the solvent was removed in vacuo to give a red powder. The residue was purified by recrystallization from THF to give an orange crystal. Yield 102 mg, 76.7%. NMR data of **17**: ^1H NMR (500 MHz, $\text{D}_8\text{-THF}$, 250 K) δ [ppm]: 8.31 (dd, 2H, $^2J_{\text{HP}} = 35.3$ Hz, $\alpha\text{-C(H)}$ of phosphinine), 7.52-7.22 (mm 26H). ^{13}C NMR (125 MHz, $\text{D}_8\text{-THF}$, 250 K) δ [ppm]: 191.3 (dd, $^1J_{\text{CP}} = 48.31$ Hz, $^2J_{\text{CP}} = 9.84$ Hz, $\alpha\text{-C-O}$ of phosphinine), 151.4 (dd, $^1J_{\text{CP}} = 46.11$, $^4J_{\text{CP}} = 7.81$ Hz, $\alpha\text{-C}$ of phosphinine), 138.4 (d, $^2J_{\text{CP}} = 14.23$ Hz, $\beta\text{-C}$ of phosphinine), 133.4 (t, $^2J_{\text{CP}} = 11.44$ Hz, $\beta\text{-C}$ of phosphinine), 131.6 (d, $^1J_{\text{CP}} = 20.87$ Hz, phenyl-C), 130.2 (s, phenyl-C), 129.4 (s, phenyl-C), 127.4 (d, $^3J_{\text{CP}} = 6.78$ Hz, phenyl-C), 125.4 (t, $^3J_{\text{CP}} = 7.27$ Hz, $\gamma\text{-C}$ of phosphinine). ^{31}P NMR (121.3 MHz, $\text{D}_8\text{-THF}$, 250 K): δ [ppm]: 134.6 (d, $^3J_{\text{PP}} = 206.41$ Hz, phosphinine-P), 96.7 (d, $^3J_{\text{PP}} = 206.41$ Hz, diphenylphosphine-P). Anal. Calcd for $\text{C}_{34}\text{H}_{28}\text{O}_2\text{P}_4\text{Cl}_2\text{Cu}_2$: C, 51.66; H, 3.57. Found: C, 51.71; H, 3.63.

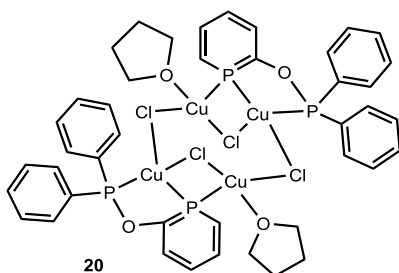


To a solution of POP (100 mg, 0.337 mmol) in THF, Copper (I) Bromide (48.34 mg, 0.337 mmol) was added. The mixture was stirred for around 0.5 h until most of Copper (I) Bromide solid was disappeared in solution. The reaction mixture was filtrated, and the solvent was removed in vacuo to give a red powder. The residue was purified by recrystallization from THF to give an orange crystal. Yield 122 mg, 82.3%. NMR data of **18**: ^1H NMR (500 MHz, $\text{D}_8\text{-THF}$, 250 K) δ [ppm]: 8.30 (dd,

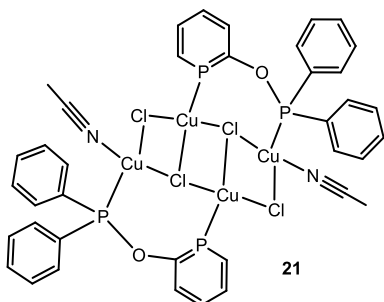
2H, $^2J_{HP} = 34.8$ Hz, α -C(H) of phosphinine), 7.53-7.29 (m, 26H). ^{13}C NMR (125 MHz, D_8 -THF, 250 K) δ [ppm]: 190.5 (dd, $^1J_{CP} = 48.21$ Hz, $^2J_{CP} = 9.77$ Hz, α -C-O of phosphinine), 150.8 (dd, $^1J_{CP} = 45.61$, $^4J_{CP} = 7.67$ Hz, α -C of phosphinine), 137.8 (d, $^2J_{CP} = 13.89$ Hz, β -C of phosphinine), 133.1 (t, $^2J_{CP} = 11.24$ Hz, β -C of phosphinine), 131.5 (d, $^1J_{CP} = 20.83$ Hz, phenyl-C), 130.2 (s, phenyl-C), 129.1 (s, phenyl-C), 127.1 (d, $^3J_{CP} = 6.72$ Hz, phenyl-C), 125.1 (t, $^3J_{CP} = 7.23$ Hz, γ -C of phosphinine). ^{31}P NMR (121.3 MHz, D_8 -THF, 250 K): δ [ppm]: 134.5 (d, $^3J_{PP} = 205.33$ Hz, phosphinine-P), 96.3 (d, $^3J_{PP} = 205.33$ Hz, diphenylphosphine-P). Anal. Calcd for $\text{C}_{34}\text{H}_{28}\text{O}_2\text{P}_4\text{Br}_2\text{Cu}_2$: C, 46.44; H, 3.21. Found: C, 46.23; H, 3.23.



To a solution of POP (100 mg, 0.337 mmol) in THF, Copper (I) iodide (64.03 mg, 0.337 mmol) was added. The mixture was stirred for around 0.5 h until most of Copper (I) iodide solid disappeared in solution. The reaction mixture was filtrated, and the solvent was removed in vacuo to give a red powder. The residue was purified by recrystallization from THF to give an orange crystal. Yield 132 mg. 80.5%. NMR data of **19**: ^1H NMR (500 MHz, D_8 -THF, 250 K) δ [ppm]: 8.33 (dd, 2H, $^2J_{HP} = 34.8$ Hz, α -C(H) of phosphinine), 7.52-7.31 (m, 26H). ^{13}C NMR (125 MHz, D_8 -THF, 250 K) δ [ppm]: 190.3 (dd, $^1J_{CP} = 47.99$ Hz, $^2J_{CP} = 9.66$ Hz, α -C-O of phosphinine), 150.6 (dd, $^1J_{CP} = 45.58$, $^4J_{CP} = 7.59$ Hz, α -C of phosphinine), 137.8 (d, $^2J_{CP} = 13.89$ Hz, β -C of phosphinine), 133.1 (t, $^2J_{CP} = 11.24$ Hz, β -C of phosphinine), 131.5 (d, $^1J_{CP} = 20.83$ Hz, phenyl-C), 130.1 (s, phenyl-C), 129.1 (s, phenyl-C), 127.2 (d, $^3J_{CP} = 6.83$ Hz, phenyl-C), 125.3 (t, $^3J_{CP} = 7.31$ Hz, γ -C of phosphinine). ^{31}P NMR (121.3 MHz, D_8 -THF, 250 K): δ [ppm]: 134.3 (d, $^3J_{PP} = 205.24$ Hz, phosphinine-P), 96.2 (d, $^3J_{PP} = 205.24$ Hz, diphenylphosphine-P). Anal. Calcd for $\text{C}_{34}\text{H}_{28}\text{O}_2\text{P}_4\text{I}_2\text{Cu}_2$: C, 41.95; H, 2.90. Found: C, 42.09; H, 2.88.



To a solution of POP (100 mg, 0.337 mmol) in THF, Copper (I) Chloride (128.1 mg, 0.674 mmol) was added. The mixture was stirred for around 0.5 h until most of Copper (I) Chloride solid disappeared in solution. The reaction mixture was filtrated, and the solvent was removed in vacuo to give a red powder. The residue was purified by recrystallization from THF to give an orange crystal. Yield 155 mg, 81.2%. NMR data of **20**: ^1H NMR (500 MHz, $\text{D}_8\text{-THF}$, 250 K) δ [ppm]: 8.30 (dd, 2H, $^2J_{\text{HP}} = 34.8$ Hz, $\alpha\text{-C(H)}$ of phosphinine), 7.53-7.29 (mm 26H). ^{31}P NMR (121.3 MHz, $\text{D}_8\text{-THF}$, 250 K): δ [ppm]: 133.7 (d, $^3J_{\text{PP}}=198.4$ Hz, phosphinine-*P*), 95.7 (d, $^3J_{\text{PP}}=198.4$ Hz, diphenylphosphine-*P*). Anal. Calcd for $\text{C}_{42}\text{H}_{44}\text{O}_2\text{P}_4\text{Cl}_4\text{Cu}_4$: C, 54.87; H, 4.40. Found: C, 54.84; H, 4.38.



40 mg of crystal **20** was solved in 5 ml acetonitrile, after laying the solution in peaceful environment for 2 hours, crystal of **21** were obtained 30 mg. Yield 79.4%. NMR data of **21**: ^1H NMR (500 MHz, CD_3CN , 250 K) δ [ppm]: 8.30 (dd, 2H, $^2J_{\text{HP}} = 34.8$ Hz, $\alpha\text{-C(H)}$ of phosphinine), 7.53-7.29 (mm 26H). ^{31}P NMR (121.3 MHz, CD_3CN , 250 K): δ [ppm]: 130.4 (d, $^3J_{\text{PP}} = 186.5$ Hz, phosphinine-*P*), 89.4 (d, $^3J_{\text{PP}} = 186.5$ Hz, diphenylphosphine-*P*). Anal. Calcd for $\text{C}_{38}\text{H}_{34}\text{O}_2\text{P}_4\text{N}_2\text{Cl}_4\text{Cu}_4$: C, 42.63; H, 3.20. Found: C, 42.61; H, 3.17.

Photophysical measurements

Excitation and emission spectra were recorded under an inert nitrogen atmosphere on an Edinburgh Instrument FLSP980 spectrometer, equipped with a 450 W Xenon lamp, double

monochromators for the excitation and emission pathways, and a red-sensitive (PMT-R928) or a near-IR photomultiplier (R5509-42) as detector. The excitation and emission spectra were fully corrected using the standard corrections supplied by the manufacturer for the spectral power of the excitation source and the sensitivity of the detector. The luminescence lifetimes were either measured using a μ F900 pulsed 60W xenon microsecond flash lamp, with a repetition rate of 100 Hz, and a multichannel scaling module, or by the use of a 5 mW pulsed EPL-375 laserdiode and a TCSPC module. The emission was collected at right angles to the excitation source with the emission wavelength selected using a double grated monochromator and detected by a R928-P PMT.

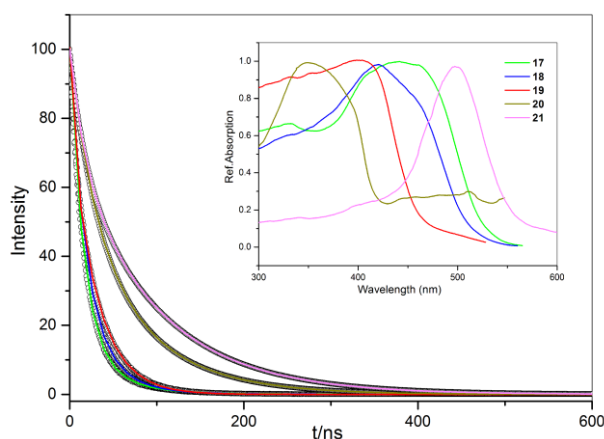
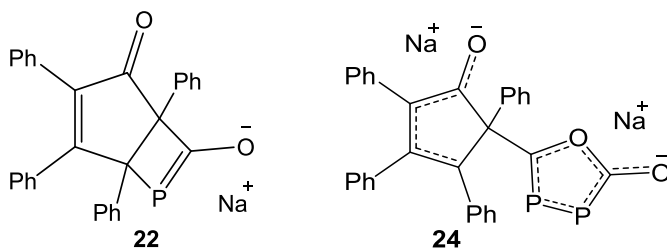


Figure 3 Emission decay of **17** (green), **18** (blue), **19** (red), **20** (Yellow) and **21** (Pink) at T = 298 K. The inset shows the corrected absorption in solid state of **17** (green), **18** (blue), **19** (red), **20** (yellow) and **21** (pink).

Table S1. Recorded emission lifetime of **17-21**

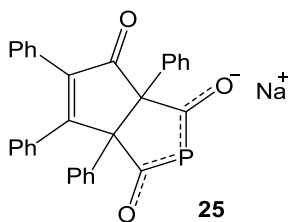
Compound	τ_1 [μ s](%)	τ_2 [μ s] (%)	R ²	τ_{av} [μ s]
17	15.73(86.05)	45.85(13.95)	0.99996	19.94
18	17.60(76.31)	38.56(23.69)	0.99995	22.56
19	4.547(18.62)	29.59(81.89)	0.99997	25.07
20	28.56(45.09)	77.37(54.91)	0.99998	55.36
21	17.36(28.89)	95.36(71.11)	0.99998	72.82

9.5 Na(OCP) AS PRECURSOR TO PHOSPHAKETENES AND PHOSPHORUS HETEROCYCLES

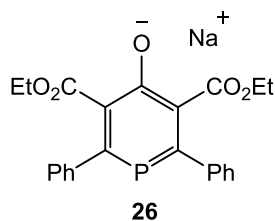


Compound **24**: Sodium phosphoethynolate ($[\text{Na}(\text{OCP}) \times 2.5 \text{ dioxane}]$, 60.4 mg, 0.2 mmol) in THF (2 mL) was added dropwise to a stirred THF solution (2 mL) of tetracyclone (38.4 mg, 0.1 mmol). The solution changed from deep red to orange. After vigorous stirring for 10 minutes, a yellow precipitate was observed. The solvent was evaporated under vacuum and then the residue was washed with toluene to obtain the pure product **24** (90 mg, yield 91%). Compound **8** is sparingly soluble in common organic solvents therefore no ^{13}C NMR could be obtained. As suspension in an organic solvent, **24** slowly converted to give compound **25** at room temperature. M.P. $>200^\circ\text{C}$
 ^1H NMR (250MHz, $[\text{D}_8]\text{THF}$, 23°C , TMS): $\delta = 6.85\text{--}7.31$ ppm (m, phenyl-H); ^{31}P NMR (100.5 MHz, $[\text{D}_8]\text{THF}$, 23°C): $\delta = 159.19$ (d, $^1J_{\text{PP}} = 361$ Hz), -35.53 ppm (d, $^1J_{\text{PP}} = 361$ Hz). Anal. Calcd. for $\text{C}_{62}\text{H}_{40}\text{O}_6\text{P}_4\text{Na}_4 \cdot 8\text{C}_4\text{H}_8\text{O}_2$: C, 67.46; H, 6.26. Found: C, 67.51; H, 6.21. IR [ATR (cm^{-1})]: 3055 (wk, CH stretch), 2977, 2876 (wk, CH stretch), 1705 (s, CO), 1655 (s, CC, Ar), 1437 (s), 1365 (s), 1241 (s, C-O), 1174 (m), 1117 (m), 1091 (m), 1027 (m), 982 (m), 889 (m), 775 (m), 613 (m), 533 (m).

Intermediate **22** was generated as above and its NMR spectra were measured at -40°C . ^{13}C NMR (100.1 MHz, $[\text{D}_8]\text{THF}$, -40°C): $\delta = 225.5$ (d, $^1J_{\text{CP}} = 47.3$ Hz, P-C(O)), 207.5 (d, $^3J_{\text{CP}} = 4.5$ Hz, C(O)), 180.4 (d, $^2J_{\text{CP}} = 2.2$ Hz, cyclone-C), 124.5 (cyclone-C), 141.2, 139.3, 135.6, 134.5, 133.88, 131.1, 129.9, 129.6, 128.6, 127.6, 127.9, 127.4, 127.0, 126.8, 125.6, 124.5 (16-phenyl-C), 78.9 (s, cyclone-C), 54.4 ppm (d, $^1J_{\text{CP}} = 16.1$ Hz, cyclone-C-P). ^{31}P NMR (163.5 MHz, THF, -40°C): $\delta = 150.3$ ppm (s)

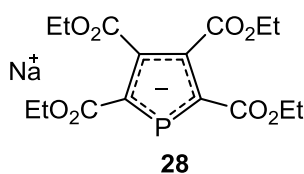
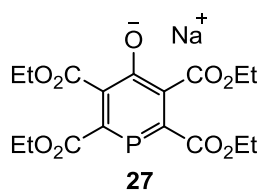


Compound **25**: By heating the THF suspension (2 mL) of compound **8** (50 mg) to 60°C, the yellow suspension turned to a reddish brown solution. After filtration, the solvent was removed under vacuum. The brown crude product was recrystallized from a mixture of 3 mL THF and 3 mL n-hexane (32 mg, 62.1%). Crystals suitable for X-ray single crystal diffraction were obtained from a THF/n-hexane solution. An alternative procedure for the synthesis of compound **9**: 1 equiv. Na(OCP) was added to a THF solution of 1 equiv. tetracyclone. After heating at 60°C for 2 h, the solvent was removed under vacuum, the product was washed with toluene, and recrystallized from THF/n-hexane solution. M.P. >200°C ^1H NMR (300MHz, $[\text{D}_8]\text{THF}$, 23°C, TMS): δ = 6.85-7.31 (m, phenyl-H); ^{13}C NMR (75.5 MHz, $[\text{D}_8]\text{THF}$, 23°C): δ = 221.8 (d, $^1J_{\text{CP}}$ = 50.2 Hz, P-C(O)), 214.9 (d, $^1J_{\text{CP}}$ = 48.2 Hz P-C(O)), 208.6 (C(O)), 149.46, 139.91, 138.3, 130.6, 130.2, 128.7, 128.1, 127.9, 127.8, 127.6, 127.2, 125.57, 125.04, 122.9, 120.9, 75.5(d, $^2J_{\text{CP}}$ = 10.2 Hz), 62.1 ppm (d, $^2J_{\text{CP}}$ = 10.6 Hz). ^{31}P NMR (100.5 MHz, $[\text{D}_8]\text{THF}$, 23°C): δ = 66.5 (s). $\text{C}_{31}\text{H}_{20}\text{O}_3\text{PNa}\cdot 2\text{C}_4\text{H}_8\text{O}$: C, 67.91; H, 7.44. Found: C, 67.65; H, 7.53. IR [ATR (cm^{-1})]: 3052 (wk, CH stretch), 2963, 2896 (wk, CH stretch), 1705 (s, CO), 1655 (s, CC, Ar), 1437 (s), 1365 (s), 1241 (s, C-O), 1174 (m), 1117 (m), 1091 (m), 1027 (m), 982 (m), 889 (m), 775 (m), 613 (m), 533 (m).



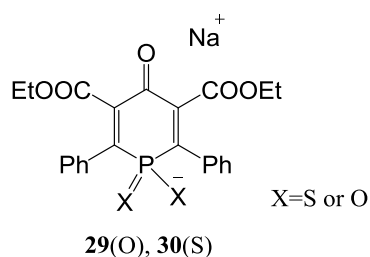
Sodium phosphoethynolate ($[\text{Na}(\text{OCP}) \times 2.5 \text{ dioxane}]$, 151 mg, 0.5 mmol) in DME (5 mL) was added dropwise to a DME solution (10 mL) of ethyl phenylpropiolate (178 mg, 1 mmol). The mixture was then heated up to 70°C under stirring over 8 hours. The solution changed from light yellow to orange, and a yellow precipitate was observed. Subsequently, the mixture was concentrated to around 5 mL and filtered, the yellow precipitate was washed with diethyl ether and dried under vacuum (150 mg, yield 86%). Crystalline **4a** was obtained from a THF solution at room temperature via slow evaporation of the solvent over 3 days. M.P. >200°C ^1H NMR (400 MHz, $[\text{D}_8]\text{THF}$, 23°C, TMS): δ = 7.35 (m, 10H, phenyl-H), 3.80 (m, 4H, O-CH₂), 0.71 ppm (t, $^3J_{\text{HH}}$ = 7.15 Hz, 6H, -CH₃). ^{13}C NMR (100.6 MHz, $[\text{D}_8]\text{THF}$, 23°C): δ = 171.8 (d, $^3J_{\text{CP}}$ = 1.2 Hz, CO), 170.7 (d,

$^1J_{CP} = 44.2$ Hz phosphinine α -C), 144.6 (d, $^2J_{CP} = 25.1$ Hz, phosphinine β -C), 130.8 (d, $^3J_{CP} = 10.4$ Hz, phosphinine γ -C), 127.9 (d, $^2J_{CP} = 12.2$ Hz, phenyl C1), 127.4, 126.4 (d, $^3J_{CP} = 1.8$ Hz, phenyl C2), 57.9, 12.7 ppm. ^{31}P NMR (161.9 MHz, $[\text{D}_8]\text{THF}$, 23°C): $\delta = 91.85$ ppm. Anal. Calcd. for $\text{C}_{27}\text{H}_{28}\text{O}_6\text{PNa}\cdot\text{C}_4\text{H}_8\text{O}$: C, 64.48; H, 5.57. Found: C, 64.65; H, 5.53. IR [ATR (cm^{-1})]: 3354 (b, CH stretch), 3055, 2977, 2876 (wk, CH stretch), 1727, 1682 (s, C=O stretch), 1548 (wk, CC, Ar), 1414 (s, CP), 1332 (s), 1258 (s, C-O), 1186 (s, C-O), 1097 (s), 1050 (s), 1022 (m), 928 (m), 901 (m), 863 (s), 831 (m), 765 (m), 699 (s), 648 (wk).



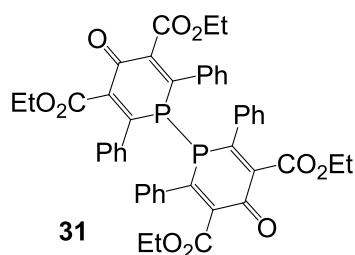
Compounds **27** and **28**: Diethyl acetylenedicarboxylate (225 mg, 1.32 mmol) in dioxane (5 mL) was added dropwise to a stirred suspension of $[\text{Na}(\text{OCP}) \times 2.5 \text{ dioxane}]$ (200 mg, 0.66 mmol) in dioxane (5 mL). An orange precipitate was obtained from the red solution. After 8 hours, the mixture was filtered. The orange precipitate which contained compound **5** was washed with dioxane and then dried under vacuum. Crystals of compound **28** (80 mg, 25% yield) were obtained from a THF-dioxane solution; M.P. $>200^\circ\text{C}$. Crystals of compound **27** were obtained from the red solution. **27**: ^1H NMR (300 MHz, $[\text{D}_8]\text{THF}$, 23°C, TMS): $\delta = 4.06$ (m, 8H), 1.22 ppm (m, 12H). ^{13}C NMR (75.5 MHz, $[\text{D}_8]\text{THF}$, 23°C): $\delta = 167.3$ (carboxylate-C bonded to phosphinine β -C), 165.6 (carboxylate-C bonded to phosphinine α -C), 165.1 (d, $^2J_{CP} = 13.5$ Hz, phosphinine β -C), 154.4 (d, $^1J_{CP} = 40.2$ Hz, phosphinine α -C), 133.6 (d, $^3J_{CP} = 10.2$ Hz, phosphinine γ -C), 62.2, 61.1, 13.1, 12.2 ppm (ethyl-C), ^{31}P NMR (121.5 MHz, $[\text{D}_8]\text{THF}$, 23°C): $\delta = 112.8$ ppm, HRMS: m/z : Calcd. for $\text{C}_{17}\text{H}_{20}\text{O}_9\text{P}_4^-$: 399.0850; found: 399.0848. **28**: ^1H NMR (300 MHz, $[\text{D}_8]\text{THF}$, 23°C, TMS): $\delta = 4.07$ (m, 8H), 1.20 ppm (m, 12H). ^{13}C NMR (75.5 MHz, $[\text{D}_8]\text{THF}$, 23°C): $\delta = 167.1$ (carboxylate-C bonded to phospholide β -C), 166.5 (d, $^2J_{CP} = 22.8$ Hz, phospholide β -C), 136.7 (d, $^1J_{CP} = 41.3$ Hz, phospholide α -C), 127.8 (d, $^2J_{CP} = 3.5$ Hz, carboxylate-C bonded to phospholide α -C), 57.8, 56.6, 12.0, 11.5 ppm (ethyl-C). ^{31}P NMR (121.5 MHz, $[\text{D}_8]\text{THF}$, 23°C): $\delta = 162.9$ ppm. Anal. Calcd. for $\text{C}_{16}\text{H}_{20}\text{O}_8\text{PNa}\cdot\text{C}_4\text{H}_8\text{O}_2$: C, 49.80; H, 5.85. Found: C, 49.81; H, 5.83. IR [ATR (cm^{-1})]: 3410 (b, CH stretch), 2973, 2857 (wk, CH stretch), 1705,

1655 (s, C=O stretch), 1437 (s, CP), 1332 (s), 1241, 1117, 1091 (s, C-O), 1027 (s), 1022 (m), 982 (m), 889 (m), 872 (s), 831 (m), 776 (m), 699 (wk), 613 (m)

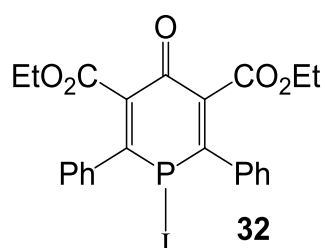


29: Sodium phosphinin-4-olate (200mg, 0.40 mmol, **26**) in THF (5 mL) was reacted with sulfur (S_8 , 26.5 mg, 0.103 mmol). The mixture was then heated up to 70°C under stirring over 8 hours. The solution changed from light yellow to red. The red solution was filtered and dried under vacuum. The orange solid remaining was washed with diethyl ether and then dried under vacuum (212 mg, yield 93.5%). Crystalline **29** was obtained by diffusion of n-hexane in a THF solution at room temperature. **29:** Sodium phosphinin-4-olate (200mg, 0.40 mmol, **26**) in THF (5 mL) was reacted with air for 3 hours. The color of the solution changed from light yellow to orange. The reaction mixture was filtered and the filtrate obtained was dried under vacuum. The remaining solid was washed with diethyl ether and then dried under vacuum (196 mg, yield 93.5%). NMR for **29**: ^1H NMR (200 MHz, $[D_8]$ THF, 23°C, TMS): δ = 7.54 (m, 4H, phenyl-H), 7.25 (m, 6H, phenyl-H), 3.68 ppm (m, 4H, O-CH₂), 0.90 ppm (m, 6H, CH₃). ^{13}C NMR (50.35 MHz, $[D_8]$ THF, 23°C): δ = 177.4 (d, $^3J_{\text{CP}}$ = 14.4 Hz, phosphinine γ -CO), 164.5 (d, $^3J_{\text{CP}}$ = 13.7 Hz, CO), 153.3 (d, $^1J_{\text{CP}}$ = 51.7 Hz, phosphinine α -C), 133.1 (d, $^2J_{\text{CP}}$ = 7.5 Hz, phosphinine β -C), 131.5 (d, $^2J_{\text{CP}}$ = 4.3 Hz, phenyl C), 130.3 (d, $^3J_{\text{CP}}$ = 3.1 Hz, phenyl C), 126.8 (d, $^4J_{\text{CP}}$ = 2.1 Hz, phenyl C), 125.9 (d, $^5J_{\text{CP}}$ = 1.5 Hz, phenyl C), 60.2, 12.8. ^{31}P NMR (80.2 MHz, $[D_8]$ THF, 23°C): δ = 4.83 ppm. Anal. Calcd. for $\text{C}_{23}\text{H}_{20}\text{O}_7\text{PNa}\cdot\text{C}_4\text{H}_8\text{O}$: C, 59.75; H, 4.36. Found: C, 59.71; H, 4.39. NMR for **30**: ^1H NMR (200 MHz, $[D_8]$ THF, 23°C, TMS): δ = 7.67 (m, 4H, phenyl-H), 7.31 (m, 6H, phenyl-H), 3.88 ppm (m, 4H, O-CH₂), 0.92 ppm (m, 6H, CH₃). ^{13}C NMR (50.35 MHz, $[D_8]$ THF, 23°C): δ = 178.3 (d, $^3J_{\text{CP}}$ = 14.3 Hz, phosphinine γ -CO), 163.8 (d, $^3J_{\text{CP}}$ = 14.5 Hz, CO), 155.14 (d, $^1J_{\text{CP}}$ = 60.6 Hz, phosphinine α -C), 134.2 (d, $^2J_{\text{CP}}$ = 6.9 Hz, phosphinine β -C), 132.2 (d, $^2J_{\text{CP}}$ = 4.6 Hz, phenyl C), 130.5 (d, $^3J_{\text{CP}}$ = 3.0 Hz, phenyl C), 127.4 (d, $^4J_{\text{CP}}$ = 2.07 Hz, phenyl

C), 126.1 (d, $^5J_{CP} = 1.6$ Hz, phenyl C), 60.0, 13.1. ^{31}P NMR (80.2 MHz, $[\text{D}_8]\text{THF}$, 23°C): $\delta = 36.88$ ppm. Anal. Calcd. for $\text{C}_{23}\text{H}_{20}\text{O}_5\text{PS}_2\text{Na}\cdot 3\text{C}_4\text{H}_8\text{O}$: C, 55.87; H, 4.08. Found: C, 55.92; H, 5.83.

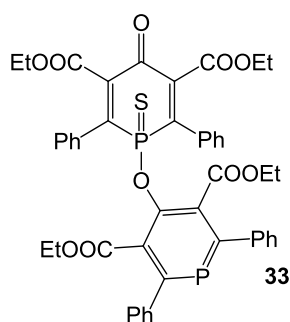


Sodium phosphinin-4-olate (200mg, 0.40 mmol, **26**) in THF (5 mL) was added dropwise to a THF solution (10 mL) of iodine (50 mg, 0.20 mmol). The solution changed from light yellow to red, and a yellow precipitate was observed. Subsequently, the mixture was dried under vacuum. Dichloromethane was used to extract the product from the colorless precipitate which was filtrated off. The yellow filtrate was dried under vacuum. The yellow solid remaining was washed with diethyl ether and dried under vacuum (153 mg, yield 94.4%). Crystalline **31** was obtained from a THF solution at room temperature via slow evaporation of the solvent over 3 days. M.P. >200°C ^1H NMR (400 MHz, $[\text{D}_8]\text{THF}$, 23°C, TMS): $\delta = 7.25$ (m, 20H, phenyl-H), 3.76 (m, 8H, O-CH₂), 0.73 ppm (t, $^3J_{\text{HH}} = 7.16$ Hz, 12H, -CH₃). ^{13}C NMR (100.6 MHz, $[\text{D}_8]\text{THF}$, 23°C): $\delta = 177.0$ (t, $^3J_{\text{CP}} = 3.67$ Hz, γ -C), 164.27 (s, CO), 153.7 (s), 140.0 (d, $^2J_{\text{CP}} = 23.07$ Hz, β -C), 140.0 (d, $^1J_{\text{CP}} = 52.29$ Hz, α -C), 131.6 (s, phenyl-C), 130.6 (s, phenyl-C), 129.3 (s, phenyl-C), 128.8 (s, phenyl-C), 128.3 (s, phenyl-C), 127.6 (s, phenyl-C), 61.8 (s), 61.5 (s), 13.9 (s) ppm. ^{31}P NMR (161.9 MHz, $[\text{D}_8]\text{THF}$, 23°C): $\delta = -36.1$ ppm. Anal. Calcd. for $\text{C}_{54}\text{H}_{56}\text{O}_{12}\text{P}_2$: C, 67.63; H, 5.89. Found: C, 67.65; H, 5.83.

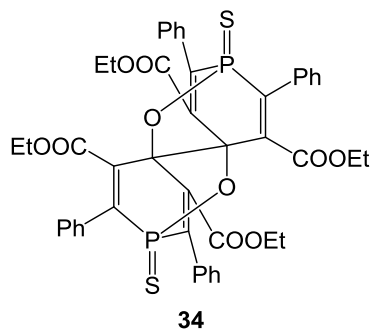


Sodium phosphinin-4-olate (200mg, 0.40 mmol, **26**) in THF (5 mL) was added dropwise to a THF solution (10 mL) of Iodine (100 mg, 0.40 mmol). The solution changed from light yellow to red.

Subsequently, the mixture was dried under vacuum. DCM was used to abstract the product, the white precipitate was filtrated and the orange solution was dried under vacuum. The orange solid remaining was washed with diethyl ether and dried under vacuum (206 mg, yield 94.9%). Crystalline **32** was obtained by diffusion of n-hexane in THF at room temperature. ^1H NMR (400 MHz, $[\text{D}_8]\text{THF}$, 23°C , TMS): δ = 7.36 (m, 10H, phenyl-H), 3.82 (m, 4H, O-CH₂), 0.70 ppm (t, $^3J_{\text{HH}}$ = 6.94 Hz, 6H, -CH₃). ^{13}C NMR (100.6 MHz, $[\text{D}_8]\text{THF}$, 23°C): δ = 171.8 (d, $^3J_{\text{CP}}$ = 1.2 Hz, CO), 170.7 (d, $^1J_{\text{CP}}$ = 44 Hz phosphinine α -C), 144.6 (d, $^2J_{\text{CP}}$ = 25 Hz, phosphinine β -C), 130.8 (d, $^3J_{\text{CP}}$ = 10 Hz, phosphinine γ -C), 127.9 (d, $^2J_{\text{CP}}$ = 12.2 Hz, phenyl C1), 127.4, 126.4 (d, $^3J_{\text{CP}}$ = 1.8 Hz, phenyl C2), 57.9, 12.7 ppm. ^{31}P NMR (161.9 MHz, $[\text{D}_8]\text{THF}$, 23°C): δ = 91.85 ppm. Anal. Calcd. for $\text{C}_{27}\text{H}_{28}\text{O}_6\text{PNa}\cdot\text{C}_4\text{H}_8\text{O}$: C, 64.48; H, 5.57. Found: C, 64.65; H, 5.53.

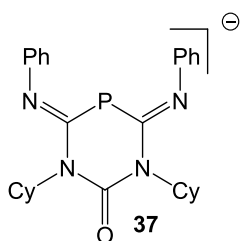


Dimer of phosphinin-4-olate **31** (100mg, 0.123 mmol, **31**) in Toluene suspension (5 mL) was added with sulfur (S_8 , 4 mg, 0.125 mmol). The mixture was then heated up to 70°C under stirring over 8 hours which turned to be clear solution. Subsequently, after the filtration, the filtrates was dried under vacuum. The remaining yellow solid was washed with diethyl ether and dried under vacuum (96 mg, yield 92.3%). Crystalline **33** was obtained by diffusion of n-hexane in THF at room temperature. ^1H NMR (400 MHz, $[\text{D}_8]\text{THF}$, 23°C , TMS): δ = 7.36-7.41 (m, 20H, phenyl-H), 4.11 (m, 8H, O-CH₂), 0.92 ppm (t, 12H, -CH₃). ^{13}C NMR (100.6 MHz, $[\text{D}_8]\text{THF}$, 23°C): δ = 191.1 (d, $^2J_{\text{CP}}$ = 13.4, phosphinine CO), 182.8 (d, $^3J_{\text{CP}}$ = 2.1 Hz, γ -CO), 170.7 (d, $^1J_{\text{CP}}$ = 43.1 Hz), 168.9 (d, $^1J_{\text{CP}}$ = 45.3 Hz), 165.1 (s), 163.4 (s), 144.3 (d, $^2J_{\text{CP}}$ = 25.2 Hz), 134.3 (d, $^2J_{\text{CP}}$ = 7.3 Hz), 132.4 (d, $^3J_{\text{CP}}$ = 9.4 Hz), 127.9 (d, $^2J_{\text{CP}}$ = 12.2 Hz, phenyl C1), 127.4, 126.4 (s), 57.3, 56.8, 12.5, 12.1 ppm. ^{31}P NMR (161.9 MHz, $[\text{D}_8]\text{THF}$, 23°C): δ = 190.04 (d, $^5J_{\text{PP}}$ = 7.86 Hz), 40.05 ppm (d, $^5J_{\text{PP}}$ = 7.86 Hz).



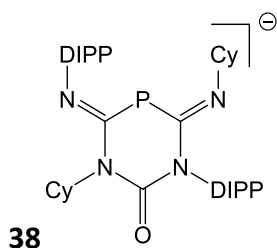
Dimer of phosphinin-4-olate **31** (100mg, 0.123 mmol, **31**) in Toluene suspension (5 mL) was added with sulfur (S_8 , 8 mg, 0.25 mmol). The mixture was then heated up to 70°C under stirring over 8 hours which turned to be clear solution. Subsequently, colorless crystals were formed, after filtration the crystals were collected, which is surprisingly good enough for X-ray diffraction. The remaining crystals were washed with diethyl ether and dried under vacuum (96 mg, yield 92.3%). However, the crystals of **34** were hardly soluble in any solvent. Anal. Calcd. for $C_{46}H_{40}O_{10}P_2S_2$, 62.86; H, 4.59. Found: C, 62.82; H, 4.53.

9.6 SYNTHESIS AND REACTIVITY OF 1,3,5-DIAZAPHOSPHINANE ANION

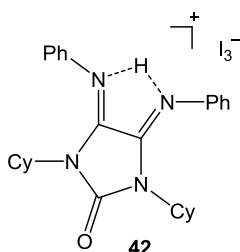


Compound Na[**37**]: Sodium phosphoethynolate ($[Na(OCP) \times 2.5 \text{ dioxane}]$, 151 mg, 0.5 mmol) in THF (5 mL) was added dropwise to a THF solution (10 mL) of N-cyclohexyl-N-phenylmethanediimine (210 mg, 1.05 mmol). The mixture was stirred over 8 hours to complete the reaction. The solution turned out to be clear yellow. Subsequently, the mixture was dried under vacuum, the remaining solid was washed with n-hexane and the yellow product was obtained (196.5 mg, yield 85%). Crystalline Na[**37**] was obtained from a DME solution at room temperature via slow evaporation of the solvent over 3 days. 1H NMR (300 MHz, CD_3CN , 23°C, TMS): δ = 7.09 (t, 4H, $^3J_{HH}$ = 6.41 Hz, phenyl-H), 6.76 (t, 2H, $^3J_{HH}$ = 7.34 Hz, phenyl-H), 6.61 ppm (d, $^3J_{HH}$ = 8.37 Hz, 4H, phenyl-H), 5.18 (t, 2H, $^3J_{HH}$ = 11.87 Hz, Cy-H), 2.58 (m, 4H, Cy-H), 1.81 (m, 4H,

Cy-H), 1.68 (m, 6H, Cy-H), 1.32 (m, 6H, Cy-H). ^{13}C NMR (100.6 MHz, CD_3CN , 23°C): δ = 176.48 (d, $^1J_{\text{CP}}$ = 69.44 Hz, CN), 155.11 (d, $^3J_{\text{CP}}$ = 13.28 Hz, CO), 128.99 (s, phenyl-C), 122.64 (d, $^3J_{\text{CP}}$ = 4.77 Hz, phenyl-C), 120.71 (s, phenyl-C), 56.02 (d, $^3J_{\text{CP}}$ = 1.91 Hz, Cy-C), 30.32 (s, Cy-C), 27.55, 26.61 (s, Cy-C). ^{31}P NMR (161.9 MHz, CD_3CN , 23°C): δ = 51.94 ppm. Anal. Calcd. for $\text{C}_{27}\text{H}_{28}\text{O}_6\text{PNa}\cdot\text{C}_4\text{H}_8\text{O}$: C, 64.48; H, 5.57. Found: C, 64.65; H, 5.53.

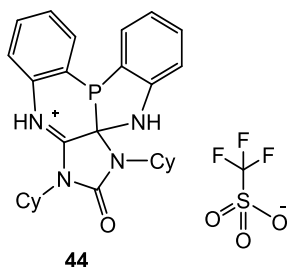


Compound Na[**38**]: Sodium phosphorimidate ($[\text{Na}(\text{OCP}) \times 2.5 \text{ dioxane}]$, 151 mg, 0.5 mmol) in DME (5 mL) was added dropwise to a DME solution (10 mL) of N-cyclohexyl-N-diisopropylphenyl methanediimine (290 mg, 1.05 mmol). The mixture was then heated up to 70°C under stirring over 8 hours. Subsequently, the mixture was dried under vacuum, the yellow solid obtained was washed with n-hexane and dried under vacuum (298 mg, yield 95%). Crystalline Na[**38**] was obtained from a DME solution at room temperature via slow evaporation of the solvent over 3 days. ^1H NMR (400 MHz, $[\text{D}_8]\text{THF}$, 23°C, TMS): δ = 7.35 (m, 10H, phenyl-H), 3.80 (m, 4H, O-CH₂), 0.71 ppm (t, $^3J_{\text{HH}}$ = 7.15 Hz, 6H, -CH₃). ^{13}C NMR (100.6 MHz, $[\text{D}_8]\text{THF}$, 23°C): δ = 171.8 (d, $^3J_{\text{CP}}$ = 1.2 Hz, CO), 170.7 (d, $^1J_{\text{CP}}$ = 44 Hz phosphinine α -C), 144.6 (d, $^2J_{\text{CP}}$ = 25 Hz, phosphinine β -C), 130.8 (d, $^3J_{\text{CP}}$ = 10 Hz, phosphinine γ -C), 127.9 (d, $^2J_{\text{CP}}$ = 12.2 Hz, phenyl C1), 127.4, 126.4 (d, $^3J_{\text{CP}}$ = 1.8 Hz, phenyl C2), 57.9, 12.7 ppm. ^{31}P NMR (161.9 MHz, $[\text{D}_8]\text{THF}$, 23°C): δ = 91.85 ppm. Anal. Calcd. for $\text{C}_{27}\text{H}_{28}\text{O}_6\text{PNa}\cdot\text{C}_4\text{H}_8\text{O}$: C, 64.48; H, 5.57. Found: C, 64.65; H, 5.53.



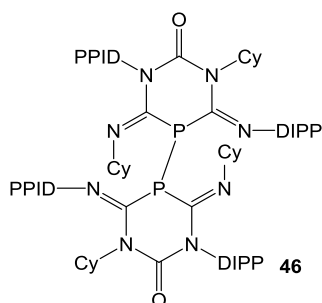
A solution of I_2 (507.6 mg, 2 mmol) in THF (1 ml) was added dropwise at room temperature to a stirred solution of Na[**37**] (482.55 mg, 1 mmol) in THF (5ml). After stirring for 15h at room

temperature, the solvent and the remaining iodine were removed under reduced pressure and the product was extracted from the brown residue with DCM (5 ml). The solvent from the filtrate was removed under reduced pressure and the rude product **41** - a brown powder- was dried in vacuo. The 100 mg rude compound **42** was recrystallized in CH₂Cl₂/n-hexane, after 1 day diffusion, the yellow crystals (32 mg, 33.6% yields) were obtained and were proved to be compound **42**. ³¹P NMR for **40** (161.9 MHz, CD₂Cl₂, 23°C): δ = 198.5 ppm. NMR for **42** ¹H NMR (400 MHz, CD₂Cl₂, 23°C, TMS): δ = 7.35 (m, 10H, phenyl-H), 6.51 (s, 1H), 3.95 (m, 2H), 1.21-1.51 ppm (m, 20H). ¹³C NMR (100.6 MHz, CD₂Cl₂, 23°C): δ = 162.8 (s, CO), 151.7 (s, NCN), 128.5 (s, phenyl-C), 126.6 (s, phenyl-C), 62.3 (s), 32.1 (s), 25.1 (s), 22.4 (s).

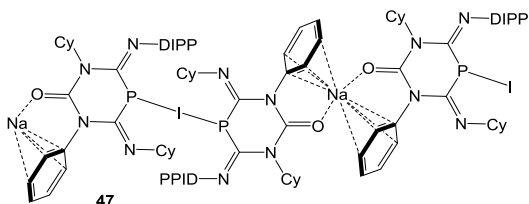


A solution of I₂ (507.6 mg, 2 mmol) in Toluene (1 ml) was added dropwise at room temperature to a stirred solution of Na[**37**] (965.1 mg, 2 mmol) in Toluene (5ml). After 20 minutes stirring, the reaction mixture was filtrated, the filtrate which contained the spectroscopically pure iodophosphane **40** (1135 mg, 1.963 mmol, 96.8% yields), was analyzed by spectroscopic methods. The following synthesis was performed under the exclusion of light. To the toluene solution of **40** (200 mg, 0.34 mmol), 90 mg silver trifoliate was added in portions over a period of 5 minutes. The solvent was removed under reduced pressure, the product was abstracted by 2 ml DCM. After filtration, the filtrate was dried under vacuum, and the remaining solid is the rude product of **44** (192.3 mg). Crystalline **44** was obtained by diffusion of n-hexane in THF at room temperature. ¹H NMR (300 MHz, CD₃CN, 23°C, TMS): δ = 10.5 (s, NH), 7.92 (t, 1H, phenyl-H), 7.37 (m, 5H, phenyl-H), 6.97 (m, 1H, phenyl-H), 6.78 (d, 1H, phenyl-H), 6.27 (s, 1H, NH), 4.22 (m, 1H, Cy-H), 2.86 (m, 1H, Cy-H), 2.33 (m, 2H, Cy-H), 2.06 (m, 2H, Cy-H), 1.75 (m, 4H, Cy-H), 1.47 (m, 1H, Cy-H), 1.31 (m, 1H, Cy-H). ¹³C NMR (75.5 MHz, CD₃CN, 23°C): δ = 161.3 (s, CO), 150.85 (d, ²J_{CP} = 4.53 Hz, phenyl-C-N), 148.62 (d, ²J_{CP} = 2.67 Hz, phenyl-C-N), 133.85 (m, ¹J_{FC} = 154.77 Hz), 131.89 (d, ¹J_{CP} = 21.90

Hz phenyl-C-P), 131.13 (d, $^1J_{CP} = 26.43$ Hz phenyl-C-P), 127.97 (s, phenyl-C), 122.85 (s, phenyl-C), 122.15 (d, $^1J_{CP} = 27.94$ Hz, P-C), 120.94 (d, $^2J_{CP} = 9.06$ Hz, NCN-C), 120.00 (s, phenyl-C), 119.96 (s, phenyl-C), 119.77 (s, phenyl-C), 118.60 (s, phenyl-C), 109.86 (s, phenyl-C), 79.84 (d, $^3J_{CP} = 15.1$ Hz, Cy-C), 56.77 (s, Cy-C), 56.02 (s, Cy-C), 56.02 (s, Cy-C), 30.11 (s, Cy-C), 29.99 (s, Cy-C), 29.89, 28.80, 27.90, 25.44, 25.33, 24.97, 24.74, 24.27, 24.55, 26.61 (s, Cy-C). ^{31}P NMR (121.3 MHz, CD_3CN , 23°C): $\delta = -7.90$ ppm. Anal. Calcd. for $\text{C}_{28}\text{H}_{32}\text{O}_6\text{F}_3\text{N}_4\text{O}_3\text{PS}$: C, 56.75; H, 5.44. Found: C, 56.63; H, 5.50.

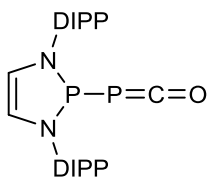


To the toluene solution of **38** (200 mg, 0.34 mmol), 90 mg iodine was added in portions over a period of 5 minutes. After filtration, the solvent was removed under reduced pressure, the product was abstracted by 2 ml n-hexane. After filtration, the filtrate was dried under vacuum, and the remaining solid is the rude product of **45** (150.5 mg, 88.3%). ^{31}P NMR (121.3 MHz, $[\text{D}_8]\text{THF}$, 23°C) δ : -12.5 and -13.9 ppm.



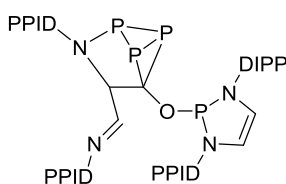
To the toluene solution of **40** (200 mg, 0.34 mmol), 90 mg silver trifoliate was added in portions over a period of 5 minutes. The solvent is removed under reduce pressure, the product was abstracted by 2 ml n-hexane. After filtration, the filtrate was dried under vacuum, and the remaining solid is the rude product of **47** (150.5 mg, 88.3%). ^{31}P NMR (121.3 MHz, THF, 23°C) δ : -75.9 ppm.

9.7 A STABLE ORGANIC PHOSPHAKETENE AND ITS REACTIVITY



48

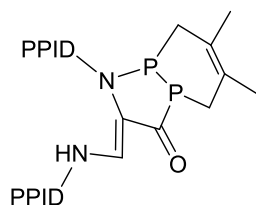
Sodium phosphoethynolate ($[\text{Na}(\text{OCP})(\text{dioxane})_{2.5}]$, 3.02 g, 10 mmol) was added to a stirred solution of chlorodiazaphospholene (4.43 g, 10 mmol) in toluene (10 mL). After 1 h stirring, the precipitate of sodium chloride was removed by filtration. The filtrate was dried under reduced pressure and the remaining solid was washed with n-hexane. Drying the residue *in vacuo* afforded **48** as a yield yellow powder (3.2 g, 6.8 mmol, 68 % yield). M. P. = 121.6 °C. ^1H NMR (C_6D_6 , 500 MHz): δ = 6.86 (m, 2 H, $\text{C}_{\text{ar}}\text{H}$), 6.77 (m, 4 H, $\text{C}_{\text{ar}}\text{H}$), 5.76 (s, 2 H, NCH), 3.25 (m, 4 H, CHMe_2), 1.06 (d, 12 H, CH_3), 0.83 (d, 12 H, CH_3); $^{13}\text{C}\{^1\text{H}\}$ NMR (C_6D_6 , 125.8 MHz): δ = 198.4 (dd, $J_{\text{CP}} = 95.6$ Hz, CPO, $J_{\text{CP}} = 22.6$ Hz, PPCO), 146.3 (*ipso*-C), 132.7 (d, $J_{\text{CP}} = 8.8$ Hz, *o*-C), 127.8 (*p*-CH), 123.6 (*m*-CH), 121.0 (d, $J_{\text{CP}} = 8.8$ Hz, NCH), 28.0 (CHMe_3), 24.0 (CH_3), 23.3 (CHMe_2); $^{31}\text{P}\{^1\text{H}\}$ NMR (C_6D_6 , 202 MHz) δ = 165.1 (d, $J_{\text{PP}} = 252.5$ Hz, PPCO), δ = -232.6 (d, $J_{\text{PP}} = 252.5$ Hz, PCO). IR (solid): 1881 cm^{-1} (s, PCO).



49

The solution of **48** (117 mg, 0.25 mmol) in THF (2 mL) was stirred for 60 hours at room temperature, or stirred in toluene (3 mL) for 2 hours at 60 °C. The solvent was removed under reduced pressure, and the remaining solids were dissolved in acetonitrile (2 mL) and diethyl ether (0.5 mL). There were yellow crystals of **49** coming out from the solution in 24 hours, after the filtration, the crystals were washed with acetonitrile and dried *in vacuo*. (81 mg, 0.09 mmol, 71 % yield). M. P. = 189.2 °C. ^1H NMR (C_6D_6 , 300 MHz): δ = 7.14 (d, 1 H, $\text{C}_{\text{ar}}\text{H}$), 6.79 (br, 9 H, $\text{C}_{\text{ar}}\text{H}$), 6.61 (m, 2 H, $\text{C}_{\text{ar}}\text{H}$), 5.63 (d, 2 H, $J_{\text{PH}} = 51$ Hz, NCH), 4.45 (s, 1 H, NCH), 3.72 (m, 1 H, CHMe_2), 3.14 (m, 3

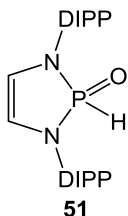
H, CHMe₂), 2.76 (m, 2 H, CHMe₂), 1.30 (d, 3 H, CH₃), 0.92 (br, 42 H, CH₃), 0.64 (d, 3 H, CH₃); ¹³C{¹H} NMR (C₆D₆, 75 MHz): δ = 162.6, 148.1, 147.6, 146.4, 145.6, 135.8, 135.6, 134.5, 135.2, 135.1, 134.9, 127.3, 123.5, 123.3, 123.2, 123.1, 121.2, 117.6, 117.1, 69.1, 28.0, 27.8, 27.5, 26.8, 26.4, 25.7, 24.9, 24.2, 24.1, 23.5, 23.3, 22.6, 22.3, 21.6; ³¹P{¹H} NMR (C₆D₆, 121 MHz) δ = 118.0 (dt, J_{PP} = 145.4 Hz, J_{PP} = 34.3 Hz), 0.1 (td, J_{PP} = 207.4 Hz, J_{PP} = 32.4 Hz), -263.4, - (ddd, J_{PP} = 33.9 Hz, J_{PP} = 145.2 Hz, J_{PP} = 208.8 Hz), -272.1 (dt, J_{PP} = 206.1 Hz, J_{PP} = 36.4 Hz).



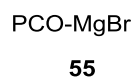
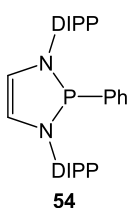
50

The solution of **48** (233 mg, 0.5 mmol) in 2,3-dimethylenebutane (3 mL) was stirred for 72 hours at room temperature. The solvent was removed under reduced pressure, and the remaining solid was dissolved in acetonitrile (1 mL) and diethyl ether (1 mL). After 48 hours, the precipitate was removed by filtration from the solution. The filtrate was dried under reduced pressure remaining a yellow-red residue. The residue was dissolved in 1 mL n-hexane, which then ran down a 6 × 1cm column of alumina with the wash of 3 mL n-hexane. Afterwards, the solvent was removed under reduced pressure and the remaining yellow solid is the product **50** (31 mg, 0.056 mmol, 11 % yield). According to the NMR, this solid has both the *trans* and *cis* isomer for which the ratio is around 2:1. M. P. = 163.7 °C. ¹H NMR (C₆D₆, 300 MHz): δ = 10.29 (d, J = 12 Hz, 1 H, NH), 6.95 (s, 2 H, C_{ar}H), 6.87 (m, 1 H, C_{ar}H), 6.77 (m, 3 H, C_{ar}H), 6.72 (m, 3 H, C_{ar}H), 6.49 (d, J = 12 Hz, 0.5 H, NH'), 5.62 (d, J = 12 Hz, 1 H, NCH), 4.97 (d, J = 12 Hz, 0.5 H, NCH'), 3.80 (m, 0.5 H, CH'Me₂), 3.27 (m, 2.5 H, CHMe₂), 2.80 (m, 5 H, CH'Me₂ and PCH₂), 2.40 (m, 1 H, CHMe₂), 1.76 (m, 1 H, PCH₂), 1.59 (m, 9 H, CH₂CH₃), 1.48 (m, 2 H, PCH'₂), 1.24 (d, J = 6 Hz, 3 H, CH₃), 1.25 (d, J = 6 Hz, 1.5 H, CH'₃), 1.11 (d, J = 6 Hz, 1.5 H, CH'₃), 1.07 (d, J = 6 Hz, 3 H, CH₃), 0.96 (d, J = 6 Hz, 3 H, CH₃), 0.78 (m, 24 H, CH₃ and CH'₃); ¹³C{¹H} NMR (C₆D₆, 75 MHz): δ = 215.2 (dd, J_{CP} = 37.5 Hz, PCO, J_{CP} = 7.5 Hz, PPCO), 148.8, 148.8, 148.2, 147.4, 143.9, 143.5, 142.6, 142.1, 136.9, 136.3, 135.0, 128.7, 126.8, 126.7, 125.7, 125.4, 124.4, 124.3, 123.9, 123.7, 123.0, 123.1, 122.4, 38.1, 37.7, 37.4, 37.1, 31.8, 29.1, 29.0, 28.4,

28.3, 28.1, 27.6, 27.5, 27.1, 26.1, 25.9, 25.3, 25.1, 24.0, 23.6, 23.5, 23.4, 22.9, 22.8, 22.2, 21.8, 21.7, 21.0, 20.6; $^{31}\text{P}\{^1\text{H}\}$ NMR (C_6D_6 , 121 MHz) δ = 39.4 (d, $J_{\text{PP}} = 290.4$ Hz, trans), 36.2 (d, $J_{\text{P}'\text{P}'} = 290.4$ Hz, cis), -45.8 (d, $J_{\text{PP}} = 290.4$ Hz, trans), -51.2 (d, $J_{\text{PP}} = 290.4$ Hz, cis).

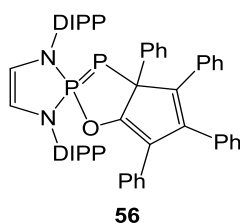


Water (5.4 mg, 0.3 mmol) was added dropwise to a stirred solution of **48** (117 mg, 0.25 mmol) in toluene (2 mL). The reaction mixture was dried after stirring for 3 minutes under reduced pressure to yield orange-red solids **51** (97.7 mg, 0.23 mmol, 92 % yield). M. P. = 69.3 °C (decompose). ^1H NMR (C_6D_6 , 300 MHz) δ [ppm]: 8.48 (d, $J_{\text{PH}} = 642$ Hz, 1 H, *PH*), 6.91 (m, 4 H, *C_{ar}H*), 6.75 (m, 2 H, *C_{ar}H*), 5.44 (d, $J_{\text{PH}} = 15$ Hz, 2 H, *NCH*), 5.39 (s, 1 H, *NCH*), 3.77 (m, 2 H, *CHMe₂*), 2.91 (m, 2 H, *CHMe₂*), 1.20 (d, 6 H, *CH₃*), 0.86 (m, 12 H, *CH₃*), 0.77 (d, 6 H, *CH₃*); $^{13}\text{C}\{^1\text{H}\}$ NMR (C_6D_6 , 75 MHz) δ [ppm]: 149.1 (d, $J_{\text{CP}} = 1.6$ Hz, *ipso-C*), 146.9 (d, $J_{\text{CP}} = 3.2$ Hz, *ipso-C'*), 131.6 (d, $J_{\text{CP}} = 3.7$ Hz, *o-C*), 128.0 (*p-CH*), 123.6 (*m-CH*), 122.8 (*m-C'H*), 115.8 (d, $J_{\text{CP}} = 11.6$ Hz, *NCH*), 27.4 (*CH₃*), 23.9 (*CHMe₂*), 23.6 (*C'HMe₂*), 23.1 (*C''HMe₂*), 22.7 (*C'''HMe₂*); $^{31}\text{P}\{^1\text{H}\}$ NMR (C_6D_6 , 121 MHz) δ [ppm]: 2.9 (td, $J_{\text{HP}} = 15$ Hz, *HCNP*, $J_{\text{HP}} = 639$ Hz, *HP*).



Phenylmagnesium bromide (1 M in thf), 0.5 mL, 0.5 mmol) was added dropwise to a stirred solution of **48** (233 mg, 0.5 mmol) in thf (3 mL) at 0 °C, and the mixture was allowed to warm to room temperature with stirring. After 2 hours stirring, the solvent was removed under reduced pressure, followed by extracting with n-hexane (2 × 2 mL) and filtrated. The filtrate was dried under reduced pressure and washed with acetonitrile (2 × 2 mL) affording **54** as yellow powder (210 mg, 0.43 mmol, 87 % yield). M. P. = 189.2 °C. ^1H NMR (C_6D_6 , 300 MHz) δ [ppm]: 7.54 (m, 2

H, $C_{ar}H$), 6.88 (m, 4 H, $C_{ar}H$), 6.73 (m, 5 H, $C_{ar}H$), 5.60 (d, $J_{PH} = 2.3$ Hz, 2 H, NCH), 3.59 (m, 2 H, $CHMe_2$), 3.22 (m, 2 H, $CHMe_2$), 1.23 (d, 6 H, CH_3), 1.07 (m, 12 H, CH_3), 0.91 (d, 6 H, CH_3), 0.20 (d, 6 H, CH_3); $^{13}C\{^1H\}$ NMR (C_6D_6 , 75 MHz) δ [ppm]: 147.6 (*ipso*-C), 146.9 (d, *ipso*-C'), 143.5, 142.7, 137.1, 136.9, 130.2, 129.8, 129.5, 126.1, 123.4, 123.0, 119.7 (d, $J_{CP} = 5.7$ Hz, NCH), 27.5 ($CHMe_2$), 27.2 (CH_3), 24.5 (CH_3), 23.4 (CH_3), 23.0 ($CHMe_2$), 22.9 (CH_3); $^{31}P\{^1H\}$ NMR (C_6D_6 , 121 MHz) δ [ppm]: 102.7. The residue from the filtration above was dried *in vacuo* affording **55** as gray powder (185 mg, 0.487 mmol, 97 % yield). According to the NMR spectrum and the titration experiment done with 1H NMR spectrum (14 mg product and 6.2 mg benzene were mixed in $[D_6]DMSO$, see the following spectrum), this solid has the composition $[55 \cdot (thf)_3]$. M. P. = 125.6 °C (decomposed, turned black). 1H NMR ($[D_6]DMSO$, 300 MHz) δ [ppm]: 3.59 (m, 4 H, OCH_2), 1.75 (m, 4 H, OCH_2CH_2); $^{13}C\{^1H\}$ NMR ($[D_6]DMSO$, 75 MHz) δ [ppm]: 169.2 (d, $J_{CP} = 60$ Hz), 67.0 (OCH_2), 25.1 (OCH_2CH_2); $^{31}P\{^1H\}$ NMR ($[D_6]DMSO$, 121 MHz) δ [ppm]: -381.1. IR (solid): 1736 cm^{-1} (s, OCP).

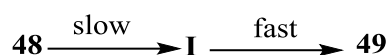


Tetraphenylcyclopentadienone (288 mg, 0.75 mmol) was added to a stirred solution of **48** (117 mg, 0.25 mmol) in THF (3 mL). After stirring for 48 hours, the solvent was removed under reduced pressure, followed by extracting with n-hexane (2×5 mL) and filtrated. The filtrate was dried under reduced pressure and washed with acetonitrile to yield **56** as yellow powder. (57 mg, 0.07 mmol, 28 % yield). M. P. = 157.5 °C. 1H NMR (C_6D_6 , 300 MHz) δ [ppm]: 7.31 (m, 2 H, $C_{ar}H$), 7.15 (m, 2 H, $C_{ar}H$), 6.92 (m, 2 H, $C_{ar}H$), 6.76 (m, 5 H, $C_{ar}H$), 6.67 (m, 5 H, $C_{ar}H$), 6.60 (m, 3 H, $C_{ar}H$), 6.48 (m, 1 H, $C_{ar}H$), 6.33 (m, 6 H, $C_{ar}H$), 5.61 (m, 1 H, NCH), 5.44 (m, 1 H, NCH), 3.66 (m, 1 H, $CHMe_2$), 3.37 (m, 1 H, $CHMe_2$), 3.03 (m, 1 H, $CHMe_2$), 2.67 (m, 1 H, $CHMe_2$), 1.36 (m, 6 H, CH_3), 1.04 (d, 3 H, CH_3), 0.89 (m, 6 H, CH_3), 0.78 (d, 3 H, CH_3), 0.70 (d, 3 H, CH_3), 0.37 (d, 3 H, CH_3); ^{13}C NMR (C_6D_6 , 75 MHz) δ [ppm]: 158.5 (d, $J_{CP} = 1.6$ Hz), 148.6, 147.9, 147.1, 146.1, 145.9, 145.8, 145.7, 141.4, 139.4, 136.8, 136.2, 135.0, 133.5, 133.4, 130.3, 129.6, 129.1, 126.9, 126.7, 126.5, 125.3, 125.6, 124.3, 124.8, 121.4, 121.0, 117.2, 66.6 (dd, $J_{CP} = 52.2$ Hz, PC, $J_{CP} = 7.5$ Hz, PPC), 65.7, 31.8, 29.6, 29.0, 28.2, 26.6,

26.2, 26.0, 25.0, 24.2, 23.7, 22.6, 22.2, 15.4, 14.2; $^{31}\text{P}\{^1\text{H}\}$ NMR (C_6D_6 , 121 MHz) δ [ppm]: 118.2, 112.8 (d, $J_{\text{PP}} = 651$ Hz), $\delta = -140.5, -145.9$ (d, $J_{\text{PP}} = 651$ Hz).

Kinetic measurement and analysis for the dimerization of **48**

From the studies of the reaction for the dimerization of **48**, the reaction is relatively slow and the intermediate **I** can be trapped by 2,3-dimethylenebutane, however **I** can't be observed from the NMR spectrum during the dimerization, so we assumed the speed of the reaction for **I** converting to **49** is very high, the barrier step for dimerization is the first step from **48** to **I**.



The ^{31}P NMR data for kinetic analysis were acquired on Bruker-200 spectrometers. All integrals were normalized versus the started concentration of **48** and plotted versus the time. The values of the integrals were fit by a non-linear least squares method to the first order equations $[3] = Ae^{-kt}$ and $[5] = B - Ce^{-kt}$ (where A, B, C and k were allowed to vary freely) using the automated routine of Gnuplot.

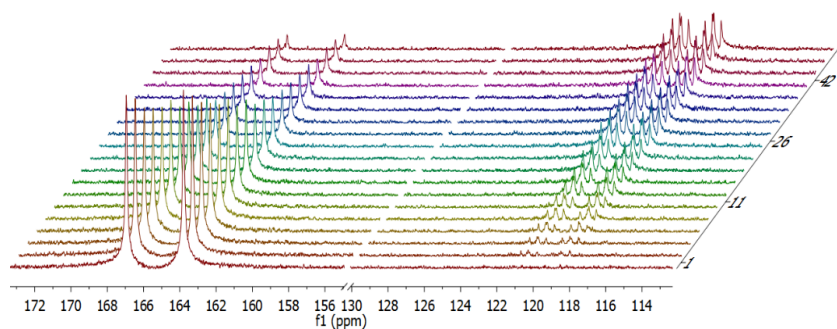


Figure 4. Dimerization of **48** to **49** in toluene (^{31}P NMR) at 0 hour to 75 hours (front to back). The left are the doublets from **48**, the right is the multiplet for **49**. The other region of chemical shifts have been omitted.

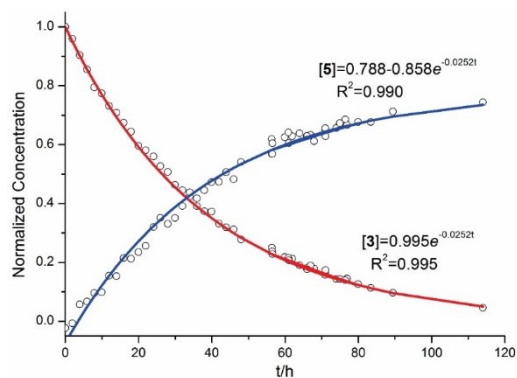


Figure 5. Representative kinetic data on the dimerization of **48** to **5** in toluene at 25 °C. The concentration versus time profile of starting material **48** and product dimer **5** fit first order equation: $[48] = Ae^{-kt}$ and $[48a] = B - Ce^{-kt}$, with a rate constant $k_{\text{obs}} = 0.23$ and 0.28 h^{-1} at 25 °C.

10 APPENDIX

10.1 CRYSTALLOGRAPHIC INFORMATION

10.1.1 Experimental Details

X-Ray diffraction was measured on a *Bruker SMART Apex II* diffractometer with CCD area detector; MoK α radiation (0.71073 Å) at T = 100 K. The refinement against full matrix (versus *F*²) was done with SHELXTL (ver. 6.12) and SHELXL-97. Empirical absorption correction was done with SADABS (ver. 2.03). All non-hydrogen atoms were refined anisotropically where not noted otherwise. The contribution of the hydrogen atoms, in their calculated positions, was included in the refinement using a riding model.

10.1.2 Crystallographic data and tables

The tables containing the crystal data and structure refinement for all of the compounds reported in this work whose solid state structures were determined, can be found in the following pages. In the cases where the structures were not discussed in the previous chapters (precursors), the selected bond distances and angles are also reported.

10.2 CRYSTALLOGRAPHIC TABLES

Identification code	Na(DME)(2)	2 × 2H × (dioxane)	5
Empirical formula	C ₃₆ H ₅₅ O ₁₂ Na ₄ P ₄	C ₁₄ H ₁₇ O ₄ NaP ₂	C ₁₇ H ₁₄ O ₂ P ₂
Formula weight	895.64	334.20	312.22
Temperature/K	100.0	200.15	100.15
Crystal system	monoclinic	monoclinic	monoclinic
Space group	P2 ₁ /n	P2 ₁ /n	P2 ₁ /c
a/Å	11.0571(5)	6.27310(10)	8.0881(16)
b/Å	33.2981(16)	7.2118(2)	11.622(2)
c/Å	12.8385(7)	17.7108(4)	18.110(3)
α/°	90	90	90.00
β/°	105.4266(10)	95.289(2)	113.525(7)
γ/°	90	90	90.00
Volume/Å ³	4556.6(4)	797.83(3)	1560.8(5)
Z	4	2	4
ρ _{calc} /cm ³	1.306	1.391	1.329
μ/mm ⁻¹	0.258	0.310	0.279
F(000)	1884.0	348.0	648.0
Crystal size/mm ³	0.3 × 0.2 × 0.2	0.5 × 0.15 × 0.15	0.18 × 0.13 × 0.05
Radiation	MoKα (λ = 0.71073)	MoKα (λ = 0.71073)	MoKα (λ = 0.71073)
2θ range for data collection/°	2.446 to 52.484	6.104 to 63	4.28 to 52.74
Index ranges	-13 ≤ h ≤ 9, -41 ≤ k ≤ 41, -15 ≤ l ≤ 15	-9 ≤ h ≤ 9, -10 ≤ k ≤ 8, -26 ≤ l ≤ 23	-10 ≤ h ≤ 10, -14 ≤ k ≤ 0, -22 ≤ l ≤ 9
Reflections collected	40295	10343	3190
Independent reflections	9160 [R _{int} = 0.0779, R _{sigma} = 0.0807]	2654 [R _{int} = 0.0208, R _{sigma} = 0.0208]	3190 [R _{int} = 0.0000, R _{sigma} = 0.0503]
Data/restraints/parameters	9160/0/533	2654/0/133	3190/0/238
Goodness-of-fit on F ²	0.919	1.099	1.027
Final R indexes [I ≥ 2σ (I)]	R ₁ = 0.0431, wR ₂ = 0.0817	R ₁ = 0.0288, wR ₂ = 0.0837	R ₁ = 0.0552, wR ₂ = 0.1131
Final R indexes [all data]	R ₁ = 0.0742, wR ₂ = 0.0913	R ₁ = 0.0390, wR ₂ = 0.0866	R ₁ = 0.0852, wR ₂ = 0.1247
Largest diff. peak/hole / e Å ⁻³	0.76/-0.35	0.38/-0.20	0.81/-0.32

Identification code	10	11
---------------------	----	----

Empirical formula	C ₁₇ H ₁₄ OP ₂ Cl ₂ Pd	C ₁₇ H ₁₄ OP ₂ Cl ₂ Pd
Formula weight	473.52	473.52
Temperature/K	100.15	100.15
Crystal system	monoclinic	monoclinic
Space group	C2/c	C2/c
a/Å	23.162(2)	23.162(2)
b/Å	9.8544(8)	9.8544(8)
c/Å	18.190(3)	18.190(3)
α/°	90.00	90.00
β/°	121.6220(10)	121.6220(10)
γ/°	90.00	90.00
Volume/Å ³	3535.3(7)	3535.3(7)
Z	8	8
ρ _{calc} /g/cm ³	1.779	1.779
μ/mm ⁻¹	1.533	1.533
F(000)	1872.0	1872.0
Crystal size/mm ³	0.15 × 0.09 × 0.037	0.15 × 0.09 × 0.037
Radiation	MoKα (λ = 0.71073)	MoKα (λ = 0.71073)
2θ range for data collection/°	4.14 to 52.04	4.14 to 52.04
Index ranges	-28 ≤ h ≤ 26, -11 ≤ k ≤ 11, -22 ≤ l ≤ 21	-28 ≤ h ≤ 26, -11 ≤ k ≤ 11, -22 ≤ l ≤ 21
Reflections collected	6990	6990
Independent reflections	3435 [R _{int} = 0.0593, R _{sigma} = 0.0694]	3435 [R _{int} = 0.0593, R _{sigma} = 0.0694]
Data/restraints/parameters	3435/0/252	3435/0/252
Goodness-of-fit on F ²	0.933	0.933
Final R indexes [I ≥ 2σ (I)]	R ₁ = 0.0279, wR ₂ = 0.0440	R ₁ = 0.0279, wR ₂ = 0.0440
Final R indexes [all data]	R ₁ = 0.0459, wR ₂ = 0.0497	R ₁ = 0.0459, wR ₂ = 0.0497
Largest diff. peak/hole / e Å ⁻³	0.70/-0.97	0.70/-0.97

	12	13	14
Identification code			
Empirical formula	C ₃₁ H ₂₉ O ₃ P ₄ Cl ₄ Rh	C ₄₈ H ₄₂ O _{3.5} P ₅ Rh	C ₆₄ H ₆₂ Li ₂ O ₈ P ₈ Rh ₂ l ₂
Formula weight	818.13	932.57	1680.39
Temperature/K	105.93(10)	100.0	100
Crystal system	monoclinic	monoclinic	monoclinic
Space group	P2 ₁ /c	P2 ₁ /c	P2 ₁ /n
a/Å	20.6756(7)	10.3260(4)	13.53806(14)
b/Å	9.4283(3)	17.0270(8)	16.20413(15)
c/Å	18.7505(7)	23.6585(10)	15.62853(13)
α/°	90	90	90
β/°	113.847(4)	100.866(2)	101.9587(9)
γ/°	90	90	90
Volume/Å ³	3343.1(2)	4085.1(3)	3354.06(6)
Z	4	4	2
ρ _{calc} /g/cm ³	1.625	1.516	1.664
μ/mm ⁻¹	1.055	0.659	1.655
F(000)	1648.0	1912.0	1664.0
Crystal size/mm ³	0.3 × 0.1 × 0.1	0.16 × 0.1 × 0.06	0.32 × 0.28 × 0.18
Radiation	MoKα (λ = 0.71073)	MoKα (λ = 0.71073)	MoKα (λ = 0.71073)
2θ range for data	5.752 to 65.092	2.966 to 55.318	5.892 to 65.288
Index ranges	-30 ≤ h ≤ 30, -14 ≤ k ≤ 13, -22 ≤ l ≤ 27	-13 ≤ h ≤ 13, -22 ≤ k ≤ 30, 0 ≤ l ≤ 30	-19 ≤ h ≤ 20, -22 ≤ k ≤ 23, -23 ≤ l ≤ 23
Reflections collected	25473	18505	32850
Independent reflections	10946 [R _{int} = 0.0444, R _{sigma} = 0.0680]	9432 [R _{int} = 0.0364, R _{sigma} = 0.0501]	11287 [R _{int} = 0.0251, R _{sigma} = 0.0301]
Data/restraints/paramet	10946/0/393	9432/0/532	11287/0/500
Goodness-of-fit on F ²	1.030	1.006	1.066
Final R indexes [I ≥ 2σ (I)]	R ₁ = 0.0498, wR ₂ = 0.0957	R ₁ = 0.0341, wR ₂ = 0.0879	R ₁ = 0.0258, wR ₂ = 0.0541
Final R indexes [all data]	R ₁ = 0.0705, wR ₂ = 0.1051	R ₁ = 0.0591, wR ₂ = 0.1097	R ₁ = 0.0310, wR ₂ = 0.0562
Largest diff. peak/hole / e	1.00/-0.63	0.79/-0.51	0.93/-0.61

Identification code	15	16
Empirical formula	C ₁₀ H ₁₀ O ₂ P ₂ Rh	C ₁₅ H ₁₂ O ₃ P ₃ ClRh
Formula weight	358.75	475.02
Temperature/K	296.15	190.0
Crystal system	triclinic	triclinic
Space group	P-1	P-1
a/Å	9.5152(8)	11.9101(5)
b/Å	9.9594(8)	12.4858(10)
c/Å	14.1462(13)	12.6286(12)
α/°	80.0276(14)	97.724(7)
β/°	79.8788(15)	106.602(6)
γ/°	62.2642(11)	98.644(5)
Volume/Å ³	1161.64(17)	1747.8(2)
Z	4	4
ρ _{calc} /cm ³	2.051	1.805
μ/mm ⁻¹	2.386	1.414
F(000)	697.0	939.0
Crystal size/mm ³	0.3 × 0.25 × 0.25	0.4 × 0.2 × 0.2
Radiation	MoKα (λ = 0.71073)	MoKα (λ = 0.71073)
2θ range for data collection/°	7.216 to 68.518	5.728 to 58.188
Index ranges	-14 ≤ h ≤ 14, -15 ≤ k ≤ 15, - 22 ≤ l ≤ 22	-15 ≤ h ≤ 15, -16 ≤ k ≤ 17, - 17 ≤ l ≤ 15
Reflections collected	13689	36884
Independent reflections	8460 [R _{int} = 0.0585, R _{sigma} = 0.0885]	8415 [R _{int} = 0.0433, R _{sigma} = 0.0414]
Data/restraints/parameters	8460/78/271	8415/0/539
Goodness-of-fit on F ²	1.012	1.036
Final R indexes [I ≥ 2σ (I)]	R ₁ = 0.0402, wR ₂ = 0.0849	R ₁ = 0.0336, wR ₂ = 0.0702
Final R indexes [all data]	R ₁ = 0.0657, wR ₂ = 0.1125	R ₁ = 0.0463, wR ₂ = 0.0765
Largest diff. peak/hole / e Å ⁻³	1.84/-1.78	0.47/-0.49

Identification code	17	18	19
Empirical formula	C ₃₄ H ₂₈ O ₂ P ₄ Cl ₂ Cu ₂	C ₃₄ H ₂₈ O ₂ P ₄ Cu ₂ Br ₂	C ₃₄ H ₂₈ O ₂ P ₄ Cu ₂ I ₂
Formula weight	790.42	879.34	973.32
Temperature/K	101.1	100.7	100
Crystal system	triclinic	triclinic	triclinic
Space group	P-1	P-1	P-1
a/Å	10.1153(7)	9.8061(6)	9.9228(6)
b/Å	10.2522(7)	10.1371(7)	10.2858(5)
c/Å	18.1667(12)	10.4135(7)	10.5582(6)
α/°	84.749(2)	118.5616(19)	118.070(5)
β/°	88.568(2)	105.859(2)	106.077(5)
γ/°	63.210(2)	94.680(2)	94.502(4)
Volume/Å ³	1674.4(2)	846.53(10)	885.52(9)
Z	2	1	1
ρ _{calc} /g/cm ³	1.568	1.725	1.825
μ/mm ⁻¹	1.652	3.836	3.154
F(000)	800.0	436.0	472.0
Crystal size/mm ³	0.41 × 0.32 × 0.25	0.26 × 0.25 × 0.21	0.2 × 0.1 × 0.08
Radiation	MoKα (λ = 0.71073)	MoKα (λ = 0.71073)	MoKα (λ = 0.71073)
2θ range for data collection/°	4.468 to 52.812	4.726 to 74.28	5.552 to 64.718
Index ranges	-12 ≤ h ≤ 12, -12 ≤ k ≤ 12, -22 ≤ l ≤ 22	-16 ≤ h ≤ 16, -17 ≤ k ≤ 17, -17 ≤ l ≤ 17	-14 ≤ h ≤ 14, -15 ≤ k ≤ 11, -14 ≤ l ≤ 15
Reflections collected	63567	20591	10600
Independent reflections	6871 [R _{int} = 0.0600, R _{sigma} = 0.0275]	8462 [R _{int} = 0.0950, R _{sigma} = 0.0817]	5763 [R _{int} = 0.0270, R _{sigma} = 0.0434]
Data/restraints/parameters	6871/0/509	8462/0/255	5763/0/255
Goodness-of-fit on F ²	1.120	0.987	1.011
Final R indexes [I ≥ 2σ (I)]	R ₁ = 0.0321, wR ₂ = 0.0702	R ₁ = 0.0402, wR ₂ = 0.0930	R ₁ = 0.0281, wR ₂ = 0.0607
Final R indexes [all data]	R ₁ = 0.0428, wR ₂ = 0.0738	R ₁ = 0.0661, wR ₂ = 0.1025	R ₁ = 0.0329, wR ₂ = 0.0631
Largest diff. peak/hole / e Å ⁻³	0.52/-0.37	1.47/-0.89	0.79/-1.01

Identification code	20	21
Empirical formula	C ₄₂ H ₄₄ O ₄ P ₄ Cl ₄ Cu ₄	C ₃₈ H ₃₄ N ₂ O ₂ P ₄ Cl ₄ Cu ₄
Formula weight	1132.61	1070.51
Temperature/K	100.15	100.15
Crystal system	triclinic	monoclinic
Space group	P-1	P2 ₁ /c
a/Å	9.6929(16)	9.9119(17)
b/Å	15.742(3)	17.631(3)
c/Å	16.427(3)	12.173(2)
α/°	66.649(2)	90
β/°	74.850(2)	110.196(2)
γ/°	80.491(3)	90
Volume/Å ³	2215.9(6)	1996.5(6)
Z	4	2
ρ _{calc} /g/cm ³	1.697	1.781
μ/mm ⁻¹	2.321	2.568
F(000)	1144.0	1072.0
Crystal size/mm ³	0.22 × 0.18 × 0.18	0.5 × 0.26 × 0.13
Radiation	MoKα (λ = 0.71073)	MoKα (λ = 0.71073)
2θ range for data collection/°	2.766 to 51.364	4.248 to 58.26
Index ranges	-11 ≤ h ≤ 11, -19 ≤ k ≤ 19, -20 ≤ l ≤ 20	-13 ≤ h ≤ 10, -24 ≤ k ≤ 23, -16 ≤ l ≤ 15
Reflections collected	16963	14434
Independent reflections	8166 [R _{int} = 0.0774, R _{sigma} = 0.1008]	5328 [R _{int} = 0.0696, R _{sigma} = 0.0752]
Data/restraints/parameters	8166/0/650	5328/0/300
Goodness-of-fit on F ²	0.818	0.897
Final R indexes [I ≥ 2σ (I)]	R ₁ = 0.0375, wR ₂ = 0.0706	R ₁ = 0.0351, wR ₂ = 0.0713
Final R indexes [all data]	R ₁ = 0.0563, wR ₂ = 0.0756	R ₁ = 0.0497, wR ₂ = 0.0757
Largest diff. peak/hole / e Å ⁻³	0.57/-0.51	0.83/-0.51

Identification code	24	25
Empirical formula	C ₉₄ H ₁₀₄ O ₁₄ Na ₄ P ₄	C ₃₉ H ₃₆ NaO ₅ P
Formula weight	1673.61	638.64
Temperature/K	293(2)	100.02
Crystal system	monoclinic	orthorhombic
Space group	P2 ₁ /c	P2 ₁ 2 ₁ 2 ₁
a/Å	14.7071(10)	10.2521(4)
b/Å	15.8795(6)	37.6012(13)
c/Å	22.3535(15)	8.6662(3)
α/°	90	90
β/°	123.792(10)	90
γ/°	90	90
Volume/Å ³	4338.5(6)	3340.7(2)
Z	2	4
ρ _{calc} /cm ³	1.281	1.27
μ/mm ⁻¹	0.171	0.139
F(000)	1768	1344
Crystal size/mm ³	0.2 × 0.16 × 0.1	0.22 × 0.12 × 0.05
Radiation	MoKα (λ = 0.71073)	MoKα (λ = 0.71073)
2θ range for data collection/°	5.58 to 49.426	4.12 to 52.74
Index ranges	-16 ≤ h ≤ 17, -18 ≤ k ≤ 18, -26 ≤ l ≤ 26	-10 ≤ h ≤ 12, -26 ≤ k ≤ 46, -10 ≤ l ≤ 5
Reflections collected	31741	14055
Independent reflections	7345 [R _{int} = 0.0686, R _{sigma} = 0.0701]	6458 [R _{int} = 0.0336, R _{sigma} = 0.0564]
Data/restraints/parameters	7345/0/723	6458/9/414
Goodness-of-fit on F ²	1.034	1.452
Final R indexes [I ≥ 2σ (I)]	R ₁ = 0.0496, wR ₂ = 0.0994	R ₁ = 0.0652, wR ₂ = 0.1474
Final R indexes [all data]	R ₁ = 0.0822, wR ₂ = 0.1159	R ₁ = 0.0802, wR ₂ = 0.1521
Largest diff. peak/hole / e Å ⁻³	0.31/-0.35	0.55/-0.47

Identification code	26	28
Empirical formula	C ₅₄ H ₅₆ Na ₂ O ₁₂ P ₂	C ₂₂ H ₃₂ O ₁₁ NaP
Formula weight	1004.91	526.43
Temperature/K	373(2)	100.2
Crystal system	monoclinic	monoclinic
Space group	P2 ₁ /c	P2 ₁ /n
a/Å	11.8005(5)	11.3291(5)
b/Å	20.4205(8)	17.6383(8)
c/Å	11.9120(5)	13.7134(7)
α/°	90.00	90
β/°	119.700(2)	109.909(2)
γ/°	90.00	90
Volume/Å ³	2493.37(18)	2576.5(2)
Z	2	4
ρ _{calc} /cm ³	1.339	1.357
μ/mm ⁻¹	0.168	0.180
F(000)	1056.0	1112.0
Crystal size/mm ³	0.26 × 0.14 × 0.07	0.2 × 0.165 × 0.12
Radiation	MoKα (λ = 0.71073)	MoKα (λ = 0.71073)
2θ range for data collection/°	4.42 to 50.7°	3.912 to 59.148
Index ranges	-13 ≤ h ≤ 14, -24 ≤ k ≤ 24, -14 ≤ l ≤ 8	-15 ≤ h ≤ 15, -24 ≤ k ≤ 24, -19 ≤ l ≤ 19
Reflections collected	13119	71695
Independent reflections	4561 [R(int) = 0.0380]	7227 [R _{int} = 0.0346, R _{sigma} = 0.0204]
Data/restraints/parameters	4561/0/373	7227/0/444
Goodness-of-fit on F ²	1.020	0.991
Final R indexes [I ≥ 2σ (I)]	R ₁ = 0.0537, wR ₂ = 0.1183	R ₁ = 0.0367, wR ₂ = 0.1122
Final R indexes [all data]	R ₁ = 0.0884, wR ₂ = 0.1381	R ₁ = 0.0491, wR ₂ = 0.1243
Largest diff. peak/hole / e Å ⁻³	0.66/-0.73	0.54/-0.25

Identification code	29	30
Empirical formula	C ₂₇ H ₂₈ NaO ₈ P	C ₇₀ H ₈₈ Na ₂ O ₁₆ P ₂ S ₄
Formula weight	548.16	1421.56
Temperature/K	296.15	101.3
Crystal system	monoclinic	monoclinic
Space group	P2 ₁ /c	P2 ₁
a/Å	13.314(7)	13.8246(9)
b/Å	18.783(9)	16.0645(10)
c/Å	11.773(6)	17.1249(11)
α/°	90	90
β/°	115.686(9)	107.8494(17)
γ/°	90	90
Volume/Å ³	2653(2)	3620.1(4)
Z	4	2
ρ _{calc} /cm ³	1.372	1.304
μ/mm ⁻¹	0.264	0.252
F(000)	1139.0	1504.0
Crystal size/mm ³	0.3 × 0.2 × 0.2	0.4 × 0.3 × 0.2
Radiation	MoKα (λ = 0.71073)	MoKα (λ = 0.71073)
2θ range for data collection/°	3.394 to 56.356	4.998 to 66.196
Index ranges	-17 ≤ h ≤ 17, -24 ≤ k ≤ 24, -15 ≤ l ≤ 15	-21 ≤ h ≤ 21, -24 ≤ k ≤ 24, -25 ≤ l ≤ 26
Reflections collected	31001	74711
Independent reflections	6200 [R _{int} = 0.2431, R _{sigma} = 0.1245]	26918 [R _{int} = 0.0720, R _{sigma} = 0.0716]
Data/restraints/parameters	6200/0/336	26918/135/912
Goodness-of-fit on F ²	1.047	1.187
Final R indexes [I ≥ 2σ(I)]	R ₁ = 0.0995, wR ₂ = 0.2106	R ₁ = 0.0794, wR ₂ = 0.1347
Final R indexes [all data]	R ₁ = 0.1283, wR ₂ = 0.2391	R ₁ = 0.1143, wR ₂ = 0.1505
Largest diff. peak/hole / e Å ⁻³	1.11/-0.90	0.49/-0.45

	31	32
Identification code	31	32
Empirical formula	C ₄₆ H ₄₀ P ₂ O ₁₀	C ₂₃ H ₂₀ O ₅ PI
Formula weight	814.72	534.26
Temperature/K	100.0	100.0
Crystal system	tetragonal	monoclinic
Space group	P4 ₃ 2 ₁ 2	P2 ₁ /n
a/Å	12.4129(14)	5.7518(3)
b/Å	12.4129(14)	23.9962(12)
c/Å	25.452(3)	16.4753(8)
α/°	90	90
β/°	90	97.2217(16)
γ/°	90	90
Volume/Å ³	3921.7(10)	2255.9(2)
Z	4	4
ρ _{calc} /cm ³	1.380	1.573
μ/mm ⁻¹	0.173	1.521
F(000)	1704.0	1064.0
Crystal size/mm ³	0.3 × 0.3 × 0.2	0.3 × 0.2 × 0.2
Radiation	MoKα (λ = 0.71073)	MoKα (λ = 0.71073)
2θ range for data collection/°	4.584 to 55.472	4.984 to 72.746
Index ranges	-16 ≤ h ≤ 16, -15 ≤ k ≤ 16, -33 ≤ l ≤ 33	-6 ≤ h ≤ 9, -39 ≤ k ≤ 37, -27 ≤ l ≤ 18
Reflections collected	167676	20282
Independent reflections	4605 [R _{int} = 0.0561, R _{sigma} = 0.0277]	9627 [R _{int} = 0.0249, R _{sigma} = 0.0277]
Data/restraints/parameters	4605/0/342	9627/0/351
Goodness-of-fit on F ²	1.194	1.069
Final R indexes [I ≥ 2σ (I)]	R ₁ = 0.0479, wR ₂ = 0.0954	R ₁ = 0.0304, wR ₂ = 0.0639
Final R indexes [all data]	R ₁ = 0.0688, wR ₂ = 0.1059	R ₁ = 0.0404, wR ₂ = 0.0675
Largest diff. peak/hole / e Å ⁻³	0.24/-0.24	1.02/-0.54

	33	34
Identification code	33	34
Empirical formula	C ₄₆ H ₄₀ O ₁₀ P ₂ S	C ₄₆ H ₄₀ O ₁₀ P ₂ S ₂
Formula weight	842.24	280.22
Temperature/K	107(2)	273.15
Crystal system	triclinic	monoclinic
Space group	P-1	C2/c
a/Å	12.0256(3)	19.6455(17)
b/Å	16.8103(5)	13.8200(12)
c/Å	21.0449(7)	17.2636(15)
α/°	90	90
β/°	95.296(3)	116.6552(12)
γ/°	90	90
Volume/Å ³	4236.2(2)	4188.9(6)
Z	4	4
ρ _{calc} /cm ³	1.321	1.777
μ/mm ⁻¹	0.21	1.618
F(000)	1750	2208
Crystal size/mm ³	0.2 × 0.15 × 0.15	0.4 × 0.3 × 0.3
Radiation	MoKα (λ = 0.71073)	MoKα (λ = 0.71073)
2θ range for data collection/°	5.832 to 65.194	3.75 to 62.858
Index ranges	-17 ≤ h ≤ 16, -24 ≤ k ≤ 23, -31 ≤ l ≤ 31	-28 ≤ h ≤ 28, -19 ≤ k ≤ 19, -24 ≤ l ≤ 25
Reflections collected	54725	24182
Independent reflections	27615 [R _{int} = 0.0560, R _{sigma} = 0.1062]	6399 [R _{int} = 0.0538, R _{sigma} = 0.0353]
Data/restraints/parameters	27615/0/1073	6399/0/351
Goodness-of-fit on F ²	1.054	1.074
Final R indexes [I ≥ 2σ (I)]	R ₁ = 0.0724, wR ₂ = 0.1149	R ₁ = 0.0357, wR ₂ = 0.0989
Final R indexes [all data]	R ₁ = 0.0999, wR ₂ = 0.1257	R ₁ = 0.0400, wR ₂ = 0.1016
Largest diff. peak/hole / e Å ⁻³	0.46/-0.45	0.56/-0.26

Identification code	37	38
Empirical formula	C ₁₀ H ₁₀ N ₂ ONaP	C ₅₁ H ₈₆ N ₄ O ₇ NaP
Formula weight	228.16	921.19
Temperature/K	100.0	100
Crystal system	monoclinic	monoclinic
Space group	P2 ₁ /n	P2 ₁ /c
a/Å	11.2038(7)	12.0139(5)
b/Å	20.9316(11)	13.4611(5)
c/Å	17.6696(10)	34.2114(13)
α/°	90	90
β/°	91.3174(18)	91.00
γ/°	90	90
Volume/Å ³	4142.7(4)	5531.8(4)
Z	15	4
ρ _{calc} /cm ³	1.372	1.106
μ/mm ⁻¹	0.260	0.106
F(000)	1770.0	2008.0
Crystal size/mm ³	0.3 × 0.2 × 0.2	0.4 × 0.4 × 0.4
Radiation	MoKα (λ = 0.71073)	MoKα (λ = 0.71073)
2θ range for data collection/°	4.524 to 64.248	2.382 to 66.968
Index ranges	-16 ≤ h ≤ 16, -31 ≤ k ≤ 31, -26 ≤ l ≤ 26	-18 ≤ h ≤ 18, -20 ≤ k ≤ 20, -52 ≤ l ≤ 52
Reflections collected	132854	190174
Independent reflections	14488 [R _{int} = 0.0503, R _{sigma} = 0.0294]	21204 [R _{int} = 0.1795, R _{sigma} = 0.0831]
Data/restraints/parameters	14488/0/713	21204/0/899
Goodness-of-fit on F ²	1.026	0.990
Final R indexes [I ≥ 2σ (I)]	R ₁ = 0.0600, wR ₂ = 0.1432	R ₁ = 0.0519, wR ₂ = 0.1238
Final R indexes [all data]	R ₁ = 0.0888, wR ₂ = 0.1633	R ₁ = 0.0948, wR ₂ = 0.1445
Largest diff. peak/hole / e Å ⁻³	1.34/-0.37	0.37/-0.51

	42	44	46
Identification code	42	44	46
Empirical formula	C ₂₈ H ₃₄ Cl ₂ I ₃ N ₄ O	C _{31.5} H ₄₀ F ₃ N ₄ O _{4.5} PS	C ₈₄ H ₁₂₆ N ₈ O ₂ P ₂
Formula weight	894.19	665.19	1341.86
Temperature/K	100.0	100.0	101.8
Crystal system	triclinic	triclinic	monoclinic
Space group	P-1	P-1	P2/n
a/Å	10.4182(6)	10.9250(5)	13.1340(5)
b/Å	10.8486(7)	11.8726(6)	13.9419(7)
c/Å	14.6771(9)	13.1288(7)	21.3836(10)
α/°	79.172(2)	94.1458(19)	90
β/°	82.503(2)	99.5637(17)	90.6064(16)
γ/°	89.072(2)	100.0991(17)	90
Volume/Å ³	1615.33(17)	1644.18(14)	3915.4(3)
Z	2	2	2
ρ _{calc} /g/cm ³	1.838	1.344	1.138
μ/mm ⁻¹	3.095	0.208	0.107
F(000)	862.0	699.0	1464
Crystal size/mm ³	0.2 × 0.1 × 0.1	0.3 × 0.25 × 0.25	0.3 × 0.2 × 0.2
Radiation	MoKα (λ = 0.71073)	MoKα (λ = 0.71073)	MoKα (λ = 0.71073)
2θ range for data	5.156 to 62.856	4.468 to 61.068	4.654 to 65.278
Index ranges	-14 ≤ h ≤ 14, -15 ≤ k ≤ 9, -20 ≤ l ≤ 20	-13 ≤ h ≤ 15, -16 ≤ k ≤ 16, -18 ≤ l ≤ 18	-19 ≤ h ≤ 19, -21 ≤ k ≤ 21, -32 ≤ l ≤ 32
Reflections collected	9411	71340	146005
Independent reflections	7197 [R _{int} = 0.0371, R _{sigma} = 0.0559]	9865 [R _{int} = 0.1049, R _{sigma} = 0.0444]	14322 [R _{int} = 0.0908, R _{sigma} = 0.0383]
Data/restraints/parameters	7197/0/343	9865/0/474	14322/0/685
Goodness-of-fit on F ²	1.043	1.037	1.061
Final R indexes [I ≥ 2σ (I)]	R ₁ = 0.0622, wR ₂ = 0.1376	R ₁ = 0.0732, wR ₂ = 0.1935	R ₁ = 0.0470, wR ₂ = 0.1071
Final R indexes [all data]	R ₁ = 0.0978, wR ₂ = 0.1609	R ₁ = 0.0917, wR ₂ = 0.2112	R ₁ = 0.0668, wR ₂ = 0.1174
Largest diff. peak/hole / e Å ⁻³	2.46/-2.29	1.55/-1.29	0.45/-0.35

Identification code	48	49
Empirical formula	C ₂₇ H ₃₆ N ₂ OP ₂	C ₅₃ H ₇₂ N ₄ OP ₄
Formula weight	466.55	905.02
Temperature/K	100.4	105(1)
Crystal system	monoclinic	triclinic
Space group	P2 ₁ /c	P-1
a/Å	9.5186(12)	9.86749(18)
b/Å	12.9781(15)	15.8674(3)
c/Å	21.293(3)	18.6581(4)
α/°	90	68.043(2)
β/°	95.781(4)	77.0428(17)
γ/°	90	73.5767(17)
Volume/Å ³	2617.0(6)	2575.71(10)
Z	4	2
ρ _{calc} /cm ³	1.1841	1.167
μ/mm ⁻¹	0.187	0.187
F(000)	1001.2	972
Crystal size/mm ³	0.477 × 0.183 × 0.129	0.28 × 0.21 × 0.13
Radiation	Mo Kα (λ = 0.71073)	MoKα (λ = 0.71073)
2θ range for data collection/°	4.96 to 61.2	5.686 to 65.138
Index ranges	-13 ≤ h ≤ 13, -15 ≤ k ≤ 18, -30 ≤ l ≤ 30	-14 ≤ h ≤ 14, -23 ≤ k ≤ 24, -26 ≤ l ≤ 28
Reflections collected	35771	82945
Independent reflections	7819 [R _{int} = 0.0296, R _{sigma} = 0.0223]	17517 [R _{int} = 0.0320, R _{sigma} = 0.0272]
Data/restraints/parameters	7819/1/432	17517/0/682
Goodness-of-fit on F ²	1.033	1.08
Final R indexes [I ≥ 2σ (I)]	R ₁ = 0.0376, wR ₂ = 0.0957	R ₁ = 0.0482, wR ₂ = 0.1228
Final R indexes [all data]	R ₁ = 0.0476, wR ₂ = 0.1042	R ₁ = 0.0559, wR ₂ = 0.1274
Largest diff. peak/hole / e Å ⁻³	0.43/-0.29	1.12/-0.47

	50	56
Identification code	50	56
Empirical formula	C ₃₃ H ₄₆ N ₂ OP ₂	C ₆₃ H ₆₅ N ₃ OP ₂
Formula weight	548.66	942.12
Temperature/K	100.8	100.7
Crystal system	triclinic	triclinic
Space group	P-1	P-1
a/Å	10.0689(11)	17.7901(14)
b/Å	11.5642(12)	18.7231(16)
c/Å	14.5238(16)	19.1169(16)
α/°	84.273(3)	73.099(3)
β/°	72.479(3)	63.618(3)
γ/°	76.618(3)	71.027(3)
Volume/Å ³	1568.1(3)	5313.5(8)
Z	2	4
ρ _{calc} /cm ³	1.162	1.178
μ/mm ⁻¹	0.166	0.126
F(000)	592	2008
Crystal size/mm ³	0.3 × 0.2 × 0.2	0.21 × 0.2 × 0.18
Radiation	MoKα (λ = 0.71073)	MoKα (λ = 0.71073)
2θ range for data collection/°	4.592 to 52.882	4.246 to 56.71
Index ranges	-12 ≤ h ≤ 12, -14 ≤ k ≤ 14, -18 ≤ l ≤ 18	-23 ≤ h ≤ 23, -24 ≤ k ≤ 24, -25 ≤ l ≤ 25
Reflections collected	42934	243043
Independent reflections	6422 [R _{int} = 0.0246, R _{sigma} = 0.0125]	26447 [R _{int} = 0.0932, R _{sigma} = 0.0409]
Data/restraints/parameters	6422/0/527	26447/3197/1234
Goodness-of-fit on F ²	1.022	1.055
Final R indexes [I ≥ 2σ (I)]	R ₁ = 0.0364, wR ₂ = 0.0958	R ₁ = 0.0654, wR ₂ = 0.1717
Final R indexes [all data]	R ₁ = 0.0398, wR ₂ = 0.0985	R ₁ = 0.0864, wR ₂ = 0.1862
Largest diff. peak/hole / e Å ⁻³	1.12/-0.22	1.60/-0.96

- [1] P. R. Hanson, *Beils. J. Organ. Chem.* **2014**, *10*, 2087-2088.
- [2] S. Trippett, *Annu. Rep. Prog. Chem., Sect. B: Org. Chem.* **1973**, *70*, 268-284.
- [3] G. Hilgetag, *Z. Chem.* **1976**, *16*, 253-259.
- [4] J. I. G. Cadogan, P. K. G. Hodgson, *Phosphorus Sulfur Silicon Relat Elem.* **1987**, *30*, 3-88.
- [5] I. L. Odinets, E. V. Matveeva, *Russ. Chem. Rev.* **2012**, *81*, 221-238.
- [6] G. Keglevich, *Curr. Org. Chem.* **2010**, *14*, 425-425.
- [7] C. Fish, M. Green, R. J. Kilby, J. M. Lynam, J. E. McGrady, D. A. Pantazis, C. A. Russell, A. C. Whitwood, C. E. Willans, *Angew. Chem. Int. Ed.* **2006**, *45*, 3628-3631.
- [8] J. F. Nixon, *Coord. Chem. Rev.* **1995**, *145*, 201-258.
- [9] F. Mathey, *Angew. Chem. Int. Ed.* **2003**, *42*, 1578-1604.
- [10] T. E. Gier, *J. Am. Chem. Soc.* **1961**, *83*, 1769-1771.
- [11] G. Becker, W. Massa, O. Mundt, R. Schmidt, *Z. Anorg. Allg. Chem.* **1982**, *485*, 23-35.
- [12] G. Becker, W. Schwarz, N. Seidler, M. Westerhausen, *Z. Anorg. Allg. Chem.* **1992**, *612*, 72-82.
- [13] F. F. Puschmann, D. Stein, D. Heift, C. Hendriksen, Z. A. Gal, H. F. Grutzmacher, H. Grutzmacher, *Angew. Chem. Int. Ed.* **2011**, *50*, 8420-8423.
- [14] I. Krummenacher, C. C. Cummins, *Polyhedron* **2012**, *32*, 10-13.
- [15] A. R. Jupp, J. M. Goicoechea, *Angew. Chem. Int. Ed.* **2013**, *52*, 10064-10067.
- [16] M. Westerhausen, S. Schneiderbauer, H. Piotrowski, M. Suter, H. Nöth, *J. Organomet. Chem.* **2002**, *643-644*, 189-193.
- [17] S. Alidori, D. Heift, G. Santiso-Quinones, Z. Benko, H. Grutzmacher, M. Caporali, L. Gonsalvi, A. Rossin, M. Peruzzini, *Chem. Eur. J.* **2012**, *18*, 14805-14811.
- [18] L. Nyulaszi, T. Veszpremi, *J. Phys. Chem.* **1996**, *100*, 6456-6462.
- [19] A. M. Tondreau, Z. Benko, J. R. Harmer, H. Grutzmacher, *Chem. Sci.* **2014**, *5*, 1545-1554.
- [20] G. Markl, *Angew. Chem. Int. Ed.* **1966**, *5*, 846-849.
- [21] A. J. Ashe, *J. Am. Chem. Soc.* **1971**, *93*, 3293-3294.
- [22] K. Dimroth, F. W. Steuber, *Angew. Chem. Int. Ed.* **1967**, *6*, 445-446.
- [23] G. Markl, F. Lieb, A. Merz, *Angew. Chem. Int. Ed.* **1967**, *6*, 87-89.
- [24] J. J. Daly, G. Markl, *J. Chem. Soc., Chem. Commun.* **1969**, 1057-1058.
- [25] C. Batich, Heilbron, E. V. Hornung, A. J. Ashe, D. T. Clark, U. T. Cobley, D. Kilcast, I. Scanlan, *J. Am. Chem. Soc.* **1973**, *95*, 928-930.
- [26] K. K. Baldridge, M. S. Gordon, *J. Am. Chem. Soc.* **1988**, *110*, 4204-4208.
- [27] L. Nyulaszi, T. Veszpremi, J. Reffy, B. Burkhardt, M. Regitz, *J. Am. Chem. Soc.* **1992**, *114*, 9080-9084.
- [28] P. D. Burrow, A. J. Ashe, D. J. Bellville, K. D. Jordan, *J. Am. Chem. Soc.* **1982**, *104*, 425-429.
- [29] L. Nyulaszi, *Chem. Rev.* **2001**, *101*, 1229-1246.
- [30] A. Modelli, B. Hajgato, J. F. Nixon, L. Nyulaszi, *J. Phys. Chem. A* **2004**, *108*, 7440-7447.
- [31] P. Le Floch, *Coord. Chem. Rev.* **2006**, *250*, 627-681.
- [32] C. Muller, D. Vogt, *Dalton Trans.* **2007**, 5505-5523.
- [33] L. Weber, *Angew. Chem. Int. Ed.* **2002**, *41*, 563-572.
- [34] N. Mezailles, F. Mathey, P. Le Floch, *Prog. Inorg. Chem.*, **2001**, *49*, 455-550.

- [35] J. Waluk, H. P. Klein, A. J. Ashe, J. Michl, *Organometallics* **1989**, *8*, 2804-2808.
- [36] J. M. Davidson, G. Dyer, *J. Chem. Soc. A*, **1968**, 1616-1619.
- [37] J. M. Davidson, *J. Chem. Soc. A*, **1969**, 193-195.
- [38] H. M. McConnell, *J. Chem. Phys.* **1957**, *27*, 226-229.
- [39] A. J. Arce, A. J. Deeming, Y. Desanctis, A. M. Garcia, J. Manzur, E. Spodine, *Organometallics* **1994**, *13*, 3381-3383.
- [40] G. Frison, A. Sevin, N. Avarvari, F. Mathey, P. Le Floch, *J. Org. Chem.* **1999**, *64*, 5524-5529.
- [41] C. Elschenbroich, M. Nowotny, B. Metz, W. Massa, J. Graulich, K. Biehler, W. Sauer, *Angew. Chem. Int. Ed.* **1991**, *30*, 547-550.
- [42] H. Vahrenkamp, H. Nöth, *Chem. Ber.* **1972**, *105*, 1148-1157.
- [43] J. Deberitz, H. Nöth, *Chem. Ber.* **1973**, *106*, 2222-2226.
- [44] M. Doux, L. Ricard, F. Mathey, Pascal L. Floch, N. Mézailles, *Eur. J. Inorg. Chem.* **2003**, *2003*, 687-698.
- [45] N. Mezailles, L. Ricard, F. Mathey, P. Le Floch, *Organometallics* **2001**, *20*, 3304-3307.
- [46] F. Nief, C. Charrier, F. Mathey, M. Simalty, *J. Organomet. Chem.* **1980**, *187*, 277-285.
- [47] B. Breit, R. Winde, T. Mackewitz, R. Paciello, K. Harms, *Chem. Eur. J.* **2001**, *7*, 3106-3121.
- [48] I. C. Tornieporthoetting, P. Buzek, P. V. Schleyer, T. M. Klapotke, *Angew. Chem. Int. Ed.* **1992**, *31*, 1338-1339.
- [49] C. Elschenbroich, M. Nowotny, A. Behrendt, K. Harms, S. Wocadlo, J. Pebler, *J. Am. Chem. Soc.* **1994**, *116*, 6217-6219.
- [50] H. Kanter, K. Dimroth, *Tetrahedron Lett.* **1975**, *16*, 541-544.
- [51] G. Yamamoto, K. Kuwahara, K. Inoue, *Chem. Lett.* **1995**, 351-352.
- [52] M. Shiotsuka, T. Tanamachi, T. Urakawa, M. Munakata, Y. Matsuda, *J. Supramol. Chem.* **2002**, *2*, 211-217.
- [53] Y. Hu, C.-Y. Li, X.-M. Wang, Y.-H. Yang, H.-L. Zhu, *Chem. Rev. (Washington, DC, U. S.)* **2014**, *114*, 5572-5610.
- [54] N. E. Kamber, W. Jeong, R. M. Waymouth, R. C. Pratt, B. G. G. Lohmeijer, J. L. Hedrick, *Chem. Rev. (Washington, DC, U. S.)* **2007**, *107*, 5813-5840.
- [55] D. Heift, Z. Benko, H. Grutzmacher, *Angew. Chem. Int. Ed.* **2014**, *53*, 6757-6761.
- [56] A. Loibl, I. de Krom, E. A. Pidko, M. Weber, J. Wiecko, C. Muller, *Chem. Commun.* **2014**, *50*, 8842-8844.
- [57] G. Markl, K. Hohenwarter, M. L. Ziegler, B. Nuber, *Tetrahedron Lett.* **1990**, *31*, 4849-4852.
- [58] C. Muller, D. Vogt, *Compt. Rend. Chim.* **2010**, *13*, 1127-1143.
- [59] R. Paciello, E. Zeller, B. Breit, M. Roeper, Basf Ag (Badi).
- [60] P. Lefloch, D. Carmichael, F. Mathey, *Organometallics* **1991**, *10*, 2432-2436.
- [61] P. Lefloch, F. Mathey, *Tetrahedron Lett.* **1989**, *30*, 817-818.
- [62] P. Lefloch, F. Mathey, *J. Chem. Soc., Chem. Commun.* **1993**, 1295-1296.
- [63] N. Avarvari, P. LeFloch, F. Mathey, *J. Am. Chem. Soc.* **1996**, *118*, 11978-11979.
- [64] N. Avarvari, N. Mezailles, L. Ricard, P. Le Floch, F. Mathey, *Science* **1998**, *280*, 1587-1589.
- [65] J. Grundy, F. Mathey, *Angew. Chem. Int. Ed.* **2005**, *44*, 1082-1084.
- [66] G. Markl, A. Kallmunzer, *Tetrahedron Lett.* **1989**, *30*, 5245-5248.
- [67] M. Nakagawa, J. Saegusa, M. Tonozuka, M. Obi, M. Kiuchi, T. Hino, Y. Ban, *Organ. Synth.* **1988**, *50*-9, 462-464.

- [68] C. Muller, D. Vogt, *Dalton Trans.* **2007**, 5505-5523.
- [69] J. Sieler, M. Pink, G. Zahn, *Z. Anorg. Allgem. Chem.* **1994**, 620, 743-748.
- [70] D. J. MacDougall, B. C. Noll, K. W. Henderson, *Inorg. Chem.* **2005**, 44, 1181-1183.
- [71] N. Tsuchida, S. Yamabe, *J. Phys. Chem. A* **2005**, 109, 1974-1980.
- [72] W. Q. Li, W. Q. Tian, J. K. Feng, Z. Z. Liu, *Eur. J. Org. Chem.* **2007**, 1669-1677.
- [73] P. J. Hore, *Nuclear Magnetic Resonance*, Oxford University Press **1995**.
- [74] P. Le Floch, M. Blug, O. Piechaczyk, M. Fustier, N. Mezaillles, *J. Org. Chem.* **2008**, 73, 3258-3261.
- [75] M. Podewitz, J. D. van Beek, M. Worle, T. Ott, D. Stein, H. Ruegger, B. H. Meier, M. Reiher, H. Grutzmacher, *Angew. Chem. Int. Ed.* **2010**, 49, 7465-7469.
- [76] P. Le Floch, *Phosphorous Heterocycles I* **2009**, 20, 147-184.
- [77] G. G. Hammes, P. J. Lillford, *J. Am. Chem. Soc.* **1970**, 92, 7578-7585.
- [78] C. B. Fischer, H. Steininger, D. S. Stephenson, H. Zipse, *J. Phys. Org. Chem.* **2005**, 18, 901-907.
- [79] E. L. Hahn, *Phys. Rev.* **1950**, 80, 580-594.
- [80] P. S. Pregosin, P. G. A. Kumar, I. Fernandez, *Chem. Rev.* **2005**, 105, 2977-2998.
- [81] P. S. Pregosin, E. Martinez-Viviente, P. G. A. Kumar, *Dalton Trans.* **2003**, 4007-4014.
- [82] E. Meister, *Grundpraktikum Physikalische Chemie*, UTB **2006**, 202.
- [83] S. Babic, A. J. M. Horvat, D. M. Pavlovic, M. Kastelan-Macan, *TrAC, Trends Anal. Chem.* **2007**, 26, 1043-1061.
- [84] J. A. Dean, *Lange's Handbook of Chemistry (15th Edition)*, McGraw Hill **1999**.
- [85] C. A. Reed, Y. Zhang, T. S. Tham, J. F. Nixon, C. Taylor, J. C. Green, *Angew. Chem. Int. Ed.* **2008**, 47, 3801-3804.
- [86] R. Ramage, *Nature* **1985**, 315, 354-354.
- [87] A. Savin, B. Silvi, F. Colonna, *Can. J. Chem.* **1996**, 74, 1088-1096.
- [88] G. P. Bean, *J. Org. Chem.* **1998**, 63, 2497-2506.
- [89] T. Shintou, K. Fukumoto, T. Mukaiyama, *Bull. Chem. Soc. Jpn.* **2004**, 77, 1569-1579.
- [90] F. Mathey, *Phosphorus-carbon heterocyclic chemistry: the rise of a new domain*, Pergamon Amsterdam, **2001**.
- [91] N. Mézailles, F. Mathey, P. L. Floch, in *Prog. Inorg. Chem.*, John Wiley & Sons, Inc., **2007**, pp. 455-550.
- [92] P. Le Floch, F. Mathey, *Coord. Chem. Rev.* **1998**, 178, 771-791.
- [93] P. Le Floch, S. Mansuy, L. Ricard, F. Mathey, A. Jutand, C. Amatore, *Organometallics* **1996**, 15, 3267-3274.
- [94] B. Schmid, L. M. Venanzi, A. Albinati, F. Mathey, *Inorg. Chem.* **1991**, 30, 4693-4699.
- [95] I. de Krom, E. A. Pidko, M. Lutz, C. Muller, *Chem. Eur. J.* **2013**, 19, 7523-7531.
- [96] C. Muller, L. E. E. Broeckx, I. de Krom, J. J. M. Weemers, *Eur. J. Inorg. Chem.* **2013**, 187-202.
- [97] A. Michaelis, R. Kaehne, *Berichte der deutschen chemischen Gesellschaft* **1898**, 31, 1048-1055.
- [98] B. A. Arbusow, in *Pure Appl. Chem.*, Vol. 9, **1964**, p. 307.
- [99] A. K. Bhattacharya, G. Thyagarajan, *Chem. Rev.* **1981**, 81, 415-430.
- [100] T. B. Brill, S. J. Landon, *Chem. Rev.* **1984**, 84, 577-585.
- [101] R. J. Haines, A. L. Dupreez, L. L. Marais, *J. Organomet. Chem.* **1970**, 24, C26-C28.
- [102] J. A. S. Howell, A. J. Rowan, M. S. Snell, *J. Chem. Soc., Dalton Trans.* **1981**, 325-327.
- [103] J. A. S. Duncan, D. Hedden, D. M. Roundhill, T. A. Stephenson, M. D. Walkinshaw, *Angew. Chem. Int. Ed.* **1982**, 21, 452-453.

- [104] O. Seven, S. Polat-Cakir, M. S. Hossain, M. Emrullahoglu, A. S. Demir, *Tetrahedron* **2011**, *67*, 3464-3469.
- [105] X. D. Chen, S. Alidori, F. F. Puschmann, G. Santiso-Quinones, Z. Benko, Z. S. Li, G. Becker, H. F. Grutzmacher, H. Grutzmacher, *Angew. Chem. Int. Ed.* **2014**, *53*, 1641-1645.
- [106] P. P. Terence, T. D. Nixon, *New Aspects in Phosphorus Chemistry li* **2003**, *223*, 45-65.
- [107] P. Le Floch, D. Carmichael, L. Ricard, F. Mathey, A. Jutand, C. Amatore, *Organometallics* **1992**, *11*, 2475-2479.
- [108] M. Bruce, G. Meissner, M. Weber, J. Wiecko, C. Müller, *Eur. J. Inorg. Chem.* **2014**, *2014*, 1719-1726.
- [109] H. Onken, J. Lottermoser, *Naturwissenschaften* **1967**, *54*, 560-561.
- [110] A. Campos-Carrasco, L. E. E. Broeckx, J. J. M. Weemers, E. A. Pidko, M. Lutz, A. M. Masdeu-Bultó, D. Vogt, C. Müller, *Chem. Eur. J.* **2011**, *17*, 2510-2517.
- [111] A. Breque, C. C. Santini, F. Mathey, J. Fischer, A. Mitschler, *Inorg. Chem.* **1984**, *23*, 3463-3467.
- [112] W. Klau, H. Otto, W. Eberspach, E. Buchholz, *Chem. Ber. Recl.* **1982**, *115*, 1922-1933.
- [113] H. Nakazawa, T. Fujita, K. Kubo, K. Miyoshi, *J. Organomet. Chem.* **1994**, *473*, 243-252.
- [114] I. Thiel, H. J. Jiao, A. Spannenberg, M. Hapke, *J. Organomet. Chem.* **2014**, *763*, 60-64.
- [115] F. F. Puschmann, J. Harmer, D. Stein, H. Ruegger, B. de Bruin, H. Grutzmacher, *Angew. Chem. Int. Ed.* **2010**, *49*, 385-389.
- [116] T. B. Brill, S. J. Landon, *Chem. Rev.* **1984**, *84*, 577-585.
- [117] T. Zweifel, J. V. Naubron, H. Grutzmacher, *Angew. Chem. Int. Ed.* **2009**, *48*, 559-563.
- [118] F. A. Cotton and G. Wilkinson, *Advanced Inorganic Chemistry*, John Wiley and Sons, 5th edn., **1988**.
- [119] V. Balzani, A. Juris, M. Venturi, S. Campagna, S. Serroni, *Chem. Rev.* **1996**, *96*, 759-834.
- [120] A. Juris, P. Ceroni, V. Balzani, *Photochemistry and photophysics : concepts, research, applications*, Weinheim : Wiley-VCH, **2014**.
- [121] A. Juris, V. Balzani, F. Barigelletti, S. Campagna, P. Belser, A. von Zelewsky, *Coord. Chem. Rev.* **1988**, *84*, 85-277.
- [122] J. G. Vos, J. M. Kelly, *Dalton Trans.* **2006**, 4869-4883.
- [123] E. M. Kober, J. V. Caspar, R. S. Lumpkin, T. J. Meyer, *J. Phys. Chem.* **1986**, *90*, 3722-3734.
- [124] M. S. Lowry, S. Bernhard, *Chem. Eur. J.* **2006**, *12*, 7970-7977.
- [125] O. Horváth, *Coord. Chem. Rev.* **1994**, *135-136*, 303-324.
- [126] J. Sýkora, *Coord. Chem. Rev.* **1997**, *159*, 95-108.
- [127] M. Maestri, N. Armaroli, V. Balzani, E. C. Constable, A. M. W. C. Thompson, *Inorg. Chem.* **1995**, *34*, 2759-2767.
- [128] D. G. Cuttall, S.-M. Kuang, P. E. Fanwick, D. R. McMillin, R. A. Walton, *J. Am. Chem. Soc.* **2002**, *124*, 6-7.
- [129] D. Felder, J.-F. Nierengarten, F. Barigelletti, B. Ventura, N. Armaroli, *J. Am. Chem. Soc.* **2001**, *123*, 6291-6299.
- [130] V. Kalsani, M. Schmittel, A. Listorti, G. Accorsi, N. Armaroli, *Inorg. Chem.* **2006**, *45*, 2061-2067.
- [131] M. Hashimoto, S. Igawa, M. Yashima, I. Kawata, M. Hoshino, M. Osawa, *J. Am. Chem. Soc.* **2011**, *133*, 10348-10351.
- [132] Q. Zhang, Q. Zhou, Y. Cheng, L. Wang, D. Ma, X. Jing, F. Wang, *Adv. Mater.* **2004**, *16*, 432-436.
- [133] W. L. Jia, T. McCormick, Y. Tao, J.-P. Lu, S. Wang, *Inorg. Chem.* **2005**, *44*, 5706-5712.
- [134] Q. Zhang, Q. Zhou, Y. Cheng, L. Wang, D. Ma, X. Jing, F. Wang, *Adv. Funct. Mater.* **2006**, *16*, 1203-1208.

- [135] C. Muller, D. Wasserberg, J. J. M. Weemers, E. A. Pidko, S. Hoffmann, M. Lutz, A. L. Spek, S. C. J. Meskers, R. A. J. Janssen, R. A. van Santen, D. Vogt, *Chem. Eur. J.* **2007**, *13*, 4548-4559.
- [136] N. N. Pham-Tran, G. Bouchoux, D. Delaere, M. T. Nguyen, *J. Phys. Chem. A* **2005**, *109*, 2957-2963.
- [137] J. Waluk, H. P. Klein, A. J. Ashe, J. Michl, *Organometallics* **1989**, *8*, 2804-2808.
- [138] J. Moussa, T. Cheminel, G. R. Freeman, L. M. Chamoreau, J. A. G. Williams, H. Amouri, *Dalton Trans.* **2014**, *43*, 8162-8165.
- [139] P. Roesch, J. Nitsch, M. Lutz, J. Wiecko, A. Steffen, C. Muller, *Inorg. Chem.* **2014**, *53*, 9855-9859.
- [140] S. Naik, J. T. Mague, M. S. Balakrishna, *Inorg. Chem.* **2014**, *53*, 3864-3873.
- [141] I. Jess, C. Nather, *Inorg. Chem.* **2006**, *45*, 7446-7454.
- [142] P. C. Ford, E. Cariati, J. Bourassa, *Chem. Rev.* **1999**, *99*, 3625-3647.
- [143] S. B. Harkins, J. C. Peters, *J. Am. Chem. Soc.* **2005**, *127*, 2030-2031.
- [144] A. Tsuboyama, K. Kuge, M. Furugori, S. Okada, M. Hoshino, K. Ueno, *Inorg. Chem.* **2007**, *46*, 1992-2001.
- [145] A. Bondi, *J. Phys. Chem.* **1964**, *68*, 441-444.
- [146] P. K. Mehrotra, R. Hoffmann, *Inorg. Chem.* **1978**, *17*, 2187-2189.
- [147] N. Marsich, G. Nardin, L. Randaccio, *J. Am. Chem. Soc.* **1973**, *95*, 4053-4054.
- [148] M. S. Balakrishna, D. Suresh, J. T. Mague, *Eur. J. Inorg. Chem.* **2010**, *2010*, 4201-4210.
- [149] B. Schmid, L. M. Venanzi, T. Gerfin, V. Gramlich, F. Mathey, *Inorg. Chem.* **1992**, *31*, 5117-5122.
- [150] M. T. Reetz, E. Bohres, R. Goddard, M. C. Holthausen, W. Thiel, *Chem. Eur. J.* **1999**, *5*, 2101-2108.
- [151] T. Pechmann, C. D. Brandt, H. Werner, *Angew. Chem. Int. Ed.* **2000**, *39*, 3909-+.
- [152] M. J. Bakker, F. W. Vergeer, F. Hartl, P. Rosa, L. Ricard, P. Le Floch, M. J. Calhorda, *Chem. Eur. J.* **2002**, *8*, 1741-1752.
- [153] C. Elschenbroich, J. Six, K. Harms, *Chem. Commun.* **2006**, 3429-3431.
- [154] Y. L. Mao, K. M. H. Lim, Y. X. Li, R. Ganguly, F. Mathey, *Organometallics* **2013**, *32*, 3562-3565.
- [155] A. Campos-Carrasco, L. E. E. Broeckx, J. J. M. Weemers, E. A. Pidko, M. Lutz, A. M. Masdeu-Bulto, D. Vogt, C. Muller, *Chem. Eur. J.* **2011**, *17*, 2510-2517.
- [156] A. Breque, C. C. Santini, F. Mathey, J. Fischer, A. Mitschler, *Inorg. Chem.* **1984**, *23*, 3463-3467.
- [157] A. C. Carrasco, E. A. Pidko, A. M. Masdeu-Bulto, M. Lutz, A. L. Spek, D. Vogt, C. Muller, *New J. Chem.* **2010**, *34*, 1547-1550.
- [158] Y. Chen, H. X. Li, D. Liu, L. L. Liu, N. Y. Li, H. Y. Ye, Y. Zhang, J. P. Lang, *Cryst. Growth Des.* **2008**, *8*, 3810-3816.
- [159] X. Y. Yang, Y. X. Li, S. A. Pullarkat, *Inorg. Chem.* **2014**, *53*, 10232-10239.
- [160] K. Naktode, R. K. Kottalanka, H. Adimulam, T. K. Panda, *J. Coord. Chem.* **2014**, *67*, 3042-3053.
- [161] J. Yuasa, M. Dan, T. Kawai, *Dalton Trans.* **2013**, *42*, 16096-16101.
- [162] D. J. Fife, K. W. Morse, W. M. Moore, *Journal of Photochemistry* **1984**, *24*, 249-263.
- [163] P. Murer, J. Wolf, S. Burkhardt, H. Gruetzmacher, D. Stein, K. Dietliker, H. Grutzmacher, J. P. Wolf, CIBA SPECIALTY CHEM HOLDING INC (CIBA) MURER P (MURE-Individual) WOLF J (WOLF-Individual) BURKHARDT S (BURK-Individual) GRUTZMACHER H (GRUT-Individual) STEIN D (STEI-Individual) DIETLIKER K (DIET-Individual) CIBA SC HOLDING AG (CIBA) CIBA SPECIALTY CHEM CORP (CIBA) BASF SE (BADI).
- [164] F. Mathey, *Angew. Chem. Int. Ed.* **2003**, *42*, 1578-1604.
- [165] A. Mack, M. Regitz, *Chem. Ber.* **1997**, *130*, 823-834.
- [166] U. Annen, M. Regitz, *Tetrahedron Lett.* **1988**, *29*, 1681-1684.

- [167] W. Roesch, M. Regitz, *Z. Naturforsch., B: Anorg. Chem., Org. Chem.* **1986**, *41B*, 931-933.
- [168] W. Roesch, M. Regitz, *Angew. Chem.* **1984**, *96*, 898-899.
- [169] T. Joh, K. Fujiwara, S. Takahashi, *Bull. Chem. Soc. Jpn.* **1993**, *66*, 978-980.
- [170] N. A. Pushkarevsky, S. N. Konchenko, A. V. Virovets, M. Scheer, *Organometallics* **2013**, *32*, 770-779.
- [171] G. Becker, M. Niemeyer, O. Mundt, W. Schwarz, M. Westerhausen, M. W. Ossberger, P. Mayer, H. Noth, Z. Y. Zhong, P. J. Dijkstra, J. Feijen, *Z. Anorg. Allg. Chem.* **2004**, *630*, 2605-2621.
- [172] J. Emsley, D. Hall, Harper and Row, London, **1976**, p. 34.
- [173] J. Sieler, M. Pink, G. Zahn, *Z. Anorg. Allg. Chem.* **1994**, *620*, 743-748.
- [174] D. J. MacDougall, B. C. Noll, K. W. Henderson, *Inorganic Chemistry* **2005**, *44*, 1181-1183.
- [175] T. Kremer, P. v. R. Schleyer, *Organometallics* **1997**, *16*, 737-746.
- [176] D. Gudat, S. Hüp, V. Bajorat, M. Nieger, *Z. Anorg. Allg. Chem.* **2001**, *627*, 1119-1127.
- [177] E. Niecke, M. Nieger, P. Wenderoth, *Angew. Chem. Int. Ed.* **1994**, *33*, 353-354.
- [178] M. Westerhausen, M. W. Oßberger, A. Keilbach, C. Gückel, H. Piotrowski, M. Suter, H. Nöth, *Z. Anorg. Allg. Chem.* **2003**, *629*, 2398-2407.
- [179] X. Chen, X. Wang, Z. Zhou, Y. Li, Y. Sui, J. Ma, X. Wang, P. P. Power, *Angew. Chem. Int. Ed.* **2013**, *52*, 589-592.
- [180] P. R. Schreiner, L. V. Chernish, P. A. Gunchenko, E. Y. Tikhonchuk, H. Hausmann, M. Serafin, S. Schlecht, J. E. P. Dahl, R. M. K. Carlson, A. A. Fokin, *Nature* **2011**, *477*, 308-311.
- [181] A. A. Fokin, L. V. Chernish, P. A. Gunchenko, E. Y. Tikhonchuk, H. Hausmann, M. Serafin, J. E. P. Dahl, R. M. K. Carlson, P. R. Schreiner, *J. Am. Chem. Soc.* **2012**, *134*, 13641-13650.
- [182] F. F. Puschmann, D. Stein, D. Heift, C. Hendriksen, Z. A. Gal, H.-F. Grützmacher, H. Grützmacher, *Angew. Chem. Int. Ed.* **2011**, *50*, 8420-8423.
- [183] A. R. Jupp, J. M. Goicoechea, *Angew. Chem., Int. Ed.* **2013**, *52*, 10064-10067.
- [184] D. Heift, Z. Benko, H. Gruetzmacher, *Angew. Chem., Int. Ed.* **2014**, *53*, 6757-6761.
- [185] M. S. J. R. A. P. Moss, M. Jr., , Hoboken, NJ,, **2004**.
- [186] M. Melaimi, M. Soleilhavoup, G. Bertrand, *Angew. Chem. Int. Ed.* **2010**, *49*, 8810-8849.
- [187] i. K. Lammertsma, *New Aspects in Phosphorus Chemistry III, Vol. vol. 229, ch. 4, pp. 95-119*, ed. J.-P. Majoral, Springer Berlin Heidelberg, **2003**.
- [188] K. L. J. C. Slootweg, *Science of Synthesis*, **2009**, *42*, 15-36.
- [189] T. Wong, J. K. Terlouw, H. Keck, W. Kuchen, P. Tommes, *J. Am. Chem. Soc.* **1992**, *114*, 8208-8210.
- [190] G. Bucher, M. L. G. Borst, A. W. Ehlers, K. Lammertsma, S. Ceola, M. Huber, D. Grote, W. Sander, *Angew. Chem. Int. Ed.* **2005**, *44*, 3289-3293.
- [191] H. Jansen, M. C. Samuels, E. P. A. Couzijn, J. C. Slootweg, A. W. Ehlers, P. Chen, K. Lammertsma, *Chem. Eur. J.* **2010**, *16*, 1454-1458.
- [192] A. Velian, C. C. Cummins, *J. Am. Chem. Soc.* **2012**, *134*, 13978-13981.
- [193] A. Velian, M. Nava, M. Temprado, Y. Zhou, R. W. Field, C. C. Cummins, *J. Am. Chem. Soc.* **2014**, *136*, 13586-13589.
- [194] D. Heift, Z. Benko, H. Grutzmacher, *Dalton Trans.* **2014**, *43*, 831-840.
- [195] F. F. Puschmann, D. Stein, D. Heift, C. Hendriksen, Z. A. Gal, H. F. Grutzmacher, H. Grutzmacher, *Angew. Chem. Int. Ed.* **2011**, *50*, 8420-8423.
- [196] I. Krummenacher, C. C. Cummins, *Polyhedron* **2012**, *32*, 10-13.
- [197] A. R. Jupp, J. M. Goicoechea, *Angew. Chem. Int. Ed.* **2013**, *52*, 10064-10067.

- [198] S. Alidori, D. Heift, G. Santiso-Quinones, Z. Benkő, H. Grützmacher, M. Caporali, L. Gonsalvi, A. Rossin, M. Peruzzini, *Chem. Eur. J.* **2012**, *18*, 14805-14811.
- [199] D. Heift, Z. Benko, H. Grutzmacher, *Dalton Trans.* **2014**, *43*, 5920-5928.
- [200] D. Heift, Z. Benkő, H. Grützmacher, *Chem. Eur. J.* **2014**, *20*, 11326-11330.
- [201] Z. Benko, R. Streubel, L. Nyulaszi, *Dalton Trans.* **2006**, 4321-4327.
- [202] G. Becker, G. Heckmann, K. Hübler, W. Schwarz, *Z. Anorg. Allg. Chem.* **1995**, *621*, 34-46.
- [203] T. Mizuta, T. Nakazono, K. Miyoshi, *Angew. Chem. Int. Ed.* **2002**, *41*, 3897-3898.
- [204] D. Tofan, C. C. Cummins, *Angew. Chem. Int. Ed.* **2010**, *49*, 7516-7518.
- [205] C. Fave, M. Hissler, T. Kárpáti, J. Rault-Berthelot, V. Deborde, L. Toupet, L. Nyulászi, R. Réau, *J. Am. Chem. Soc.* **2004**, *126*, 6058-6063.
- [206] Y.-y. Carpenter, C. A. Dyker, N. Burford, M. D. Lumsden, A. Decken, *J. Am. Chem. Soc.* **2008**, *130*, 15732-15741.
- [207] S. L. Hinchley, C. A. Morrison, D. W. H. Rankin, C. L. B. Macdonald, R. J. Wiacek, A. Voigt, A. H. Cowley, M. F. Lappert, G. Gundersen, J. A. C. Clyburne, P. P. Power, *J. Am. Chem. Soc.* **2001**, *123*, 9045-9053.
- [208] S. Burck, K. Götz, M. Kaupp, M. Nieger, J. Weber, J. Schmedt auf der Günne, D. Gudat, *J. Am. Chem. Soc.* **2009**, *131*, 10763-10774.
- [209] S. Burck, D. Gudat, M. Nieger, *Angew. Chem. Int. Ed.* **2004**, *43*, 4801-4804.
- [210] R. Appel, B. Niemann, M. Nieger, *Angew. Chem. Int. Ed.* **1988**, *27*, 957-958.
- [211] M. A. Serra, R. B. Honzatko, *Acta Crystallographica Section C* **1986**, *42*, 1755-1757.
- [212] O. Back, G. Kuchenbeiser, B. Donnadieu, G. Bertrand, *Angew. Chem. Int. Ed.* **2009**, *48*, 5530-5533.
- [213] E. Niecke, O. Altmeyer, M. Nieger, *J. Chem. Soc., Chem. Commun.* **1988**, 945-946.
- [214] D. Förster, H. Dilger, F. Ehret, M. Nieger, D. Gudat, *Eur. J. Inorg. Chem.* **2012**, *2012*, 3989-3994.
- [215] R. Appel, W. Paulen, *Tetrahedron Lett.* **1983**, *24*, 2639-2642.
- [216] V. Plack, J. R. Goerlich, A. Fischer, R. Schmutzler, *Z. Anorg. Allg. Chem.* **1999**, *625*, 1979-1984.
- [217] N. A. Piro, J. S. Figueroa, J. T. McKellar, C. C. Cummins, *Science* **2006**, *313*, 1276-1279.
- [218] J. D. Masuda, W. W. Schoeller, B. Donnadieu, G. Bertrand, *J. Am. Chem. Soc.* **2007**, *129*, 14180-14181.
- [219] J. D. Masuda, W. W. Schoeller, B. Donnadieu, G. Bertrand, *Angew. Chem. Int. Ed.* **2007**, *46*, 7052-7055.
- [220] The isolated 2+4 Diels-Alder adduct is actually the mixture of cis/trans isomers which are obtained in a 2:1 ratio as confirmed by NMR spectroscopy and single-crystal X-ray crystallography (for details see the supporting information).
- [221] M. T. Nguyen, A. F. Hegarty, M. A. McGinn, P. Ruelle, *J. Chem. Soc., Perkin Trans. 2* **1985**, 1991-1997.
- [222] C. Dimur, F. Pauzat, Y. Ellinger, G. Berthier, *Spectrochim. Acta, Part A* **2001**, *57*, 859-873.
- [223] S. Burck, D. Gudat, M. Nieger, *Angew. Chem. Int. Ed.* **2004**, *43*, 4801-4804.
- [224] D. Heift, Z. Benko, H. Grutzmacher, *Dalton Trans.* **2014**, *43*, 5920-5928.
- [225] M. Westerhausen, S. Schneiderbauer, H. Piotrowski, M. Suter, H. Noth, *J. Organomet. Chem.* **2002**, *643*, 189-193.
- [226] S. Shah, J. D. Protasiewicz, *Coord. Chem. Rev.* **2000**, *210*, 181-201.
- [227] S. Shah, J. D. Protasiewicz, *Chem. Commun.* **1998**, 1585-1586.
- [228] S. Shah, M. C. Simpson, R. C. Smith, J. D. Protasiewicz, *J. Am. Chem. Soc.* **2001**, *123*, 6925-6926.

- [229] A. H. Cowley, B. Pellerin, J. L. Atwood, S. G. Bott, *J. Am. Chem. Soc.* **1990**, *112*, 6734–6735.
- [230] Y. L. Mao, Z. Y. Wang, R. Ganguly, F. Mathey, *Organometallics* **2012**, *31*, 4786–4790.
- [231] A free phosphanyl phosphinidene as intermediate is very unlikely. The computed dissociation energy $A \rightarrow (HC)_2(NMe)_2P-P + CO$ is endothermic by 29.0 kcal mol⁻¹ and is associated with a high activation barrier of 48.7 kcal mol⁻¹ (at the BP86/RI/def2-TZVP level).
- [232] M. J. T. Frisch, G. W.; Schlegel, H. B.; Scuseria, G. E.; Robb, M. A.; Cheeseman, J. R.; Scalmani, G.; Barone, V.; Mennucci, B.; Petersson, G. A.; Nakatsuji, H.; Caricato, M.; Li, X.; Hratchian, H. P.; Izmaylov, A. F.; Bloino, J.; Zheng, G.; Sonnenberg, J. L.; Hada, M.; Ehara, M.; Toyota, K.; Fukuda, R.; Hasegawa, J.; Ishida, M.; Nakajima, T.; Honda, Y.; Kitao, O.; Nakai, H.; Vreven, T.; Montgomery, Jr., J. A.; Peralta, J. E.; Ogliaro, F.; Bearpark, M.; Heyd, J. J.; Brothers, E.; Kudin, K. N.; Staroverov, V. N.; Kobayashi, R.; Normand, J.; Raghavachari, K.; Rendell, A.; Burant, J. C.; Iyengar, S. S.; Tomasi, J.; Cossi, M.; Rega, N.; Millam, N. J.; Klene, M.; Knox, J. E.; Cross, J. B.; Bakken, V.; Adamo, C.; Jaramillo, J.; Gomperts, R.; Stratmann, R. E.; Yazyev, O.; Austin, A. J.; Cammi, R.; Pomelli, C.; Ochterski, J. W.; Martin, R. L.; Morokuma, K.; Zakrzewski, V. G.; Voth, G. A.; Salvador, P.; Dannenberg, J. J.; Dapprich, S.; Daniels, A. D.; Farkas, Ö.; Foresman, J. B.; Ortiz, J. V.; Cioslowski, J.; Fox, D. J., Gaussian 09, Revision A.1 ed., Gaussian, Inc., Wallingford CT, **2009**.
- [233] M. B. R. Ahlrichs, M. Häser, H. Horn, C. Kölmel, *Chem. Phys. Lett.* **1989**, *162*, 165–169.
- [234] C. H. A. Schäfer, R. Ahlrichs, *J. Chem. Phys.* **1994**, *100*, 5829-5835.
- [235] R. A. F. Weigend, *Phys. Chem. Chem. Phys.* **2005**, *7*, 3297-3305.
- [236] A. D. Becke, *Phys. Rev. A* **1988** *38*, 3098-3100.
- [237] J. P. Perdew, *Phys. Rev. B* **1986**, *33*, 8822-8824.
- [238] A. D. Becke, *J. Chem. Phys.* **1993**, *98*, 5648-5652.
- [239] F. J. D. P. J. Stephens, C. F. Chabalowski, M. J. Frisch, *J. Phys. Chem* **1994**, *98*, 11623-11627.
- [240] W. Y. C. Lee, R. G. Parr, *Phys. Rev. B* **1988**, *37*, 785-789.
- [241] H. H. A. Schäfer, R. Ahlrichs, *J. Chem. Phys.* **1992**, *97*, 2571-2577.
- [242] W. L. D. S. S. C. DeLano, CA, 2002.

Chen Xiao-dan

Bergacker 70 8046 Zurich, Switzerland

Email: xiaochen@inorg.chem.ethz.ch; chxdlzhsh@gmail.com

Phone number: 0041762929958

Birthday: Sep.1th 1986

● Education:

11/2010-9/2015(defense on 16th of September) ETH Zürich, Switzerland

Thesis: Synthesis and reactivity of phosphorus heterocycles using sodium phosphoethynolate as the building block.

9/2008—9/2010 Southeast University (985, 211) Technology Master Degree

Subject: School of Chemistry and Chemical Engineering (Material Science and Engineering)

9/2004—6/2008 Southeast University (985, 211) Technology Bachelor Degree

Subject: School of Chemistry and Chemical Engineering

● Skills:

English: Passed CET-6; IELTS: 6.

Computer: National Computer Rank Examination Grade 2.

Software: Originlab, ChemDraw, Shelxtl, Olex, Diamond, Platon, Magpack, Magfit, Endnote and so on.

Professional knowledge: Proficient in analyzing compounds with UV, IR, CV, MS, NMR, X-ray

● Scholarships and Awards:

Award for Best courses studies (such as Math, C++, Organic chemistry, Physics) nine times.

Excellent League Member in 2005

Tri-A Student in 2006

Scholarship of Changzhou Government in 2006, 2009

Excellent Project of Student's Research out of School in 2007

The second place in women's 800m match in of my School in 2006

Top one Scholarship for Graduates in 2008

Outstanding Student Leader Award in 2009

● Experience:

League Branch Secretary 2005–2007

Librarian 9/2007–6/2008

Monitor 9/2008–6/2010

The member of Academic Department of SEU 9/2008–6/2010

The member of Swiss Chemistry Society 9/2011–Present

TEACHING ASSISTANT, ETH Zürich, Switzerland, 9/2011–2/2014

- Inorganic and Organic Practicum I